

# Polylactic acid core-shell fibres by coaxial electrospinning

by

**Haydn Kriel**

*Thesis presented in partial fulfilment of the requirements for the degree of Master of Science*



*Stellenbosch University*

Department of Chemistry and Polymer Science  
Faculty of Natural Sciences

**Promoter:** Prof. Ron D. Sanderson  
**Co-Promoter:** Mrs Adine Gericke

March 2010

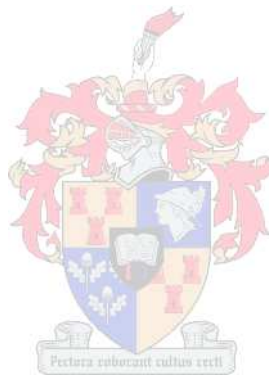
## Declaration

By submitting this thesis electronically, I declare that the entirety of the work contained therein is my own, original work, that I am the owner of the copyright thereof (unless to the extent explicitly otherwise stated) and that I have not previously in its entirety or in part submitted it for obtaining any qualification.



**Haydn Kriel**

*Stellenbosch, March 2010*



Copyright © 2010 Stellenbosch University

All rights reserved

## Abstract

The work presented in this dissertation describes the use of coaxial electrospinning of two miscible polymer solutions in the preparation of core-shell fibres with a semi-crystalline core of poly(L-lactic acid) and an amorphous shell of poly(D,L-lactic acid). Additionally it describes using these fibres in the production of single polymer composite yarns and films. These materials can potentially be used in applications that require biodegradable and fibre-reinforced composite materials e.g. suture yarns.

Traditional methods, such as TEM, when used to analyse the core-shell fibre structure were not successful with the polymer system used. A method was developed to validate core-shell fibre structure by selective dissolution of the shell material and correlating analyses of the separated components using differential scanning calorimetry (DSC) and optical rotation. The effects of solution concentration and flow rate on resultant core-shell fibre diameters were investigated. Core-solution flow rate was shown to be the most significant variable affecting the core and core-shell fibre diameters.

A thermal processing window exists between the glass transition temperature of the amorphous PDLA shell material and the crystalline melting temperature of the semi-crystalline PLLA core material. Heating these core-shell fibres within this processing window resulted in flow and fusion of overlapping shells of these core-shell fibres at their surfaces while the fibrous core components remained intact and reinforced the resulting composite material. This approach was used to produce single polymer composite yarns and films. Thermal treatments on yarns were shown to increase crystallinity of the cores and therefore the modulus and yield strength of the fibres when compared to untreated yarns.

## Opsomming

Die werk wat in hierdie tesis voorgelê word, beskryf die gebruik van koaksiale elektro-spinnery van twee wedersydoplosbare polimeeroplossings in die vervaardiging van kern-skilvesels met 'n gedeeltelik-kristallyne kern van poli-L-melksuur (PLLA) en 'n amorfe skil van poli-D,L-melksuur (PDLLA). Verder beskryf dit die gebruik van hierdie vesels in die vervaardiging van enkel-polimeer saamgestelde-materiaalgarings en -films. Hierdie materiale kan moontlik gebruik word in toepassings wat bio-afbreekbare en veselversterkte saamgestelde materiale vereis, soos byvoorbeeld chirurgiese steke.

Die polimeervesels wat in hierdie studie gebruik is, kon nie gekarakteriseer word met behulp van transmissie-elektronmikroskopie (TEM), wat gewoonlik gebruik word in die bestudering van kern-skilvesels, nie. 'n Alternatiewe karakteriseringsmetode is ontwikkel om te bevestig dat die gevormde vesels wel 'n kern-skilstruktuur het. Hierdie metode het behels dat die skil van die kern-skilvesel selektief opgelos is, waarna beide komponente (d.i. kern en skilmateriale) bestudeer is met behulp van differensiële skanderingskalorimetrie en optiese rotasie. Die invloed van polimeeroplossingskonsentrasie en -vloeitempo op die gevormde kern-skilvesels is daarna ondersoek en die vloeitempo van die kernoplossing is geïdentifiseer as die prosesinsetwaarde wat die mees beduidende invloed het op die deursnee van die vesels.

Daar bestaan 'n temperatuurinterval tussen die glasoorangstemperatuur van die amorfe PDLLA skilmateriaal en die kristallyne smeltpunt van die gedeeltelik-kristallyne PLLA kernmateriaal. Verwerking van die kern-skilvesels by 'n temperatuur binne hierdie interval het gelei tot vervloeiing en samesmelting van die oorvleuelende skille van die kern-skilvesels, terwyl die veselagtige kernkomponente van die vesels heel gebly het en opgetree het as versterking binne-in die saamgestelde materiaal wat gevorm het. Hierdie benadering is gebruik om enkel-polimeersaamgestelde-materiaalgarings en -films te vervaardig. 'n Vergelykende studie tussen onbehandelde en hitte-behandelde enkel-polimeer-saamgestelde-materiaalgarings het aangetoon dat die hittebehandeling gelei het tot 'n verhoging in die kristalliniteit van die veselkerne en daarom ook 'n verhoging in die modulus en breeksterkte van die garings tot gevolg gehad het.



I dedicate this work and everything I am to my parents whose unyielding love, guidance and support has allowed me to face any challenge as an opportunity and accept any defeat as a learning experience. With you I can fly!

I would like to give thanks to the following:

- All my friends and especially my family for all the encouragement and for helping me learn and grow. Especially my circle of trust Brynn, Storm, Leboganster, Leslie, Donald, Richard and Lewis. You guys are awesome and I take a part of you guys with me wherever I go!
- Mrs Gericke for your open door policy, always giving me great advice and for always looking for ways to help me out! Thanks for everything!
- My mentor and friend, Eugene, I can't tell you how much I appreciate all that you do for me! You saved my masters and gave me the tools to look at life through different eyes. I admire your hard work ethic, attention to detail and your unyielding enthusiasm. I aspire to reach your heights!
- Prof. Sanderson for providing me the opportunity to study further, to travel and to grow into an independent researcher. I thank you for your patience with me and for your enthusiasm for my work!
- The electrospinning group: Abdu, Ilana, Carla and Liesl thanks for the support and most importantly for your friendship! (and our surrogate member Tiaan for inspiring me with all your ideas and energy).
- The Dean of Science, Prof. Cloete, you inspire me!
- The unsung heroes of the Chemistry and Polymer Science Department, especially Cavlin (for being just awesome), Dorothy, Gabriel (pleasure), Lettie, Roderick, William, Anothony, Jim, Deon, Erinda, Margie, Oom Hennie, Anneli and Mr Groenewald.
- Free Radical Group: Lebohang, Khotso, Reuben, Niels, Eric and Zaskia...you guys saved me on so many levels thank you!
- All the people who helped make my masters possible especially Ulrich Buttner, Eyal Zussman, Dr. Kuhn, Mohamed Jaffer, Miranda Waldron, Madeline Frazenburg, Jan Gertenbach, Alfius, Zakhele Khumalo, Remy Bucher, Ben Loos, Dr. Verhoeven, Dr. Bredenkamp, Simon Herbert, Gareth Harding and Gareth Bailey.

Finally I would like to acknowledge the NRF and CTFL SETA for all the financial support during my masters.

## Table of Contents

Declaration.....	II
Abstract.....	III
Opsomming.....	IV
Acknowledgements.....	V
List of Figures.....	XI
List of Tables.....	XXI
List of Symbols and Abbreviations.....	XXIII
<b>Chapter 1. Introduction and Objectives.....</b>	<b>1</b>
1.1. Background.....	1
1.2. Goals and Objectives.....	3
1.3. Outline of document.....	4
References	
<b>Chapter 2. Literature Review.....</b>	<b>5</b>
2.1. Fibre technology.....	5
2.1.1. Background.....	5
2.1.2. Fine structure.....	6
2.1.3. Fine fibres.....	8
2.2. Composites and composite/bicomponent fibres.....	9
2.2.1. Fibre reinforced composites.....	9
2.2.2. Composite/Bicomponent fibres.....	10
2.2.2.1. Introduction.....	10
2.2.2.2. Core-shell fibres.....	12
2.2.3. Single polymer composites (SPC's).....	14
2.2.3.1. Background.....	14
2.2.3.2. SPC polylactic acid core-shell fibres.....	15
2.3. Polylactic acid (PLA).....	16
2.3.1. Introduction.....	16
2.3.2. PLA fibres.....	20
2.3.3. PLA nanofibres.....	20

2.4.	Coaxial electrospinning of nano- to meso-scale core-shell fibres .....	20
2.4.1.	Introduction.....	20
2.4.2.	Background.....	22
2.4.2.1.	Classical single capillary electrospinning.....	22
2.4.2.2.	Coaxial electrospinning .....	24
2.4.3.	Parameters.....	26
2.4.3.1.	System parameters .....	26
	<i>i) Miscibility of core and shell solutions.....</i>	<i>26</i>
	<i>ii) Effect of solution concentration, viscosity and molecular weight.....</i>	<i>27</i>
	<i>iii) Solvent Volatility .....</i>	<i>27</i>
	<i>iv) Conductivity.....</i>	<i>28</i>
	<i>v) Dielectric Constant.....</i>	<i>29</i>
	<i>vi) Surface tension and interfacial surface tension.....</i>	<i>29</i>
2.4.3.2.	Process parameters.....	30
	<i>i) Applied Voltage, Spinning/Gap Distance and Electric Field Strength</i>	<i>30</i>
	<i>ii) Applied voltage polarity.....</i>	<i>31</i>
	<i>iii) Flow rate .....</i>	<i>31</i>
	<i>iv) Capillary tip.....</i>	<i>32</i>
	<i>v) Coaxial spinneret configuration.....</i>	<i>32</i>
	<i>vi) Core-needle protrusion.....</i>	<i>33</i>
	<i>vii) Collector .....</i>	<i>33</i>
2.4.3.3.	Ambient conditions.....	34

*References*

<b>Chapter 3.</b>	<b>Experimental .....</b>	<b>42</b>
3.1.	Electrospinning Inputs .....	43
3.1.1.	Raw materials.....	43
3.1.2.	Solution preparation.....	43
3.1.3.	Materials and Equipment .....	44
3.1.4.	Electrospinning environment (ambient conditions).....	45
3.2.	Single-capillary Electrospinning.....	45
3.2.1.	Set-up and Electrospinning Procedure.....	45
3.2.2.	Analysis of resultant fibre diameters: Scanning electron microscopy (SEM).....	46

3.3.	Coaxial Electrospinning.....	47
3.3.1.	Set-up and Electrospinning Procedure.....	48
3.3.2.	Fibre collection and preparation of yarns .....	51
3.3.2.1.	Static collection.....	51
3.3.2.2.	Dynamic collection .....	51
3.3.2.3.	Yarn formation.....	52
3.3.3.	Process validation: coaxial Taylor cone and jet.....	53
3.3.4.	Core-shell structure validation.....	54
3.3.4.1.	Fluorescent microscopy .....	54
3.3.4.2.	Selective dissolution method: core-shell fibre structure validation .....	55
	<i>i) Background</i> .....	55
	<i>ii) Overview</i> .....	56
	<i>iii) Procedure</i> .....	57
	<i>iv) Analyses</i> .....	58
3.3.5.	Parameter Effects .....	60
3.3.5.1.	Effect of solution concentration and flow rate on core-shell fibre diameters.....	60
3.3.6.	Applications of core-shell fibres: Properties of yarns and films.....	61
3.3.6.1.	Thermal treatments .....	62
	<i>i) Yarns</i> .....	62
	<i>ii) Films</i> .....	62
3.3.6.2.	Analyses: Yarns and Films .....	63
	<i>i) Cryo-fracture</i> .....	63
	<i>ii) Light Microscopy</i> .....	63
	<i>iii) DSC and Modulated Differential Scanning Calorimetry (MDSC)</i> ....	63
	<i>iv) X-ray Diffraction</i> .....	63
	<i>v) Mechanical Testing</i> .....	64

*References*

<b>Chapter 4.</b>	<b>Results and Discussions - Coaxial Electrospinning .....</b>	<b>68</b>
4.1.	Core-shell structure validation.....	68
4.1.1.	Fluorescent microscopy .....	70
4.1.2.	Selective dissolution method: core-shell fibre structure validation.....	73

4.1.2.1. Analyses.....	73
i) SEM.....	73
ii) Optical rotation .....	73
iii) DSC.....	75
4.2. Parameter effects on core-shell fibre diameter .....	76
4.2.1. Concentration.....	76
4.2.2. Flow rate .....	80

*References*

**Chapter 5. Results and Discussions – Single Polymer Composite Applications:**

<b>Yarn and Films.....</b>	<b>85</b>
5.1. SPC Yarns .....	85
5.1.1. Morphology.....	86
5.1.2. Fine structure .....	87
5.1.3. Mechanical testing .....	95
5.2. SPC Films .....	99

*References*

**Chapter 6. Conclusions and Recommendations for Further Study ..... 108**

6.1 Conclusions specific to set objectives.....	108
6.2 Recommendations for further study.....	111

*References*

**Appendix A. Single-Capillary Electrospinning..... 113**

A.1. Experimental .....	113
A.1.1. Solution preparation and electrospinning .....	113
A.1.2. Determination of solution viscosity .....	113
A.2. Results and Discussion.....	114
A.2.1. Solution parameter effects on fibre diameter, uniformity and process stability .....	114
A.2.1.1. Electrospinning PLLA and PDLLA solutions .....	115
i) Effects of Concentration .....	115
ii) Effects of Solvent Ratio.....	118
A.2.2. Determination of solution viscosity (Berry number ( <i>Be</i> )).....	123

A.3. Conclusions ..... 125  
A.4. Supporting information ..... 127

*References*

**Appendix B. Direct Methods for Analysis of Core-Shell Fibre Structure..... 141**

B.1. Experimental ..... 141  
    B.1.1. Outline..... 141  
    B.1.2. Materials ..... 142  
    B.1.3. Light and Optical Microscopy ..... 142  
    B.1.4. Cryo-SEM ..... 142  
    B.1.5. TEM ..... 143  
        B.1.5.1. Standard conditions..... 143  
        B.1.5.2. Cryo condition ..... 144  
        B.1.5.3. Cross-sections ..... 144  
B.2. Results and Discussions ..... 145  
    B.2.1. Light microscopy ..... 145  
    B.2.2. SEM ..... 145  
    B.2.3. TEM ..... 147  
B.3. Conclusions ..... 154  
B.4. Supporting Information..... 155

*References*

**Appendix C. Additional Results Relevant to Chapter 4 and Chapter 5 ..... 157**

*References*

**Appendix D. Materials Synthesis and PLA Molecular Mass Determination ..... 180**

D.1 Fluorescent labelling of PLLA ..... 181  
D.2 Synthesis of Zinc Sulphide (ZnS) particles capped with polyvinylpyrrolidone (PVP)..... 181  
D.3 Determination of molecular mass of PLLA and PDLLA with size exclusion chromatography (SEC)/gas permeation chromatography (GPC) ..... 182

## Chapter 2

<b>Figure 2.1</b>	<i>Structure levels leading up to a fibre and ultimately fibre-based assemblies .....</i>	<i>6</i>
<b>Figure 2.2</b>	<i>Outmoded fringed micelle model .....</i>	<i>7</i>
<b>Figure 2.3</b>	<i>Fibre reinforcement forms in fibre reinforced composites .....</i>	<i>10</i>
<b>Figure 2.4</b>	<i>Bi-constituent fibre .....</i>	<i>11</i>
<b>Figure 2.5</b>	<i>Bicomponent structure of a wool fibre: a) by illustration (image obtained from <a href="http://www.rei.com">www.rei.com</a>: last accessed 18/09/2009) and b) by preferential dye-accessible (DA) staining of the ortho-cortex while the para-cortex is non-DA and resists staining .....</i>	<i>11</i>
<b>Figure 2.6</b>	<i>Bicomponent fiber cross-section configurations a) side-by-side even, b-c) side-by-side uneven, d) concentric core-shell e) eccentric core-shell</i>	<i>12</i>
<b>Figure 2.7</b>	<i>Islands in the sea morphology; a) cross-sectional and b) longitudinal View.....</i>	<i>12</i>
<b>Figure 2.8</b>	<i>Extrusion methods used to prepare a) side-by-side, b) core-shell and c) multi-segmented bicomponent fibre configurations.....</i>	<i>13</i>
<b>Figure 2.9</b>	<i>Isomers of lactic acid and lactide: L-lactic acid, D-lactic acid, L-lactide, D,L-lactide (meso), D-lactide and PLLA and PDLA polylactic acid polymers .....</i>	<i>17</i>
<b>Figure 2.10</b>	<i>Successive bending instabilities of the electrified jet (picture adapted from).....</i>	<i>24</i>
<b>Figure 2.11</b>	<i>Schematic of coaxial electrospinning showing a compound Taylor cone and whipping jet .....</i>	<i>25</i>
<b>Figure 2.12</b>	<i>Core-shell Taylor cone formation (A: Surface charges on the shell solution, B: Viscous drag exerted on the core by the deformed shell droplet, C: Core-shell compound Taylor cone formed due to continuous viscous drag). .....</i>	<i>26</i>
<b>Figure 2.13</b>	<i>The effect of increasing applied voltage on the core-shell droplet.....</i>	<i>30</i>
<b>Figure 2.14</b>	<i>Schematic of “L” shape coaxial electrospinning set-up.....</i>	<i>32</i>

## Chapter 3

<b>Figure 3.1</b>	<i>Single capillary electrospinning set-up</i> .....	47
<b>Figure 3.2</b>	<i>Fibre diameter measurements on SEM image using SEM Image Studio software</i> .....	48
<b>Figure 3.3</b>	<i>Coaxial electrospinning set-up and wire drum collector</i> .....	49
<b>Figure 3.4</b>	<i>Capillary-in-capillary spinneret with compound Taylor cone and linear jetting region</i> .....	50
<b>Figure 3.5</b>	<i>Hydraulic system and coaxial spinneret</i> .....	51
<b>Figure 3.6</b>	<i>Core-shell fibre yarn preparation by a) coaxial electrospinning on wire drum collector, b) rolling edges of the mat and cutting through the width of the mat, c) removing the mat from the collector, d,e) twisting the mat into a yarn, and f) maintaining the twist in the yarns by use of clamps</i> .....	53
<b>Figure 3.7</b>	<i>Digital image showing the stable compound Taylor cone with two menisci, the core-shell jetting region and the onset of the first bending instability</i> .....	55
<b>Figure 3.8</b>	<i>Yarn holder with yarn in poly top filled with ethyl acetate</i> .....	58
<b>Figure 3.9</b>	<i>Rocking action administered to poly tops</i> .....	59
<b>Figure 3.10</b>	<i>Custom yarn holder with yarn parallel to radiation in the BRUKER AXS D8 Advance diffractometer</i> .....	65
<b>Figure 3.11</b>	<i>Template with yarn mounted with tape for mechanical testing</i> .....	67

---

## Chapter 4

<b>Figure 4.1</b>	<i>Fluorescent image of electrospun PLLA-rhodamine B fibres under 100X magnification (0.02mm scale bar)</i> .....	70
<b>Figure 4.2</b>	<i>a) and b) Fluorescence microscopy image of coaxial electrospun PLLA-PDLLA core-shell fibres under 100X magnification indicating no observable fluorescence (0.02mm scale bar)</i> .....	71
<b>Figure 4.3</b>	<i>Fluorescence microscopy image (0.02mm scale bar) of excited PLLA(Rhodamine B)-PDLLA core-shell and twin fibres</i> .....	72



<b>Figure 4.4</b>	<i>Coaxial electrospun yarns and fibres a,c) before and b,d) after washing in ethyl acetate. The average fibre diameters are shown in boxes .....</i>	74
<b>Figure 4.5</b>	<i>DSC thermogram of coaxial electrospun fibre yarn, and separated core and shell components after washing in ethyl acetate .....</i>	75
<b>Figure 4.6</b>	<i>Solution concentration effects on resultant core and total fibre diameters.....</i>	77
<b>Figure 4.7</b>	<i>Core-shell fibre diameters as a function of core polymer concentrations a-b) 4wt%, c-d) 6wt%, e-f) 8wt% before and after washing in ethyl acetate. The core and shell solution flow rates during electrospinning were 0.3 and 1.2 ml/h respectively. The shell solution concentration was 10wt% .....</i>	79
<b>Figure 4.8</b>	<i>Solution concentration effects on the percentage crystallinity of coaxial electrospun fibre yarns at 10wt% and 12wt% shell solution concentrations.....</i>	80
<b>Figure 4.9</b>	<i>Solution flow rate effects on resultant core and total fibre diameters ....</i>	81
<b>Figure 4.10</b>	<i>SEM images showing core-shell fibres spun with PLLA core solution flow rates a-b) 0.1ml/h, c-d) 0.2ml/h, e-f) 0.3ml/h and a shell solution flow rate of 1.2 ml/h before and after washing in ethyl acetate. The core and shell solution concentrations used were 8wt% PLLA and 10wt% PDLA respectively. ....</i>	83
<b>Figure 4.11</b>	<i>Solution flow rate effects on the melt endotherm of coaxial electrospun fibre yarns at 1.2 ml/h and 1.4ml/h shell solution flow rate .....</i>	85

---

## Chapter 5

<b>Figure 5.1</b>	<i>Coaxial electrospun fibre yarns before (left) and after (right) heat treatments.....</i>	86
<b>Figure 5.2</b>	<i>Cryo-fracture point of a heat-set core-shell fibre yarn showing the difference in fusion between the yarn surface and core .....</i>	87
<b>Figure 5.3</b>	<i>X-ray diffractogram: yarns prepared from as-spun PLLA-core/PDLA-shell fibres .....</i>	89
<b>Figure 5.4</b>	<i>X-ray diffractogram: heat-set (HS) yarns prepared from PLLA-core/PDLA-shell fibres .....</i>	90

List of Figures

---

<b>Figure 5.5</b>	<i>XRD diffractograms comparing as-spun PLLA, PDLLA and PLLA-core/PDLLA-shell yarns with a heat-set PLLA-core/PDLLA-shell yarn</i>	91
<b>Figure 5.6</b>	<i>DSC thermogram comparing thermal transitions for as-spun versus heat-set yarns</i>	93
<b>Figure 5.7</b>	<i>DSC thermogram: Double melting behaviour of PLLA-core/PDLLA-shell fibre yarn</i>	93
<b>Figure 5.8</b>	<i>MDSC thermogram: reversing/ non-reversing thermal transitions of fibres prepared by coaxial electrospinning PLLA-PDLLA core-shell solutions</i>	94
<b>Figure 5.9</b>	<i>Stress vs. Strain of as-spun fibre yarns</i>	96
<b>Figure 5.10</b>	<i>Stress vs. Strain of heat-set yarns</i>	96
<b>Figure 5.11</b>	<i>Comparison of stress vs. strain curves of as-spun and heat-set yarns for sample no.7</i>	96
<b>Figure 5.12</b>	<i>As-spun fibre yarn sample after mechanical testing</i>	97
<b>Figure 5.13</b>	<i>Heat-set fibre yarn after mechanical testing</i>	97
<b>Figure 5.14</b>	<i>Average maximum yield stress (MPa) of as-spun versus heat-set yarns</i>	98
<b>Figure 5.15</b>	<i>Average maximum extension (%) of as-spun versus heat-set yarns</i>	98
<b>Figure 5.16</b>	<i>Coaxial electrospun PDLLA-PLLA mat before heat pressing (left) and the SPC film in front of a piece of paper with the word 'FILM' written on it to show the transparency of the film</i>	99
<b>Figure 5.17</b>	<i>DSC thermogram showing 1<sup>st</sup> heating cycle of heat-pressed film</i>	100
<b>Figure 5.18</b>	<i>XRD diffractogram comparing electrospun PDLLA, PLLA, PLLA-PDLLA core-shell and heat-set PLLA-PDLLA core-shell fibre yarns with that of the SPC film</i>	100
<b>Figure 5.19</b>	<i>DSC thermograms of PDLLA and PLLA raw polymer, a yarn prepared from PLLA-core/PDLLA-shell fibres, a heat-set yarn of the same, and the SPC film</i>	101
<b>Figure 5.20</b>	<i>SEM and light microscopy images of a film having one hemisphere soaked in ethyl acetate</i>	102
<b>Figure 5.21</b>	<i>Fibre diameter distributions of fibre mat before heat pressing and the exposed remaining fibres after selective dissolution of PDLLA from the film with ethyl acetate (average fibre diameters are shown in boxes)</i>	

---

.....	103
<b>Figure 5.22</b> <i>DSC thermogram of the fibres exposed at the film edge that was exposed to selective dissolution by ethyl acetate compared with the polymer film that was extracted from the ethyl acetate .....</i>	104
<b>Figure 5.23</b> <i>Cryo fractured film.....</i>	105
<b>Figure 5.24</b> <i>Cryo fractured film.....</i>	105

---

## Appendix A

<b>Figure A.1</b> <i>Fibre diameter distributions: Electrospun PLLA solutions of increasing concentration in 70/30 DCM/DMF .....</i>	117
<b>Figure A.2</b> <i>Fibre diameter distributions: increasing polymer wt% concentration of PDLLA solutions spun from 70/30 DCM/DMF .....</i>	117
<b>Figure A.3</b> <i>SEM images illustrating a change in fibre morphology on varying solvent ratio of an 8wt% PLLA solution with a) 80/20, b) 70/30, c) 60/40 DCM/DMF solvent ratio.....</i>	120
<b>Figure A.4</b> <i>Average fibre diameter (nm) vs. polymer wt% concentration of PLLA solutions spun from 80/20, 70/30, 60/40 DCM/DMF solvent ratios.....</i>	120
<b>Figure A.5</b> <i>SEM images illustrating a change in fibre morphology on changing the solvent ratio of an 8wt% PDLLA solution with a) 80/20, b) 70/30, c) 60/40 DCM/DMF solvent ratio.....</i>	121
<b>Figure A.6</b> <i>Average fibre diameter (nm) vs. polymer wt% concentration of PDLLA solutions spun from 80/20, 70/30, 60/40 DCM/DMF solvent ratios ....</i>	121
<b>Figure A.7</b> <i>Fibre diameter distributions: comparison of 8wt% concentration of PLLA solutions spun from DCM/DMF .....</i>	122
<b>Figure A.8</b> <i>Fibre diameter distributions: comparison of 10wt% concentration of PDLLA solutions spun from DCM/DMF .....</i>	122
<b>Figure A.9</b> <i>Viscosity readings for PLLA and PDLLA 70/30 DCM/DMF solutions with concentration intervals 4,6,8,10,12wt%.....</i>	124
<b>Figure A.10</b> <i>Effect of increasing solution concentration and viscosity of average fibre diameter.....</i>	124
<b>Figure A.11</b> <i>SEM images illustrating a change in fibre morphology and distribution with on increasing PLLA polymer solution concentration a) 4wt%, b)</i>	

---

	6wt%, c) 8wt%, d) 10wt%, e) 12wt% polymer solution with 80/20 DCM/DMF solvent ratio.....	127
<b>Figure A.12</b>	<i>Fibre diameter distributions: Electrospun PLLA solutions of increasing concentration in 80/20 DCM/DMF .....</i>	128
<b>Figure A.13</b>	<i>SEM images illustrating a change in fibre morphology with on increasing PLLA polymer solution concentration a) 4wt%, b) 6wt%, c) 8wt%, d) 10wt%, e) 12wt% polymer solution with 70/30 DCM/DMF solvent ratio .....</i>	129
<b>Figure A.14</b>	<i>SEM images illustrating a change in fibre morphology with on increasing PLLA polymer solution concentration a) 4wt%, b) 6wt%, c) 8wt%, d) 10wt% polymer solution with 60/40 DCM/DMF solvent ratio .....</i>	130
<b>Figure A.15</b>	<i>Fibre diameter distributions: increasing polymer wt% concentration of PLLA solutions spun from 60/40 DCM/DMF .....</i>	131
<b>Figure A.16</b>	<i>SEM images illustrating a change in fibre morphology with on increasing PDLA polymer solution concentration a) 4wt%, b) 6wt%, c) 8wt%, d) 10wt%, e) 12wt% polymer solution with 80/20 DCM/DMF solvent ratio .....</i>	132
<b>Figure A.17</b>	<i>Fibre diameter distributions: increasing polymer wt% concentration of PDLA solutions spun from 80/20 DCM/DMF .....</i>	133
<b>Figure A.18</b>	<i>SEM images illustrating a change in fibre morphology on increasing PDLA polymer solution concentration a) 4wt%, b) 6wt%, c) 8wt%, d) 10wt%, e) 12wt% polymer solution with 70/30 DCM/DMF solvent ratio.....</i>	134
<b>Figure A.19</b>	<i>SEM images illustrating a change in fibre morphology with on increasing PDLA polymer solution concentration a) 4wt%, b) 6wt%, c) 8wt%, d) 10wt% polymer solution with 60/40 DCM/DMF solvent ratio.....</i>	135
<b>Figure A.20</b>	<i>Fibre diameter distributions: increasing polymer wt% concentration of PDLA solutions spun from 60/40 DCM/DMF .....</i>	136

---

# Appendix B

<b>Figure B.1</b>	<i>Attempting to break ductile yarn sample under Cryo-SEM conditions</i>	143
<b>Figure B.2</b>	<i>Trapezium cut resin tablet with coaxial electrospun fibre yarn</i>	144
<b>Figure B.3</b>	<i>Light microscope image of coaxial electrospun fibres under 400X magnification</i>	145
<b>Figure B.4</b>	<i>SEM images of exposed fibre ends under a) low and b) high magnification</i>	146
<b>Figure B.5</b>	<i>Resin tablet edge exposed by ultramicrotomy showing fibres sticking out of the resin</i>	147
<b>Figure B.6</b>	<i>Bubble formation from interaction between electrons and coaxial electrospun PLA fibre</i>	148
<b>Figure B.7</b>	<i>Nucleation of pores within the coaxial electrospun PLA fibres observed under cryo conditions</i>	149
<b>Figure B.8</b>	<i>a) TEM image and b) expanded view of a coaxial electrospun PLA fibre stable under the electron beam showing contrast of a continuous core</i>	150
<b>Figure B.9</b>	<i>Wool fibre with preferential staining of ortho- and para-cortex (DA – dye accepted sites)</i>	150
<b>Figure B.10</b>	<i>Coaxial electrospun fibre that shows a lighter peripheral region and a darker interior which is too thick to allow transmission of electrons</i>	151
<b>Figure B.11</b>	<i>a), b), c), and d) Coaxial electrospun fibres with 0.1wt% (of dry fibre mass) dye in the core</i>	151
<b>Figure B.12</b>	<i>a) ZnS-PVP particles and b) Coaxial electrospun PLA fibres with 0.1wt% (of dry fibre mass) ZnS-PVP in the core</i>	152
<b>Figure B.13</b>	<i>Coaxial electrospun PLA fibres with 0.1wt% AgNO<sub>3</sub> particles (of dry fibre mass) in the core</i>	152
<b>Figure B.14</b>	<i>a) and b 1-3) coaxial electrospun fibre cross-section prepared by ultramicrotomy of yarns embedded in resin</i>	153
<b>Figure B.15</b>	<i>a) Dark field TEM image of coaxial electrospun PLA fibres and b) expanded view of the fibre showing a possible eccentric core-shell fibre</i>	154
<b>Figure B.16</b>	<i>Fibres exposed from microtomed resin tablet</i>	155

---

<b>Figure B.17</b>	<i>TEM images of ZnS-PVP loaded core-shell fibres cross-sections.....</i>	<i>155</i>
<b>Figure B.18</b>	<i>a) TEM image and b) expanded view of electrospun PLLA yarn cross-sections.....</i>	<i>156</i>

---

## Appendix C

<b>Figure C.1</b>	<i>PDLLA polymer film after evaporation of ethyl acetate.....</i>	<i>157</i>
<b>Figure C.2</b>	<i>a) and b) Coaxial electrospun PLLA(Rhodamine B)-PLLA fibres with 0.1 and 0.3ml/h core flow rate respectively.....</i>	<i>157</i>
<b>Figure C.3</b>	<i>Average fibre diameter distributions of coaxial electrospun fibres before and after washing in ethyl acetate.....</i>	<i>157</i>
<b>Figure C.4</b>	<i>DSC thermogram showing the melt endotherms of the cores.....</i>	<i>159</i>
<b>Figure C.5</b>	<i>DSC thermogram of the separated shell components compared with one PLLA core sample.....</i>	<i>159</i>
<b>Figure C.6</b>	<i>Effects of solution concentration on actual vs. theoretical core mass yield.....</i>	<i>160</i>
<b>Figure C.7</b>	<i>Beads-on-string morphology of fibres electrospun from 4wt% PLLA (70/30 v/v DCM/DMF) solutions.....</i>	<i>162</i>
<b>Figure C.8</b>	<i>Core-shell fibre diameters as a function of core polymer concentrations a-b) 4wt%, c-d) 6wt%, e-f) 8wt% before and after washing in ethyl acetate. The core and shell solution flow rates during electrospinning were 0.3 and 1.2 ml/h respectively. The shell solution concentration was 12wt%.....</i>	<i>163</i>
<b>Figure C.9</b>	<i>Fibre remaining after washing in ethyl acetate - fibre diameter distributions: Effect of increasing core solution concentration at 10wt% shell solution concentration.....</i>	<i>164</i>
<b>Figure C.10</b>	<i>Fibre remaining after washing in ethyl acetate - fibre diameter distributions: Effect of increasing core solution concentration at 12wt% shell solution concentration.....</i>	<i>164</i>
<b>Figure C.11</b>	<i>As-spun fibre diameter distributions: Effect of increasing core solution concentration at 10wt% shell solution concentration.....</i>	<i>165</i>
<b>Figure C.12</b>	<i>As-spun fibre diameter distributions: Effect of increasing core solution concentration at 12wt% shell solution concentration.....</i>	<i>165</i>



<b>Figure C.13</b>	<i>Shell solution concentration effects on core (shell removed) and core-shell (As-spun) fibre diameter - Parameter Effects*Upper Level; Least-square (LS) Means .....</i>	167
<b>Figure C.14</b>	<i>Solution concentration effects on core (shell removed) and core-shell (As-spun) fibre diameter - Parameter Effects*Upper Level*Lower Level; LS Means.....</i>	167
<b>Figure C.15</b>	<i>Solution concentration effects on the melt endotherm of coaxial electrospun fibre yarns at a 10wt% shell solution concentration.....</i>	168
<b>Figure C.16</b>	<i>Solution concentration effects on the melt endotherm of coaxial electrospun fibre yarns at a 12wt% shell solution concentration.....</i>	168
<b>Figure C.17</b>	<i>Solution concentration effects on core-shell fibre crystallinity – UpperLevel; Least-square (LS) Means.....</i>	179
<b>Figure C.18</b>	<i>Solution concentration effects on core-shell fibre crystallinity – Upper Level*Lower Level; LS means .....</i>	170
<b>Figure C.19</b>	<i>Effects of solution concentration flow rate on actual vs. theoretical core mass yield.....</i>	170
<b>Figure C.20</b>	<i>SEM images showing core-shell fibres spun with PLLA core solution flow rates a-b) 0.1ml/hr, c-d) 0.2ml/hr, e-f) 0.3ml/h and a shell solution flow rate of 1.4 ml/h before and after washing in ethyl acetate. The core and shell solution concentrations used were 8wt% PLLA and 10wt% PDLLA respectively .....</i>	171
<b>Figure C.21</b>	<i>Fibre remaining after washing in ethyl acetate - fibre diameter distributions: Effect of increasing core solution flow rate at 1.2ml/h shell solution flow rate.....</i>	172
<b>Figure C.22</b>	<i>Fibre remaining after washing in ethyl acetate - fibre diameter<sup>3</sup> distributions: Effect of increasing core solution flow rate at 1.4ml/h shell solution flow rate.....</i>	172
<b>Figure C.23</b>	<i>As-spun fibre diameter distributions: Effect of increasing core solution flow rate at 1.2ml/h shell solution flow rate .....</i>	173
<b>Figure C.24</b>	<i>As-spun fibre diameter distributions: Effect of increasing core solution flow rate at 1.4ml/h shell solution flow rate.....</i>	173
<b>Figure C.25</b>	<i>Shell solution flow rate effects on core (shell removed) and core-shell (As-spun) fibre diameter - Parameter Effects*Upper Level; Least-square (LS) Means .....</i>	175

<b>Figure C.26</b>	<i>Solution flow rate effects on core (shell removed) and core-shell (As-spun) fibre diameter - Parameter Effects*Upper Level*Lower Level; LS Means.....</i>	175
<b>Figure C.27</b>	<i>Solution flow rate concentration effects on the melt endotherm of coaxial electrospun fibre yarns at a 1.2 ml/h shell solution flow rate.....</i>	176
<b>Figure C.28</b>	<i>Solution flow rate effects on the melt endotherm of coaxial electrospun fibre yarns at a 1.4 ml/h shell solution flow rate .....</i>	176
<b>Figure C.29</b>	<i>Solution flow rate effects on core-shell fibre crystallinity – UpperLevel; Least-square (LS) Means .....</i>	177
<b>Figure C.30</b>	<i>Solution solution effects on core-shell fibre crystallinty – Upper Level*Lower Level; LS means .....</i>	178
<b>Figure C.31</b>	<i>a) and b) Cryo fractured film prepared from coaxial electrospun PLLA-PDLLA fibres.....</i>	189
<b>Figure C.32</b>	<i>Cryo factured film prepared from single capillary electrospun PDLLA fibres .....</i>	189

---

**Appendix D** ..... 180

<b>Figure D.1</b>	<i>GPC curve for PLLA and PDLLA polymer in THF .....</i>	183
-------------------	--	-----





## Chapter 3

<b>Table 3.1</b>	<i>Calibration data of DC voltage vs. linear velocity</i> .....	52
<b>Table 3.2</b>	<i>Coaxial electrospinning parameters</i> .....	57
<b>Table 3.3</b>	<i>Coaxial electrospinning parameters</i> .....	62

---

## Chapter 5

<b>Table 5.1</b>	<i>Coaxial electrospinning parameters</i> .....	100
<b>Table 5.2</b>	<i>Parameters investigated: A) Effects of solution concentration and B) Effects of solution flow rate on resultant fibre diameters</i> .....	105
<b>Table 5.3</b>	<i>Optical rotation measurements for cores and films dissolved in Chloroform</i> .....	106

---

## Appendix A

<b>Table A.1</b>	<i>Effect of concentration and solvent ratio on average fibre diameters (nm) of electrospun PLLA and PDLLA solutions</i> .....	116
<b>Table A.2</b>	<i>Effect of concentration and solvent ratio on electrospinning conditions and resultant fibre morphology</i> .....	116
<b>Table A.3</b>	<i>DCM and DMF solvent properties</i> .....	118

---

## Appendix C

<b>Table C.1</b>	<i>Specific optical rotation measurements for cores and films dissolved in chloroform</i> .....	158
<b>Table C.2</b>	<i>Specific optical rotation measurements for cores and films dissolved in chloroform</i> .....	158
<b>Table C.3</b>	<i>Parameter effects on as-spun yarn mass before and after washing in ethyl acetate</i> .....	161
<b>Table C.4</b>	<i>Parameters investigated: A) effects of solution concentration and B) effects of solution flow rate on resultant fibre diameters</i> .....	162

<b>Table C.5</b>	<i>Bonferroni Tests for significance from ANOVA of solution concentration effects on core and core-shell fibre diameters.....</i>	<i>166</i>
<b>Table C.6</b>	<i>Bonferroni Tests for significance from ANOVA of increasing core solution concentration effects on core-shell fibre crystallinity: 10wt% shell solution concentration.....</i>	<i>169</i>
<b>Table C.7</b>	<i>Bonferroni Tests for significance from ANOVA of increasing core solution concentration effects on core-shell fibre crystallinity: 12wt% shell solution concentration.....</i>	<i>169</i>
<b>Table C.8</b>	<i>Bonferroni Tests for significance from ANOVA of solution flow rate concentration effects on core-shell (as-spun) fibre diameters.....</i>	<i>174</i>
<b>Table C.9</b>	<i>Bonferroni Tests for significance from ANOVA of solution flow rate concentration effects on core (shell removed) fibre diameters.....</i>	<i>174</i>
<b>Table C.10</b>	<i>Bonferroni Tests for significance from ANOVA of increasing core solution flow rate effects on core-shell fibre crystallinity: 1.2ml/h and 1.4ml/h shell solution flow rate .....</i>	<i>177</i>
<b>Table C.11</b>	<i>Young's modulus (E) for as-spun and heat-set yarns .....</i>	<i>178</i>

---

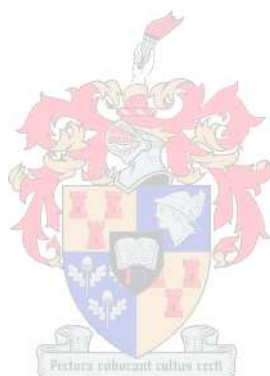
## Appendix D

<b>Table D.1</b>	<i>Molecular weight distributions .....</i>	<i>182</i>
------------------	---	------------



<b><math>A_0</math></b>	- original cross-sectional area of the yarn (m <sup>2</sup> )
<b><math>[\alpha]_{\lambda}^0</math></b>	- Specific optical Rotation for core
<b><math>Be</math></b>	- Berry number
<b><math>D</math></b>	- nanofibre cross-sectional diameter
<b><math>D_a</math></b>	- diffusion coefficient of the dopant
<b><math>D_p</math></b>	- polymer diffusion coefficient
<b><math>DCM</math></b>	- dichloromethane
<b><math>DMF</math></b>	- dimethyl formamide
<b><math>DSC</math></b>	- differential scanning calorimetry
<b><math>E</math></b>	- Young's modulus measured in Pascals (or N/m <sup>2</sup> )
<b><math>F</math></b>	- force applied to the object (N)
<b><math>FTIR</math></b>	- Fourier transform infrared spectroscopy
<b><math>GPC</math></b>	- gel permeation chromatography
<b><math>\Delta H</math></b>	- change in enthalpy
<b><math>H_{of}</math></b>	- theoretical heat of fusion value of 100% crystalline material
<b><math>H_f</math></b>	- area under the melt endotherm (J/g)
<b><math>\Delta L</math></b>	- displacement at maximum load (m)
<b><math>L_0</math></b>	- original length of the yarn test specimen (m)
<b><math>M_n</math></b>	- number average molecular weight
<b><math>M_w</math></b>	- weight average molecular weight
<b><math>PDI</math></b>	- polydispersity index
<b><math>PDLLA</math></b>	- poly(D,L-lactic acid)
<b><math>PLA</math></b>	- poly(lactic acid)
<b><math>PLLA</math></b>	- poly(L-lactic acid)
<b><math>PLLA-PDLLA</math></b>	- poly(L-lactic acid)-poly(D,L-lactic acid) core-shell configuration
<b><math>MDSC</math></b>	- modulated differential scanning calorimetry
<b><math>rH</math></b>	- relative humidity
<b><math>RT</math></b>	- room temperature
<b><math>SEM</math></b>	- scanning electron microscopy
<b><math>SPC</math></b>	- single polymer composite
<b><math>\Delta S</math></b>	- change in entropy
<b><math>TEM</math></b>	- transmission electron microscopy
<b><math>T_g</math></b>	- glass transition temperature

<b><math>T_m</math></b>	- crystalline melting temperature
<b>(v/v)</b>	- solvent volume:volume ratio
<b>XRD</b>	- x-ray diffraction
<b>WAXD</b>	- wide angle x-ray diffraction
<b><math>\chi\%</math></b>	- percentage crystallinity



# Chapter 1

## *Introduction and Objectives*

### 1.1 Introduction

Composite materials are ubiquitous in daily life. Almost every daily activity is teeming with composite materials, from those that allow us to ride waves (e.g. composites used in surfboards) to the most technical composites that aid human kind explore the universe (e.g. composite used in space craft). The use of these materials is advantageous as the combination of two or more complementary materials into a composite can yield specialised properties unattainable with the individual components alone. This is important when designing materials for particular end-uses that require specific properties.

The vast amount of these materials used raises concerns for the environment in terms of recycling after the useful life time of the product. There are also concerns over the use of non-renewable fossil fuels to prepare materials for these composites. The concept of a composite material requires that two or more materials are incorporated into its structure. Recycling and biodegradability of these heterogeneous composites are difficult as it is not often that the methods of reduction are the same for all the components of the composite. Delamination and moisture absorption at the interface between components of the composite, as a result of the compatibility issues between the different material properties, may be problematic.

Single polymer composites have a matrix and reinforcing component of the same material that can be recycled or degraded in one process. Therefore, questions of recycling and compatibility issues at the interface between the matrix and the reinforcing component are answered. Single polymer composite (SPC) structures made from a completely biodegradable and biocompatible polymer such as poly(lactic acid) (PLA) are ideal candidates for implantable medical devices as well as commodity materials. PLA polymer has gained popularity as it is a commercial polymer produced from renewable feedstock, has commercially significant material properties, is non-toxic, and can be hydrolysed (ester bond hydrolysis) and assimilated

by natural metabolic pathways. Variation of the relative ratio of D/L isomers along the polymer backbone can produce either semi-crystalline or amorphous PLA.<sup>1,2</sup>

Nano- to micro-diameter fibres are highly favourable for use in fibre reinforced composites. This is a function of their higher aspect, surface area-to-volume and strength-to-weight ratios compared with larger diameter fibres. These qualities provide composite materials with improved optical properties, improved barrier properties, and higher strength as a result of higher loading of finer reinforcing material and more intimate contact between the matrix and fibres at their interface.<sup>3</sup>

Biodegradable PLA fibres can be used in fibre-reinforced composites. These are ideal candidates for implantable medical devices such as tissue scaffolds, drug delivery media and sutures. This is because specific material performance can be tailored and can be balanced with biocompatibility as well as biodegradability. Composite core-shell nano-to micro- diameter fibres can be prepared by coaxial electrospinning. This is a fibre spinning technique that uses an electrostatic force to draw two polymer fluids through a concentric capillary-in-capillary spinneret into composite core-shell micro-nanofibres.

In this work SPC core-shell microfibres are prepared by coaxial electrospinning from poly(lactic acid) (PLA) solutions. The core-shell microfibres have a poly(L-lactic acid) (PLLA) semi-crystalline core and poly(D,L-lactic acid) PDLA amorphous shell. The novelty of this combination lies in the difference in properties of the core and shell materials. The shell is softened in a thermal operating window between the glass transition temperature of the PDLA shell and crystalline melting temperature of the PLLA core. Any temperature in this operating window will be high enough to fuse overlapping fibres at the shell surfaces (to form adhesive bonds on cooling) but also be low enough so as not to melt the reinforcing core fibre component.

Transmission electron microscopy (TEM) is the classic method used to study the structure of core-shell micro-nano diameter fibres. PLA polymer is sensitive to radiation<sup>4</sup> and because the polymers have the same chemistry it was foreseen that TEM analysis would be challenging as the PLA fibres would possibly not be stable nor show sufficient contrast respectively under the electron beam. A method, based on

the selective dissolution of the PDLLA shell from the composite fibre, was developed to validate that the PLLA-PDLLA core-shell fibre structure existed and that the coaxial electrospinning technique used to produce them was successful. Fluorescent microscopy was also used to study the core-shell fibre structure by coaxial electrospinning with a fluorescently labelled core polymer. The selective dissolution method was additionally used to study electrospinning solution and process parameters effects on resultant core-shell fibre diameters.

Electrospinning of polymers, specifically slow crystallising polymers such as PLLA, produces fibres with a high degree of molecular order but no extensive crystal structures. Thermal treatments of core-shell fibre yarns, in the thermal operating window between the glass transition temperature of the shell polymer and the crystalline melting temperature of the core polymer, were used to influence the crystallinity of the core material and thereby also the mechanical properties of the yarns.

A transparent SPC film was prepared in a similar fashion and analysed to validate the proof of concept in a composite application.

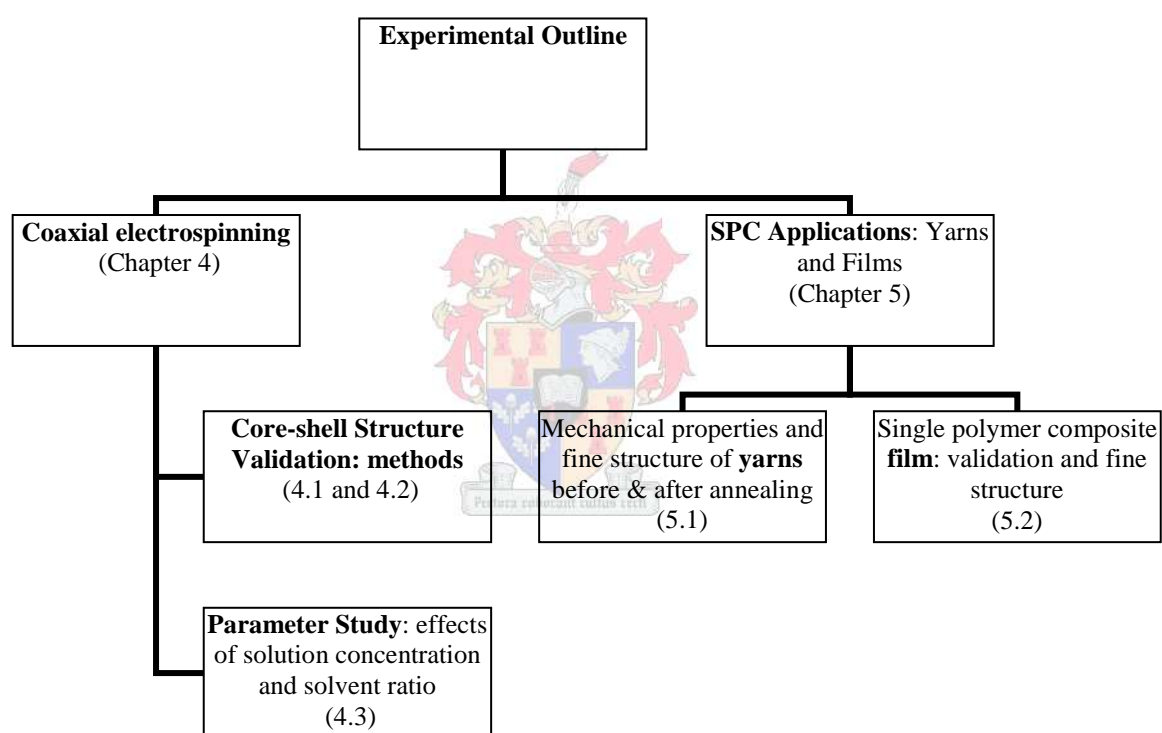
## 1.2 Goals and Objectives

The following goals and objectives were set out at the start of the study:

- A.** *Development of a coaxial electrospinning process that could produce core-shell fibres from miscible solutions of amorphous PDLLA and semi-crystalline PLLA*
- B.** *Development of a method to analyse the core-shell fibre structure and study the effects of solution and other electrospinning process parameters on fibre morphology*
- C.** *Evaluation of internal molecular arrangement within the fibres and the potential to enhance the crystallinity of the core and heat-bond neighbouring fibres within the thermal operating window*

### 1.3 Outline of Document

The document continues with a review of the literature (Chapter 2 Literature Review) followed by an experimental section (Chapter 3 Experimental) describing research methodology and materials used. The experimental outcomes are presented and discussed in Chapter 4 (Results and Discussion - Coaxial Electrospinning) and Chapter 5 (Results and Discussion – SPC Applications: Yarns and Films). An organogram outlining the experiments conducted in this study is shown below. Finally the findings are summarised and recommendations for future work is given in Chapter 6 (Conclusions and Recommendations for Further Study). All relevant supporting information can be found in the Appendices.



#### References

1. Gupta BS, Revagade N, Hilborn J. Poly(lactic acid) fiber: An overview. *Progress in Polymer Science*. 2007;32:433-82.
2. Garlotta D. A Literature review of poly(lactic acid). *Journal of Polymers and the Environment*. 2002;9(2):63-84.
3. Huang Z-M, Zhang Y-Z, Kotaki M, Ramakrishna S. A review on polymer nanofibers by electrospinning and their applications in nanocomposites. *Composite Science and Technology*. 2003 08/04/2003;63:2223-53.
4. Derch R, Liu T, Schaper AK, Greiner A, Wendorff JH. Electrospun nanofibers: internal structure and intrinsic orientation. *Journal of Polymer Science*. 2003;41:545-53.



# Chapter 2

## *Literature Review*

*This chapter starts with a discussion on fibre technology as background to understanding the unique properties of fibres that result from their high length-to-thickness geometry and complex ordering of macromolecular chains. Composite fibres and fibre-reinforced composites are discussed with a focus on biodegradable single polymer composites where the novelty of core-shell polylactic acid fibres is explained. Synthetic polylactic acid technology is presented to understand the intrinsic material properties and how these create unique properties for fibre applications. Finally, coaxial electrospinning and the parameters affecting the resultant fibre morphology are discussed in detail.*

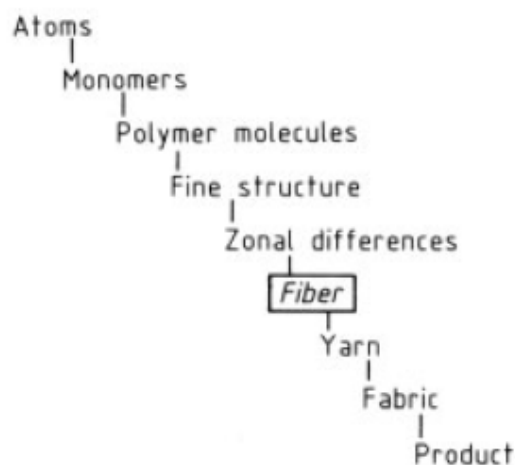
### 2.1 Fibre technology

#### 2.1.1 Background

Fibres, by definition of the Textile Institute are units of matter characterized by flexibility, fineness, and high ratio of length to thickness.<sup>1</sup>

Fibres are intermediate components and can be manipulated at different levels (Figure 2.1). Fibre properties are dependent on physical and chemical factors but more generally are a function of the geometry and fine structure.<sup>2</sup> Fibre geometry is of significant importance as large structural defects found in bulk materials cannot be present in the smaller diameters of fibres. Hence, brittle bulk materials that are above their glass transition temperature ( $T_g$ ) at room temperature (RT), such as glass, can be spun into flexible fibres.<sup>2</sup>

The high length-to-thickness offers high surface area-to-volume and high axial strength-to-weight ratios. These properties are responsible for the ubiquitous use of fibres and textiles across all industries and in nature.



**Figure 2.1** *Structure levels leading up to a fibre and ultimately fibre-based assemblies*<sup>2</sup>

### 2.1.2 Fine structure

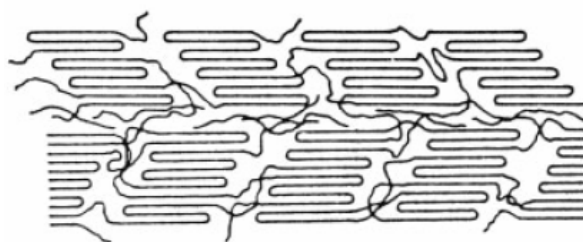
A fibre's fine structure is a description of the internal structure of the fibre. It is composed of different structural regions that are formed by the arrangement of the polymers and the intermolecular forces that exist between them.<sup>2</sup>

Fibres were used for centuries before the polymer/macromolecular hypothesis was introduced by Herman Staudinger (1920). The polymer hypothesis and the development of the electron microscope contributed to the understanding of the fibre structure.<sup>3</sup>

Fibres can be broadly classed as man-made or natural fibres. Man-made fibres are formed by spinning that involves; pushing a polymer melt or solution through small holes/dies in a spinneret, the solidification of liquid polymer into fibres and drawing of the fibres to increase molecular alignment. Spinning leads to the preliminary orientation of polymer molecules along the fibre axis. The molecular orientation, as well as partial crystallisation, can later be enhanced by drawing of the extruded fibres directly or as a post-spinning procedure (with or without heat). During spinning individual segments within the fibre crystallise independently of each other and result in free volume and amorphous intercrystalline regions.

The internal structure of a fibre has been a topic of much debate over the years. In general all hypotheses have some form of agreement that the internal structure of a fibre is a two-phase mixture of a crystalline component and an amorphous component separated by a poorly defined interface.<sup>1,2,4</sup> The internal structure is defined by the complex manner in which polymer chains fold and pack together. The molecules within fibres are highly anisotropic yet possess molecular order intermediate between perfectly crystalline and amorphous materials.

There are many models pictorially describing this partially crystalline yet partially amorphous structure. A common model used is the modified fringed micelle model (Figure 2.2) which describes a distribution of crystalline micelles embedded in an amorphous matrix. Each model may support experimental data, for a particular fibre, to varying degrees. In reality the internal fibre structure is a more complicated distribution of order, consisting of intermediate degrees of order of paracrystals in a matrix of simultaneous disorder, which could be described by several models.<sup>2</sup>



**Figure 2.2** *Outmoded fringed micelle model*<sup>2</sup>

Crystalline regions are closely packed fibrils and lamellae comprised of folded polymer chains from different polymer molecules. Usually the more crystalline the fibre is the greater its resistance to elongation and to break, resulting in higher elastic modulus and tensile strength respectively. Other properties derived from a greater degree of orientation and crystallinity includes lower moisture absorbance, lower dyeability, greater chemical resistance and more stability to effects of temperature and moisture.<sup>5</sup>

These crystalline regions are denser and pack more efficiently, which results in less free volume between polymer molecules than in the disordered amorphous regions. The crystalline regions within fibres are very small compared to bulk material, they

are imperfect and stressed by chain entanglements. Larger crystal structures such as spherulites are usually not present within fibres, as there is insufficient space.

Fibre strength and flexibility are a function of the orientation and packing of polymer chains within the fibres and can be described by six parameters: degree of order, degree of localization of order, aspect (length-to-width) ratio of crystalline units, degree of orientation, size of crystalline units and molecular extent.<sup>2</sup>

Varying degrees of order are influenced not only by processing conditions and thermal history of the fibre but also by factors such as by degree of polymerisation and back bone flexibility or rigidity as a function of polymer chemistry and side groups.

### 2.1.3 Fine fibres

Commercial spinning techniques used to produce man-made polymer fibre filaments include melt, dry, wet and gel spinning. Other spinning techniques of lower significance include reactive, dispersion and flash spinning.<sup>5-8</sup>

Fibres with finer diameters are significant as they possess superior properties (e.g. reduced flaws and higher strength per weight) that result from an even higher aspect ratio of fibre geometry. These superior properties stretch the application base for traditional fibres and textiles to meet higher end-uses. The fibre fineness refers to the linear density (mass per length) of fibre or yarn. Commercially available fibres (staple/short and filament/continuous) have diameters ranging 2-100 $\mu$ m.

Fibres with diameters smaller than 1 $\mu$ m are entering into the scale that is marketed as nano-fibres or ultra-fine fibres, although strictly nanofibres are those fibres that have diameters <100nm. It is only when fibres have diameters <100nm that quantum effects occur.<sup>9-11</sup>

The theoretical possibility of a fully stretched polymer is almost realised with fibres of diameters <100nm. This would result in perfectly oriented bundles of extended-chain crystals and therefore for the same linear density a stronger yarn can be made with significantly fewer flaws.<sup>12</sup>

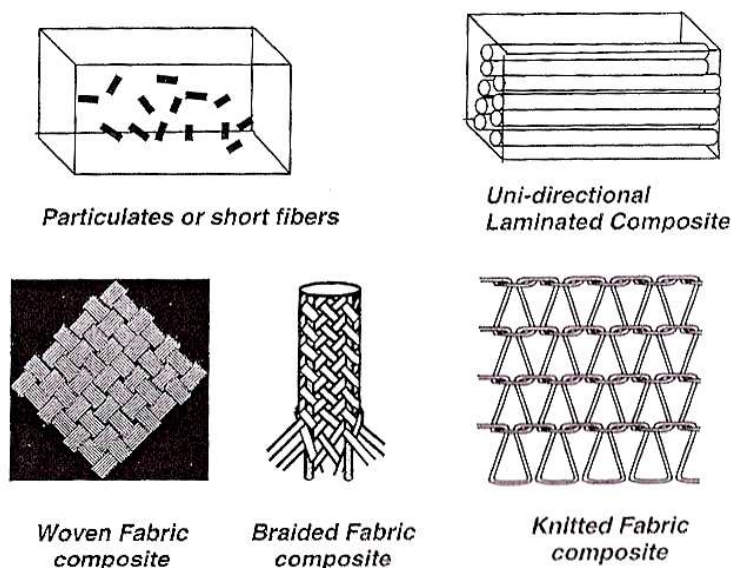
Nanofibres are characterised by flexibility, superior directional strength-to-weight ratio, high surface area-to-volume ratio, and a high aspect ratio of  $\geq 1000:1$ . A proportionally larger number of atoms exist on the nanofibre surfaces compared with larger fibres with diameters  $>2000\text{nm}$ .<sup>13</sup> Commercial spinning technologies used to create very fine fibres with diameters in the lower ( $2\text{-}5\mu\text{m}$ ) micro-metre scale includes melt blown and multicomponent technologies (i.e. islands in the sea).<sup>7,4</sup>

## 2.2 Composites and composite/bicomponent fibres

### 2.2.1 Fibre reinforced composites

Fibre reinforced composites have a long history in engineered functional materials. Strong stiff materials can be created by combining a ‘glue’ with a reinforcing fibre component to deliver superior performance unattainable by either material alone. The said glue is the matrix material that impregnates a reinforcing fibre assembly. The matrix acts to transfer loads to the stronger fibres (strength along fibre axis) and to hold the fibres together in some fixed form. The elements of a composite material are therefore the reinforcing fibres, the matrix and the interface around the matrix-fibre boundary. The organisation of these elements determines the properties of the composite and the material is strongest in the fibre direction.<sup>14</sup>

The level of interaction at the matrix-fibre interface determines many of the mechanical properties of the composite. The interaction determines the relationship and transfer of stresses across this two-phase boundary. The adhesion mechanism between matrix and fibre can be wetting, chemical bonding (covalent and/or secondary intermolecular forces) or mechanical interlocking (high surface areas of fibres, fibre surface roughness, resin shrinkage during solidification). The nature of the matrix and fibre surface chemistry is important for adhesion and the actual wetting of the fibres by the matrix. In pre-impregnated (prepreg) composites reinforcement is achieved by several means; short fibres, uniaxial fibres, woven, braided and knitted fabrics (Figure 2.3).<sup>14</sup>



**Figure 2.3** Fibre reinforcement forms in fibre reinforced composites

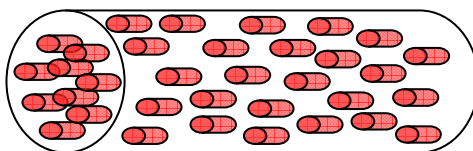
## 2.2.2 Composite/Bicomponent fibres

### 2.2.2.1 Introduction

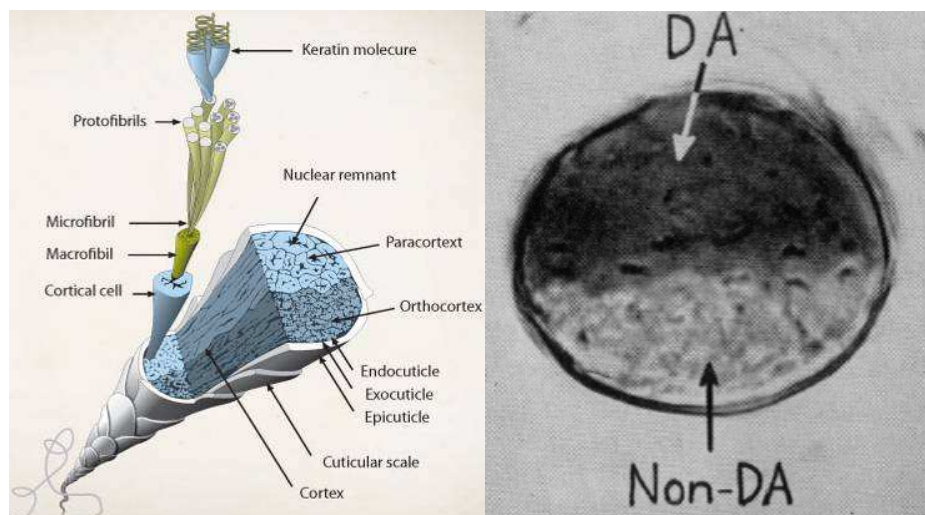
Composite or bicomponent fibers by definition consist of two components divided, along the length of the fibre, into two more or less distinct regions. These fibres are also referred to as “composite”, “conjugate” and “hetero” fibres. These fibres must be differentiated from **bi-constituent** fibres (Figure 2.4), whereby one component consists of small discrete units i.e. carbon nano-tubes or clay particles embedded in a continuous matrix of another component, and **blends** which have a mixture of two components that most likely have phase separated morphology.<sup>15-17</sup>

Wool is a natural bicomponent fibre and its inherent crimping properties can be explained by its bicomponent structure. It is a multicellular protein fibre and has a cortex that consists of two halves, the ortho- and para-cortex (Figure 2.5), which adhere strongly and rotate in a helical arrangement along the length of the fibre. These two components differ in their degree of crystallinity. Differential shrinkage occurs when the fibre is dry (approximately straight when wet). The fibre is therefore crimped in a helical structure and has a high degree of bulk.<sup>5,17</sup>



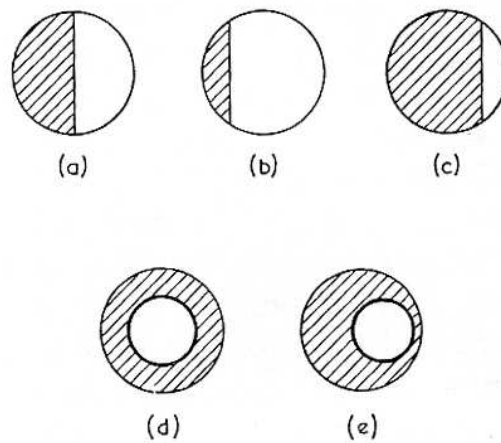


**Figure 2.4** *Bi-constituent fibre*

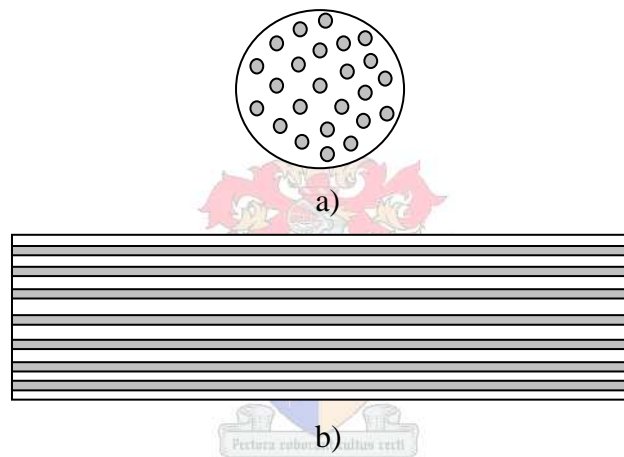


**Figure 2.5** *Bicomponent structure of a wool fibre: a) by illustration (image obtained from [www.rei.com](http://www.rei.com): last accessed 18/09/2009) and b) by preferential dye-accessible (DA) staining of the ortho-cortex while the para-cortex is non-DA and resists staining<sup>18</sup>*

Synthetic bicomponent fibres can be designed when properties for specific end-uses cannot be obtained from homogenous fibres. The properties of these fibres depend on the polymer selected, relative amounts of these polymers and their configuration within the fibres. These polymers are generally physically or chemically different. Commercial examples of these are fibres with side-by-side, matrix-fibril (islands in the sea and segmented pie), and eccentric and concentric core-shell configuration (Figure 2.6 & 2.7).



**Figure 2.6** *Bicomponent fiber cross-section configurations a) side-by-side even, b) side-by-side uneven, d) concentric core-shell e) eccentric core-shell*  
17



**Figure 2.7** *Islands in the sea morphology; a) cross-sectional and b) longitudinal view*

#### 2.2.2.2 Core-shell fibres

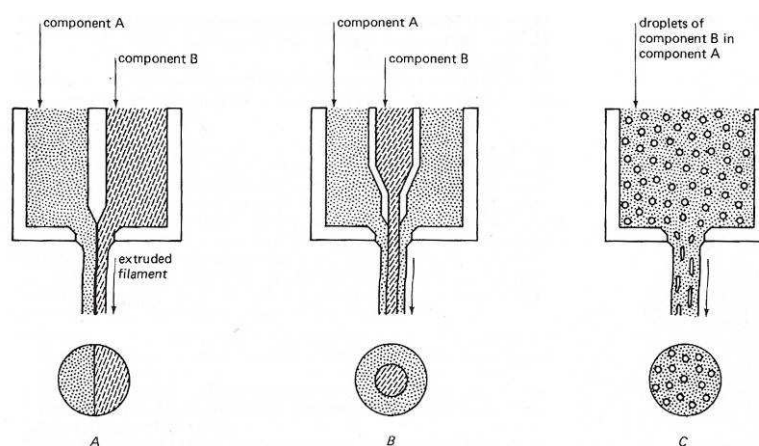
A core-shell fibre (also known as core-sheath, core-clad or coaxial fibre) can be described as a fibre possessing, along the entirety of its length, one or multiple continuous core components concentrically encapsulated by a sheath or clad component.<sup>15-17</sup> These fibres have long been used in the commercial textile industry for various applications.<sup>17</sup>



Core-shell fibres and yarns fulfil a number of applications, both novel and commercially exploited, including but not limited to the following:

- Binder/bonding/“prepreg” fibres for fibre reinforced matrices and thermally bonded non-wovens<sup>16,19-21</sup>
- Crimping fibres for increasing material bulk and therefore insulation properties in the fashion and non-woven industry<sup>20</sup>
- Conducting component i.e. either core or shell forms conductive material, for antistatic products<sup>22</sup>
- Optical fibres<sup>23</sup>
- Structural reinforcement: fibre-reinforced plastic bars for concrete reinforcement (re-bars)<sup>24</sup>
- Controlled drug release in medical stent applications<sup>25</sup>
- Aesthetic/functional fibres i.e. core-spun yarns that have cotton fibres wrapped around polyester core filaments to have a comfortable and aesthetically pleasing yarn that has a strong core

Bicomponent fibres are generally formed by extrusion; when two polymer melts/solutions (component A and component B), with different physical or chemical properties, are channelled separately to an orifice where they are extruded with the intention of having both components contained within the same filament (Figure 2.8).<sup>17,20,26</sup>



**Figure 2.8** Extrusion methods used to prepare a) side-by-side, b) core-shell and c) multi-segmented bicomponent fibre configurations<sup>27</sup>

### 2.2.3. Single Polymer Composites (SPC's)

#### 2.2.3.1 Background

Fibre reinforced composites are traditionally heterogeneous materials comprised of a matrix of one type of material and reinforcing fibre component of a different material. These materials are being used increasingly in commodity products and raise environmental concerns as they are often difficult to recycle as they are generally made from different materials.

Single polymer composites (SPC's), a concept introduced 31 years ago by Mead and Porter, offer a recyclable alternative as they are composed of compatible homogenous (of the same polymer) matrix and fibre reinforcement.<sup>28</sup> SPC's have the advantage of physical and chemical compatibility between fibre and matrix components promoting greater adhesion between the two enhancing matrix-fibre interfacial bonding.<sup>29,30</sup>

The governing concept behind SPC's is that the processing/fusing temperature of the reinforcing fibres is significantly higher (>20°C) than that of the matrix. This is achieved by preparing highly-oriented fibres of high molecular weight (slowly crystallisable) polymer by post-drawing procedures and constrained crystallisation below the melting temperature of that polymer.<sup>30</sup>

A workable processing window is dependent on the ability to control the melting point of either the matrix or the fibres. This can be understood from studying the Gibbs free energy equation:

$$T_m = \Delta H_f / \Delta S_f$$

$T_m$ ,  $\Delta H_f$  and  $\Delta S_f$  are the crystalline melting temperature, change in enthalpy of fusion and the change in entropy of fusion respectively. The change in enthalpy ( $\Delta H_f$ ) of a polymer is a function of the interaction between molecular chains (in crystalline regions - typically one conformational state) and entropy describes the many conformational possibilities for the chains (in liquid polymer). Upon heating, even highly oriented semi-crystalline fibres will tend to relax to a more preferential isotropic structure. It is possible to prevent this relaxation by constraining the polymer chains by fixing the ends of the fibre and heat treating it at the onset of the

crystallisation temperature for that polymer. The chains in the constrained fibres have no freedom to change conformation and cannot relax. The entropy is reduced and the crystalline melting temperature ( $T_m$ ) shifts to higher temperatures.<sup>30</sup>

By heat-pressing, the fibre surfaces become sticky (small portion of amorphous regions remain in the fibre) and under low contact pressure for a short time can fuse to create a consolidated material. This processing temperature should be much lower than the crystalline  $T_m$  so as not to anneal the fibre and negatively impact its mechanical performance.

Fusion occurs above the glass transition temperature ( $T_g$ ) where two processes occur:

- First is the glass transition or softening of the amorphous phase where diffusion occurs across the interface between the two sticky surfaces of the fibre and matrix
- The second is the competing process of crystallisation where the amorphous phase will crystallise (cold crystallisation above the  $T_g$ )

The ideal goal is to promote the first process and restrict the second. This can be achieved by promoting fusion by rapidly heating above the  $T_g$  to achieve interfacial diffusion within a short time period to ensure no crystallisation occurs. If crystallisation occurs the result would be a hard crystalline matrix material. Interfacial bonding strength can be measured with tensile strength experiments.

To enhance the processing gap between the reinforcing fibre material and the matrix material slowly crystallisable polymers such as polyethylene terephthalate (PET) and PLA can be used. Alternatively a less crystalline matrix material could be used.<sup>29</sup>

### 2.2.3.2 SPC polylactic acid core-shell fibres

The SPC concept can be used in conjunction with a bicomponent fibre configuration as described in patent literature for biodegradable PLA core-shell fibres, composites of the core-shell fibres and devices created there from.<sup>31,32</sup>

The fibres should comprise a core polymer that should be a semi-crystalline, high strength fibre-forming polymer and the shell of a less crystalline or preferably an amorphous polymer with a glass transition temperature significantly below the crystalline melting temperature of the core. Barrows describes in his patent “Bioabsorbable fibers and reinforced composites produced therefrom” the preparation of a core-shell fibre configuration, by melt spinning, of a semi-crystalline polylactic acid polymer for the core and amorphous polylactic acid polymer for shell.<sup>32</sup> These composites are completely biodegradable and the interfacial bonds between either of the components are sufficient and will not suffer from water penetration or delamination in use.

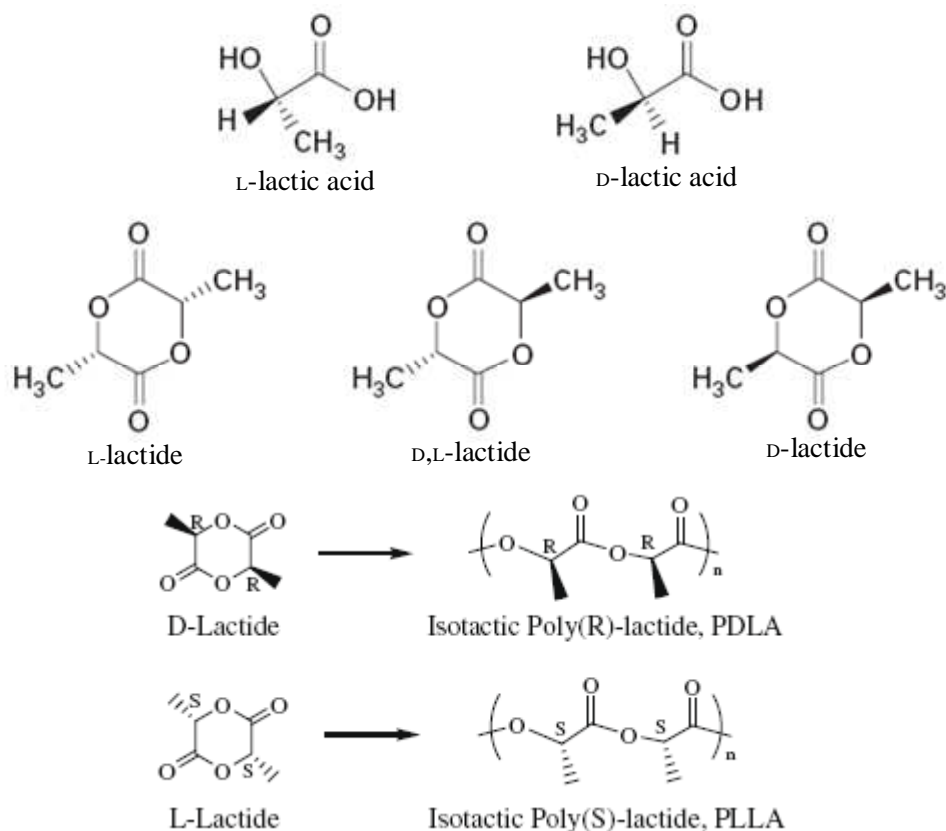
## 2.3 Polylactic acid (PLA)

### 2.3.1 Introduction

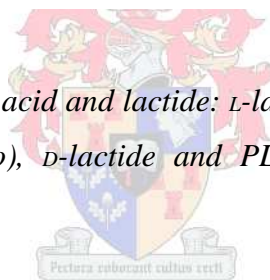
Poly(lactic acid) or polylactide (PLA), one of a range of synthetic biodegradable poly( $\alpha$ -hydroxy esters) that are FDA approved, has fashioned wide interest as it is the first commodity biodegradable polymer manufactured from renewable resources.<sup>33,34</sup>

PLA was initially limited to high-end applications and fundamental research until Cargill Dow Polymer LLC began commercial production of PLA via a green chemistry approach in 2002.<sup>35</sup> The Cargill Dow process is inherently “green” as it substitutes petroleum-based feedstock with corn starch. Solvents or other hazardous materials are not used in this process and efficient utilization of catalysts in polymerisation steps allows reduced energy consumption. Cargill Dow NatureWorks™ PLA products can be recycled or composted after use.<sup>33</sup>

The chemical structures of various isomers of lactic acid, as well as that of polylactic acid, are given in Figure 2.9. Chemical and physical properties of PLA can be manipulated around the pendent methyl group on the alpha carbon atom. The methyl group gives chirality to the carbon of lactic acid. Poly(L-lactic acid), poly(D-lactic acid) and poly(D,L-lactic acid) can therefore be polymerised from optically active L(-), D(+), and optically inactive D,L-lactic acid isomers (Figure 2.9) respectively to yield distinctive properties.<sup>36</sup>



**Figure 2.9** *Isomers of lactic acid and lactide: L-lactic acid, D-lactic acid, L-lactide, D,L-lactide (meso), D-lactide and PLLA and PDLA polylactic acid polymers*<sup>36,37</sup>



Lactic acid is a product of a biochemical fermentation process (although a less common petrochemical route also exists) by lactic acid bacteria on 100% annually renewable resources such as corn or potato starch, beet sugar, and cheese whey. The fermentation feed stock to be used and nutrients available will determine which optimised/modified strain of homofermentive *Lactobacillus* will be used to produce lactic acid.<sup>36,38</sup>

The raw material for PLA is lactic acid or lactide for which there are three commonly used polymerization routes through which high molecular weight PLA can be obtained. These routes include condensation/coupling and azeotropic dehydrative condensation of lactic acid, or ring-opening polymerisation of lactide.<sup>36</sup>

PLA is a unique biodegradable polymer that typically has a glass transition temperature approximately 50°C and crystalline melting temperature approximately 180°C. These physical properties give PLA processing characteristics similar to polyethylene terephthalate (PET) and performance characteristics approximating that of polypropylene (PP). PLA can be stress or thermally crystallised, impact modified or filled, copolymerised, and can be processed using existing polymer processing equipment. Transparent films, fibres, or injection molded into blow-moldable preforms are possible. PLA also has excellent organoleptic characteristics and is excellent for food contact and related packaging applications.<sup>33</sup>

The chirality of lactic acid allows for the stereochemistry of PLA to be tailored to meet desired requirements. The PLA chain may contain homo stereocentres (L:L or D:D) yielding stereoregular highly crystalline PLLA polymer or enantiomeric stereocentres (L/D) yielding more amorphous stereoirregular PDLLA polymer. Isotacticity and syndiotacticity with different enantiomeric units can be tailored by special catalysts. Relatively high D content (>20%) results in nearly completely amorphous materials whereas highly crystalline material is obtained when the D content is <2%.<sup>35</sup>

Manipulating the thermal and processing history, molecular weight, copolymer composition and blending semi-crystalline PLLA with less crystalline material are routes to reduce crystallinity. These techniques can therefore be used to reduce the modulus and increase the degradation rate of PLLA expanding the scope of use for the material in controlled-release drug applications or other applications where the degradation profile needs to be tailor made, such as tissue engineering

PLA is biodegradable and degradation occurs mainly by hydrolysis. There are many factors that affect the rate of hydrolysis including temperature, humidity, processing conditions (shear force), presence of bacteria and enzymes and also the autocatalytic degradation by lactic acid monomer present in the environment or in the polymer.<sup>35</sup>

The instability of PLA has both positive and negative implications. In a positive sense this leads to the biodegradation which occurs when PLA products are composted after completing their useful life or are required to be bioabsorbable for medical implants.

On the other hand, thermal degradation during melt-processing is a negative effect of PLA's instability. Very high molecular weight polymers, with associated high viscosity, must be processed under harsher conditions (elevated temperatures to reduce viscosity) and are not ideal for melt-processing PLA. Additives such as plasticisers can be added but can influence biocompatibility and toxicology if they can leach out easily into body fluids and the environment. It is preferable therefore to achieve property adjustment through chemical or physical structure factors and/or blending with other biocompatible polymers, and not through additives. The optimum processing conditions must be found so that thermal degradation processes during melt-processing are inhibited while still maintaining a commercially viable rate of production. Stabilizing agents in the form of anti-oxidants and water scavengers may be added but need to be declared for possible toxicological effects.<sup>35</sup>

### 2.3.2 PLA fibres

PLA fibres are of great interest for filament and non-woven applications as a result of thermoplasticity, ease of processing, biodegradability, biocompatibility and superior mechanical performance compared to other biodegradable fibres. PLA is a polar polymer that displays dipole-dipole interactions resulting in good attraction between PLA molecules. This results in enhanced adhesion in single polymer composites (SPC) where matrix and reinforcing fibre components are of the same polymer.

Properties of PLA that are of interest for different commodity products include low moisture absorption and high wicking (apparel), low flammability and smoke generation, high resistance to ultraviolet light (outdoor textiles) and low index of refraction (aesthetic benefits, low density (light weight textiles)). Properties of interest in medical applications are biocompatibility by assimilation of degradation products by natural metabolic pathways in the body, and high mechanical performance over the product life time. In a recent review paper, Gupta discusses the many applications for PLA fibres and composites made therefrom.<sup>35</sup> These applications include commodity products (apparel and packaging) and a host of biotextiles (pharmaceuticals, tissue engineering, sutures and implants).

Properties of the fibres can be tailored by processing methods, copolymerisation with glycolic acid and blending with other additives and polymers.



Commercial production rates of PLA fibres have been achieved by means of melt spinning, dry spinning, wet spinning, and by dry-jet-wet spinning. Melt spinning has some advantages over wet spinning: it is a solvent-free process and has higher production speeds resulting in a more environmentally and economically friendly approach. Melt spinning does, however, have some drawbacks. PLA may undergo degradation reactions involving thermohydrolysis, depolymerisation, intermolecular and cyclic oligomerisation, and/or transesterification during melting. This is the result of the combination of high temperatures, shearing forces and residuals (moisture and monomer) present in the polymer.<sup>35</sup>

PLA fabrics can be constructed by bonding, thermal bonding, knitting and weaving. Non-woven products can be made by meltblown and spunlaid technologies.

### 2.3.3 PLA nanofibres

Electrospinning of PLA nanofibres has been popular among researchers as the surface morphology and porosity of the fibre can be easily controlled, and the possibility exists to incorporate active agents into polymer solutions and the resultant fibre matrix. The most interest in these fibres has been for tissue engineering applications i.e. to mimic extra-cellular matrices that are porous and have high surface area. This is a result of the biocompatibility and biodegradability characteristics of pure PLA as well as its copolymers with other precursor's e.g. glycolic acid.<sup>39-44</sup>

## 2.4 Coaxial electrospinning of nano- to micro-scale core-shell fibres

### 2.4.1 Introduction

Coaxial electrospinning has gained much interest as it is a facile production method for the preparation of core-shell fibres with diameters in the nano- to micro-scale. Core-shell nanofibres afford an extra dimension to the usual one dimensional (1D) nanofibre materials by further enhancing the fibre properties. Encapsulation of one material inside another may serve a multitude of purposes e.g in bio-engineering applications to isolate an unstable component from an aggressive environment, or to avoid decomposition of a labile component under a certain atmosphere, or to deliver a given substance to a particular receptor.<sup>45-57,58</sup> It also allows the processing of hard-



to-process materials i.e. low molecular weight materials that are not fibre forming by the classic electrospinning method.

Core-shell nanofibres have been fabricated through various processing techniques based on template and self-assembly methods. These methods include laser ablation, polymerisation of monomers on a template<sup>59</sup>, polymerisation of wire/sheath self assembled precursors<sup>60</sup>, growing a semiconductor nanowire inside polymer tubules<sup>61</sup> and the coating on a fibre template or TUFT process (tubes by fibre templates)<sup>62-64</sup>. Core-shell nanostructures have also been fabricated via the filling of carbon nanotubes with fluorescent particles.<sup>65</sup> These techniques are not ideal as they require very specific multi-step chemical processes, while providing poor versatility and low throughput.

Another technique that has been used to create core-shell fibres is coaxial electrospinning. Electrospinning is an electrohydrodynamic fibre forming process that uses electrostatic forces to draw fibre forming precursors or “electrospinnable” fluids into fibres with diameters from the micro- to nano-metre range.<sup>66</sup> The electrospinning process was first patented in 1902 by Cooley and later some modifications to the process were patented by Formals in 1934.<sup>67,68</sup> Electrospinning was essentially lost to the world for over half a century until its revival by the work of Reneker *et al.*<sup>69,70</sup> The process has since received enormous attention, based on its ability to produce nano-diameter fibres simply, continuously and robustly.

The spin-off electrospinning technologies that have been used to fabricate core-shell and bicomponent fibres include blend electrospinning<sup>71</sup>, emulsion electrospinning<sup>72</sup>, conjugate electrospinning<sup>73</sup>, side-by-side bicomponent spinning<sup>15</sup>, and capillary-in-capillary coaxial<sup>45</sup> and “L” shape electrospinning<sup>74</sup>. Capillary-in-capillary coaxial electrospinning has been the most preferred choice based in its simplicity and success in forming continuous core-shell fibres.<sup>45,47,48,51,54,55,58,75-90</sup> Other common names found in literature for the coaxial electrospinning technique include core-shell/core-sheath, compound, composite, two-fluid and co-electrospinning.

## 2.4.2 Background

A short background and description of the classic single capillary electrospinning is given. This is followed by an in-depth look at coaxial electrospinning technology and the parameters that affect the process and resultant fibres.

### 2.4.2.1 Classical single capillary electrospinning

Nanostructures can be manufactured/synthesized by Top-Down, Bottom-Up or hybrid routes.<sup>10,91</sup> Bottom-up involves the building-up of nanomaterials using single atoms and molecules allowing superior versatility. The top-down approach involves converting large uniform materials into nanostructures via specialised techniques e.g. lithography. Electrospinning is a top-down process as it takes already formed macromolecules and processes them into solid fibres and has the benefit of making use of existing technology, materials and equipment.<sup>11</sup>

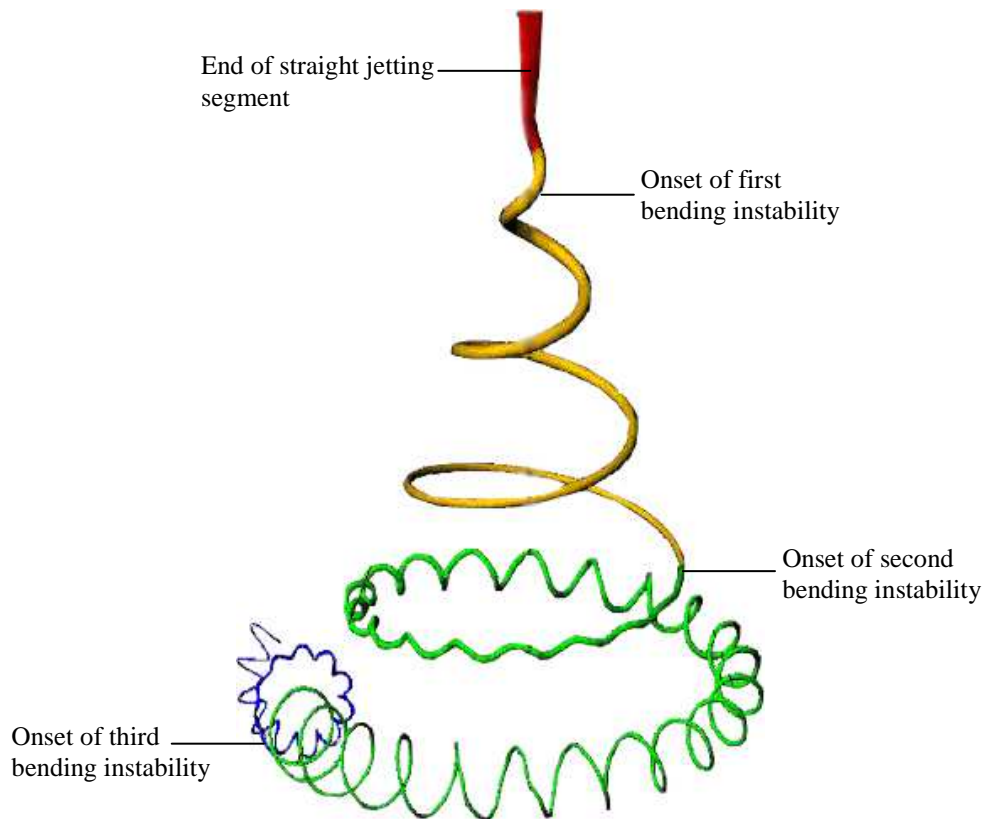
Electrospinning is the preferred method for producing nano-scale fibres as a result of three inherent process benefits: low cost simplistic apparatus design, and scalability.<sup>92</sup> The versatility of the electrospinning technique is illustrated by the broad spectrum of materials processed, including synthetic and natural polymers, polymer alloys, metals, ceramics, and polymers loaded with chromophores, nanoparticles, or active agents.<sup>57</sup>

The electrospinning technique uses electrostatic forces to spin and draw fibres compared with mechanical drawing used in conventional dry spinning. Electrospinning requires that a charged “electrospinnable” fluid droplet be brought into an electric field. This electric field must have the appropriate field line configuration and strength. The droplet, held together by surface tension, is charged with an applied voltage. Increasing the applied voltage above a certain point causes the droplet to taper into a conical geometry called a Taylor cone. Increasing the applied voltage further causes more charge build-up and repulsion. Above some critical voltage the surface tension is eventually overcome and a fluid jet emerges from the apex of the Taylor cone. The jet transcends a straight segment, known as the jetting region. At the end of the jetting region, whipping begins. Whipping is a process caused by instabilities that arise from charge repulsions between the charges present on the surface of the jet. The mutual charge repulsions initiate a series of consecutively smaller bending coils (Figure 2.10), with each coil comprising turns of

increasing radius. In this process of jetting and whipping the fibres are stretched and aligned with typical stretching rates of up to  $10^5 \text{ s}^{-1}$ .<sup>57</sup> In solution electrospinning the jet whipping thins the fibre and expels solvent molecules. Finally dry continuous fibres are deposited onto a conductive collector that is oppositely charged (or grounded) to voltage initially applied to the polymer fluid. Fibres may be collected in random or aligned fibre arrays.<sup>57,93</sup>

There are many variations to the conventional electrospinning process including melt electrospinning<sup>94</sup>, reactive spinning<sup>95</sup>, emulsion electrospinning<sup>96</sup>, pressure assisted<sup>97</sup>, vibrational-assisted electrospinning<sup>98</sup>, field assisted<sup>99</sup>, conjugate<sup>73</sup>, coaxial<sup>45</sup> fibre spinning. There are numerous process and design variations that can be used in the electrospinning set-up to direct and order the collected fibres.<sup>92</sup>

Control of the process and various set-up configurations allows the fabrication of fibres possessing nano-scale diameters having various morphologies and fiber arrangements i.e. cross-sectional shapes, beads, branches and buckling coils or zigzags, aligned or randomly laid webs. Pre-loading electrospinning fluids with active, functional or reinforcing components allows their inclusion along the length of the nanofibres i.e. dispersed particles<sup>100</sup> and viable cells<sup>52</sup>. Post-treating nanofibers can further enhance the property profiles i.e. conglutination, vapour coating, chemical treatment of the surfaces, and thermal processing.<sup>93</sup>



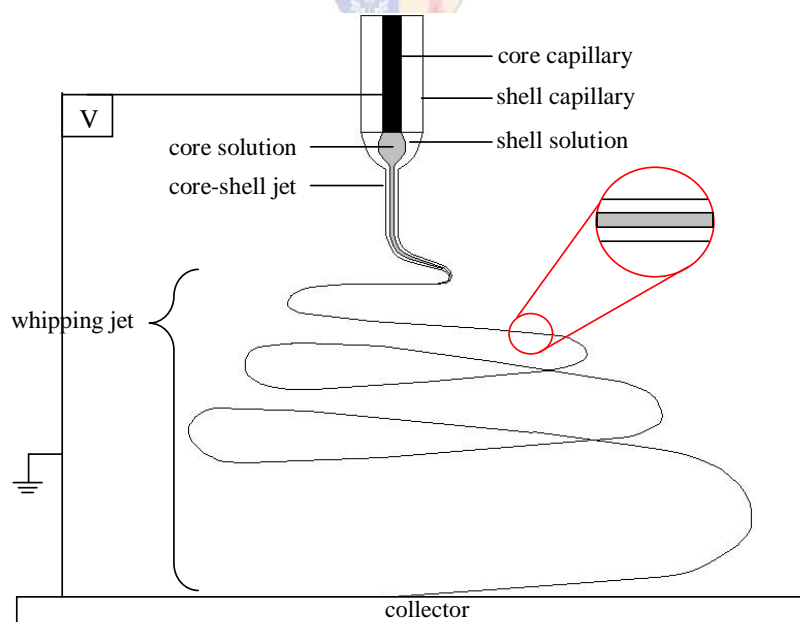
**Figure 2.10** *Successive bending instabilities of the electrified jet (picture adapted from)<sup>93</sup>*

#### 2.4.2.2 Coaxial electrospinning

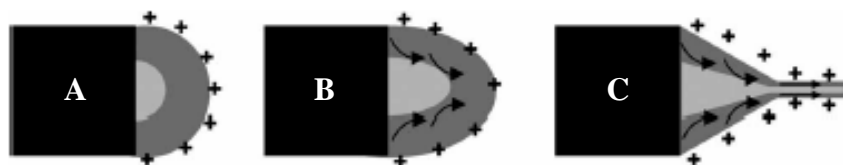
Coaxial **electrospinning** has its roots in coaxial **electrospraying** but the first work on the subject was reported by Sun et al. in 2003.<sup>45,46</sup> Coaxial electrospinning is a technique that can be used to process traditionally non-electrospinnable materials (limited by solubility, molecular weights, rigid or compact architectures). The electrospinnable shell acts as a template and prevents the varicous break-up into droplets (from Rayleigh instability) of the non-electrospinnable core. A viscoelastic core can also resist Rayleigh instability and impart even greater elasticity to the interface between core and shell components due to strain hardening and thereby also stabilise the shell.<sup>88</sup>

Classical single capillary electrospinning occurs from a Taylor cone that consists of only one material, whereas in coaxial electrospinning you have a compound Taylor cone made up of two different, concentric fluids.<sup>45,66,88</sup>

Capillary-in-capillary coaxial electrospinning (Figure 2.11) involves two fluids; a core fluid and a shell fluid. These fluids are co-extruded, from a spinneret consisting of two capillaries/needles positioned concentrically in a capillary-in-capillary arrangement. The core-shell fluids are separately fed at appropriate flow rates (via pump or gravity) into a spinneret. A compound droplet is formed at the spinneret orifice. The spinneret is attached to one electrode of a high voltage supply and the collector to the oppositely charged (or grounded) electrode. Increasing the voltage applied to the spinneret deforms the compound droplet in a compound Taylor cone. Increasing the applied voltage further increases the charge build-up and above a critical voltage the repulsions of the charges overcome the surface tension of the shell fluid. A fluid jet of the shell fluid jets out of the apex of the Taylor cone. The core fluid increases in diameter upon exiting the capillary orifice (die swell effect). If all the system and operating parameters meet the critical conditions then viscous dragging will be induced by the electrically driven shell on the core fluid. The core fluid will therefore be dragged into the electrospinning jet of shell fluid (Figure 2.12).<sup>56,88</sup> As in classical electrospinning the compound jet remains linear for as few millimetres until bending instability sets in and whipping of the jet commences. Dry core-shell fibres are deposited on the collector.<sup>66</sup>



**Figure 2.11** Schematic of coaxial electrospinning showing a compound Taylor cone and whipping jet



**Figure 2.12** Core-shell Taylor cone formation (A: Surface charges on the shell solution, B: Viscous drag exerted on the core by the deformed shell droplet, C: Core-shell compound Taylor cone formed due to continuous viscous drag).<sup>56</sup>

### 2.4.3 Parameters

The electrospinning process is complex and many of the system, process and ambient parameters are inter-dependent. Changing one parameter directly or indirectly affects other parameters e.g. changing a solvent to increase the dielectric constant of the solution can affect other parameters such as conductivity, surface tension, polymer chain conformation in solution and ultimately polymer chain entanglements. There is no general set of system, process and ambient parameters that can be applied to a given polymer-solvent system that will ensure continuous electrospinning of uniform fibres.

Core-shell electrospinning of continuous concentric core-shell fibres is strongly dependent on the stability of the process. Factors known to affect this stability are discussed in literature.<sup>56,101</sup> Ideal conditions for core-shell electrospinning have been described as “achieved when both solutions are sufficiently viscous and even spinnable (at least the shell)” and when solvents of the solution pair are immiscible (but may be miscible).<sup>101</sup>

Some of the most significant process parameters in coaxial electrospinning will be discussed in the following section.

#### 2.4.3.1 System parameters

##### *i) Miscibility of core and shell solutions*

Li and Xia report that of all parameters the immiscibility of core and sheath liquids is the most critical in the formation of continuous and uniform hollow fibres (after extraction of core component).<sup>88</sup> Sun *et al.*, in agreement with Yu *et al.*, showed that

core-shell electrospinning occurs at a rate fast enough to prevent any mixing of the core-shell polymers (as polymers have a low diffusion coefficient relative to the rate of stretching/solidification of fibres).<sup>45,66</sup> Immiscible core-shell solvents produce defined core-shell boundary interfaces whereas miscible core-shell solvents yield less defined interfaces.<sup>45,88</sup> It has also been shown by members of our group that using the same solvent reduced the interfacial tension between the two solutions, which could aid viscous drag of the shell on the core solution and lead to more effective core entrainment.

ii) *Effect of solution concentration, viscosity and molecular weight*

Coaxial electrospinning will only occur if the shell solution is electrospinnable under single capillary electrospinning and will readily form continuous fibres. The shell fluid should therefore possess significant polymer chain entanglements in solution ( $\geq 2.5$  entanglements per chain).<sup>102</sup> The polymer molecular weight and concentration will determine the number of entanglements in solution and therefore affect stable fibre formation. Shell solutions with less than 2.5 entanglements per chain result in instabilities, which with single capillary electrospinning, leads to beads-on-string fibre morphology or electrospaying of droplets. Coaxial electrospinning with such solutions will not allow sufficient wrapping of the core fluid. Core concentrations that are too low in viscosity result in discontinuous cores and jet break-up.<sup>55,56</sup>

Sun *et al.* reported that increasing the core concentration had no effect on the fibre morphology but resulted in a broad distribution of fibre diameters.<sup>78</sup> Zhang *et al.* reported that by increasing the core concentration the core and total fibre diameters were increased while yielding a thinner shell.<sup>90</sup> Increasing the shell concentration results in greater shell wall thickness and smaller core volume. The inverse occurs with lower concentrations for the shell solution.<sup>48,103</sup>

iii) *Solvent Volatility*

Under certain circumstances it has been shown that it is possible to prepare composite hollow fibres by coaxial electrospinning.<sup>85,101</sup> Under these circumstances the shell rapidly solidifies due to solvent evaporation and will therefore solidify faster than the solvent in the core can evaporate. The slow diffusion of the solvent trapped in the interior creates a vacuum and a hollow core. This hollow core structure collapses



(under atmospheric pressure) and causes the fibre structure to change from round to a ribbon configuration.

The time available for significant stretching of the jet and alignment of polymer molecules is also determined by the solvent volatility. Solvents that are highly volatile will evaporate too quickly for the critical elongation viscosity\* to be maintained for maximum orientation of polymer molecules.<sup>104</sup>

If the vapour pressure is too high the Taylor cone may also form a skin on its surface and eventually block the needle and halt electrospinning so that further electrospinning is only possible after removing the blockage and renewing the droplet.<sup>105</sup>

Low vapour pressure solvents on the other hand may remain in the fibres and wet-fused fibres may be collected. Toxic residues may restrict applications.

The vapour pressure of the solvent plays a major role in creation of nanostructures by influencing the phase separation process that occurs during fibre solidification and drying. Solvents with higher vapour pressure increase the rate of phase separation and result in more porous structures compared with low vapour pressure solvents.<sup>106</sup>

The effect of solvent volatility can also be compounded by the ambient conditions, such as relative humidity (covered in Section 2.4.3.3). Solvent mixtures can be used to either increase or decrease the volatility of a solution for stable spinning and to change the kinetics of phase separation<sup>107</sup> to create specific fibre morphologies.

#### iv) *Conductivity*

Free charges or ions in the polymer solution are forced to move in the electric field and the force applied is transferred to the polymer solution.<sup>69</sup> The process of electrospinning occurs more readily with solutions that are more conductive as a greater force is applied to those charges.<sup>69</sup> Non-conductive solutions will not spin as readily on their own. A conductive shell or core solution can be used to pull a

---

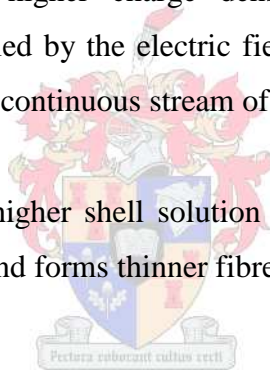
\* Critical elongation viscosity – the viscosity required for optimal alignment of polymer molecules and stretching of the electrospinning jet to produce fibres that are thin, smooth and uniform

respective non-conductive core or shell solution to permit the electrospinnability of the non-conductive solution.<sup>108</sup> The electrical conductivity of a solution determines the charge density on the electrospinning fluid jet. The electrical force experienced by the jet with higher conductivity under the same electric field will cause greater stretching of the jet along its axis and therefore produce fibre with smaller diameters.<sup>109</sup>

Surface charge density opposes Rayleigh instability and acts to enhance the whipping and bending instabilities of the jet. Conductivity is, therefore, important when trying to obtain finer fibre diameters when working with dilute solutions, where bead formation is problematic. Strategies to reduce bead formation include adding ionic salts to the polymer solution or using a more polar solvent.<sup>109,110</sup>

When the core fluid has a higher charge density than the shell in coaxial electrospinning, the core is pulled by the electric field at a higher rate than the feed line can supply resulting in a discontinuous stream of core solution.<sup>66</sup>

A spinning system that has a higher shell solution conductivity results in a greater elongation of the whipping jet and forms thinner fibres with thinner cores.<sup>66</sup>



v) *Dielectric Constant*

The dielectric constant is the ability of a solution to hold and disperse electric charge, and concentrate the electric field lines of flux, when placed in an electric field. It is related to the solution conductivity (charge density) and to the nature of the intervening medium.<sup>104</sup>

Materials with higher dielectric constants tend to disperse the surface charge density more evenly which improves fibre uniformity and productivity. Fibres spun from solutions of higher dielectric constant result in finer fibre diameters.<sup>111</sup>

vi) *Surface tension and interfacial tension*

Surface tension is an important parameter in jet initiation as there is a critical amount of charge that is required to overcome the surface tension in the Taylor cone and to eject a jet of polymer solution from the apex.<sup>93</sup>

It is the balance between the surface tension and the coulombic repulsions in the electrospinning jet that determine the nature of perturbations experienced by the whipping jet. Rayleigh instability is caused by the surface tension of the polymer solution but is countered by solution viscosity (entanglements) and electrical Maxwell forces. Solutions with high surface tensions are prone to bead formation.<sup>112</sup>

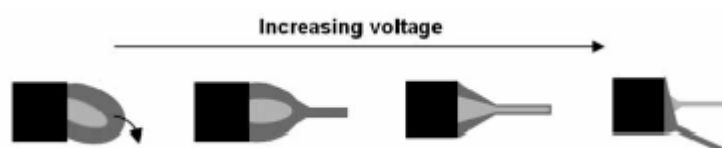
Surface tension is mainly a function of the solvent and is less sensitive to the variations in polymer concentration. The surface tension can be reduced by addition of surfactants and salts.<sup>109</sup>

Interfacial tension between core and shell solutions affects the stability of the Taylor cone and also the translation of shearing forces from the shell solution to the core. Core and shell solutions with low interfacial tension/interfacial energy are desired (miscible or nearly miscible solvents) as they allow the viscous dragging forces of the shell fluid to pull the core continuously into the jet to form uniform core-shell fibres.<sup>56</sup>

#### 2.4.3.2 Process parameters

##### i) Applied Voltage, Spinning/Gap Distance and Electric Field Strength

The applied voltage, spinning distance and electric field strength are related parameters. The electric field strength can be described in a simplified form as the applied voltage over the spinning distance (expressed in kV/cm). The effect of increasing voltage on a core-shell droplet is shown in Figure 2.13. Applied voltage is responsible for the surface charge on the jet. Higher applied voltages therefore, increase the instability of the whipping jet. In coaxial electrospinning this is important for stretching the shell solution that in turn pulls the core along with it. Above a certain threshold voltage the core-shell Taylor cone splits into two jets as a means to spread the charge on the surface of the Taylor cone.<sup>113</sup> Very high voltages usually produce broad fibre diameter distributions.<sup>93,109</sup>



**Figure 2.13** The effect of increasing applied voltage on the core-shell droplet<sup>113</sup>

In general the core-shell fibre diameters can be reduced by increasing electrical field strength.<sup>88</sup> This, however, will not be the case if the solution feed rates are increased simultaneously with the electric field strength. The increase in electrostatic forces induces higher volumetric flow rate and therefore more solution is pulled out of the spinneret. Higher viscosity solutions with higher surface tensions require greater electric charge build-up and greater electric field strength to be electrospun and also to form thinner fibres.

The nature of the field lines of a potential gap is determined by the capillary and collector geometry, as well as the electric field strength (electric force/ distance).<sup>92</sup>

For the same surface charge density a greater electric field will enhance the pulling forces on the fluid jet and increase jet thinning and molecular orientation.<sup>112</sup>

The spinning distance is the distance between the capillary orifice and the collector surface. This distance influences the electric field strength and also the time allowed for whipping and solvent evaporation before fibre collection. Increasing the distance, while fixing all other parameters, reduces the fibre diameter by allowing more time for whipping instability and solvent evaporation. Decreasing the distance can yield wet fibres and therefore a network of connected fibres from solvent diffusion at the points where fibres overlap. If the capillary is too close to the collector corona discharge may result.<sup>104</sup>

*ii) Applied voltage polarity*

The polarity of the applied voltage has been reported to significantly affect the mobility of charges in the polymer solutions. Negatively charged solutions are shown to produce larger fibre diameters and narrower spinning envelopes (therefore a smaller area covered by the fibres on the collector). AC voltages have also been used and produced greater alignment of fibres.<sup>114,115</sup>

*iii) Flow rate*

The core and shell fluids should be fed to the spinneret at rates required to maintain a continuous core-shell jet and optimum stability for core entrainment. If the core fluid

flow rate is too high the core jet breaks-up into droplets within the fibre, and if the shell flow rate is too high a non-continuous core results.<sup>66, 78</sup>

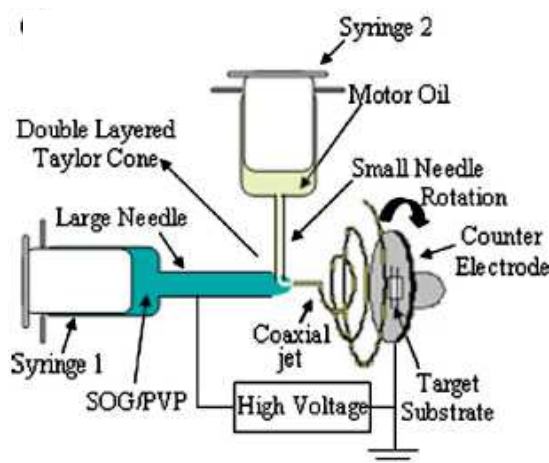
The core-shell flow rates can be used to manipulate the core and shell component ratios; increasing the core flow rate results in a fibre with a larger core diameter and a thinner shell diameter.<sup>90</sup> Increasing the core flow rate past a certain threshold for low molecular weight cores results in fibre collapse as the shell wall is too thin to support the core. Increasing the shell flow rate increases the shell wall thickness and decreases the relative core volume.<sup>103</sup>

#### iv) *Capillary tip*

A narrow electrode is required to efficiently charge the electrospinning solution. Although the effects of capillary size on core-shell fibre diameters prepared by coaxial electrospinning have not been reported specifically, a smaller diameter capillary has been said to produce smaller fibres in single capillary electrospinning.<sup>116</sup> The size of the orifices that can be used in coaxial electrospinning is limited by the solution viscosity.

#### v) *Coaxial spinneret configurations*

The most common coaxial electrospinning spinneret is the capillary-in-capillary configuration.<sup>56</sup> Another more simple design that has been used with success is the L-shape configuration (Figure 2.14).<sup>103</sup>



**Figure 2.14** Schematic of “L” shape coaxial electrospinning set-up

*vi) Core-needle protrusion*

Entrainment of a core fluid in an attempt to produce core-shell fibres is not always successful as explained in a paper by Reznik *et al.*<sup>117</sup> This they attributed to the rapid movement of free charges from both fluids and their interface to the free surface of the shell fluid. This causes the electric field to act only on the free surface. They showed that this phenomenon could be resolved by extending the core nozzle by a distance of about half the radius of the shell needle and thereby place the core solution closer to the free surface where the greatest charge density (apex of the cone) and resultant viscous dragging is felt. Problems of entrainment and concentricity could be remedied through the use of the single nozzle (eliminating the need for an inner nozzle) core-shell electrospinning technique proposed by Bazilevsky *et al.* (although this would not be applicable to all core-shell solution combinations).<sup>72</sup>

*vii) Collector*

Fibres may be collected on conductive receptors or can be intercepted on route to such collectors. These may be static or dynamic collectors and are either grounded or oppositely charged. Various collectors can be used to collect non-woven or aligned fibre webs. The fibres may be deposited directly onto a substrate. Smit *et al.*<sup>118,119</sup> showed how yarns can also be created by using a water bath method or by using an electrostatic gap-alignment collector. Spinning onto a water bath may also affect the fibre morphology and allow removal of toxic non-volatile solvents. A review by Teo and Ramakrishna describes in detail the various collectors that have been used to collect electrospun fibres.<sup>92</sup>

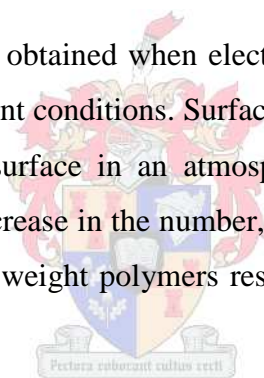
The dielectric properties of the collector material are important with regard to packing densities of the fibres. Polymer fibres in general are good insulators and after the first few layers are plied onto the collector the conducting effect is diluted and electrostatic repulsion between succeeding fibre layers increases. After the first layer of fibres is deposited on a gap alignment collector there is no space for the fibres to be pushed into space by the charged fibre repulsion. The fibres can therefore not be aligned parallel between the gaps and they are therefore less ordered than the first gap aligned fibres. This reduces the packing density of the fibre mat and creates a more open structure. Use of a rotating collector can aid in alignment through high linear collecting velocities.<sup>104</sup>

### 2.4.3.3 Ambient conditions

Most electrospinning experiments are conducted in air under normal atmospheric conditions. The surface morphology and surface area, and more specifically the surface porosity, of electrospun nanofibres can be controlled (size, shape, density, and depth of pores) by choice of polymer/solvent properties as well as setting the ambient conditions under which electrospinning is conducted.<sup>105, 120</sup>

The control of surface area, by creating porosity on the fibre surface, is important for some applications i.e. filtration applications or drug release media. Porous surface features of a known size and distribution are essential if nanoparticles need to be deposited on the surface (and inside the pores) of the fibre or if drug molecules are to be incorporated in the core for release through the pores for controlled release applications.<sup>105,120</sup>

Porous/rough fibre surfaces are obtained when electrospinning with solvents of high vapour pressure in humid ambient conditions. Surface features and/or pores have been shown to occur on the fibre surface in an atmosphere of high relative humidity. Elevated humidity causes an increase in the number, diameter, shape, and distribution of the pores. Higher molecular weight polymers result in larger non-uniform shaped pores.<sup>120</sup>



The porosity seen in electrospun fibres is attributed to two mechanisms of phase-separation, *Thermally-induced* (TIPS) and *Vapour-induced* (VIPS) *phase separation*.<sup>105</sup> Another type of surface feature, termed 'breath figure', has been attributed to similar mechanisms.<sup>69</sup> These mechanisms are related to the evaporative cooling of the electrospinning jet surface due to the rapid solvent evaporation. Different morphologies may be observed based on electrospinning at different relative humidity.<sup>70,105,121</sup>

It is advantageous to control the spinning environment to control the solidification rate of the electrospinning jet (by control of evaporation to facilitate sufficient jet elongation to create fine fibres). This can be done by spinning in various atmospheres, controlling the temperature and humidity of the spinning environment. Another way to control the spinning environment around the spinneret and jetting region would be



to spin using a gas-jacketed capillary tip. This would surround the jet with gas saturated with solvent to prevent drying and allow stable Taylor cones at higher voltages.<sup>122</sup> A gas jacket of high air pressure can create additional drag and allow enhanced drawing of the fibre and is called electroblowing.<sup>123</sup> The rate of drying can also be influenced by using a heated air jacket or heating lamp.

## References

1. Hearle JWS, Peters RH (eds). *Fibre Structure*. Manchester and London: Butterworths & Co. Ltd. and the Textile Institute; 1963.
2. Hearle JWS. *Fibers, 2. Structure*. Ullmann's Encyclopedia of Industrial Chemistry 8th ed, 2006:1-42.
3. Sperling LH. The macromolecular hypothesis. *Introduction to Physical Polymer Science*. 4 ed: John Wiley & Sons, Inc, 2006:19.
4. Hatch KL. *Fiber Morphology and Formation*. Textile Science: West Publishing Company, 1993:88-107.
5. Hatch KL. *Fiber Morphology*. Textile Science: West Publishing Company, 1993:88-107.
6. Schultze-Gebhardt F, Herlinger K-H. *Fibres, 1. Survey*. Ullmann's Encyclopedia of Industrial Chemistry 8th ed: Wiley-VCH GmbH & Co. KGaA, Weinheim, 2005:1-36.
7. Smith PA. Technical fabric structures - 3. Nonwoven fabrics. In: Horrocks AR, Anand SC (eds). *Handbook of Technical Textiles*: Woodhead Publishing Ltd., 2000:130-51.
8. Chen X, Gong R-H. Technical Yarns. In: Horrocks AR, Anand SC (eds). *Handbook of Technical Textiles*: Woodhead Publishing Limited, 2000:42-61.
9. Ko FK. *Nanofiber Technology: Bridging the gap between nano and macro world*. NATO ASI on Nanoengineered Nanofibrous Materials, 2004.
10. Fahlman BD. *Nanomaterials*. Materials Chemistry. 1st ed: Springer, 2007:498.
11. Ramakrishna S, Fujihara K, Teo W-E, Lim T-C, Ma Z. *An introduction to electrospinning and nanofibers*. Singapore: World Scientific; 2005.
12. Bergshoef MM, Vansco GJ. Transparent nanocomposites with ultrafine electrospun nylon-4,6 fiber reinforcement. *Advanced Materials*. 1999;11:1362.
13. He J-H, Wan Y-Q, Xu L. Nano-effects, quantum-like properties in electrospun nanofibers. *Chaos, Solutions and Fractals*. 2007;33:26-37.
14. Peacock JA, Cogswell FN. Fibre reinforced advanced structural composites. In: Miles IS, Rostami S (eds). *Multicomponent Polymer Systems*: Longman Scientific & Technical, 1994:319-61.
15. Gupta P, Wilkes GL. Some investigations on the fiber formation by utilizing a side-by-side bicomponent electrospinning approach. *Polymer*. 2003;44:6353-9.
16. Mattern S. *Kraton announces breakthrough in bicomponent fiber technology* <[http://findarticles.com/p/articles/mi\\_pwwi/is\\_200606/ai\\_n16487247](http://findarticles.com/p/articles/mi_pwwi/is_200606/ai_n16487247)>. Accessed 2008/05/07, 2006.
17. Jeffries R. *Bicomponent Fibers*. Volume 13. Manchester: Marrow Publishing; 1971.

18. Horio M, Kondo W. Crimping of Wool Fibers. *Textile Research Journal*. 1953;23:373-86.
19. Reemay®. Celbond® Particulate Structures <<http://www.fiberwebfiltration.com/Celbond.html>>. Accessed 2008/05/06, 2008.
20. Hedge RR, Dahiya A, Kamath MG. Bicomponent Fibers <<http://www.engr.utk.edu/mse/Textiles/Bicomponent%20fibers.htm>>. Accessed 2008/05/06, 2004.
21. Swicofil. Polyamide Grilon BA 3100 fiber for non woven <<http://www.swicofil.com/nonwovenpafiber.html>>. Accessed 2008/05/06, 2008.
22. Solutia. No-Shock® Antistatic Fiber Products <<http://www.noshockfiber.com/products.aspx>>. Accessed 2008/05/06, 2008.
23. Ferenets M, Myllymaki H, Grahn K, Sipila A, Harlin A. Manufacturing methods for multi step index plastic optical fiber materials. *AUTEX Research Journal*. 2004;4(4):164-74.
24. Cui Y, Cheung MMS, Noruziaan B, Lee S, Tao J. Development of ductile reinforcement bars for concrete structures. *Materials and Structures*. Volume Online First, 2007.
25. Kraitzer A, Ofek L, Schreiber R, Zilberman M. Long-term *in vitro* study of paclitaxel-eluting bioresorbable core/shell fiber structures. *Journal of Controlled Release*. 2007;126:139-48.
26. Source F. Bicomponent Fiber <<http://www.fibersource.com/f-tutor/bicomponent.htm>>. Accessed 2008/05/06, 2008.
27. Joseph ML. Basic Fibre Theory. In: Sheinis LA (ed). *Essentials of Textiles*. 4th ed: Holt, Rinehart and Winston, Inc, 1998:1-30.
28. Mead WT, Porter RS. *Journal of Applied Polymer Science*. 1978;22(11):3249.
29. Li R, Yao D. Preparation of single poly(lactic acid) composites. *Journal of Applied Polymer Science*. 2007 10/08/2007;107:2909-16.
30. Barkoula N-M, Peijs T, Schimanski T, Loos J. Processing of single polymer composites using the concept of constrained fibers. *Polymer Composites*. 2005:114-20.
31. Tsai F-J, Etzel BT; Multicomponent fiber PCT International Patent Application WO 1998/024951. 1998.
32. Barrows TH; Bioabsorbable fibers and reinforced composites produced therefrom PCT International Patent Application WO/1999/034750. 1999.
33. Henton DE, Gruber P, Lunt J, Randall J. Polylactic acid technology. *Natural Fibers, Biopolymers and Biocomposites*, 2005:527-77.
34. Li W-J, Cooper Jr JA, Mauck RL, Taun RS. Fabrication and characterization of six electrospun poly( $\alpha$ -hydroxy ester)-based fibrous scaffolds for tissue engineering applications. *Acta Biomaterialia*. 2006;2:377-85.
35. Gupta BS, Revagade N, Hilborn J. Poly(lactic acid) fiber: An overview. *Progress in Polymer Science*. 2007;32:433-82.
36. Garlotta D. A Literature review of poly(lactic acid). *Journal of Polymers and the Environment*. 2002;9(2):63-84.
37. Yi Q, Wen X, He B, et al.. The chiral effects on the responses of osteoblastic cells to the polymeric substrates. *European Polymer Journal*. 2009;45:1970-8.
38. Gupta AP, Kumar V. New emerging trends in synthetic biodegradable polymers - Polylactide: A critique. *European Polymer Journal*. 2007;43:4053-74.

39. Inai R, Kotaki M, Ramakrishna S. Structure and properties of electrospun PLLA single nanofibres. *Nanotechnology*. 2005;16:208-13.
40. Xu X, Yang Q, Wang Y, Yu H, Chen X, Jing X. Biodegradable electrospun poly(L-lactide) fibers containing antibacterial silver nanoparticles. *European Polymer Journal*. 2006;42(9):2081-7.
41. Li W-J, Jr JAC, Mauck RL, Taun RS. Fabrication and characterization of six electrospun poly( $\alpha$ -hydroxyester)-based fibrous scaffolds for tissue engineering applications. *Acta Biomaterialia*. 2006;2(4):377-85.
42. Kim K-W, Joo YL, Giannelis EP. Effects of nanoclays on molecular structures of poly (L-lactic) acid in electrospinning. *Polymer Preprints*. 2003;44(2):74-5.
43. Zeng J, Yang L, Liang Q, et al.. Influence of the drug compatibility with polymer solution on the release kinetics of electrospun fiber formulation. *Journal of Controlled Release*. 2005;105(1-2):43-51.
44. Zong X, Kim K, Fang D, Ran S, Hsiao BS, Chu B. Structure and process relationship of electrospun bioabsorbable nanofiber membranes. *Polymer*. 2002;43:4403-12.
45. Sun Z, Zussman E, Yarin AL, Wendorff JH, Greiner A. Compound core-shell polymer nanofibers by co-electrospinning. *Advanced Materials*. 2003;15(2003):1929-32.
46. Loscertales IG, Barrero A, Guerrero I, Cortijo R, Marquez M, Ganan-Calvo AM. Micro/Nano encapsulation via electrified coaxial liquid jets. *Science*. 2002;1695-8.
47. Jiang H, Hu Y, Li Y, Zhao P, Zhu K, Chen W. A facile technique to prepare biodegradable coaxial electrospun nanofibers for controlled release of bioactive agents. *Journal of Controlled Release*. 2005;108:237-43.
48. Jiang H, Hu Y, Zhao P, Li Y, Zhu K. Modulation of protein release from biodegradable core-shell structured fibers prepared by coaxial electrospinning. *Journal of biomedical Materials Research Part B: Applied Biomaterials*. 2006;79B:50-7.
49. Townsend-Nicholson A, Jayasinghe SN. Cell electrospinning: a unique biotechnique for encapsulation living organisms for generating active biological microthreads/scaffolds *Biomacromolecules*. 2006;7(12):3364-9.
50. Jun Z, Aigner A, Czubyko F, Kissel T, Wendorff JH, Greiner A. Poly(vinyl alcohol) nanofibers by electrospinning as a protein delivery system and the retardation of enzyme release by additional polymer coatings. *Biomacromolecules*. 2005;6(1484-1488):1484.
51. Greiner A, Wendorff JH, Yarin AL, Zussman E. Biohybrid nanosystems with polymer nanofibers and nanotubes. *Applied Microbiology Biotechnology*. 2006;71:387-93.
52. Salalha W, Kuhn J, Dror Y, Zussman E. Encapsulation of bacteria and viruses in electrospun nanofibres. *Nanotechnology*. 2006;17:4675-81.
53. Deutsch S, Tarbell JM, Manning KB, Rosenberg G, Fontaine AA. Experimental fluid mechanics of pulsatile artificial blood pumps. *Annual Review of Fluid Mechanics*. 2006;38:65-86.
54. Yarin AL, Zussman E, Wendorff JH, Greiner A. Material encapsulation and transport in core-shell micro/nanofibers, polymer and carbon nanotubes and microchannels. *Journal of Materials Chemistry*. 2007;17:2585-99.
55. McCann JT, Marquez M, Xia Y. Melt coaxial electrospinning: a versatile method for the encapsulation of solid materials and fabrication of phase change nanofibers. *Nano Letters*. 2006;6(12):2868-72.

56. Moghe AK, Gupta BS. Co-axial electrospinning for nanofiber structures: preparation and applications. *Polymer Reviews*. 2008;48(2):353-77.
57. Greiner A, Wendorff JH. Electrospinning: A fascinating method for the preparation of ultrathin fibers. *Nanotechnology*. 2007 2007;46:5670-703.
58. McCann JT, Li D, Xia Y. Electrospinning of nanofibers with core-sheath, hollow, or porous structures. *Journal of Materials Chemistry*. 2005;15:735-8.
59. Jang J, Lim B, Lee J, Hyeon T. Fabrication of a novel polypyrrole/poly(methyl methacrylate) coaxial nanocable using mesoporous silica as a nanoreactor. *Chemical Communications*. 2001:83-4.
60. Xie Y, Qiao Z, Chen M, Liu X, Qian Y.  $\gamma$ -Irradiation route to semiconductor/polymer nanocable fabrication. *Advanced Materials*. 1999;11(18):1512-5.
61. Luo Y, Lee SK, Hofmeister H, Steinhart M, Gosele U. Pt nanoshell tubes by template wetting. *Nano Letters*. 2004;4(1):143-7.
62. Dong H, Prasad S, Nyame V, Jones WE. Sub-micrometer conducting polyaniline tubes prepared from polymer fiber templates. *Chem Mater*. 2004;16:371-3.
63. Hou H, Jun Z, Reuning A, Schaper A, Wendorff JH, Greiner A. Poly(p-xylylene) nanotubes by coating and removal of ultrathin polymer template fibers. *Macromolecular*. 2002;35:2429-31.
64. Yang Y, Wang H, Lu X, Zhao Y, Li X, Wang C. Electrospinning of carbon/CdS coaxial nanofibers with photoluminescence and conductive properties. *Material Science and Engineering*. 2007;140:48-52.
65. Kim BM, Qian S, Bau HH. Filling carbon nanotubes with particles. *Nano Letters*. 2005;5(5):873-8.
66. Yu JH, Fridrikh SV, Rutledge GC. Production of submicrometer diameter fibers by two-fluid electrospinning. *Advanced Materials*. 2004;16(17):1562-6.
67. Cooley JF; Apparatus for electrically dispersing fluids US Patent 692631. 1902.
68. Formhals A; Process and apparatus for preparing artificial threads US Patent 1975504. 1934.
69. Reneker DH, Chun I. Nanometre diameter fibres of polymer, produced by electrospinning. *Nanotechnology*. 1996 1996;7:216-23.
70. Doshi J, Reneker DH. Electrospinning process and applications of electrospun fibers. *Journal of Electrostatics*. 1995 1995;35:151-60.
71. Wei M, Lee J, Kang B, Mead J. Preparation of core-sheath nanofibers from conducting polymer blends. *Macromolecular Rapid Communications*. 2005;26:1127-32.
72. Bazilevsky AV, Yarin AL, Megaridis CM. Co-electrospinning of core-shell fibers using a single-nozzle technique. *Langmuir*. 2007;23:2311-4.
73. Li X, Yao C, Sun F, Song T, Li Y, Pu Y. Conjugate electrospinning of continuous nanofiber yarn of poly(L-lactide)/Nanotricalcium phosphate nanocomposite. *Journal of Applied Polymer Science*. 2008;107:3756-64.
74. Wang M, Jing N, Su CB, et al.. Electrospinning of silica nanochannels for single molecule detection. *Applied Physics Letters*. 2006;88(033106):1-3.
75. Loscertales I, Barrero A, Marquez M, Spretz R, Velarde-Ortiz R, Larsen G. Electrically forced coaxial nanojets for one-step hollow nanofiber design. *Journal of the American Chemical Society*. 2004;126:5376-7.



76. Wang M, Yu JH, Kaplan DL, Rutledge GC. Production of submicron diameter silk fibers under benign processing conditions by two-fluid electrospinning. *Macromolecules*. 2006;39:1102-7.
77. Diaz JE, Barrero A, Marquez M, Loscertales I. Controlled encapsulation of hydrophobic liquids in hydrophilic polymer nanofibers by co-electrospinning. *Advanced Functional Materials*. 2006;16:2110-6.
78. Sun B, Duan B, Yuan X. Preparation of core/shell PVP/PLA ultrafine fibers by coaxial electrospinning. *Journal of Polymer Science*. 2006;102:39-45.
79. Lallave M, Bedia J, Ruiz-Rosas R, et al.. Filled hollow carbon nanofibers by coaxial electrospinning of alcell lignin without binder polymers. *Advanced Materials*. 2007;19:4292-6.
80. Srivastava Y, Loscertales I, Marquez M, Throsen T. Electrospinning of hollow and core/sheath nanofibers using a microfluidic manifold. *Microfluid Nanofluid*. 2007;1-6.
81. Han X-J, Haung Z-M, He C-L, Liu L. Coaxial electrospinning of PC(shell)/PU(core) composite nanofibers for textile application. *Polymer Composites*. 2006;27:381-7.
82. Huang Z, Zhang Z, Ramakrishna S. Double-layered composite nanofibers and their mechanical performance. *Journal of Polymer Science Part B - Polymer Physics*. 2005;43(2852-2861).
83. Song T, Zhang Y, Zhou T, Lim CT, Ramakrishna S, Liu B. Encapsulation of self-assembled FePt magnetic nanoparticles in PCL nanofibers by coaxial electrospinning. *Chemical Physics Letters*. 2005;415:317-22.
84. Zhang YZ, Venugopal J, Haung Z-M, Lim CT, Ramakrishna S. Characterization of the surface biocompatibility of the electrospun PCL-collagen nanofibers using fibroblasts. *Biomacromolecules*. 2005.
85. Li D, Babel A, Jenekhe SA, Xia Y. Nanofiber of conjugated polymers prepared by electrospinning with a two-capillary spinneret. *Advanced Materials*. 2004;16(2062-2066).
86. Jiang H, Fridrikh SV, Rutledge GC. Production of submicrometer diameter fibers by two-fluid electrospinning. *Advanced Materials*. 2004;16:1562-6.
87. Li D, McCann JT, Xia Y. Use of electrospinning to directly fabricate hollow nanofibers with functionalized inner and outer surfaces. *Small*. 2005;1(1):83-6.
88. Li D, Xia Y. Direct fabrication of composite and ceramic hollow nanofibers by electrospinning. *Nano Letters*. 2004;4(5):933-8.
89. Xin Y, Huang Z, Li W, Jiang Z, Tong Y, Wang C. Core-sheath functional polymer nanofibers prepared by co-electrospinning. *European Polymer Journal*. 2008;34:2-16.
90. Zhang Y, Huang Z-M, Xu X, Lim CT, Ramakrishna S. Preparation of core-shell structured PCL-r-gelatin bi-component nanofibers by coaxial electrospinning. *Chem Mater*. 2004;16(18):3406-9.
91. Teo BK, Sun XH. From top-down to bottom-up to hybrid nanotechnologies: road to nanodevices. *Journal of Cluster Science*. 2006;17(4):529-40.
92. Teo WE, Ramakrishna S. A review on electrospinning design and nanofibre assemblies. *Nanotechnology*. 2006;17:R89-R106.
93. Reneker DH, Yarin AL. Electrospinning jets and polymer nanofibers. *Polymer*. 2008;49:2387-425.
94. Lyons J, Li C, Ko F. Melt-electrospinning part 1: processing parameters and geometric properties. *Polymer*. 2004;45:7597-603.

95. Kim SH, Kim S-H, Nair S, Moore E. Reactive electrospinning of cross-linked poly(2-hydroxyethyl methacrylate) nanofibers and elastic properties of individual hydrogel nanofibers in aqueous solutions. *Macromolecules*. 2005;38:3719-23.
96. Qi H, Hu P, Xu J, Wang A. Encapsulation of drug reservoirs in fibers by emulsion electrospinning: morphology characterisation and preliminary release assessment. *Biomacromolecules*. 2006;7:2327-30.
97. Arumuganathar S, Jayasinghe SN. Pressure-assisted spinning: A versatile and economical, direct fibre to scaffold spinning methodology. *Macromolecules Rapid Communication*. 2007;28:1491-6.
98. Wan Y, He J, Wu Y, Yu J. Vibrorheological effect on electrospun polyacrylonitrile (PAN) nanofibers. *Materials Letters*. 2006.
99. Theron A, Zussman E, Yarin AL. Electrostatic field-assisted alignment of electrospun nanofibres. *Nanotechnology*. 2001;12:384-90.
100. Fong H, Liu W, Wang C-S, Vaia RA. Generation of electrospun fibers of nylon 6 and nylon 6-montmorillonite nanocomposite. *Polymer*. 2002;43:775-80.
101. Dror Y, Salalha W, Avrahami R, et al.. One-step production of polymeric microtubes by co-electrospinning. *Small*. Volume 3, 2007.
102. Shenoy SL, Bates WD, Frisch HL, Wnek GE. Role of chain entanglements on the fiber formation during electrospinning of polymer solutions: good solvent, non-specific polymer-polymer interaction limit. *Polymer*. 2005;46:3372-84.
103. Wang M, Jing N, Su CB, Kameoka J. Electrospinning of silica nanochannels for single molecule detection. *Applied Physics Letters*. 2006;88.
104. Andradý AL. Factors affecting nanofiber quality. *Science and technology of polymer nanofibers*. 1st ed. New Jersey: John Wiley & Sons, Inc, 2008:81-109.
105. Megelski S, Stephens JS, Chase DB, Rabolt JF. Micro- and nanostructured surface morphology on electrospun polymer fibers. *Macromolecules*. 2002;35:8456-66.
106. Subbiah T, Bhat GS, Tock RW, Parameswaran S, Ramkumar SS. Electrospinning of nanofibers. *Journal of Applied Polymer Science*. 2005;96:557-69.
107. Larsen G, Spretz R, Velarde-Ortiz R. Use of coaxial gas jackets to stabilize Taylor cones of volatile solutions and to induce particle-to-fiber transitions. *Advanced Materials*. 2004;16(2):166-9.
108. Lopez-Herrera JM, Barrero A, Lopez A, Loscertales IG, Marquez M. Coaxial jets generated from electrified Taylor cones. *Scaling Laws. Aerosol Science*. 2003;34:535-52.
109. Tan S-H, Inai R, Kotaki M, Ramakrishna S. Systematic parameter study for ultra-fine fiber fabrication via electrospinning process. *Polymer*. 2005;46(16):6128-34.
110. Zeng J, Chen X, Xu X, et al.. Ultrafine fibers electrospun from biodegradable polymers. *Journal of Applied Polymer Science*. 2002;89:1085-92.
111. Stanger SS. Charge transfer mechanisms in electrospinning. *Canterbury: University of Canterbury*, 2008. 134 p.
112. Theron SA, Zussman E, Yarin AL. Experimental investigation of the governing parameters in the electrospinning of polymer solutions. *Polymer*. 2004;45(9):2889-99.

113. Moghbeli MR, Mohammadi N, Bagheri R, Ghaffarian SR. Wet spinning of low gel content SBR/PMMA core/shell particles dispersed in a good solvent for the shell. *Polymer*. 2003;44:4011-9.
114. Kessick R, Fenn J, Tepper G. The use of AC potentials in electrospinning and electrospinning processes. *Polymer*. 2004;45(9):2981-4.
115. Kalayci VE, Patra PK, Kim YK, Ugbolue SC, Warner SB. Charge consequences in electrospun polyacrylonitrile (PAN) fibers. *Polymer*. 2005;46(18):7191-200.
116. Katti DS, Robinson KW, Ko FK, Laurencin CT. Bioresorbable nanofiber based systems for wound healing and drug delivery: optimization of fabrication parameters. *Journal of Biomedical Materials Research Part B: Applied Biomaterials*. 2004;70B(2):286-96.
117. Reznik SN, Yarin AL, Zussman E, Bercovici L. Evolution of a compound droplet attached to a core-shell nozzle under the action of a strong electric field. *Physics of fluids*. 2006;18:1-13.
118. Smit E, Buttner U, Sanderson RD. Continuous yarns from electrospun fibers. *Polymer*. 2005;46:2419-23.
119. Smit AE; A yarn and a process for manufacture thereof PCT International Patent Application WO 2008/062264. 2008.
120. Casper CL, Stephens SS, Tassi NG, Chase DB, Rabolt JF. Controlling surface morphology of electrospun polystyrene fibers: effect of humidity and molecular weight in the electrospinning process. *Macromolecules*. 2003;37:573-8.
121. Srinivasarao M, Collings D, Philips A, Patel S. Three-dimensionally ordered array of air bubbles in a polymer film. *Science*. 2001;292:79-83.
122. Larsen G, Spretz R, Velarde-Ortiz R. Use of coaxial gas jackets to stabilize taylor cones of volatile solutions and induce particle-to-fiber transitions. *Advanced Materials*. 2004;16(2):166-9.
123. Wang X, Um IC, Fang A, Okamoto A, Hsiao BS, Chu B. Formation of water-resistant hyaluronic acid nanofibers by blowing-assisted electrospinning and non-toxic post treatments. *Polymer*. 2005;46(13):4853-67.



# Chapter 3

## *Experimental*

*This chapter describes the **materials, procedures and analyses** required for electrospinning solution preparation, fibre/yarn/film formation and the study of the resultant material properties. The methods and analyses used in this study have been compartmentalised into relevant sections*

*A method for monitoring the presence of a **coaxial Taylor cone and jet**, as a pre-requisite for continuous entrainment of the core during the coaxial electrospinning process is described. The formation of a **core-shell fibre structure** was then investigated by using a fluorescent microscopy and a new selective dissolution method. An investigation into the **effects of solution concentration and flow rate** on the resultant core shell fibre diameters and amount of crystallisable material entrained in the fibres is also described. **Single polymer composite yarns and films** were prepared to demonstrate potential applications of the core-shell fibres. The fine structure and mechanical properties of the yarns before and after thermal treatments were investigated. The fine structure of the films was investigated and the presence of the cores as reinforcement was explored.*



### 3.1. Electrospinning Inputs

#### 3.1.1. Raw Materials

The raw materials were used as received from the supplier. The materials were:

<i>Raw Material</i>	<i>Supplier</i>
<i>Electrospinning solutions</i>	
Poly(L-lactic acid) (PL24, $M_w \cong 291k^I$ g/mol)	Purac Biomaterials, Netherlands
Poly(D,L-lactic acid) (PDL20, $M_w \cong 265k^{II}$ g/mol)	
Analytical grade N,N Dimethylformamide (DMF) (98%)	Sigma Aldrich, South Africa
Industrial grade Dichloromethane (DCM)	Sasol Solvents, South Africa
<i>Selective dissolution method for core-shell structure validation</i>	
Analytical grade Ethyl acetate (99%)	Saarchem/Merck, South Africa
<i>Optical rotation measurements</i>	
Analytical grade Chloroform	Saarchem/Merck, South Africa
<i>Contrasting agents added to core polymer solution</i>	
DIANIX SBR blue disperse dye	Dye Star, South Africa

#### 3.1.2. Solution preparation

The range of concentrations and optimum solvent ratios for coaxial electrospinning solutions were determined by single-needle electrospinning experiments.<sup>III</sup> The results of these single-needle electrospinning experiments are detailed in Appendix A. From these studies it was determined that a DCM/DMF solvent ratio of 70/30 allowed the widest range of solution concentrations to be investigated. This solvent ratio allowed for good dissolution of both polymers and made for stable electrospinning solutions that displayed minimal blocking of the capillaries during electrospinning. This solvent

<sup>I</sup> Appendix D: Section D.3 Molecular mass determination of PLLA and PDLLA by GPC

<sup>II</sup> Appendix D: Section D.3 Molecular mass determination of PLLA and PDLLA by GPC

<sup>III</sup> Note: Additionally the use of a the Berry (*Be*) number as an *a priori* method to determine the solution concentrations that would yield bead-free electrospun fibres was investigated for the PLLA and PDLLA solutions made with 70/30 DCM/DMF solvent ratio (Appendix A).

ratio produced smooth fibres with the narrowest fibre diameter distributions compared with other solvent ratios for the concentration ranges studied.

PLLA and PDLLA solutions were prepared by first dissolving the polymer in DCM for 24hrs and later DMF was added to create solutions with a 70/30 volume/volume (vol/vol) solvent ratio combination of DCM/DMF. These solutions were stirred for 24hrs at room temperature (RT). The polymer solution concentrations are described in terms of weight percentage based on the solvent mass. Where applicable contrasting agents were mixed with the core solutions to discern the core from the shell solution in the Taylor cone. This was done to monitor the presence of the core-shell Taylor cone and coaxial jet when electrospinning (discussed in Section 3.3.3). Where contrasting agents were used, these materials were stirred with a small amount of DMF and mixed with the core solutions at RT for 24 hrs prior to spinning.

### 3.1.3. Materials and Equipment

In this section, the materials and equipment used for single- and coaxial-electrospinning are described as well as equipment used to monitor and control ambient conditions.

<i>Materials</i>	<i>Supplier</i>
1mL disposable syringes with plunger tips covered with thin aluminium foil	Various
1mL teflon plunger gas tight syringes	1000 series, Hamilton, USA
Disposable hypodermic blunted needle (0.49/0.81mm i.d./o.d. measured via optical microscopy)	Fine-Ject, Germany
PTFE tubing assembly with dual hub	24 guage, Hamilton, USA
Polypropylene female barbed luer lock (1.2mm i.d.)	1/16", 45500-50 Cole Parmer, USA

<i>Equipment</i>	<i>Supplier</i>
Custom built 50kV potential high voltage source (+25kV & -25kV)	Department of Electronic and Electrical Engineering, Stellenbosch University
Rotating wire-drum collector (18cm in length with 10cm diameter. Copper wires were parallel and spaced alternately 1 and 2cm apart)	
Programmable dual action syringe pump	Pump 33, Harvard Apparatus, USA
Portable thermo-hygrometer	Model 30.5015, Jörghöfer, Germany

### 3.1.4. Electrospinning environment (ambient conditions)

All electrospinning experiments were conducted in a fume hood under weak laminar flow. The temperature and humidity inside the fume hood was monitored at various intervals during the experiments with a portable thermo-hygrometer. Humidity was controlled between 40-55%rH.

## 3.2. Single-capillary Electrospinning

Single-capillary (or single-needle) electrospinning<sup>IV</sup> was used to study the electrospinnability of the solutions to be used in coaxial electrospinning.

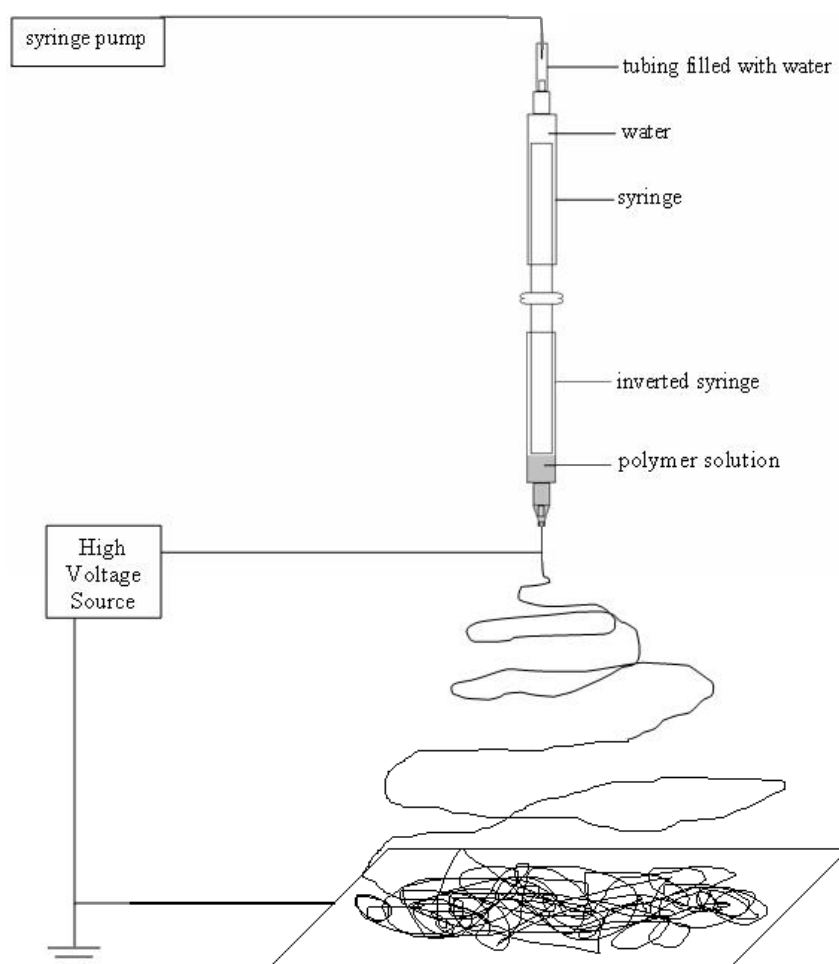
### 3.2.1. Set-up and Electrospinning Procedure

The single capillary electrospinning set-up is shown in Figure 3.1. A 1mL plastic syringe with an aluminium capped plunger was used as the solution reservoir. A blunt needle (0.49mm internal diameter/id) was used as the spinneret. A programmable syringe pump (Pump 33 Harvard Apparatus USA) connected to a home made hydraulic system (two syringes connected by tubing that is filled with water). The hydraulic system was used to translate the pumping action to the syringe carrying the polymer solution. The reason for using the hydraulic system was to reduce the amount (<1ml solution volumes) of polymer solution required for each experiment. The syringes used in the hydraulic system and those carrying the polymer solution were all equivalent 1ml syringes. The polymer solutions were brought to the needle orifice at

<sup>IV</sup> Appendix A: see for more detail on these experiments

1.5ml/h<sup>V</sup> solution flow rate. The high voltage source was used to generate electrostatic build-up within the polymer solution via the metal electrode attached to the needle.

An electric field was generated between the polymer solution and a grounded flat-aluminium-foil-coated collector. The spinning distance was 15cm in all experiments. A stable jet was obtained at each set of spinning conditions by adjusting the electrostatic potential (approximately 13.5-15.5kV). Intermittent blockage<sup>VI</sup> of the capillary tip from solvent evaporation was wiped clean with a paper towel affixed to a glass rod. Thin non-woven mats consisting of dry electrospun fibres were collected on the surface on a grounded counter electrode covered with aluminium foil.



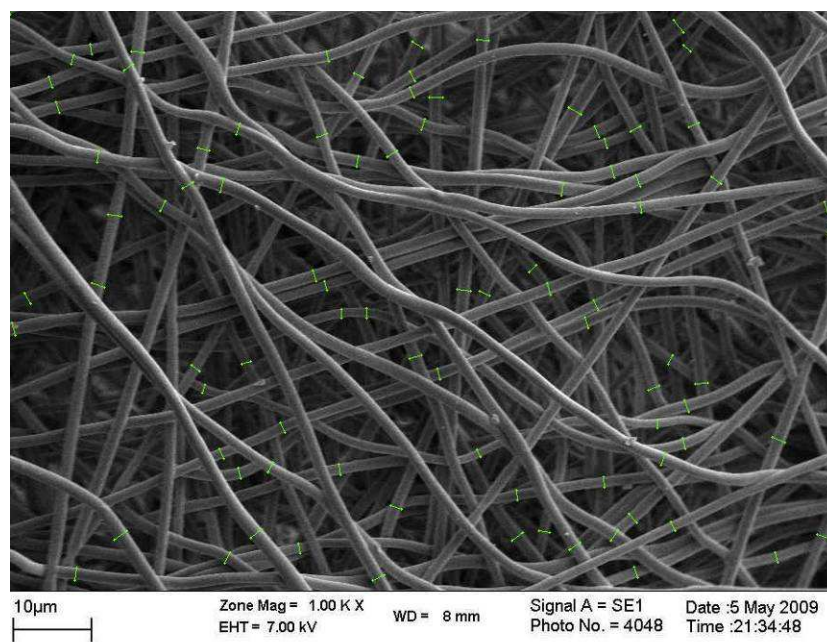
**Figure 3.1** *Single capillary electrospinning set-up*

<sup>V</sup> This flow rate was used for all single-capillary electrospinning experiments where not specified; the applied voltage was varied to provide stable electrospinning

<sup>VI</sup> A consequence of solvent evaporation and congealing of the polymer solution at the Taylor cone

### 3.2.2. Analysis of resultant fibre diameters: Scanning electron microscopy (SEM)

Sections cut from electrospun fibre mats and yarn specimens were fixed to SEM stubs. The samples were sputter-coated with gold for 2.5min. Imaging of the electrospun fibre mat samples and analysis of the fibre morphology were done using a Leo® 1430VP Scanning Electron Microscope (Central Analytical Facility, Stellenbosch University). The average fibre diameters were determined from analysis of the SEM images with custom image analysis software (SEM Image Studio). Three images per sample were captured at various locations on the yarns and approximately 100 measurements per image were taken (Figure 3.2).



**Figure 3.2** *Fibre diameter measurements on SEM image using SEM Image Studio software*

### 3.3. Coaxial electrospinning

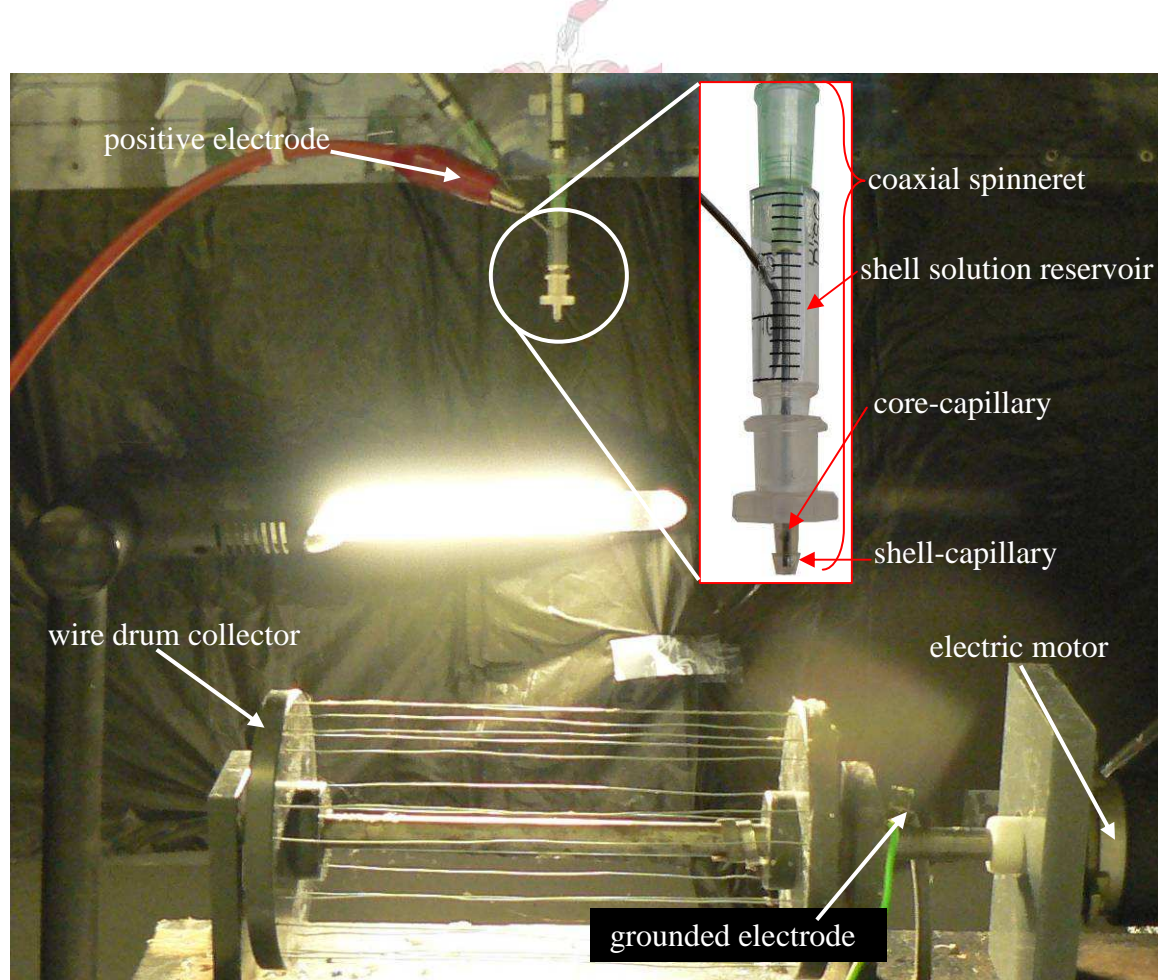
PLLA and PDLLA solutions, made with a 70/30 DCM/DMF solvent ratio, were used as core and shell solutions respectively. These solutions were miscible and precipitation of one component by the other component was not a concern. The miscibility of the solvents meant that there existed a low interfacial tension between the two solutions. The range of solution flow rates which gave stable coaxial electrospinning was determined experimentally. Stable electrospinning occurs when a



stable Taylor cone and continuous whipping jet is maintained. This occurs when the core-shell solution feed rates are balanced with the rate of spinning. The core solutions investigated were of sufficient viscosity that the viscous dragging forces from the shell solution were significant to pull the core along with it (via shearing force) and resulted in the continuous entrainment of the core into the electrospinning jet.

### 3.3.1. Set-up and Electrospinning Procedure

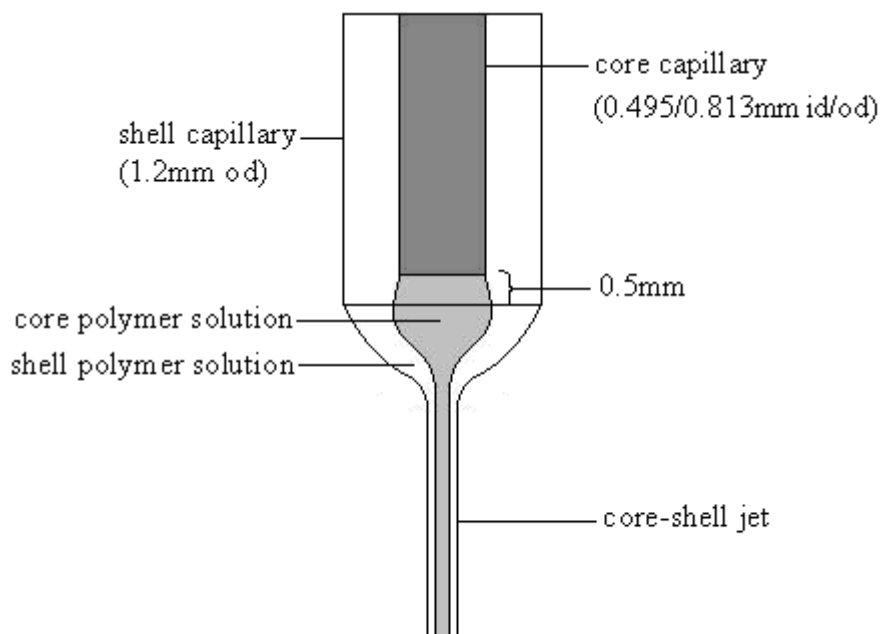
The coaxial electrospinning set-up (Figure 3.3) used consisted of five main components: a coaxial spinneret, hydraulic system, syringe pump, high voltage source and a rotating wire drum collector. This coaxial spinneret design is an adaptation of the popular concentric capillary-in-capillary used by research group of Professor E. Zussman<sup>1-3</sup> (Faculty of Mechanical Engineering, Technion, Israel Institute of Technology, Haifa, Israel) and other research groups.



**Figure 3.3** Coaxial electrospinning set-up and wire drum collector



The spinneret (Figure 3.4) had a core capillary with an inner- (id) and outer- diameter (od) of 0.49 and 0.81mm respectively. The inner diameter of the outer (shell) capillary was 1.2mm. The core capillary was retracted approximately 0.5mm within the orifice of the shell capillary. The core capillary in this configuration produced the most stable jet during electrospinning.



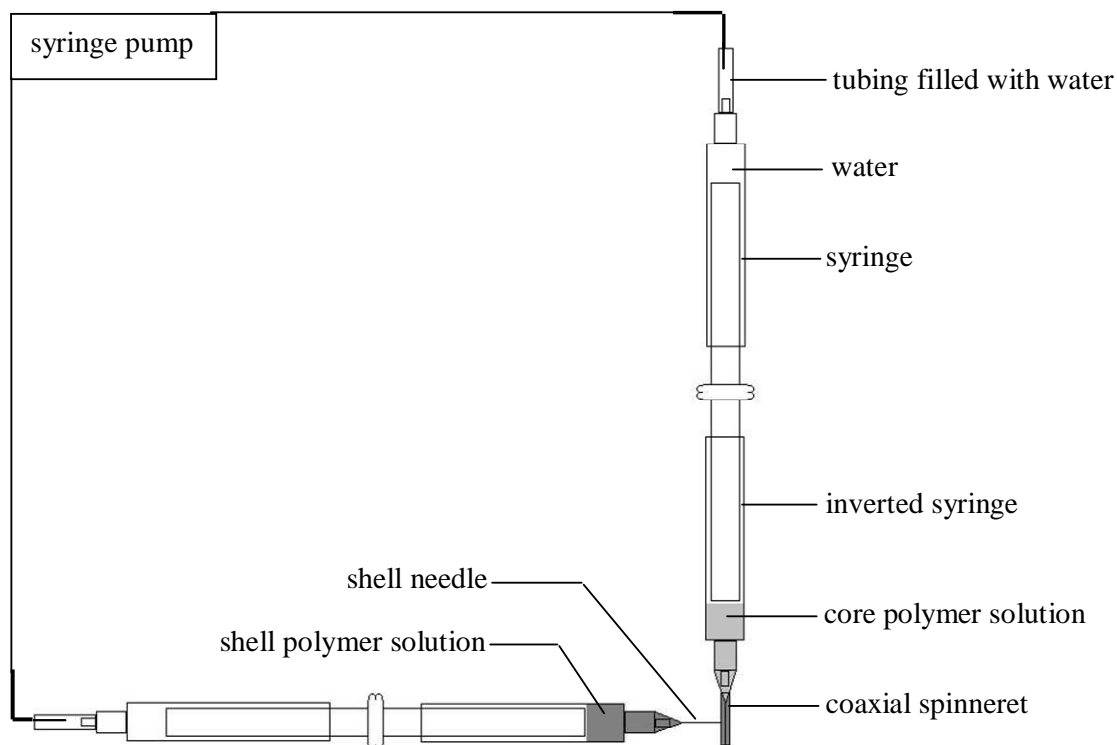
**Figure 3.4** *Capillary-in-capillary spinneret with compound Taylor cone and linear jetting region*

The PLLA core and the PDLLA shell solutions were independently pumped through the capillaries to produce a compound droplet at the tip of the coaxial spinneret (Figure 3.5).

The high voltage was applied to the shell solution capillary only, but the same electrical potential was transferred to the core capillary via contact with the needle feeding the shell capillary. A critical voltage (13.5-15.5kV depending on solution and processing parameters used) was therefore applied to the core-shell droplet and an electric field of approximately 1.kV/cm was maintained over a 15cm spinning distance.

Intermittent blockage of the spinneret tip was cleaned up with paper towel affixed to a glass rod. The fibre mats, consisting of bundles of aligned fibres, were made for each set of experimental conditions. These mats were collected on a rotating grounded wire

drum (Figure 3.4) using the gap alignment effect as used by Smit.<sup>4</sup> The wire drum was 18cm in length with a diameter of 10cm. The copper wires were parallel and were spaced alternately 1 and 2cm apart. The fibres were collected on the collector rotating at a linear velocity of approximately 1.8m/s). The ambient conditions were controlled within 20-25°C and 50-60% rH respectively. The formation of a compound Taylor cone and a coaxial jet was visually monitored as a control pre-requisite for the formation of core-shell fibres (Section 3.3.3).



**Figure 3.5** *Hydraulic system and coaxial spinneret*

### 3.3.2. Fibre collection and preparation of yarns

#### 3.3.2.1. Static collection

Electrospun fibres were deposited on a grounded aluminium foil covered substrate. A random non-woven assembly of fibres in an area that is roughly circular in shape was obtained.

#### 3.3.2.2. Dynamic collection

Electrospun fibres were initially deposited between the gaps of a grounded rotating wire drum collector. The gap alignment effect<sup>4,5</sup> and linear velocity of the collector

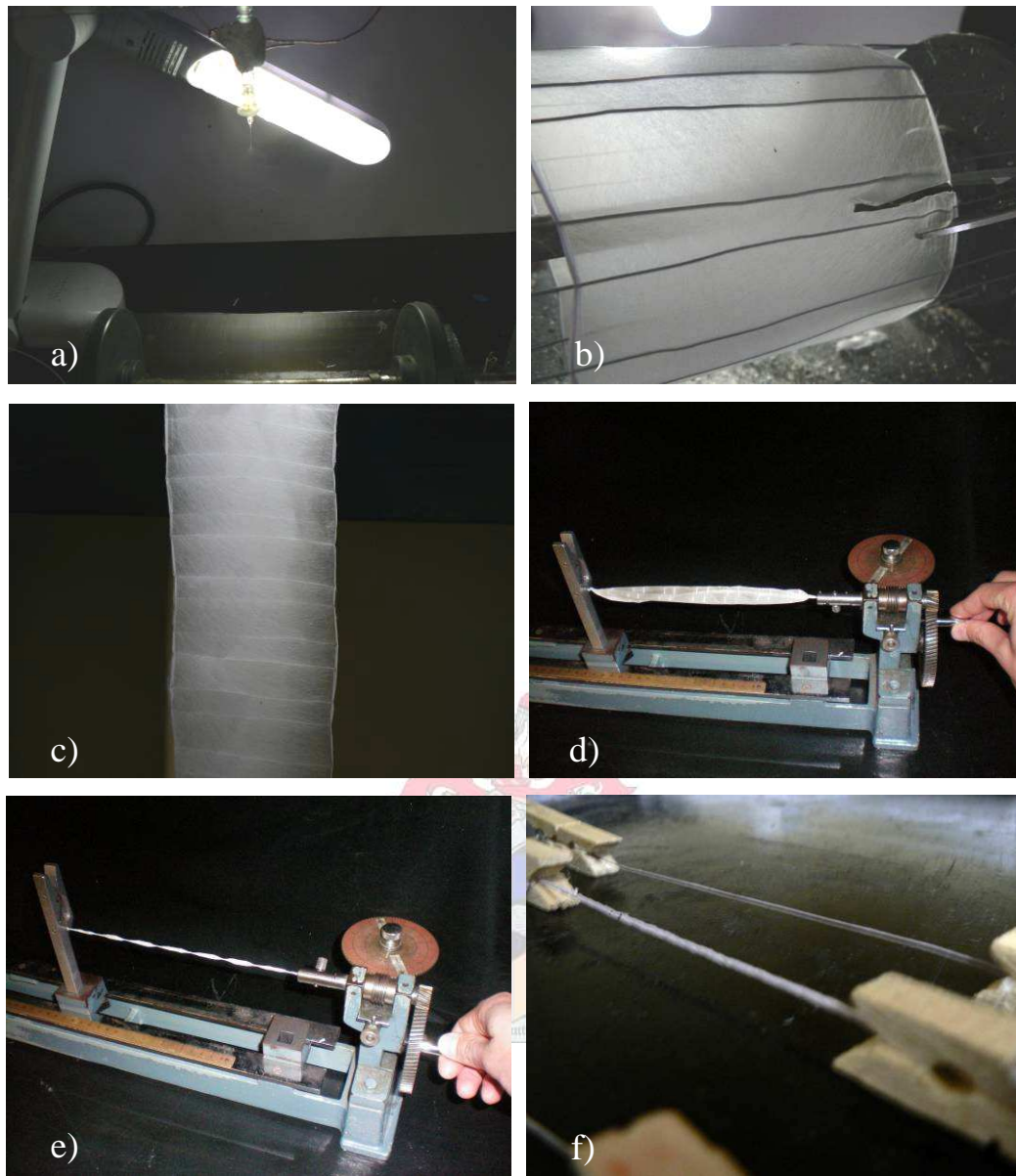
initially aligned the fibres parallel to one another. After some time the succeeding layers of fibres could not be pushed into alignment by the already gap aligned fibres as there was no space between the fibres already laid across the gaps. Further fibre additions were therefore only approximately aligned in the direction of the rotating direction as the charge repulsions of the deposited fibres and incoming fibres could not position the incoming fibres in a parallel fashion. The collector speed was controlled with an AC/DC converter which was calibrated with a digital meter to give the rotations speed (rpm). The linear velocity was calculated based on circumference of the wire drum. The conversions of voltage, rotation speed (rpm) and resultant linear velocity of the wire drum are given below:

**Table 3.1** Calibration data of DC voltage vs. linear velocity

DC voltage (V)	Digital reading (rpm)	Linear velocity (m/s)
4.5	162.5	0.85
6	234.5	1.23
7.5	342.5	1.80
9	410	2.15
12	495	2.60

### 3.3.2.3. Yarn formation

Electrospun fibre mats were removed from the wire drum collector by hand and twisted into short yarns (Figures 3.6 a-f) with 1.5 twists/cm in a mechanical yarn twisting device (ASANO Machine MFG 60, Osaka, Japan) and held taut by clamping. Yarns were used because of ease of handling and simple sample preparations for analysis.



**Figure 3.6** *Core-shell fibre yarn preparation by a) coaxial electrospinning on wire drum collector, b) rolling edges of the mat and cutting through the width of the mat, c) removing the mat from the collector, d,e) twisting the mat into a yarn, and f) maintaining the twist in the yarns by use of clamps*

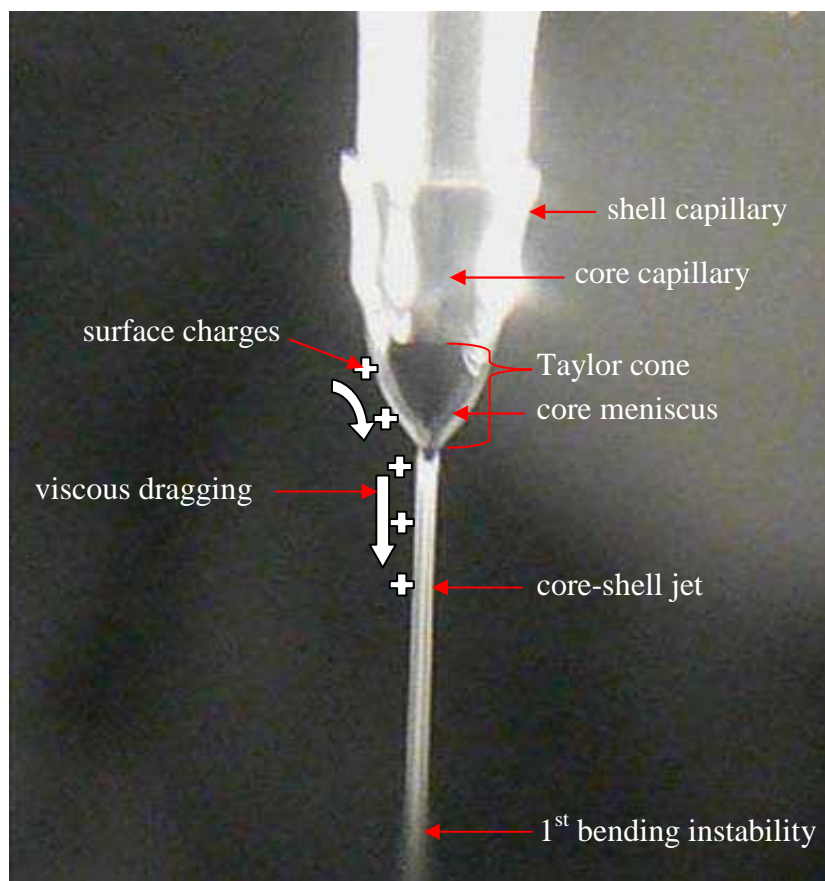
### 3.3.3. Process validation: coaxial Taylor cone and jet

The aim of visually monitoring the Taylor cone was to confirm the incorporation of the core fluid into the electrospinning shell fluid for coaxial electrospinning. It is reasonable to postulate that in the presence of a stable Taylor cone with two menisci, subsequent dragging of the core solution into the electrospinning shell solution jet stream will occur, and the presence of a core-shell jet should result in a stable coaxial electrospinning process. Stable coaxial electrospinning was postulated to be necessary for the formation of continuous core-shell fibres where the core is continuously entrained within the shell along the length of the fibre.

To study the compound Taylor cone a blue disperse dye was mixed with the core solution (0.1wt% based on dry polymer mass). The Taylor cone was viewed through a magnifying glass. A lamp was placed behind the spinning jet to refract light through the electrospinning jet to better monitor the narrow whipping jet. Prior to spinning, the concentricity of the inner capillary in relation to the shell capillary within the spinneret, was confirmed visually.

The shell solution was first fed into the coaxial spinneret to form a large pendent droplet. Electrospinning was initiated when the appropriate applied voltage was applied ( $\pm 15\text{kV}$ ). Once a stable electrospinning process (solution feed rate = spinning rate) was achieved with only the shell solution, the core solution was fed into the coaxial spinneret. When observing the Taylor cone through the magnifying glass, the blue core solution could be seen after some time exiting the core capillary orifice. The core solution experienced dye swell and after some amount of core solution had built up in the compound droplet, it was dragged into the jet of the electrospinning shell solution by viscous forces translated onto the core solution. A compound Taylor cone with two menisci was clearly seen in all cases (Figure 3.7).

The resultant fibres deposited on the wire drum collector were coloured (faint blue/purple colour) from the dye.



**Figure 3.7** Digital image showing the stable compound Taylor cone with two menisci, the core-shell jetting region and the onset of the first bending instability

### 3.3.4. Core-shell structure validation

Two strategies were used to analyse the core-shell fibre structure:

1. Tagging the core polymer with a fluorescent compound and analysing the core-shell fibres with fluorescent microscopy
2. Selective dissolution of the shell from the core-shell fibres and measurement of the fibre diameters before and after separation. The chemical composition of the separated polymer components were further confirmed by supporting analyses based on the differences in thermal properties and optical rotation of PLLA and PDLA.

#### 3.3.4.1. Fluorescent microscopy

The aim of tagging the core polymer with a fluorescent compound (rhodamine B) was to observe the presence of that compound continuously along the length of the fibre and thereby confirm the likely existence of a core-shell fibre structure. Continuous

entrainment of the core by the shell along the entire length of the fibre is not always achieved as a result of varicose break-up of the core solution or splitting of the core and shell solutions into separate jets).<sup>6-9</sup> Fluorescent microscopy of the core-shell fibres was expected to shed light on the manner in which the core was entrained into the fibre (if at all). Since the Rhodamine B was only attached to one end of the high molecular ( $M_w \cong 291k$ ) PLLA polymer chains, the intensity of the fluorescence was expected to be relatively mild. The fluorescent labelling was also not expected to significantly affect the solution properties of the core polymer.

An earlier attempt to validate the core-shell structure by mixing, as opposed to covalent bonding, 0.01wt% (based on dry polymer mass) rhodamine B into the core solution and analysing the fibres with fluorescent microscopy was not successful. The fluorescence was too intense and the fibres were completely masked under fluorescent microscopy.

Fluorescent agent Rhodamine B was covalently bonded to the PLLA core polymer solution (for reaction scheme see Appendix D: Section D.1). Coaxial fibres were collected on glass slides by intercepting fibres in their flight path between the spinneret and collector during electrospinning. Image acquisition of the fibres was performed on an Olympus Cell<sup>R</sup> system attached to an IX 81 Inverted fluorescence microscope equipped with a F-view-II cooled CCD camera (Soft Imaging Systems). Using a Xenon-Arc burner (Olympus Biosystems GMBH) as light source, images were acquired using the 572nm excitation filter. Emission was collected using a UBG triple-bandpass emission filter cube (Chroma). Images were acquired using an Olympus Plan Apo N60x/1.4 Oil objective and 1.6x lens. The fibres were analysed at an excitation wavelength of 479nm (specified for Rhodamine B) at 100X magnification.

#### 3.3.4.2. Selective dissolution method: core-shell fibre structure validation

##### i) *Background*

As stated earlier, transmission electron microscopy (TEM) and light microscopy could not be used in this study to validate the core-shell fibre structure of the fibre prepared by coaxial electrospinning. The various approaches evaluated for direct visualisation



of the core shell structure using TEM and other methods are documented in Appendix B. A new selective dissolution method was used to validate the core-shell fibre structure of the fibres.

*ii) Overview*

PLLA-core/PDLLA-shell solutions were coaxially electrospun into fibre mats (electrospinning parameters Table 3.2). Twisted core-shell fibre yarns were washed in ethyl acetate which is a solvent for PDLLA and not PLLA. Fibre mass before and after washing in ethyl acetate was measured and compared with theoretical mass yield calculations. The fibre diameters before and after exposure to ethyl acetate were measured using scanning electron microscopy. The remaining fibres and the polymer dissolved in ethyl acetate were dried. The separated materials analysed with differential scanning calorimetry (DSC) and optical rotation measurements (after each component was re-dissolved in 5ml chloroform).

**Table 3.2** *Coaxial electrospinning parameters*

Designation	Polymer Solutions	Polymer Conc. (wt%)	Flow Rate (ml/h)	Applied Voltage (kV)	Distance (cm)	Collector Speed (m/s)	Temp. & Humidity
Core	PLLA 70/30 DCM/DMF	8	0.3	15.5	15	1.23	20-24°C / 40- 50%rH
Shell	PDLLA 70/30 DCM/DMF	10	1.2				

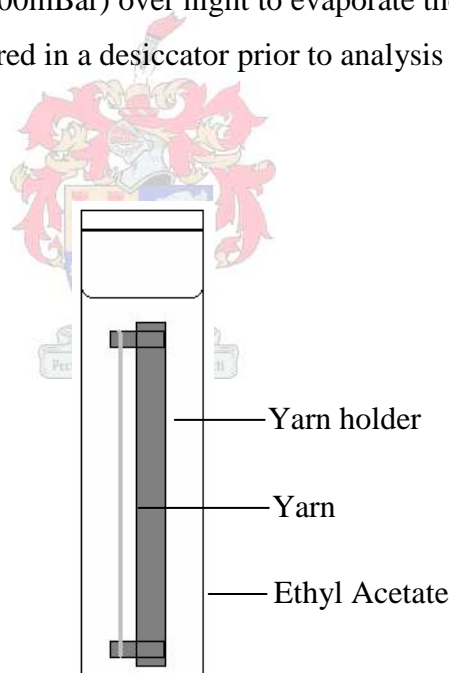
It was postulated that if,

- coaxial electrospinning occurs with a stable coaxial Taylor cone and jet,
- and the mass and fibre diameters of the core-shell fibres decrease after washing in ethyl acetate,
- so that one polymer is dissolved in ethyl acetate and the other remains in fibrous form,
- and the polymer selectively dissolved displays neither optical rotation nor a melt endotherm,
- and the fibres remaining on the yarn holders rotate light and display a melt endotherm,

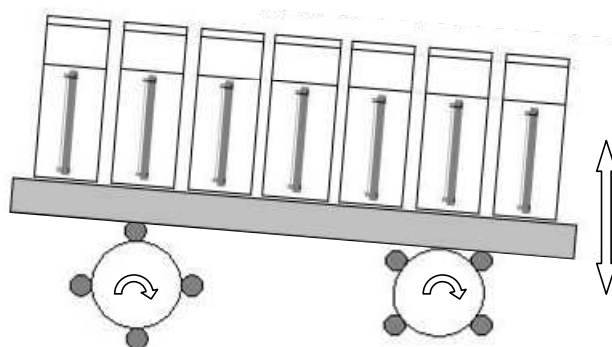
then the polymer that was selectively dissolved is PDLLA and the remaining fibres are PLLA. It is then reasonable to propose that the initial fibres have a core-shell structure with a continuous PLLA core entrained in a PDLLA shell.

*iii) Procedure*

The twisted yarns were secured under tension in a clamping device (herein referred to as the yarn holder). The yarn holders were immersed into glass poly-tops filled with ethyl acetate (Figure 3.8). The poly-tops were subjected to two washing steps to dissolve the PDLLA shell: (1) slow rocking action (Figure 3.9) at room temperature for 2hrs and (2) replacing initial ethyl acetate with clean ethyl acetate followed by sonication for 30mins in an ultra-sonic bath (50Hz) and rocking for another 2hrs. Steps 1 and 2 were repeated three times. The yarns before and after washing with ethyl acetate as well as the ethyl acetate solutions were placed in a vacuum oven at room temperature (vacuum of 100mBar) over night to evaporate the ethyl acetate. The dried polymer samples were stored in a desiccator prior to analysis



**Figure 3.8** *Yarn holder with yarn in poly top filled with ethyl acetate*



**Figure 3.9** *Rocking action administered to poly tops*

iv) *Analyses*

**Gravimetry**

The mass of the coaxial electrospun yarns before and after selective dissolution with ethyl acetate were measured. The theoretical mass of the cores and core-shell fibres were calculated as follows:

$$\text{Theoretical Mass (g)} = \text{Flow rate (ml/h)} * \text{Spinning duration (h)} * \text{concentration of the polymer solution (g/ml)}$$

**Scanning Electron Microscopy (SEM)**

The electrospun fibre mats were collected on a wire drum collector and were twisted into yarns. Three yarns for each experimental condition were prepared and therefore approximately 900 fibre diameter measurements per sample were made (100 measurements per image X 3 images per specimen X 3 yarn repeats = 900). Only fibres with clearly defined boundaries were measured. The fibre diameter measurements before and after washing in ethyl acetate were carried out as described in Section 3.2.2.

**Optical rotation**

Optical rotation measurements were performed for the separated fibre components (the remaining fibres on the yarn holders and the polymer extract recovered from ethyl acetate) after re-dissolution in chloroform, using a polarimeter (Bellingham & Stanley Ltd ADP 220). The average of three optical rotation measurements was taken for the each separated component for each yarn sample. A 100mm sample tube was

used and measurements were recorded at room temperature (RT) at a nominal wavelength 589nm. The specific optical rotation was calculated as follows,

$$[\alpha]_{\lambda}^{\theta} = \frac{\alpha}{\gamma.l}$$

where  $\alpha$  is the angle of rotation in rad,  $\gamma$  is the mass concentration in  $\text{kg/m}^3$ , and 'l' is the length of the sample tube in m.

### Differential scanning calorimetry (DSC)

Differential scanning calorimetry (DSC) measurements (TA Instruments Q100) were conducted under nitrogen atmosphere. 5-10mg samples were sealed in aluminum pans for the measurements. The samples were heated from 10 to 200°C at a rate of 10°C/min, held at 200°C for 1 min, and cooled at the same rate to 10°C. This cycle was repeated twice. The percentage crystallinity was determined using TA Universal Analysis software: by calculating the area under the melt endotherm of the thermogram and using 93.7J/g as the heat of fusion for a theoretical 100% crystalline PLLA material.<sup>10</sup> The percentage crystallinity was determined using equation

$$\chi\% = \Delta H_f / \Delta H_{of} \times 100\%$$

where  $\chi\%$  is the percentage crystallinity,  $\Delta H_f$  area under the melt endotherm (J/g) from DSC thermograms and  $\Delta H_{of}$  is the theoretical heat of fusion value of 100% crystalline PLLA polymer material which is taken to be 93.7J/g.<sup>10</sup> The area of the melt endotherm was calculated for the 1<sup>st</sup> heating cycle in DSC of the samples as the areas obtainable from the second heating cycle, (i.e. for the study of parameter effects on crystallisable material present in the yarn) were too small as the result of dilution effects of PDLA on PLLA crystallisation.<sup>11</sup>

### 3.3.5. Parameter Effects

#### 3.3.5.1. Effect of solution concentration and flow rate on core-shell fibre diameters

The aim of these experiments was to investigate the effects of

- A. polymer solution concentration and
- B. polymer solution flow rate

on the resultant core-shell fibre diameters prepared by coaxial electrospinning. The parameter effects investigated are shown in Table 3.3.

The importance of varying the core-shell fibre diameters can be seen in tissue engineering applications. Control over the mechanical properties and degradation rate of the fibres in tissue scaffolds is vital. The balance between these will determine the success of the tissue repair. The scaffold should provide specific mechanical support until the tissue cells are seeded and eventually proliferate.<sup>12</sup> The fibre diameters are closely correlated with the material surface area and fluid permeation. These properties influence the hydrolytic degradation of the hydrophobic PLA polymer.

It was postulated that increases in the core solution concentration and core flow rate would have the effect of making more PLLA polymer material available in the region of the compound Taylor cone where viscous dragging (of the shell solution) can be experienced. Increasing the core solution concentration and/or core solution flow rate was expected to lead to an increase in the core diameter (the amount of crystallisable material in the core-shell fibres) as well as the total diameter of the core-shell fibre. Furthermore, it was expected that an increase in the amount of core material entrained in the shell could be shown by an increase in crystallinity measured by DSC of core-shell fibres.

Increasing the shell solution concentration and shell solution flow rate was expected to lead to an increase in the shell thickness as well as the total core-shell fibre diameter. This would mean that, by weight, less crystallisable material would be present in the fibres with the higher shell solution concentration and/or flow rates.

The selective dissolution method (Section 3.3.4.2) was used to confirm that core-shell fibres were obtained in all cases. Additionally it would be used to investigate the effects of various process parameters on the diameters of the resulting core shell fibres. The change in core and total fibre diameters were measured from SEM images, the change in core fractions in core-shell fibres was investigated by DSC analysis of the as-spun core-shell fibres, and the change in mass of both components was measured. Three mats (repeats), per variable, were spun for exactly 20mins and twisted (1.5 twist/cm) into yarns.

**Table 3.3** *Coaxial electrospinning parameters*

Experiment	no	Core wt% Conc.	Shell wt% Conc.	Core flow rate (ml/h)	Shell flow rate (ml/h)
<b>A</b>	1	4%	10%	0.3	1.2
	2	6%	10%	0.3	1.2
	3	8%	10%	0.3	1.2
	4	4%	12%	0.3	1.2
	5	6%	12%	0.3	1.2
	6	8%	12%	0.3	1.2
<b>B</b>	7	8%	10%	0.1	1.2
	8	8%	10%	0.2	1.2
	9	8%	10%	0.3	1.2
	10	8%	10%	0.1	1.4
	11	8%	10%	0.2	1.4
	12	8%	10%	0.3	1.4

### 3.3.6. Applications of core-shell fibres: Properties of yarns and films

Potential applications of the core-shell fibres are found in the preparation of yarns and films for applications that require biodegradable reinforced composite structures e.g. medical implants and recyclable hygiene products.<sup>13,14</sup>

The fine structure and mechanical properties of the yarns before and after thermal treatments were investigated by DSC, x-ray diffraction (XRD) and mechanical

testing. The selective dissolution method (Section 3.3.4.2) was used to ensure that core-shell fibres were produced in all cases and also to prove that the cores acted as a reinforcement for the film. SEM was used to investigate the yarn surface morphology before and after heating.

The fine structure of the films were analysed by DSC and XRD. One section of the film was immersed in ethyl acetate for 48hrs. The ethyl acetate was circulated around the film by stirring. It was assumed that if a PDLA film reinforced by PLLA core fibres was obtained, that washing the one half of the film in ethyl acetate would expose the core fibre components as well as selectively dissolve the PDLA matrix from that half of the film. Additionally if this was true fracturing the film would expose the core fibres at the point of fracture. SEM was used to study the fibre diameters of the mats before film formation, the reinforcing fibres after selective dissolution of the PDLA from the prepared SPC films and also the point of fracture of cryo-fractured SPC films.

#### 3.3.6.1. Thermal treatments

##### *i) Yarns*

Initial DSC analysis in this work showed that cold crystallisation of electrospun PLLA occurs below 100°C. Although some crystallinity may exist during electrospinning, additional crystallisation can be induced by post heating yarns under tension above this temperature. The yarns were held under tension by tape or clamps and were placed in a convection oven set at 110°C for 5h. The yarns were removed from the oven and allowed to condition in a standardised air-conditioned laboratory (standard temperature: 20 ± 2 °C and relative humidity 65 ± 2%) prior to analysis by SEM, DSC, XRD and mechanical testing.

##### *ii) Films*

Core-shell fibre mats, each plied ten times, were processed into transparent films by pressing between two metal plates at 110°C under 10kN pressure for 30mins in hot-press. It was postulated that with temperature and pressure that shell components would flow and fill in the spaces between the fibres. At the same time the core fibre crystallinity would be enhanced through cold-crystallisation (at the isothermal



crystallisation temperature) of the oriented molecules. It was expected that the film would be transparent as the two materials have similar optical refraction indices, are in intimate contact at their interface and because the core fibrous reinforcement was expected to be in the nano-diameter scale.

### 3.3.6.2. Analyses: Yarns and Films

#### *i) Cryo-fracture*

It was expected that if the shell components fused and the cores reinforce the film then, on fracturing the films, the cores should protrude by some small degree at the point of fracture. Films were cryo-fractured under cryo conditions (liquid nitrogen  $\cong -196^{\circ}\text{C}$ ) and the point of fracture was analysed by SEM. The point of fracture of the SPC film was compared to that of a film prepared from a PDLA mat spun by single-capillary electrospinning.

#### *ii) Light Microscopy*

Fibres and films placed on glass slides were analysed under 400X magnification with light microscopy. (Olympus CX31, JVC Colour Video Camera, Compro DTV 4 image software, Japan)

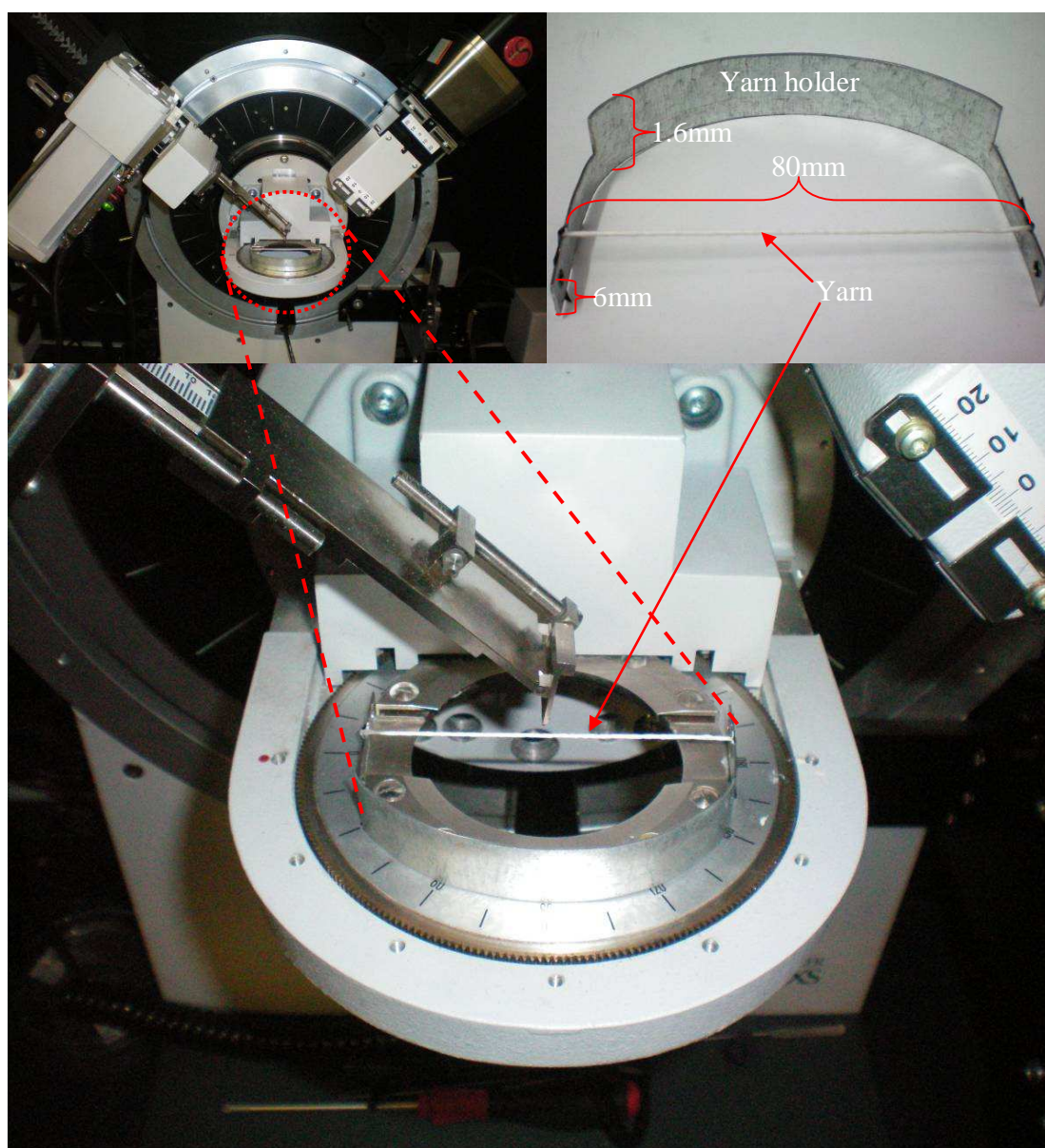
#### *iii) DSC and Modulated Differential Scanning Calorimetry (MDSC)*

Yarns and films were analysed by DSC and MDSC. DSC analysis was carried out as described earlier. MDSC was used to study reversing and non-reversing thermal events. Samples were heated from 10-200 $^{\circ}\text{C}$  with a step ramp rate of amplitude 1 $^{\circ}\text{C}$  and a period of 6seconds. The underlying heating rate was 1 $^{\circ}\text{C}/\text{min}$ .

#### *iv) X-ray Diffraction*

The internal molecular structure of the polymers (yarns and film) was investigated by 2D wide-angle x-ray diffraction (WAXD) (Instrument: BRUKER AXS D8 Advance diffractometer) with Cu-  $K\alpha_1$  radiation ( $\lambda K\alpha_1=1.5406\text{\AA}$ ) source and PSD Lynx-Eye, Si-strip detector (196 channels). In the case of XRD analysis of yarns a custom made yarn holder (Figure 3.10) was fabricated to eliminate any background effects from conventional supports (e.g. glass slides can give an amorphous halo that overlaps with significant peaks in the diffractograms). The yarn was positioned in one plane and is

parallel to the x-ray source. The yarn was held straight at both ends of the yarn holder by adhesive tape. Films and polymer chips were analysed on a glass slide support. WAXD settings: tube voltage 40kV, tube current 40mA and variable slits V12. The angles scanned in the  $2\theta$  range were between  $5 - 35^\circ$  in increments  $\Delta 2\theta$  of 0.01 deg/step. The software used was EVA software from BRUKER.



**Figure 3.10** Custom yarn holder with yarn parallel to radiation in the BRUKER AXS D8 Advance diffractometer

v) Mechanical testing

The mechanical behaviour of dried, twisted yarns was examined using an INSTRON 4444 with an INSTRON Max 50N Load Cell. Flat pneumatic action grips with a

50mm grip width were used to clamp the yarns in place. The accompanying INSTRON series IX software for windows (Merlin Version) processed the instrumental data automatically. Yarn samples were conditioned for 24 hours in a standardized climate controlled laboratory (standard temperature:  $20 \pm 2$  °C and relative humidity  $65 \pm 2\%$ ) prior to mechanical testing. 70mm test specimens (50 mm test length plus 10 mm for grips) were cut from yarn sections that appeared uniform (visually inspected). The yarns were mounted into a paper frame template (Figure 3.11) to allow the yarn to be mounted parallel and taut in the direction of mechanical testing. Once mounted the two sides of the template frame were cut on the dotted lines and the measurement commenced.

Determination of the single-end breaking force and elongation at break of yarns was followed at a constant-rate-of-extension 50mm/min and the load-displacement measurements were obtained. The cross-sectional area was calculated from the yarn diameters measured from the SEM images.

The modulus (E), tensile strength and elongation for each yarn were calculated using the following equations:

**Modulus:**

$$E = \frac{\text{tensile stress}}{\text{tensile strain}} = \frac{F / A_0}{\Delta L / L_0}$$

where

$E$  is the Young's modulus measured in Pascals (or  $\text{N/m}^2$ )

$F$  is the force applied to the object (N)

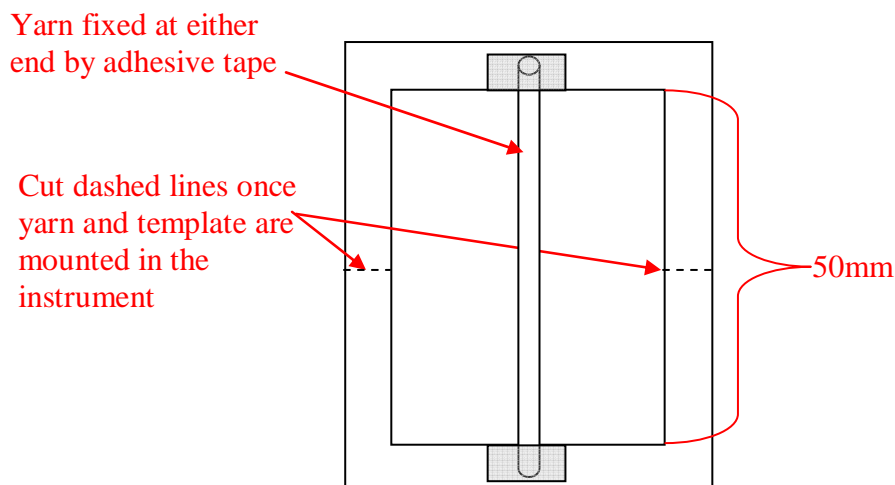
$A_0$  is the original cross-sectional area of the yarn ( $\text{m}^2$ )

$\Delta L$  is the displacement at maximum load (m)

$L_0$  is the original length of the yarn test specimen (m).

**Tensile strength** = Max load / Cross-sectional area =  $F/A_0$

**Elongation** = (Displacement at maximum load ÷ Original length of specimen) x 100  
 =  $\Delta L/L_0 \times 100$

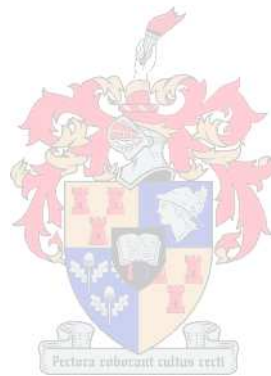


**Figure 3.11** Template with yarn mounted with tape for mechanical testing

#### References

1. Sun Z, Zussman E, Yarin AL, Wendorff JH, Greiner A. Compound core-shell polymer nanofibers by co-electrospinning. *Advanced Materials*. 2003;15(2003):1929-32.
2. Yarin AL, Zussman E, Wendorff JH, Greiner A. Material encapsulation and transport in core-shell micro/nanofibers, polymer and carbon nanotubes and microchannels. *Journal of Materials Chemistry*. 2007;17:2585-99.
3. Greiner A, Wendorff JH, Yarin AL, Zussman E. Biohybrid nanosystems with polymer nanofibers and nanotubes. *Applied Microbiology Biotechnology*. 2006;71:387-93.
4. Smit AE; A yarn and a process for manufacture thereof PCT International Patent Application WO 2008/062264. 2008.
5. Teo WE, Ramakrishna S. A review on electrospinning design and nanofibre assemblies. *Nanotechnology*. 2006;17:R89-R106.
6. Sun B, Duan B, Yuan X. Preparation of core/shell PVP/PLA ultrafine fibers by coaxial electrospinning. *Journal of Polymer Science*. 2006;102:39-45.
7. McCann JT, Marquez M, Xia Y. Melt coaxial electrospinning: a versatile method for the encapsulation of solid materials and fabrication of phase change nanofibers. *Nano Letters*. 2006;6(12):2868-72.
8. Diaz JE, Barrero A, Marquez M, Loscertales I. Controlled encapsulation of hydrophobic liquids in hydrophilic polymer nanofibers by co-electrospinning. *Advanced Functional Materials*. 2006;16:2110-6.
9. Moghe AK, Gupta BS. Co-axial electrospinning for nanofiber structures: preparation and applications. *Polymer Reviews*. 2008;48(2):353-77.
10. Gupta BS, Revagade N, Hilborn J. Poly(lactic acid) fiber: An overview. *Progress in Polymer Science*. 2007;32:433-82.
11. Pan P, Liang Z, Zhu B, Dong T, Inoue Y. Blending effects on polymorphic crystallization of poly(L-lactide). *Macromolecules*. 2009;42:3374-80.
12. Li W-J, Cooper Jr JA, Mauck RL, Taun RS. Fabrication and characterization of six electrospun poly( $\alpha$ -hydroxy ester)-based fibrous scaffolds for tissue engineering applications. *Acta Biomaterialia*. 2006;2:377-85.

13. Yao D, Li R, Nagarajan P. Single-polymer composites based on slowly crystallizing polymers. *Polymer Engineering and Science*. 2006;46:1223-30.
14. Barrows TH; Bioabsorbable fibers and reinforced composites produced therefrom PCT International Patent Application WO/1999/034750. 1999.





## Chapter 4

### **Results and Discussion: Coaxial Electrospinning**

*This chapter presents the results and the discussion of the use of coaxial electrospinning to prepare PLLA-core/PDLLA-shell fibres and the methods developed to validate the core-shell structure of the same. The influence of solution concentration and flow rate of the coaxial electrospinning solutions on the diameters of the fibres is shown and discussed.*

**Note:** In reporting of the experimental results in the following sections, various figures, tables, etc have been included to illustrate different trends and observations. In many instances though, the results obtained for various sets of experimental conditions were very similar and the trend observed could be sufficiently described using the figure/table for one set of experimental conditions. In these cases, it was deemed unnecessary and in some cases even disruptive to also include the very similar figures/tables for the other similar sets of experimental conditions (e.g. effect of flow rate on fibre diameters at both shell solution concentrations of **10 and 12 wt%**). For completeness sake these figures and tables have been included, but they have been moved to various Appendices at the back of the text so as not to disrupt the normal flow of the main text. In instances where this has been done, cross references in the form of footnotes have been included to direct the reader to the relevant Appendix where additional information can be found. The footnote references in the text takes the form of small Roman numerals, e.g. I, II, III, etc.

#### **4.1. Core-shell structure validation**

Transmission electron microscopy (TEM) is classically used to study the core-shell structure of fibres prepared by coaxial electrospinning.<sup>1,2</sup> In this study a significant amount of work was done to evaluate SEM, TEM and light microscopy as possible techniques to analyse the core-shell fibre structure. The findings from this work are documented in great detail in Appendix B. Problems arose when using SEM and TEM for analysing PLLA-core/PDLLA-shell fibres. The fibres were extremely sensitive to the radiation of the electron beam. This could be attributed to the intrinsic radiation sensitivity of PLA polymer, coupled with the release of frozen-in molecular stress (in

the axial direction during electrospinning), under the electron beam irradiation. The fibre diameters (averaging 500-2000nm) were at the upper limit for transmission of electrons in TEM and at the lower limit of resolution for light microscopy. This meant that most samples were too thick to allow electron transmission in TEM and on the other hand were too small to be resolved by light microscopy. Under certain circumstances the fibres were stable and small enough to allow transmission under the electron beam in TEM analysis. These fibres, however, showed little or no contrast between what might have been the core and shell components. This poor contrast was attributed to the similar electron densities existing for the core and shell components as both are made from polymers with the same chemical groups that, as-spun, are non-crystalline. A poor interfacial boundary for the core and shell components as a result of the core and shell solution miscible would have also contributed to the poor contrast between the two components. Various approaches were also used to reduce the effects of the electron beam on fibres and to enhance the contrast between the core and shell components (Appendix B). The results of these approaches were inconclusive.

Although these attempts proved mostly unsuccessful, as anticipated, there was however some evidence for the existence of core-shell fibre structure. This however was inconclusive. Alternative strategies were required to analyse the core-shell fibre structure.

As described in Chapter 3, two alternative strategies were used to analyse the core-shell fibre structure:

1. **Tagging the core** polymer with a fluorescent compound and analysing the core-shell fibres with fluorescent microscopy
2. **Selective dissolution of the shell** from the core-shell fibres and measurement of the fibre diameters before and after separation. The chemical composition of the separated polymer components were further confirmed by supporting thermal and optical rotation analyses.

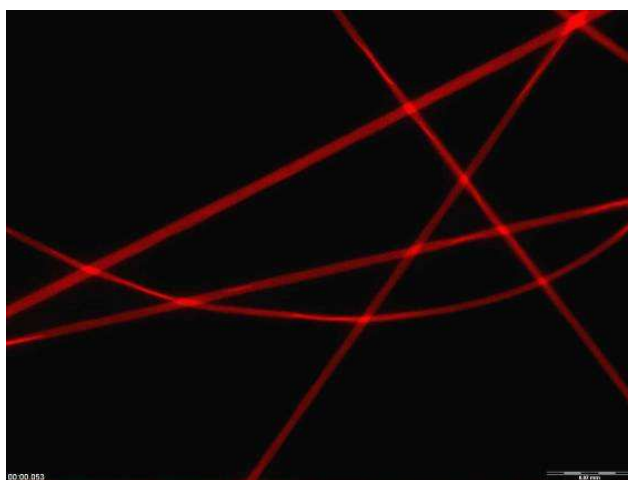


#### 4.1.1. Fluorescent microscopy

After covalently coupling the rhodamine B to PLLA, the polymer appeared a very faint pink colour after washing. This shows that the polymer was washed well and that the unreacted rhodamine B was removed (usually it is an intense red or bright pink when concentrated in the fibres).

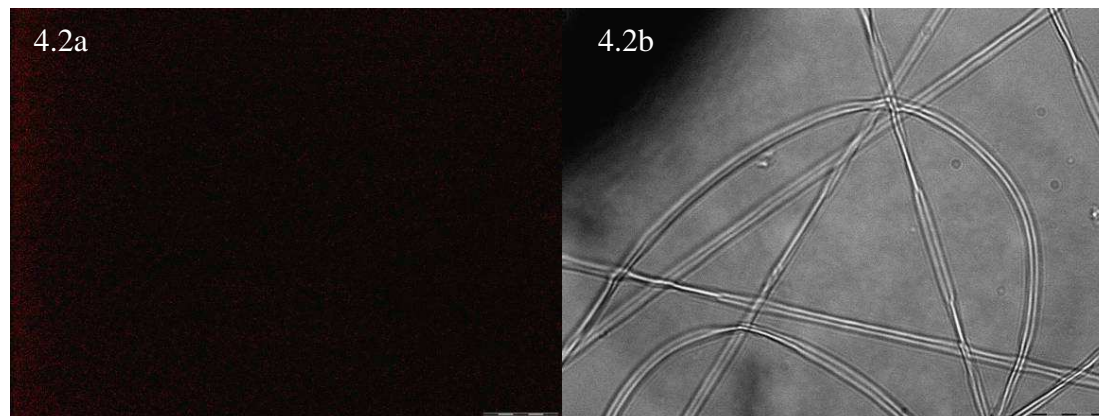
Single capillary electrospinning of PLLA-rhodamine B dissolved in 70/30 DCM/DMF was performed as a control. Coaxial electrospinning of un-labelled PLLA and PDLLA as the core and shell solutions respectively were carried out as a reference. PLLA(rhodamine B)-PDLLA core-shell solutions were coaxially electrospun with core solution flow rates of 0.1ml/h and 0.3ml/h whilst maintaining a constant shell flow rate (1.2ml/h). The two different core solution flow rates were used in an attempt to prepare fibres with different fluorescent intensities. It was hypothesised that the fibres spun with a lower core solution flow rate could potentially yield a less intense fluorescent glow as a result of a thinner core.

Single capillary electrospinning of PLLA-rhodamine B fluoresced with an intense red colour under excitation (Figure 4.1). The reference, of coaxially electrospun un-labelled PLLA and PDLLA as the core and shell solutions respectively clearly showed that, without coupling of fluorescent agent rhodamine B, the fibres showed no fluorescence (Figures 4.2 a) and b)).



**Figure 4.1** *Fluorescent image of electrospun PLLA-rhodamine B fibres under 100X magnification (0.02mm scale bar)*

Increasing the core solution flow rate did not lead to an increase in fluorescent intensity.<sup>I</sup> It is likely that a larger amount of fluorescent material would be required to see a noticeable difference.



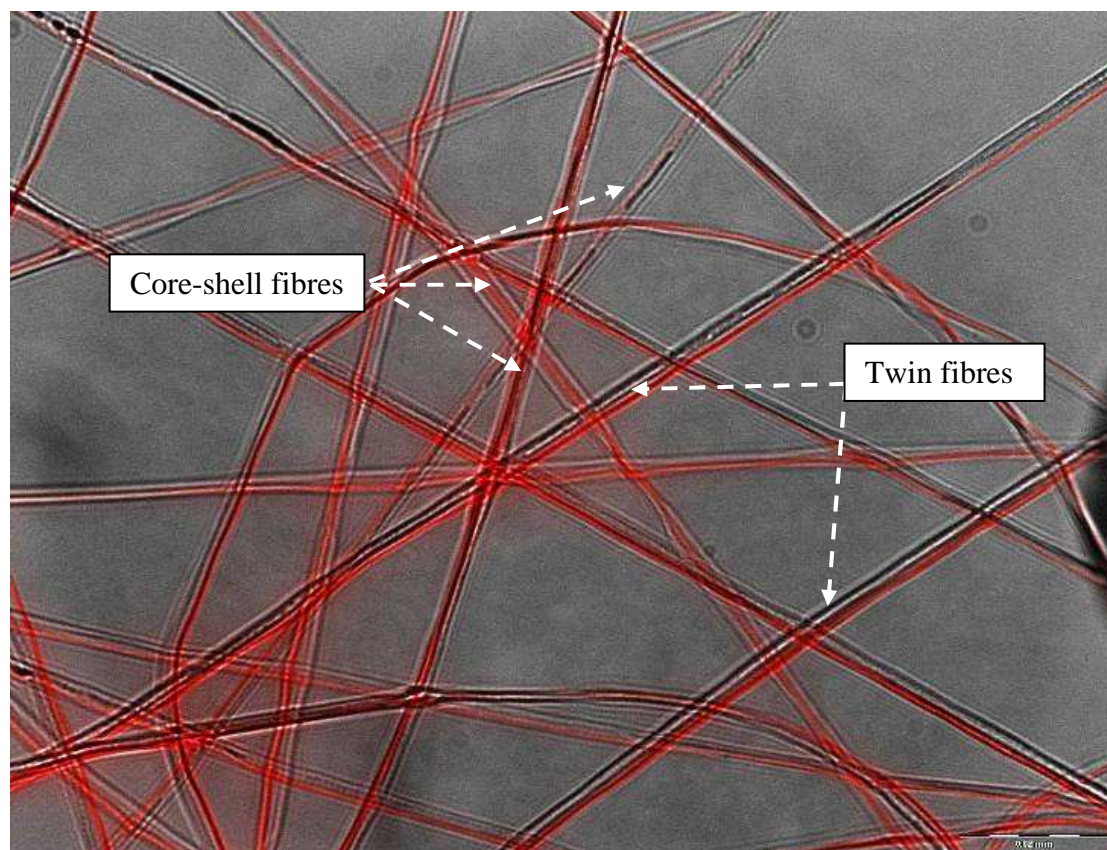
**Figure 4.2** a) and b) Fluorescence microscopy image of coaxial electrospun PLLA-PDLLA core-shell fibres under 100X magnification indicating no observable fluorescence (0.02mm scale bar)

Coaxial electrospinning<sup>II</sup> PLLA(rhodamine B)-core/PDLLA-shell solutions resulted in fibres that had the fluorescent polymer continuously incorporated along the length of the fibre. The fluorescent polymer was observed in the form of core-shell and also twin fibre structures (Figure 4.3). The existence of both fibre configurations produced by coaxial electrospinning has been reported in literature.<sup>3,4</sup>

Covalently linking rhodamine B to only one end of the high molecular mass ( $M_w \cong 291k$ ) PLLA chains resulted in a reduced intensity of fluorescence as compared with the mixture described earlier (where the fluorescence was so intense that it masked the fibres). The core polymer was successfully incorporated along the length of the fibres. This continuous entrainment of the core is important for the preparation of SPC's as sections where the core might not be entrained could create weak points or defects. The presence of a core component in a core-shell fibre configuration or part of a twin fibre configuration was confirmed.

<sup>I</sup> Appendix C: Figure C.1a and C.1b

<sup>II</sup> Coaxial electrospinning process parameters: 8wt% PLLA-core and 10wt% PDLLA-shell solutions (70/30 DCM/DMF) were coaxially electrospun with core and shell flow rates of 0.3 and 1.2ml/h respectively, the applied voltage used was 15.0-15.5kV and the temperature/relative humidity was measured as 22°C/53%rH.



**Figure 4.3** Fluorescence microscopy image (0.02mm scale bar) of excited PLLA(Rhodamine B)-PDLLA core-shell and twin fibres

Although a core-shell fibre structure is the goal of this study, the presence of these twin fibres is equally attractive as both materials are evenly distributed along the length of the fibres. The twisting of the twin fibres over their length would ensure that sufficient shell material is available to fuse with other overlapping fibres when making a SPC.

This strategy was successful in determination of the structure of the fibres. However due to uncertainties of the actual measured fibre diameters, caused by optical/light diffraction effects, this method was not preferred for the measurements of the actual fibre diameters. Hence, the selective dissolution method was used in the following section in conjunction with SEM to obtain more accurate fibre diameter measurements.

#### 4.1.2. Selective dissolution method: core-shell fibre structure validation

The selective dissolution method was used to reveal the core-shell fibre structure of fibres prepared by coaxial electrospinning 8wt% PLLA-core and 10wt% PDLLA-shell solutions (70/30 DCM/DMF). The core and shell flow rates were 0.3 and 1.2ml/h respectively. The applied voltage used was 15.5kV and the temperature/relative humidity was measured as 20°C/50%rH. Ten yarns were prepared under the conditions shown in Table 4.1 and they were analysed using the selective dissolution method.

##### 4.1.2.1. Analyses

###### i) SEM

The diameters of the yarns decreased after the washing procedures (Figure 4.4). Continuous fibres (Figure 4.4d) remained on the yarn holders and, on evaporation of the ethyl acetate, a film<sup>III</sup> was recovered from the washing solvent. The fibres remaining on the yarn holders appeared crimped or curled (Figure 4.4d), compared to the smooth uniform as-spun fibres (Figure 4.4c), and had decreased by an average of 44% in total fibre diameter after washing in ethyl acetate. The fibre diameter distributions before and after washing in ethyl acetate are shown in Appendix C: Figure C.3.

###### ii) Optical rotation

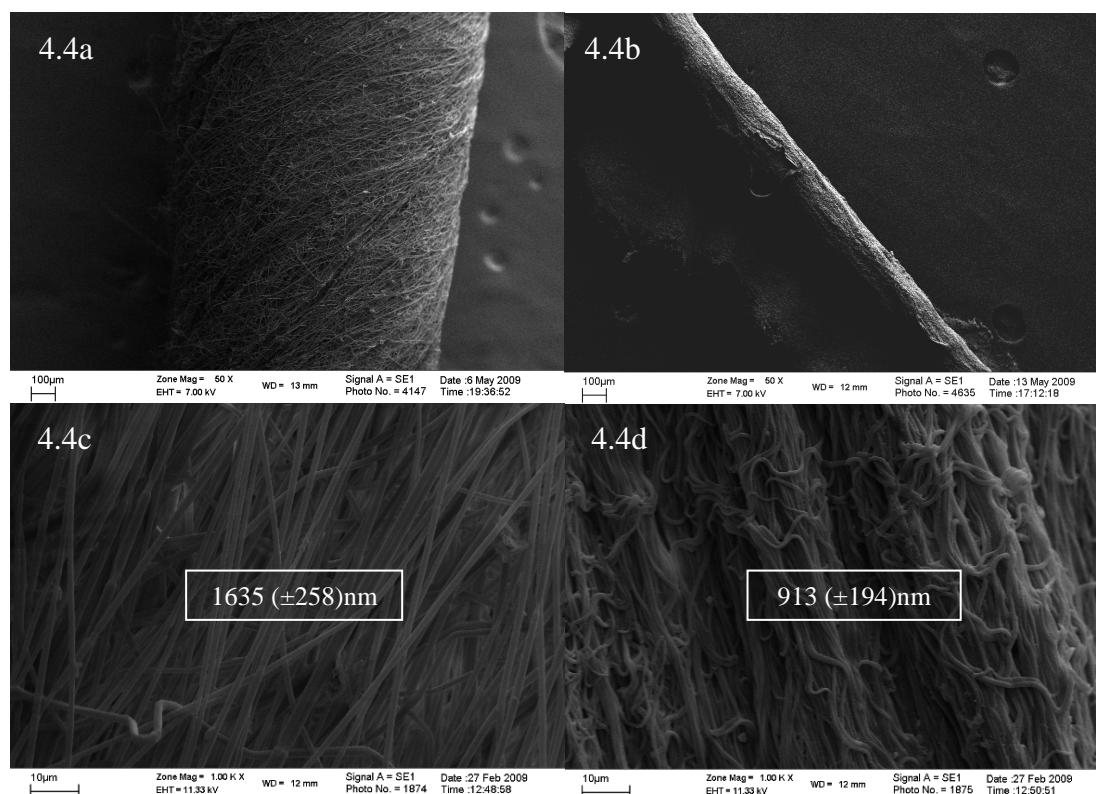
The dried polymer fibres remaining on the yarn holders, after washing in ethyl acetate, all rotated polarized light when re-dissolved in chloroform. The specific optical rotation  $[\alpha]$  for PLLA has been reported to be between  $-150 - -160^\circ$ .<sup>5,6</sup> The optical rotation values are dependent on concentration of the chemical species in solution. However the values obtained in this study for the fibres that remained on the yarn holders (after re-dissolution chloroform) did not reflect the values found in literature. However, the degree of optical rotation for the fibres remaining on the yarn holders in each case were significant when compared to the films recovered from the washing solutions. These films (from the washing solution) when dissolved in chloroform, did not rotate polarised light at all and repeatedly gave absolute 'zero' values of optical rotation. It was, therefore, reasonable to assume that despite the

---

<sup>III</sup> Appendix C: Figure C.2



optical rotation values for the remaining fibres on the yarn holders not representing true optical rotation values when dissolved in chloroform, these values were significant when compared to the 'zero' values<sup>IV</sup> obtained for the chloroform solution of the film extracted from ethyl acetate.



**Figure 4.4** Coaxial electrospun yarns and fibres a,c) before and b,d) after washing in ethyl acetate. The average fibre diameters are shown in boxes.

The PLLA polymer used for the core solution is a semi-crystalline material, is not soluble in ethyl acetate and when dissolved in chloroform rotates polarised light. PDLLA is a completely amorphous material, is soluble in ethyl acetate and when dissolved in chloroform does not rotate polarised light. It is therefore, reasonable to assume that the polymer comprising the fibres remaining on the yarn holders is only PLLA. The polymer extracted with the ethyl acetate, therefore, is only comprised of PDLLA. These results confirm that the remaining fibres on the yarn holders are the core components and the extracted (selectively dissolved) film the shell material. This was true for all the yarn samples. Both core and shell components were present in the fibres, and the core component was shown to be continuous along the full length of the composite fibres.

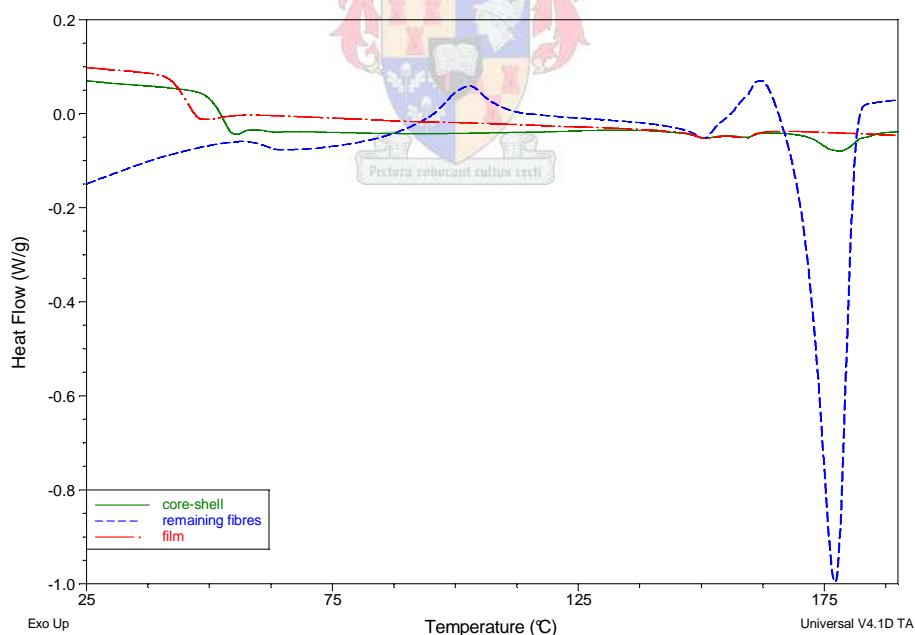
<sup>IV</sup> Appendix C: Table C.1

## iii) DSC

The conclusions drawn from the optical rotation data were supported by information acquired from the 1<sup>st</sup> heating cycle in DSC analysis of the remaining fibres and from the film extracted from ethyl acetate.

All of the remaining fibres on the yarn holders revealed a sharp melt endotherm with onset of melting at  $\approx 170^\circ\text{C}$ , a melt temperature maximum of  $\approx 177^\circ\text{C}$  and an average of 53% crystallinity (Figure 4.5). These fibres on the yarn holders showed significantly larger melt endotherms than for the as-spun core-shell fibre yarns (crystallinity values  $< 7\%$ ). The remaining fibres therefore consisted of semi-crystalline polymer and it is reasonable to assume these were the PLLA cores, as the PDLA shell is amorphous and would not show a melt endotherm.

The film extracted from the ethyl acetate solution did not show any melt endotherm and the polymer displayed only a glass transition at  $\pm 40^\circ\text{C}$ . The film is therefore the amorphous PDLA shell component.



**Figure 4.5** DSC thermogram of coaxial electrospun fibre yarn, and separated core and shell components after washing in ethyl acetate

## 4.2. Parameter effects on core-shell fibre diameter

As previously observed the diameters of core-shell fibres and yarns were reduced after washing with ethyl acetate. The PDLLA shell was dissolved in ethyl acetate while the insoluble PLLA cores remained on the yarn holders. The remaining fibres on the holders, when dissolved in chloroform, all rotated polarised light.<sup>V</sup> The polymer films recovered from the ethyl acetate displayed no optical rotation when dissolved in chloroform. The remaining fibres on the yarn holders showed a sharp melt endotherm ( $\cong 170^{\circ}\text{C}$ ) whereas the film extracted from the ethyl acetate showed no melt endotherm in all cases.<sup>VI</sup>

### 4.2.1. Concentration

The core-shell fibre mass decreased after washing in ethyl acetate as the shell components were successfully dissolved and separated from the cores. The mass of the remaining fibres on the yarn holders was observed to increase when the core spinning solution concentration was increased.<sup>VII</sup> No obvious trend could be observed with increasing shell solution concentration.

The fibres coaxially electrospun with 4wt% and 6wt% core solutions showed broad core-shell fibre diameter distributions. Some of these fibres had a twin fibre structure. The fibres spun with an 8wt% core solution concentration showed narrow core-shell fibre diameter distributions and smooth individual fibres.

It should be noted that a 4wt% PLLA solution in 70/30 DCM/DMF spun with a single needle electrospinning set-up produced only beads-on-string morphology fibres but when spun as the core in a coaxial electrospinning set-up smooth cores resulted.<sup>VIII</sup> An 8wt% PLLA solution spun with a single needle set-up produced fibers with average diameters of approximately 1300nm but when coaxially electrospun produced bead-free cores with average diameters in the 900nm range. This potentially has an

---

<sup>V</sup> Appendix C: Table C.2

<sup>VI</sup> Appendix C: Figures C.4 and C.5

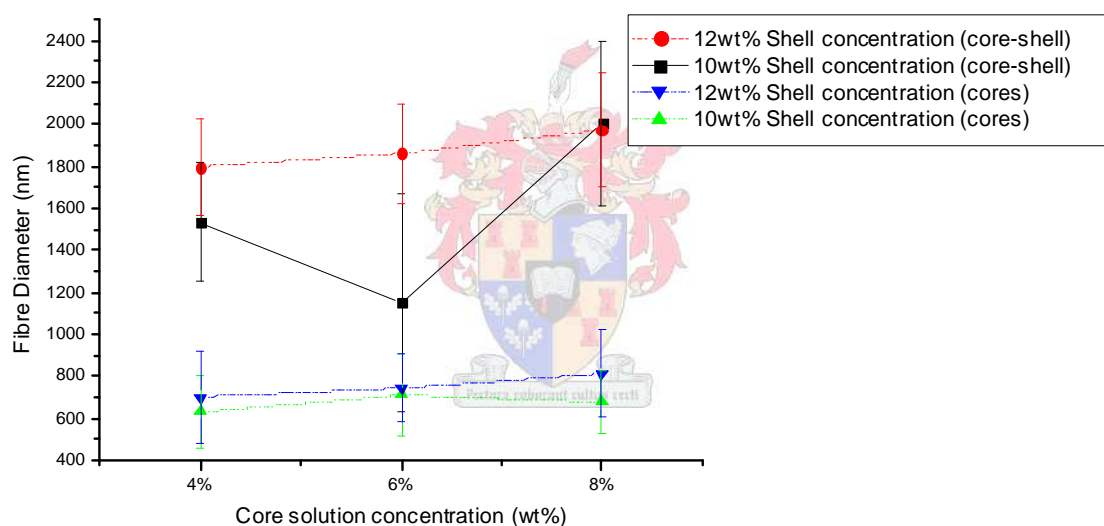
<sup>VII</sup> Appendix C: Figure C.6 and Table C.3 The theoretical mass, in all cases of core solution concentration, was greater than the actual mass. This can be explained by the loss of material during processing and handling but is also due to the fact that the fibres were not perfect cylinders. When the diameter of a flat ribbon was measured and that same diameter translated into a perfect cylinder, that cylinder would have a greater volume than the total mass volume of the actual ribbon. Hence, the theoretical mass estimates had built-in inaccuracy that tended to overestimate the mass.

<sup>VIII</sup> Appendix C: Figure C.7



additional benefit for spinning core-shell fibres and removing the shell polymer. A bead-free fibre (core polymer solution) of finer fibre diameter, than achievable with traditional electrospinning can, therefore, be prepared by spinning a core-shell fibre and subsequent removal of the shell polymer by dissolution.<sup>3</sup>

The effect of increasing the core solution concentration on the average core fibre diameters can be observed in Figures 4.6 and 4.7.<sup>IX</sup> The fibre diameter distributions are shown in Appendix C.<sup>X</sup> An ANOVA (analysis of variance) was done comparing core solution concentration and flow rate (Lower Level) and shell solution concentration and flow rate (Upper Level) parameters effects on core and core-shell fibre diameters. The significance of the parameter effects on the core and core-shell fibre diameters investigated was determined by Bonferroni tests.<sup>XI</sup>



**Figure 4.6** *Solution concentration effects on resultant core and total fibre diameters*

Increasing the core solution concentration, with a 10wt% shell solution concentration, showed no significant trend in the change in core-shell or core fibre diameters. The result of increasing the core solution concentration, when electrospinning with a shell solution of 12wt% concentration, showed a trend of increasing core-shell and core

<sup>IX</sup> Appendix C: Table C.4 and Figure C.8

<sup>X</sup> Appendix C: Figures C9-12.

<sup>XI</sup> Appendix C: Table C.5 -  $P < 0.05$  indicates that the difference between two actual means are significant and  $P > 0.05$  indicates that the difference is not significant. These analyses were used to see if there exists any trend for increasing parameters that affect the size of the core and core-shell fibre diameters and confirm that the increments along the trend are significant.

fibre diameters. This increasing trend was, however, shown to be statistically significant only for the increase in core and core-shell fibre diameters when the core solution concentration was increased from 4wt% to 6wt% and 6wt% to 8wt% respectively.<sup>XII</sup> Therefore, increasing the core solution concentration had the effect of increasing the core and core-shell fibre diameters but only when electrospun with 12wt% shell solutions.<sup>XIII</sup>

The influence of increasing the shell solution concentration was statistically significant between 4wt% and 8wt% core solutions concentrations. Although there was a clear difference in fibre diameters at these two core solution concentrations this was not large relative to the increase in core-shell fibre diameters. At 6wt% core solution concentrations there was no statistical significant difference between the core fibre diameters coaxially spun with 10 and 12wt% shell solution concentrations. Therefore increasing the shell solution concentration only influences the core-shell diameter (increasing the volume of shell material) considerably and has only a minor effect on the core diameter.

The percentage crystallinity values, as calculated from DSC thermograms, of the as-spun core-shell fibres all showed a trend of increasing crystallinity (Figure 4.8).<sup>XIV</sup> with increasing core solution concentration. This indicated that by weight, more semi-crystalline (crystallisable) material is incorporated in the core-shell fibre yarns. The increasing trend for all increments of core solution concentration on crystallinity for yarn samples prepared from coaxial electrospun fibres with a 10wt% shell solution concentration, was statistically significant.<sup>XV</sup> Whereas, only the effect of increasing the core solution concentration from 6wt% to 8wt% increased the crystallinity significantly for yarn samples prepared from a 12wt% shell solution concentrations.<sup>XVI</sup>

---

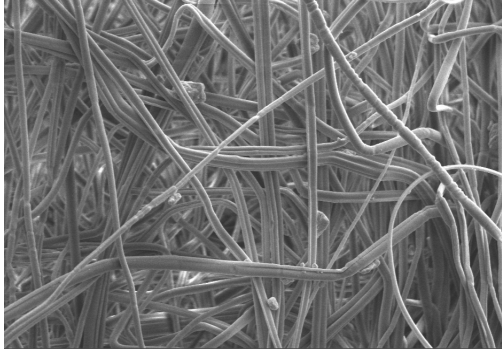
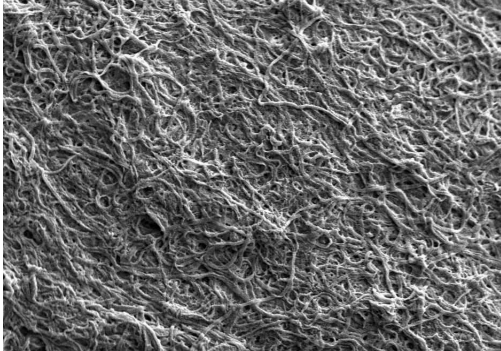
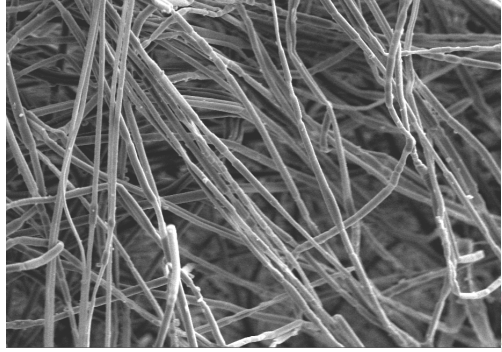
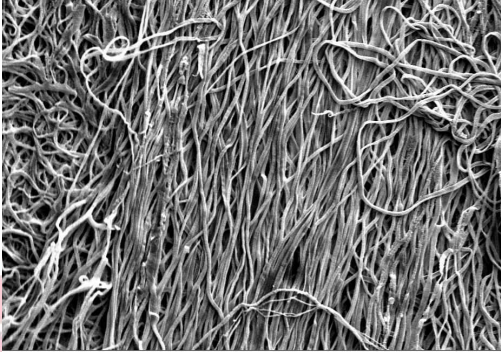
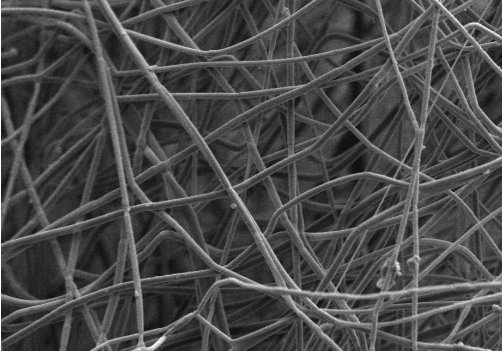
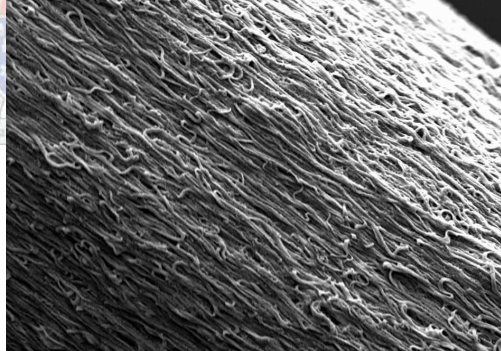
<sup>XII</sup> Appendix C: Table C.5

<sup>XIII</sup> Appendix C: Figure C.13 and C.14

<sup>XIV</sup> DSC Thermograms - Appendix C: Figures C.15 and C.16

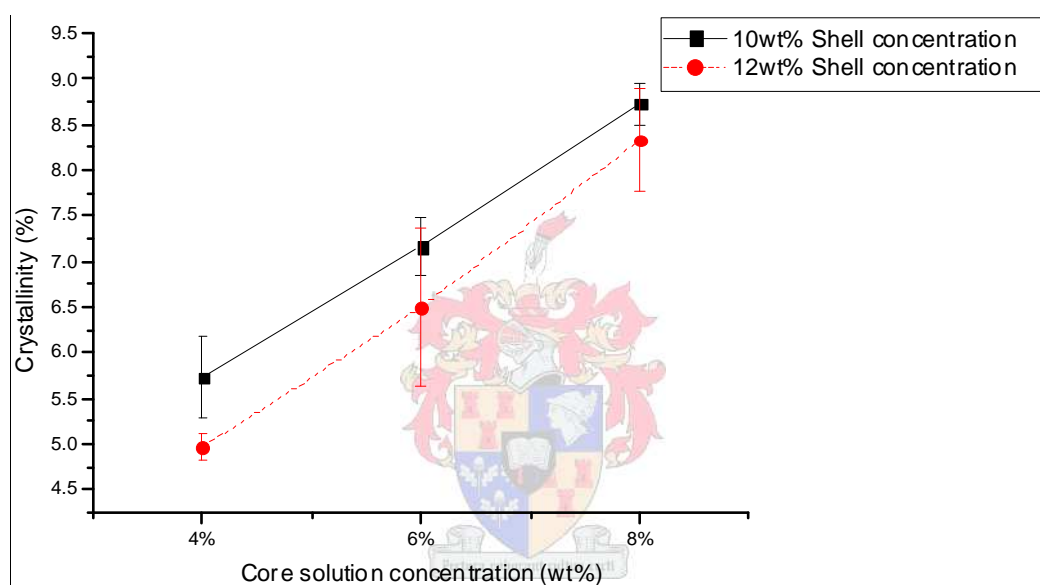
<sup>XV</sup> Appendix C: Table C.6

<sup>XVI</sup> Appendix C: Table C.7

Before washing in ethyl acetate		After washing in ethyl acetate		Core solution conc.
4.7a	Ave 1725nm	4.7b	Ave 630nm	
				4wt%
				
				

**Figure 4.7** Core-shell fibre diameters as a function of core polymer concentrations a-b) 4wt%, c-d) 6wt%, e-f) 8wt% before and after washing in ethyl acetate. The core and shell solution flow rates during electrospinning were 0.3 and 1.2 ml/h respectively. The shell solution concentration was 10wt%.

When the core concentrations were increased, while spinning with a 12wt% PDLA shell solution concentration, the melt endotherms were slightly smaller than when spinning with 10wt% PDLA shell solutions. The overall difference between the crystallinity of the samples coaxially electrospun with 10 and 12wt% solutions at each core solution concentration increment was, however, not shown to be statistically significant.<sup>XVII</sup> Therefore, the variation in shell solution concentration does not directly influence the amount of core material incorporated into the fibres but the very slight reduction of the crystallinity values at the higher shell solution concentration is a function of the increase in mass of non-crystallisable material (PDLA shell) into the core-shell fibre yarns which “dilutes” the heat-flow readings in DSC analyses.



**Figure 4.8** Solution concentration effects on the percentage crystallinity of coaxial electrospun fibre yarns at 10wt% and 12wt% shell solution concentrations

#### 4.2.2. Flow rate

The mass of the remaining fibres on the yarn holders increased when the core solution flow rate was increased.<sup>XVIII</sup> No obvious trend could be observed with increasing shell solution flow rate. The theoretical mass, in all cases of core solution flow rate, was greater than the actual mass.<sup>XIX</sup>

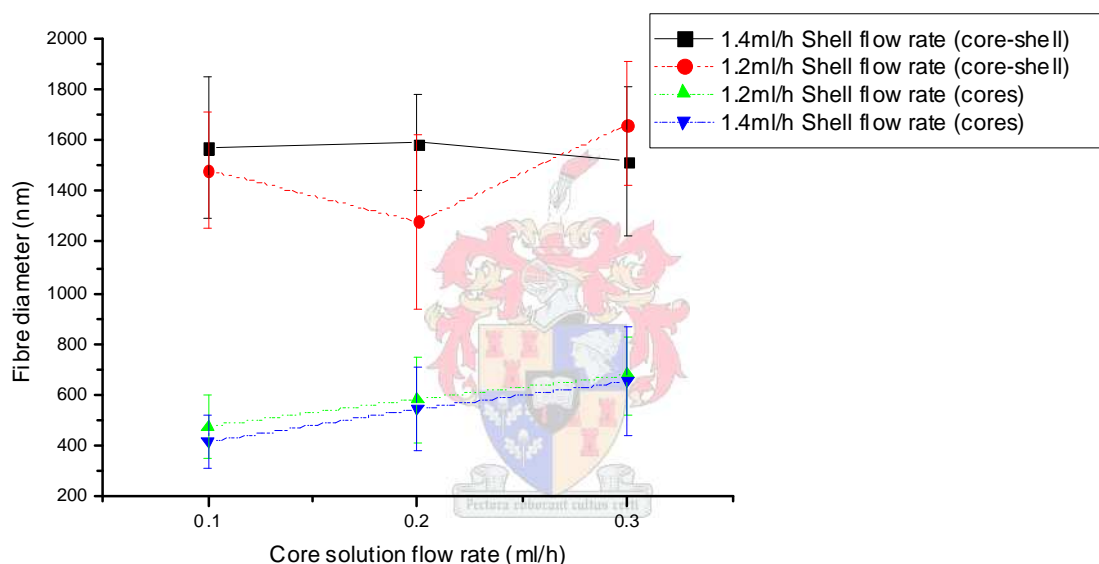
<sup>XVII</sup> Appendix C: C.17 and C.18

<sup>XVIII</sup> Appendix C: Figure C.19 and Table C.3

<sup>XIX</sup> Attributed to material loss e.g. clearing blocked needles/gelled Taylor cones during electrospinning or where some fibres were not deposited on the collector or during the selective dissolution method.



The average change in fibre diameters and their distributions as a result of varying the core and shell solution flow rates are shown in Figures 4.9 and 4.10 and Appendix C.<sup>XX</sup> The core diameters showed an increasing trend with increased core solution flow rate. This magnitude of increase in average core fibre diameter with increasing core solution flow rate was shown to be statistically significant for each increment.<sup>XXI</sup> The core-shell fibre diameter was increased only slightly for increasing core flow rate increments. This slight increase in core-shell fibre diameter was only statistically significant when the core flow rate was increased from 0.1 to 0.2ml/h for fibres coaxially electrospun with a shell solution flow rate of 1.2ml/h. This was also only statistically significant when the core flow rate was increased from 0.2 to 0.3ml/h for fibres coaxially electrospun with a shell solution flow rate of 1.4ml/h.<sup>XXII</sup>



**Figure 4.9** Solution flow rate effects on resultant core and total fibre diameters

Least-square means showed that the core-shell fibre diameters were slightly larger for the fibres spun with a 1.4ml/h shell solution flow rate than for the fibres spun with a shell solution flow rate 1.2ml/h.<sup>XXIII</sup> The other consequence of increasing the shell solution flow rate was that the core fibre diameters were smaller when the shell flow rate was higher.<sup>XXIV</sup> This means that the increase of the shell flow rate reduces the

<sup>XX</sup> Appendix C: Figures C.20 –C.24

<sup>XXI</sup> Appendix C: Table C.8

<sup>XXII</sup> Appendix C: Figure C.25 and Table C.8

<sup>XXIII</sup> Appendix C: Figures C.25

<sup>XXIV</sup> Appendix C: Figure C.26 and Table C.9

amount of core material entrained with the core-shell fibres. This effect was not seen for variations in solution concentration.

The change in core fibre diameter due to increased core solution flow rate was therefore more significant than that of concentration within the parameter ranges studied.

The change in the size of the endotherms when varying solution flow rate indicated a change of semi-crystalline crystallisable material incorporated in the core-shell fibre yarns. There was an almost linear increase in percentage crystallinity as core solution flow rate was increased from 0.1 to 0.3 ml/h (Figure 4.11).<sup>XXV</sup> The increments were all statistically significant.<sup>XXVI</sup> Increases in the shell solution flow rate resulted in a lower percentage crystallinity for those fibres spun with a higher shell solution concentration.<sup>XXVII</sup> This reduction of the melt endotherm at the higher shell solution flow rate is a function of the increase in mass of non-crystallisable material (PDLLA shell) into the core-shell fibre yarns causing the aforementioned dilution effect and also interrupting crystallisation of the core.


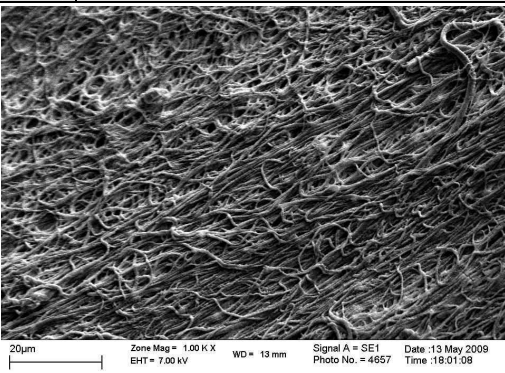
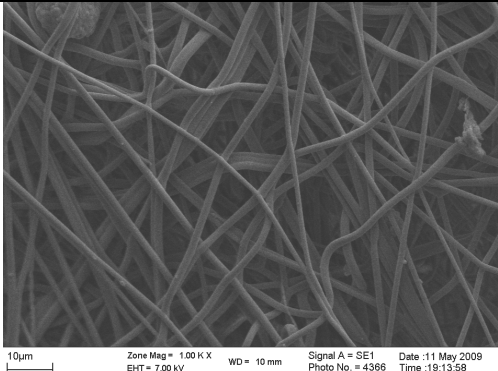
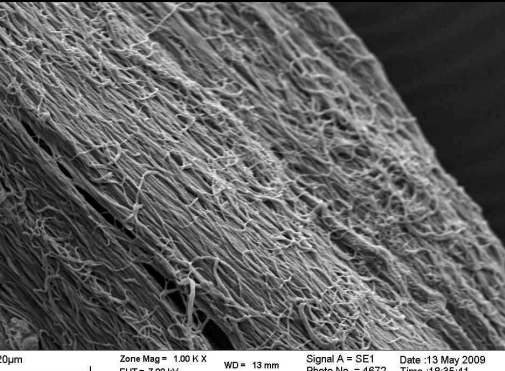
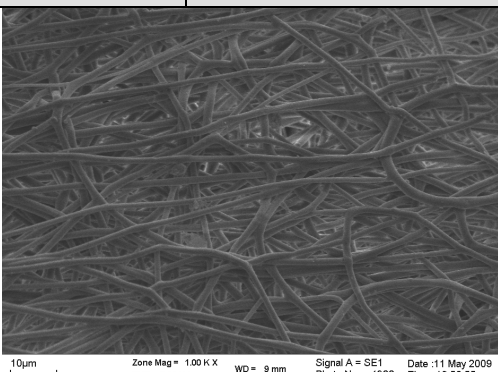
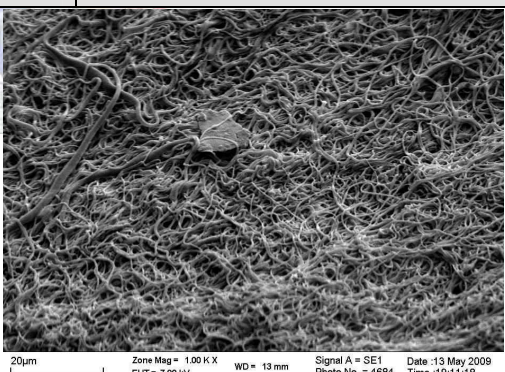
The hypothesis that increasing the core solution concentration and flow rate would result in an increase in the amount of PLLA in the core-shell fibres was shown to be correct. The increase in PLLA in the fibres resulted in increased core and core-shell fibres diameters. The increase in core diameters was reiterated by the increase in crystallinity which was the result of the increase in crystallisable material shown in DSC analysis. The size of the melt endotherms and therefore crystallinity of core-shell fibres increased almost linearly with increasing core solution concentration and flow rate.

---

<sup>XXV</sup> DSC Thermograms - Appendix C: Figures C.27 and C.28

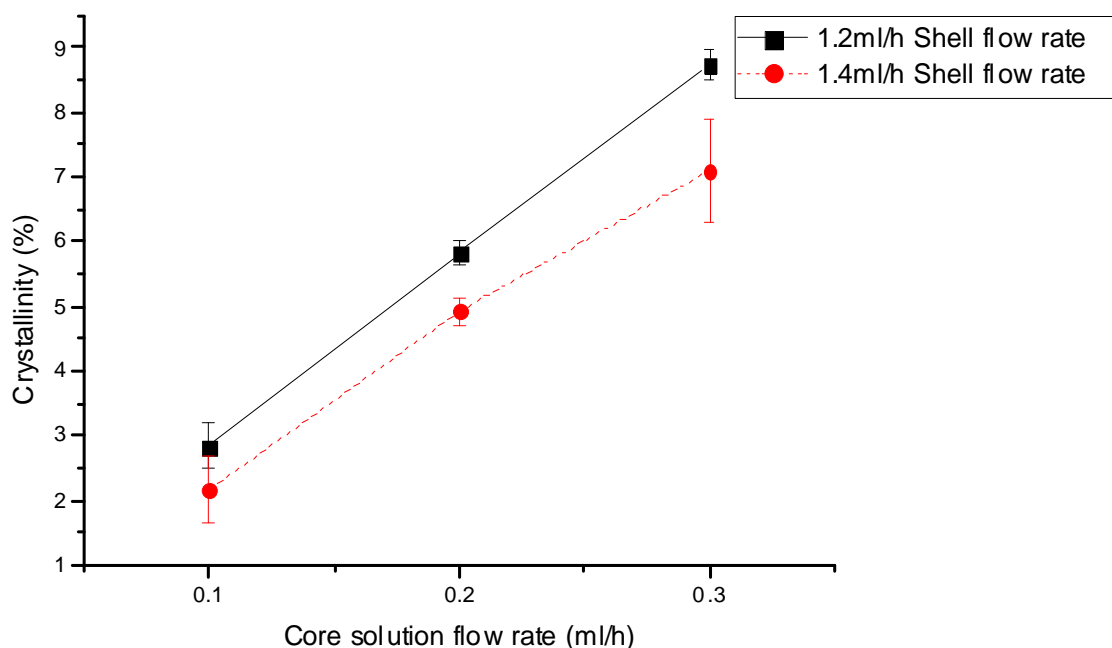
<sup>XXVI</sup> Appendix C: Table C.10

<sup>XXVII</sup> Appendix C; Figures C.29 and C.30

Before washing in ethyl acetate		After washing in ethyl acetate		Shell solution flow rate
4.10a	Ave 1436nm	4.10b	Ave 472nm	
				0.1 ml/h
				
				0.3 ml/h

**Figure 4.10** SEM images showing core-shell fibres spun with PLLA core solution flow rates a-b) 0.1ml/h, c-d) 0.2ml/h, e-f) 0.3ml/h and a shell solution flow rate of 1.2 ml/h before and after washing in ethyl acetate. The core and shell solution concentrations used were 8wt% PLLA and 10wt% PDLA respectively.





**Figure 4.11** Solution flow rate effects on the melt endotherm of coaxial electrospun fibre yarns at 1.2 ml/h and 1.4ml/h shell solution flow rate

#### References

1. Sun Z, Zussman E, Yarin AL, Wendorff JH, Greiner A. Compound core-shell polymer nanofibers by co-electrospinning. *Advanced Materials*. 2003;15(2003):1929-32.
2. Moghe AK, Gupta BS. Co-axial electrospinning for nanofiber structures: preparation and applications. *Polymer Reviews*. 2008;48(2):353-77.
3. Wang M, Yu JH, Kaplan DL, Rutledge GC. Production of submicron diameter silk fibers under benign processing conditions by two-fluid electrospinning. *Macromolecules*. 2006;39:1102-7.
4. Sun B, Duan B, Yuan X. Preparation of core/shell PVP/PLA ultrafine fibers by coaxial electrospinning. *Journal of Polymer Science*. 2006;102:39-45.
5. Garlotta D. A Literature review of poly(lactic acid). *Journal of Polymers and the Environment*. 2002;9(2):63-84.
6. Sarasua JR, Lopez Arraiza A, Balerdi P, Maiza I. Crystallization and thermal behaviour of optically pure polylactides and their blends. *Journal of Materials Science*. 2005;40:1855-62.

## Chapter 5

### **Results and discussions:**

#### **Single Polymer Composite Applications: Yarns and Films**

*In this chapter investigation into the processing of core-shell fibres into SPC yarns and films is presented to demonstrate potential application of the fibres. The novelty of the PLLA-PDLLA core-shell fibre, with a semi-crystalline core and amorphous shell structure, is explored in the preparation of these composite materials. Core-shell fibre mats were twisted into yarns and annealed under tension. The physical and mechanical properties of the yarns before and after thermal treatments were investigated. Core-shell mats were also plied and heat-pressed into thin films. The physical properties of the films were investigated. The selective dissolution of the PDLLA material from the film and cryo-fracturing techniques were used to investigate if the semi-crystalline cores retained their structure to act as reinforcement within the films.*

### **5.1. SPC Yarns**

The novelty of PLLA-core/PDLLA-shell fibres was explored by studying the structure–property relationships of yarns prepared of the same, before and after heat treatments (annealing under tension). Core-shell fibres were prepared by coaxial electrospinning from 8wt% PLLA-core and 10wt% PDLLA-shell solutions in 70/30 DCM/DMF.<sup>I</sup> Twenty core-shell fibre mats were collected and twisted into yarns (1.5twists/cm).<sup>II</sup> The yarns were secured under light tension at either end (constrained). Ten of the yarns were heat-set/annealed at 110°C for 5hrs in a convection oven and the other ten were left un-treated.

The morphology, fine-structure and mechanical properties of the yarns were investigated and compared using SEM, XRD, DSC and mechanical testing.

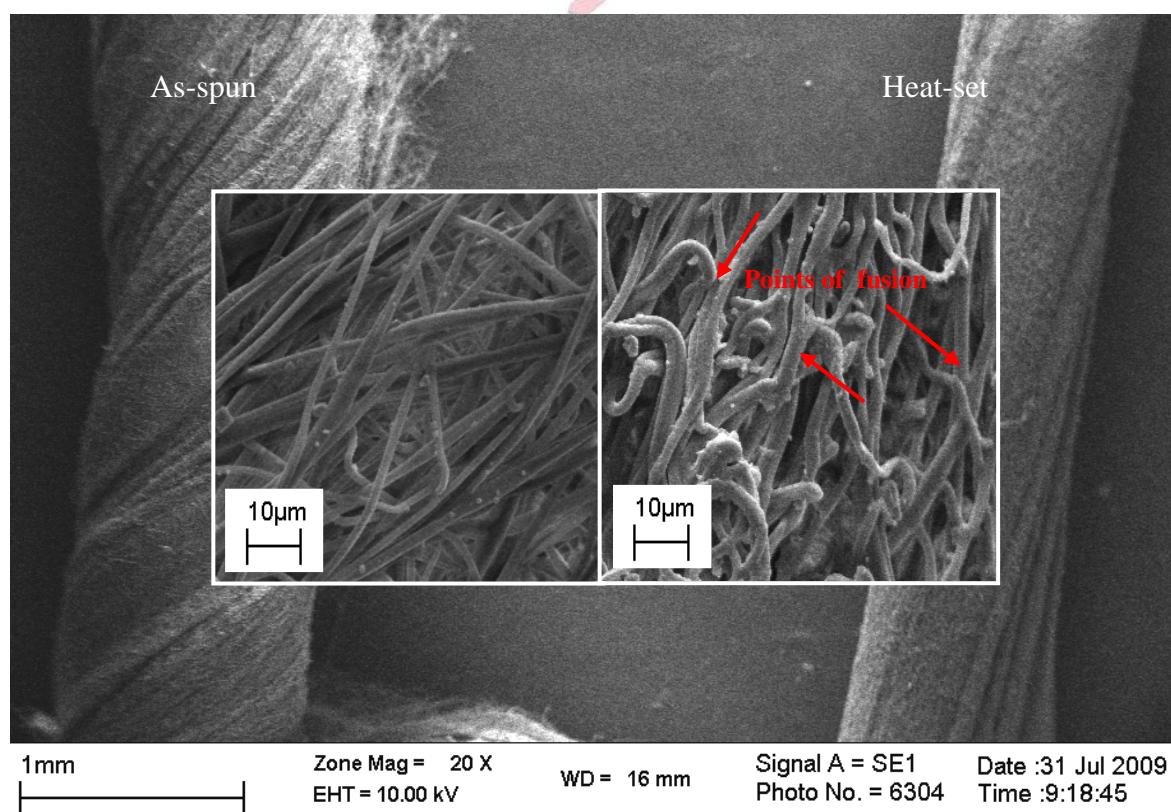
---

<sup>I</sup> Coaxial electrospinning process parameters: 8wt% PLLA-core and 10wt% PDLLA-shell solutions (70/30 DCM/DMF) were coaxially electrospun with core and shell flow rates of 0.3 and 1.2ml/h respectively, the applied voltage used was 15.0-15.5kV and the temperature/relative humidity was measured as 22°C/53.

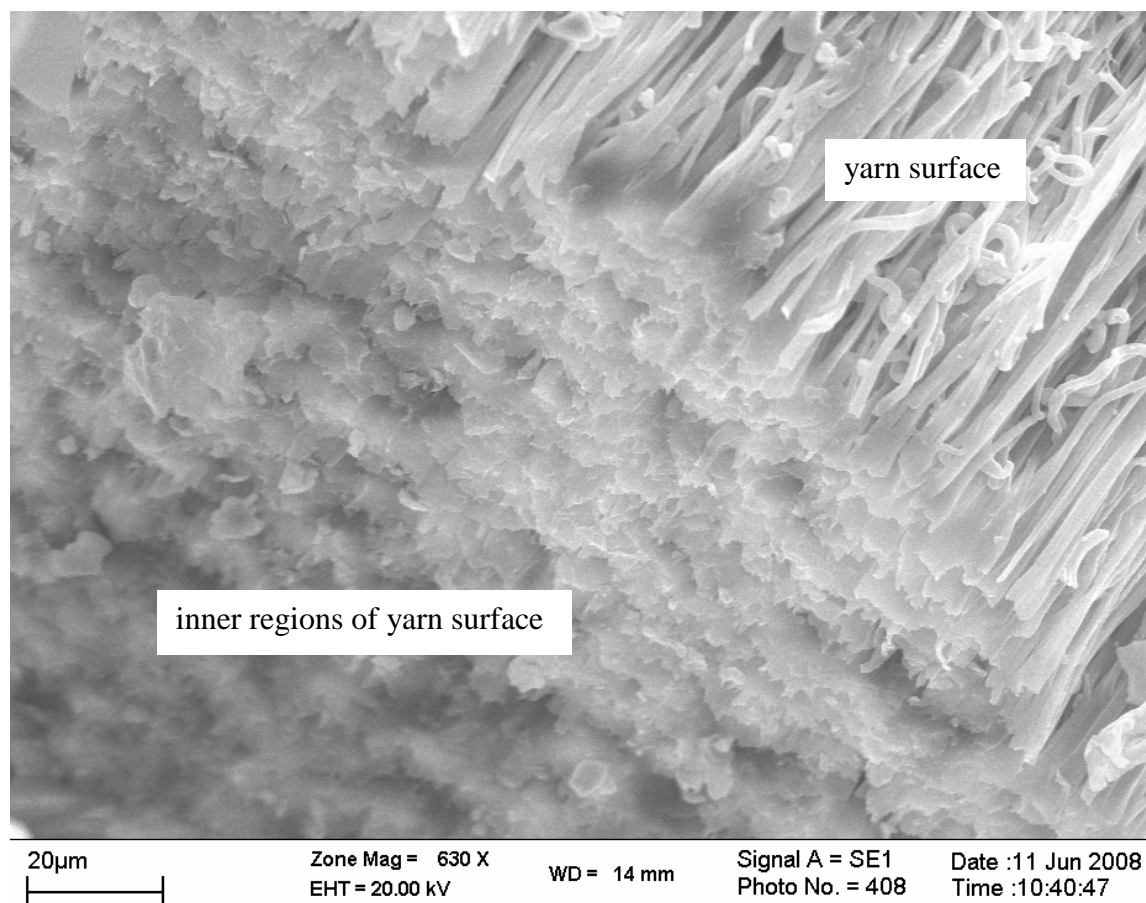
<sup>II</sup> As described in Chapter 3 (Section 3.36)

### 5.1.1. Morphology

The yarns before and after thermal treatment are shown in Figure 5.1. The yarns observed after thermal treatments had reduced diameters. This was the result of thermally induced molecular chain relaxation of non-crystalline oriented regions and because the yarns were fixed at either end during thermal treatments the twist in the yarn was distorted.<sup>1</sup> The fusion of the shell components of the heat-set yarn was not so apparent on the surface of the yarn. Fusion at the surface was seen only between overlapping fibres. An exposed cross-section of the heat-set yarn (Figure 5.2) revealed that there was however significant fusion of the fibres on the inner regions of the yarn. This was the result of the fibres on the yarn surface being too light for gravity induced flow to overcome the surface tension of the polymer. The fibres on the inner regions of the yarn were mostly fused together since they were in more intimate contact with each other.



**Figure 5.1** Coaxial electrospun fibre yarns before (left) and after (right) heat treatments



**Figure 5.2** *Cryo-fracture point of a heat-set core-shell fibre yarn showing the difference in fusion between the yarn surface and core*

### 5.1.2. Fine structure

The fibres used to prepare the yarns have a PLLA core. PLLA is a ‘slowly crystallisable’ polymer and due to the high deformation rates and rapid solidification process during the electrospinning process, electrospun PLLA fibres have little or no initial crystallinity.<sup>2-5</sup> To induce crystallographic packing within electrospun PLLA fibres, thermal annealing at the crystallisation temperature of PLLA is required.<sup>4</sup> The yarns in this study were heats-set/annealed under mild tension at 110°C for 5 hours. This was the isothermal crystallisation temperature of the PLLA material used in this study.<sup>III</sup> By inducing crystallographic packing of the PLLA chains in the cores and fusing the PDLA-shell components of overlapping fibres, it was expected that the modulus and breaking strength of the yarns would be increased.<sup>6</sup>

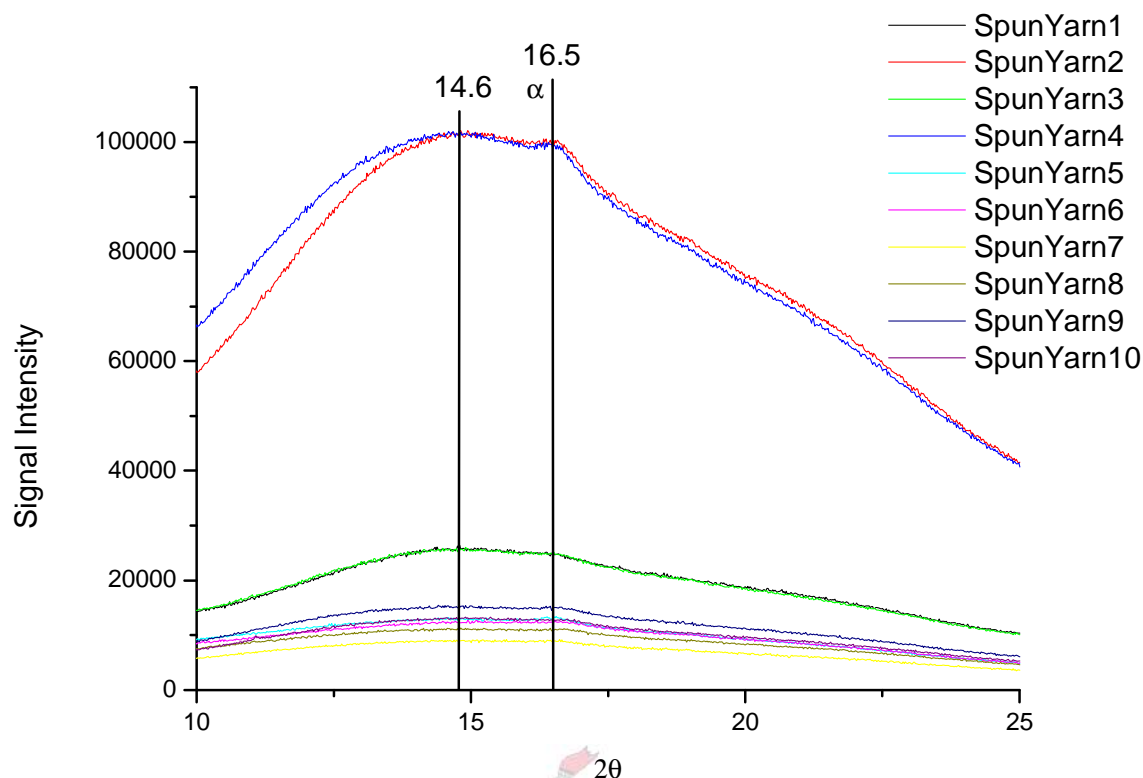
<sup>III</sup>Two cold-crystallisations occur for the PLLA entrained in the core-shell fibres on heating. The first is a significant cold crystallisation the result of the combination of the slow crystallising nature of PLLA and the high deformation rates in electrospinning. The second is an intrinsic cold-crystallisation that is less significant but is a reversible event.

The molecular orientation and crystallographic packing of polymer chains are determined by the formation, growth, and deformation of the phase-separated domains in the electrospun fibres.<sup>5,7,8</sup> This fine structure is important for mechanical strength and the biodegradability.<sup>3</sup>

Two main crystal structures,  $\alpha$  and  $\beta$ , are likely to be formed when heat-setting the yarns prepared from PLLA-core/PDLLA-shell fibres.<sup>4,9,10</sup> The preference between the two structures is determined by chain packing considerations. Crystals of  $\alpha$  structure have lamellar folded-chain morphology.  $\beta$  crystals are meta-stable structures and have a frustrated fibrillar morphology.<sup>4</sup> The presence of  $\beta$  crystal structures in as-spun electrospun fibres is attributed to the substantial elongational deformation during electrospinning and slowly crystallisable nature of PLLA. On heating,  $\beta$  crystals undergo chain relaxation and are transformed into  $\alpha$  crystals.  $\beta$  crystals melt at a lower temperature than the more stable  $\alpha$  crystals.<sup>4,9,10</sup> The formation of other PLLA crystal types are possible and the fine structure may be described in much greater detail.<sup>11</sup> However, such a detailed study of fine structure falls far beyond the scope of this study.

X-ray diffractograms of the yarns before heat-setting are shown in Figure 5.3. No extensive crystal peaks were present. An amorphous halo or strong scattering anisotropy with mid-point  $14.56^\circ$  was evident. The low extent of crystallinity means that the majority of the chains are in the non-crystalline state.<sup>3</sup> This was attributed to high deformation and rapid solidification of stretched chains during electrospinning and the slow crystallisable nature of PLLA. Crystal development is therefore hindered as the chains are not allowed sufficient time for crystallographic packing prior to solidification. The amorphous halo intensity for the as-spun yarn samples show two samples that deviate from the sample population. They have far greater intensities. These deviations could possibly be caused by misalignment of the yarn samples off the x-ray beam direction.<sup>12</sup> There is additionally a small bump or bulge on the shoulder of the amorphous halo at  $16.5^\circ$ . This has been attributed to disordered  $\alpha$  crystals.<sup>4</sup>

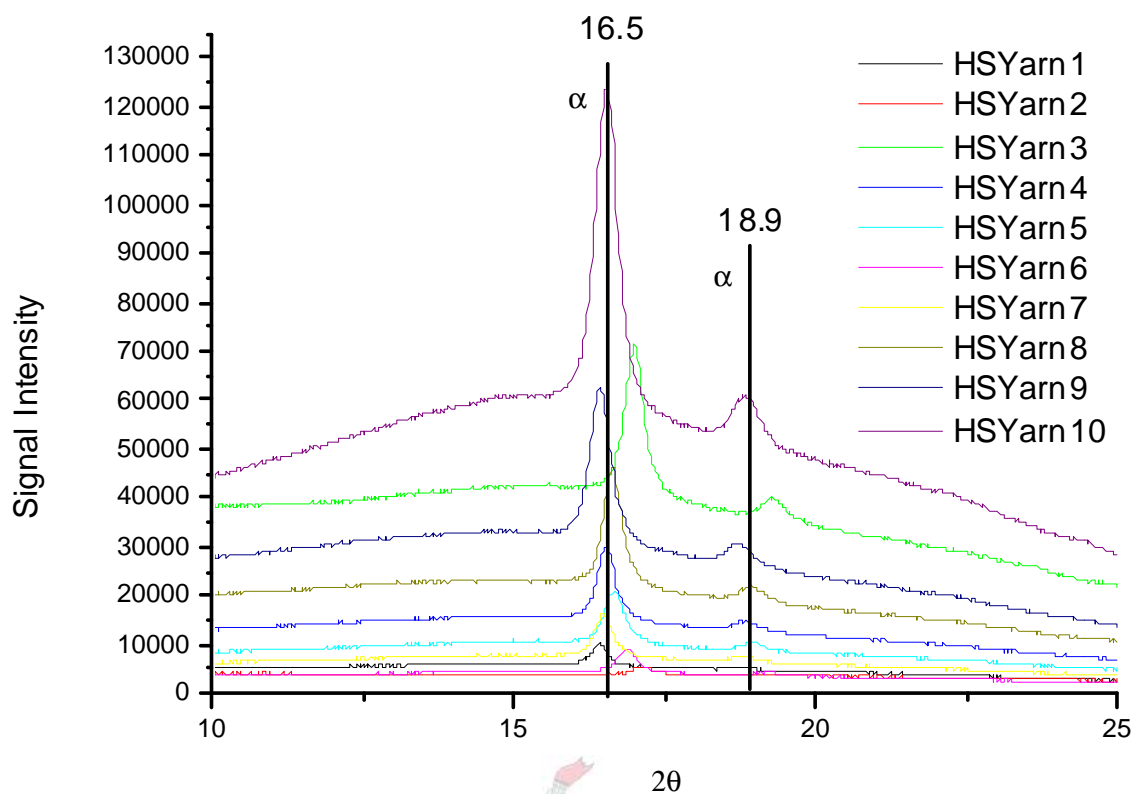




**Figure 5.3** X-ray diffractogram: yarns prepared from as-spun PLLA-core/PDLLA-shell fibres

XRD analyses of the heat-set yarns reveal sharp crystal peaks (Figure 5.4) in positions  $16.5^\circ$  and  $18.9^\circ$ . Peaks in these positions have been attributed to  $\alpha$  crystals for PLLA.<sup>4,11,13-15</sup>  $\beta$  structures would usually be present at  $17.2^\circ$  and in the region  $28.8-30.84^\circ$ .<sup>10,11,13</sup> The absence of peaks in these positions for the as-spun and heat-set yarns indicate that the rapid drawing of the polymer molecules experienced during electrospinning simply orient the molecules along the fibre axis without formation of  $\beta$  crystals.<sup>13</sup>

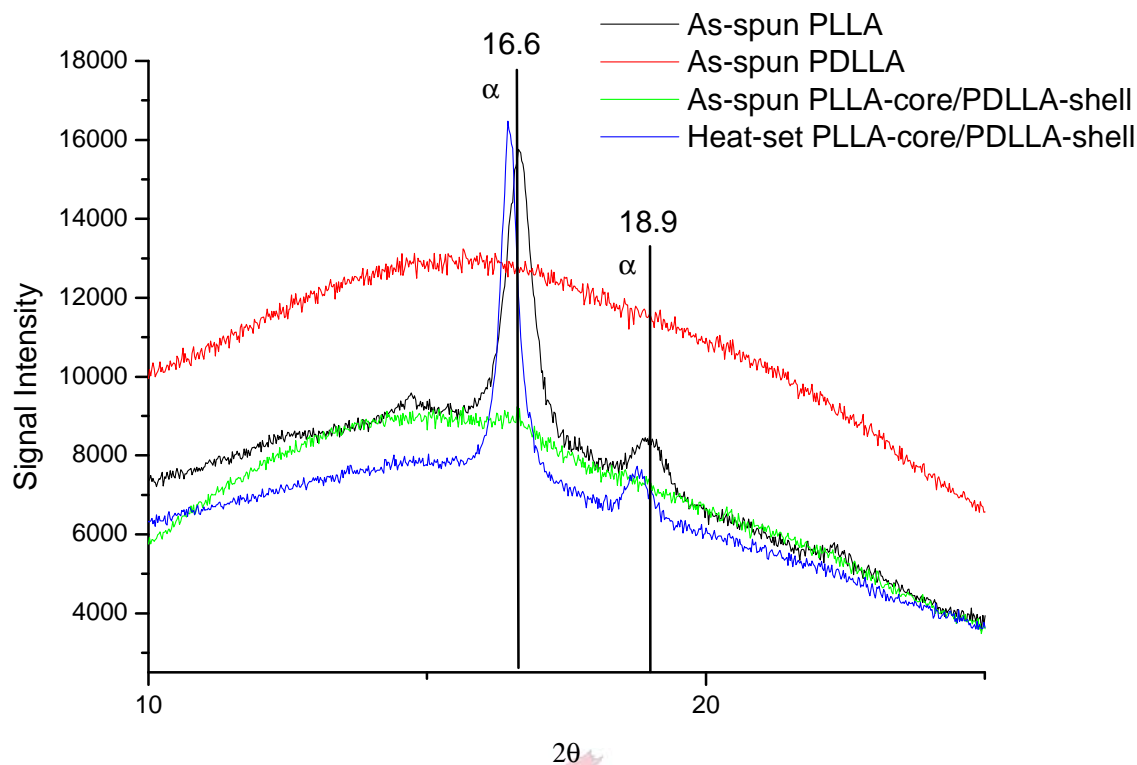
Although all the heat-set yarns were prepared under the same coaxial electrospinning parameters and heated under isothermal conditions, small deviations or shifts in the peaks such as for the two dominant  $\alpha$  crystal peaks in the amorphous halo were evident between yarn samples. These shifts may be attributed to heating at  $110^\circ\text{C}$  (isothermal heat-setting temperature used) as it has been reported that at a temperature range  $105-115^\circ\text{C}$  a tipping point exists for PLLA polymer where two types of crystal modifications may occur, the perfect  $\alpha$  form and a frustrated  $\alpha'$  form.<sup>11,14,16</sup>



**Figure 5.4** X-ray diffractogram: heat-set (HS) yarns prepared from PLLA-core/PDLLA-shell fibres

A comparison of x-ray spectra of yarns prepared from as-spun PLLA, PDLLA and PLLA-core/PDLLA-shell respectively with a heat-set yarn prepared from PLLA-core/PDLLA-shell fibres is shown in Figure 5.5. Comparing the XRD peaks of the as-spun PLLA yarn and the heat-set PLLA-core/PDLLA-shell, it is clear that the PLLA yarn displays two peaks that are slightly off-set to the right of the two  $\alpha$  crystals peaks of the PLLA-core/PDLLA-shell yarn. The off-set peaks could be due to differences in packing order between the two  $\alpha$  crystal forms. The sharp peaks are evidence of  $\alpha$  crystals which is contradictory to the anisotropic scattering and the existence of small  $\beta$  peaks recorded in literature for as-spun PLLA fibres.<sup>3,4,8</sup> The reason for this was not investigated in greater detail.





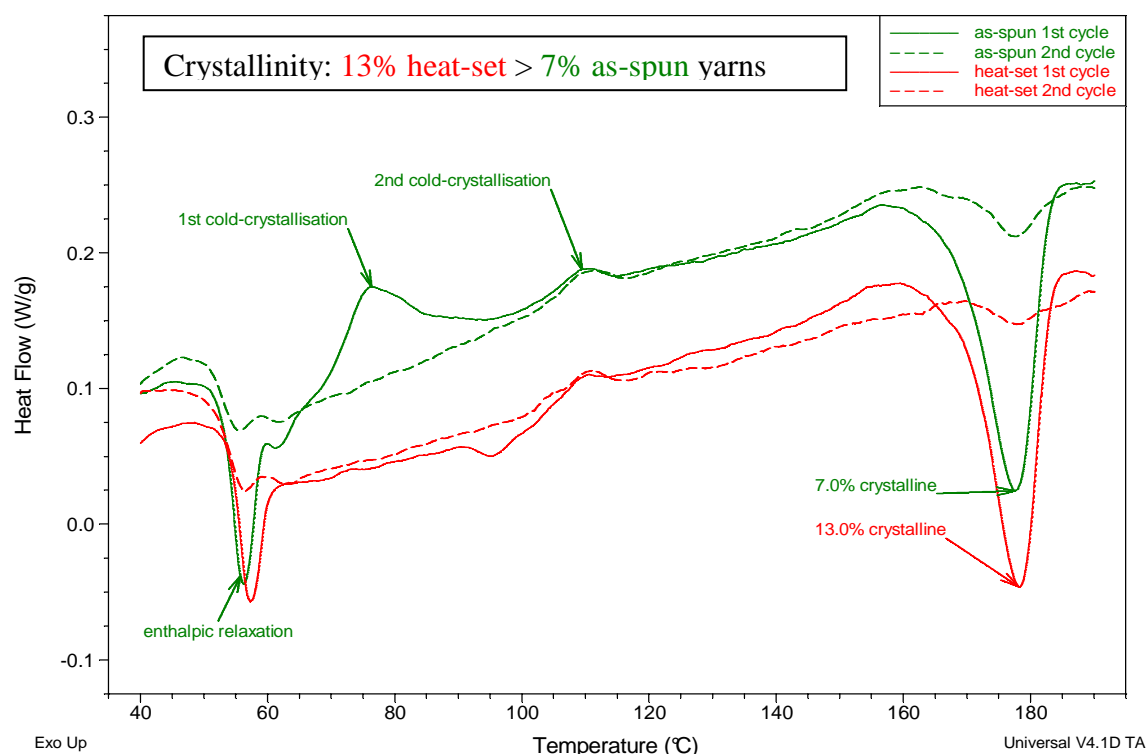
**Figure 5.5** XRD diffractograms comparing as-spun PLLA, PDLLA and PLLA-core/PDLLA-shell yarns with a heat-set PLLA-core/PDLLA-shell yarn

DSC analysis (Figure 5.6) of all as-spun and heat-set yarns showed that the  $T_g$  was always immediately followed by a sharp endothermic peak. This is a non-reversing thermal phenomenon and was attributed the relaxation enthalpy of frozen-in-stress of the oriented polymer molecules. These molecules were blocked from free movement in the glassy state, in a quasi-stable oriented conformation, as a result of the rapid solidification of the electrospinning jet. This stress should have been removed on heat-setting the yarns but it is present on the 1<sup>st</sup> heating cycle. Possible explanations for its presence include that the yarns were fixed at both ends on heat-setting and perhaps inhibited an amount of the oriented chains from relaxing, or alternatively, on pressing the samples in the DSC pans, the pressure may have induced cold drawing effects on the fibres.<sup>IV</sup>

A considerable cold crystallisation exotherm was seen for the as-spun yarns in the temperature range 65-90°C. This heat-flow out of the system is due to the packing and

<sup>IV</sup> Intermolecular interactions are relatively weak (no hydrogen bonds) and therefore cold drawing can occur under sufficient pressure/strain

transformation of oriented PLLA chains into crystal structures. This thermal phenomenon was not observed for the heat-set yarns as the isothermal crystallisation temperature used for heat-setting was above this cold-crystallisation temperature. A second, less pronounced, cold crystallinity exothermic peak was observed in the range 105-115°C for both as-spun and heat-set yarns. This could be called the intrinsic crystallisation region for PLLA as this is a reversible thermal event, whereas the first cold crystallisation region for PLLA as this is a reversible thermal event, whereas the first cold crystallinity peak is non-reversible, which confirms that the first peak was due to non-crystalline but oriented PLLA molecules.

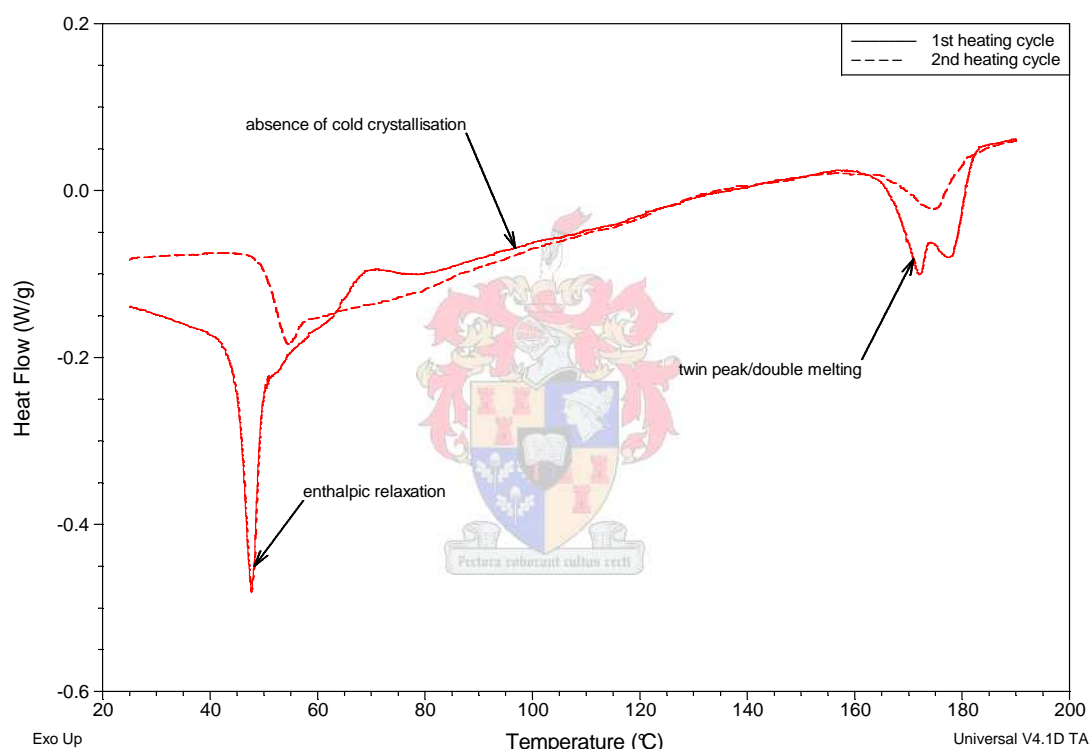


**Figure 5.6** DSC thermogram comparing thermal transitions for as-spun versus heat-set yarns

Significant melt endotherms were present for both as-spun and heat-set yarns in the region 165-190°C on the first heating cycle in DSC analyses. The melt endotherm on the second heating cycle was significantly smaller as there would be some disruption of the crystallisation by a fast cooling rate (10°C/min), the slow crystallisation nature of PLLA and mixing of PLLA and PDLA (miscible in the molten state).<sup>17</sup> The PDLA would there for interrupt crystal formation and cause a ‘dilution effect’ and the PLLA would not have sufficient time to crystallize as a result of the rapid rate of cooling.<sup>17</sup>

A double-peak melt endotherm fused at the base or a large melt endotherm with an endothermic shoulder on the left of the endotherm was seen in literature and on the 1st heating cycle for conventional DSC analysis of some (sporadic event not consistently seen) of the as-spun PLLA-core/PDLLA-shell fibres (Figure 5.7).<sup>3,4,8</sup>

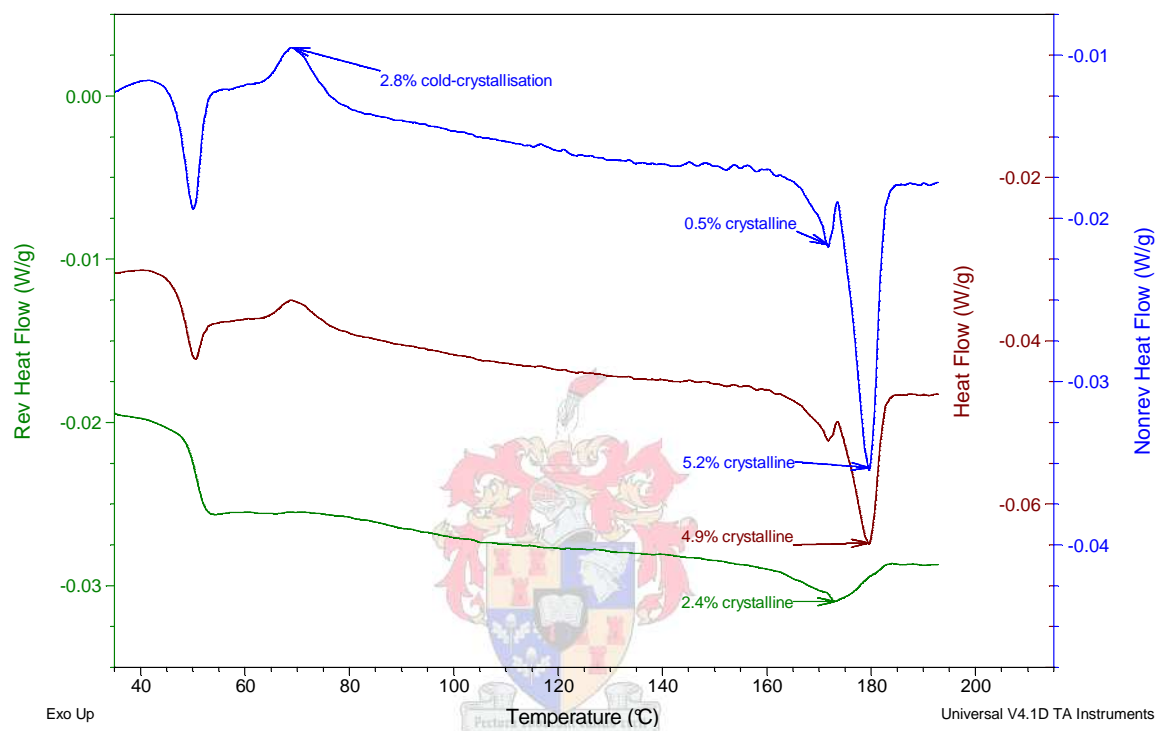
This phenomenon could be described by overlapping thermal events. This may be due to lower order (not  $\alpha$  crystals) crystal forms.<sup>4,10,18</sup> These lower order crystal forms may either be the  $\beta$  or a frustrated  $\alpha$  (denoted  $\alpha'$ ) crystal form.<sup>419</sup> The second endotherm at the higher melting temperature is due to the more stable  $\alpha$  crystal form.



**Figure 5.7** DSC thermogram: Double melting behaviour of PLLA-core/PDLLA-shell fibre yarn

This overlapping double-peak thermal phenomenon was resolved with some success using modulated differential scanning calorimetry (MDSC) (Figure 5.8) and represented using reversing and non-reversing curves. This was achieved by superimposing a faster sinusoidal heating rate onto a slower underlying linear heating rate. The MDSC analysis of the core-shell fibres in this case shows no re-crystallisation peak on the non-reversing curve. The transformation of the lower order crystals into more perfect  $\alpha$  crystals should be indicated by an exotherm for re-

crystallisation visible on the on-reversible heating curve.<sup>12</sup> This was not seen in Figure 5.8. The absence of this peak could indicate that there was no melting and reorganization of fibrillar  $\beta$  crystals into the more ordered  $\alpha$  crystals. A more likely explanation could be that  $\alpha'$  (imperfect  $\alpha$  created during cold crystallisations) crystal packing was melted first (1<sup>st</sup> endotherm) and then at the higher temperature perfect  $\alpha$  crystal packing was melted (2<sup>nd</sup> endotherm).



**Figure 5.8** MDSC thermogram: reversing/ non-reversing thermal transitions of fibres prepared by coaxial electrospinning PLLA-PDLLA core-shell solutions

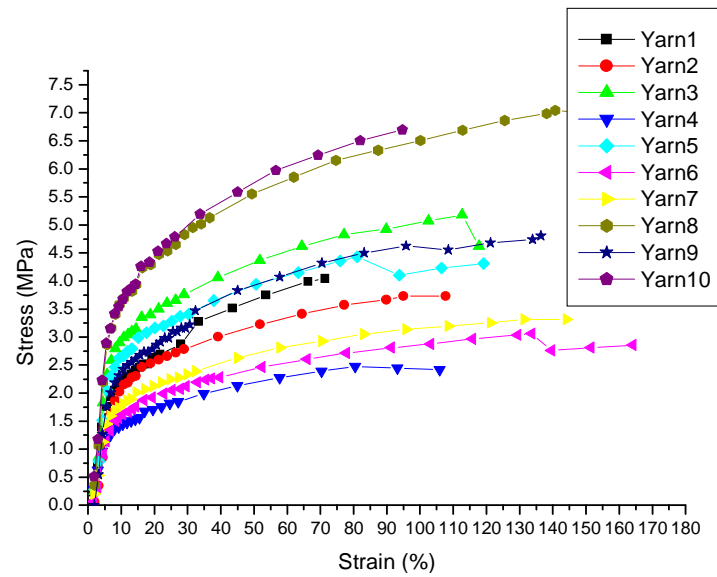
### 5.1.3. Mechanical properties

The yarns prepared from PLLA-core/PDLLA-shell fibres were shown to have only ordered chains and no notable crystal structures by XRD analysis (save a small 'bump' in the x-ray diffraction near  $16.5^\circ$  in the amorphous halo). Heat treating the yarns at the isothermal crystallisation temperature ( $110^\circ\text{C}$ ) and allowing them to cool to room temperature induced crystal structures. The annealed yarns were fused at the surfaces where fibres overlapped.

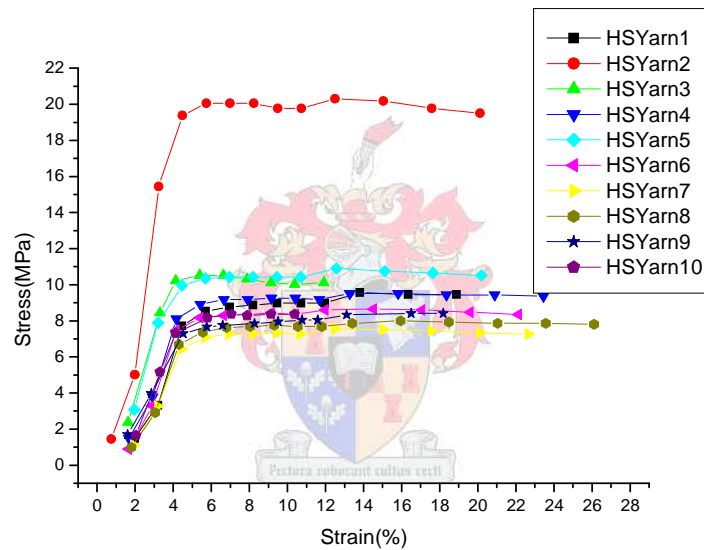
Since the crystallinity within the fibres was shown to be enhanced after heat-setting and the PDLA shell of the overlapping fibres fused, it was expected that the modulus and yield breaking strength would be higher for the heat-set yarns versus as-spun fibres. Flexibility and elongation would be sacrificed as a result of the crystallinity because the yarns would essentially be a reinforced monofilament compared to the multi-filamentous as-spun fibre yarn. This was therefore not an ‘apples with apples’ comparison, but it is reasonable to assume a structure-property comparison could be drawn between heat-set and as-spun yarns as this should be a function of increasing crystallinity for an equivalent volume of material.

Stress/strain curves from the mechanical testing of the as-spun and heat-set yarns are shown in Figures 5.9 and 5.10 respectively. A comparison of stress/strain of an as-spun versus a heat-set sample from prepared from the same original yarn is shown in Figure 5.11. The heat-set yarns showed that the crystallinity induced into the core of the fibres resulted in an increase in the modulus and yield strength, and a decrease in elongation compared with as-spun fibres.

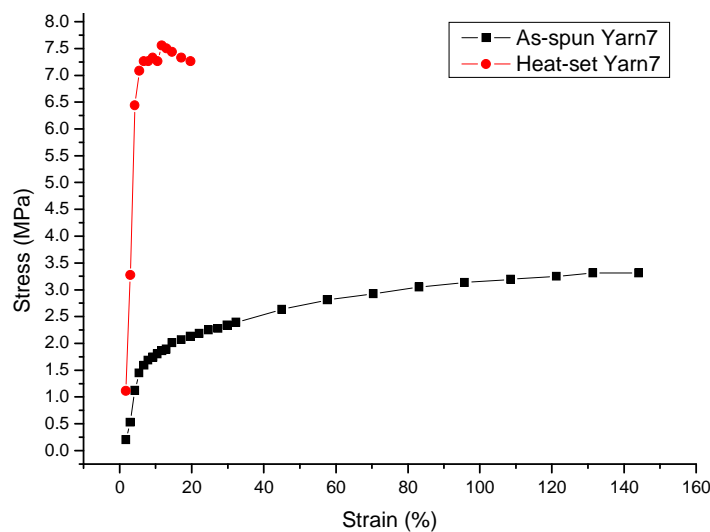
High yield extension was observed for as-spun fibre yarns, as opposed to heat set yarns. This is the result enhanced crystallinity of the cores and because of fusion at the overlapping fibre surfaces for heat-set yarns that resist slippage. Necking was seen for both as-spun (Figure 5.12) and heat set samples (Figure 5.13) indicating the ability of the fibre to tolerate a certain amount of force (load) before breaking. This could be attributed to the deformation of the non-crystalline regions and the amorphous PDLA shell material.



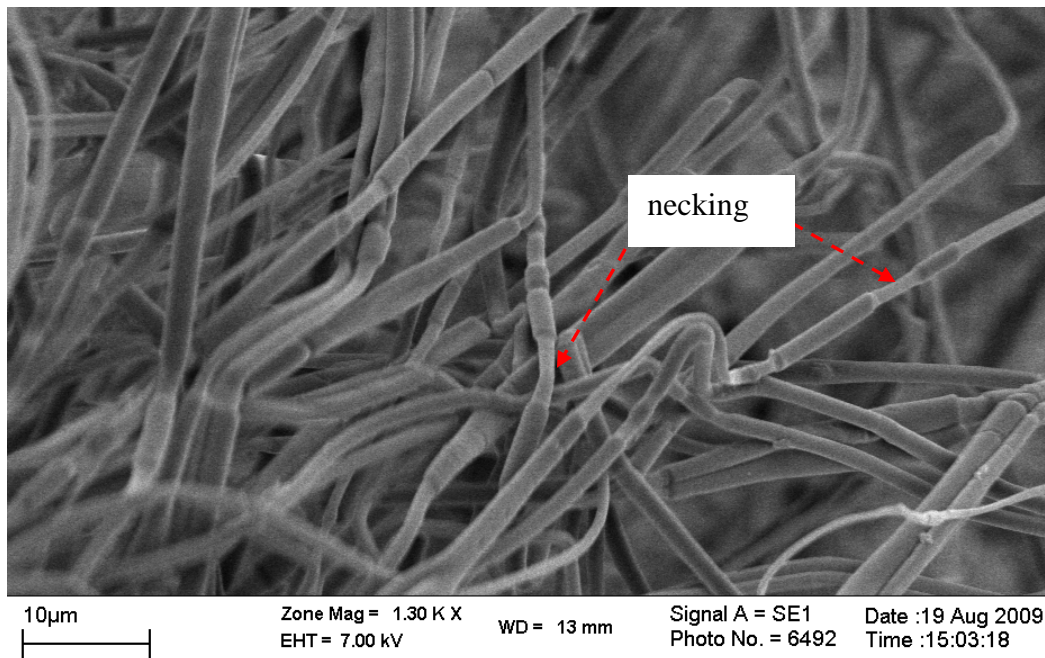
**Figure 5.9** Stress vs. Strain of as-spun fibre yarns



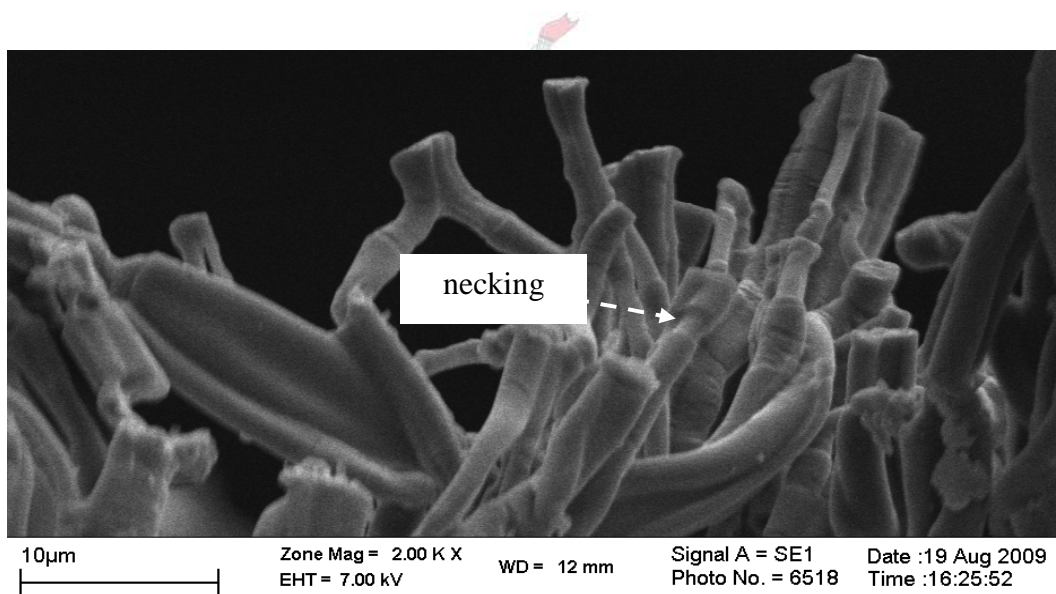
**Figure 5.10** Stress vs. Strain of heat-set yarns



**Figure 5.11** Stress vs. strain curves of as-spun and heat-set yarns for sample no.7



**Figure 5.12** *As-spun fibre yarn sample after mechanical testing*

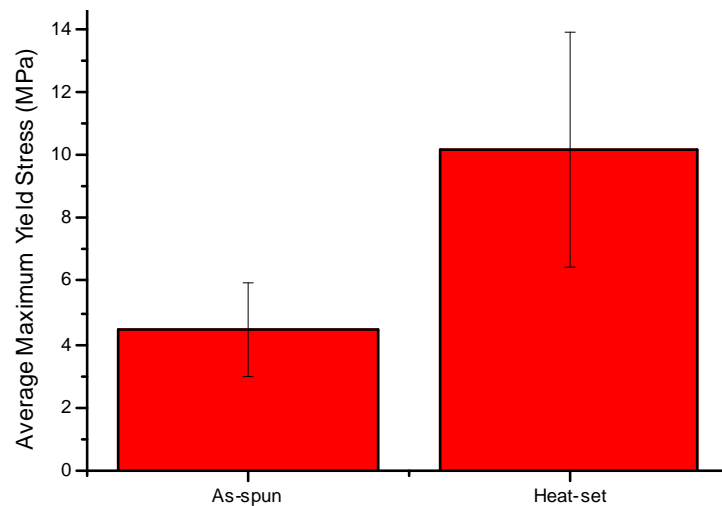


**Figure 5.13** *Heat-set fibre yarn after mechanical testing*

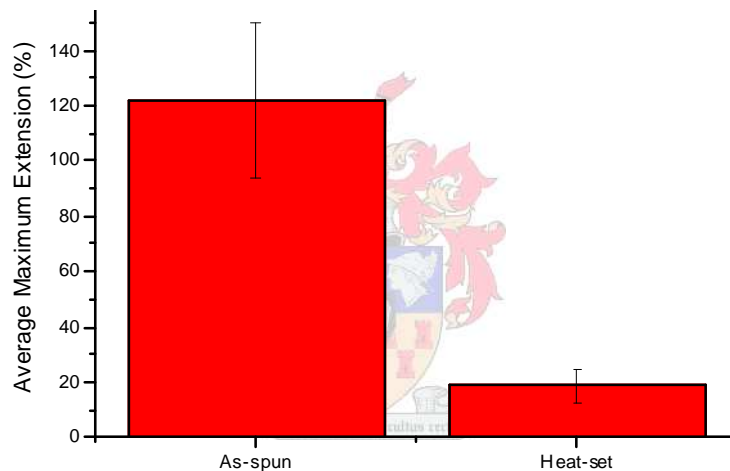
The average maximum stress and maximum extension of as-spun and heat-set yarns are shown in Figures 5.14 and 5.15 respectively.<sup>V</sup> It was shown that by inducing significant crystal structures in the cores of the heat-set yarns, and simultaneously fusing the shell components, a stronger material is attainable. This material does not however possess the toughness or extension characteristics seen in the as-spun yarns.

<sup>V</sup> the data is shown in Appendix C: Table C.11





**Figure 5.14** Average maximum yield stress (MPa) of as-spun versus heat-set yarns



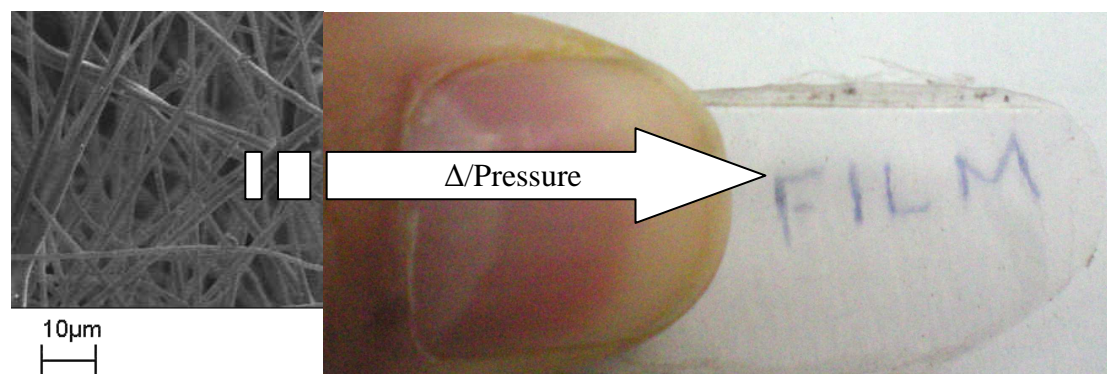
**Figure 5.15** Average maximum extension (%) of as-spun versus heat-set yarns

The Young's modulus (average 215.5MPa) and yield strength ( $\pm 4.5$ MPa) of the heat-set yarns, although significantly higher than the as-spun yarns, were not that high when compared to individual fibres prepared by conventional dry spinning ( $\pm 2.5$ GPa and  $\pm 65$ MPa respectively).<sup>19</sup> A recent study of braided electrospun PLLA and Chitosan-PLLA core-shell fibres for sutures were shown to have yield strengths between 80-90MPa and young's modulus between 380-580MPa. The braided sutures samples showed a yield strength of around 8.8N (yarn diameter 0.35mm) which was close to a typical commercially available suture. The heat-set core-shell fibre yarns in this study displayed an average yield strength of  $6.5 \pm 1.3$ N ( $\pm 4.5$ MPa for yarns with

average diameters of  $0.46 \pm 0.06 \text{ mm}$ ) and therefore further investigations in future work should be undertaken to improve these properties.<sup>20</sup>

## 5.2. SPC Films

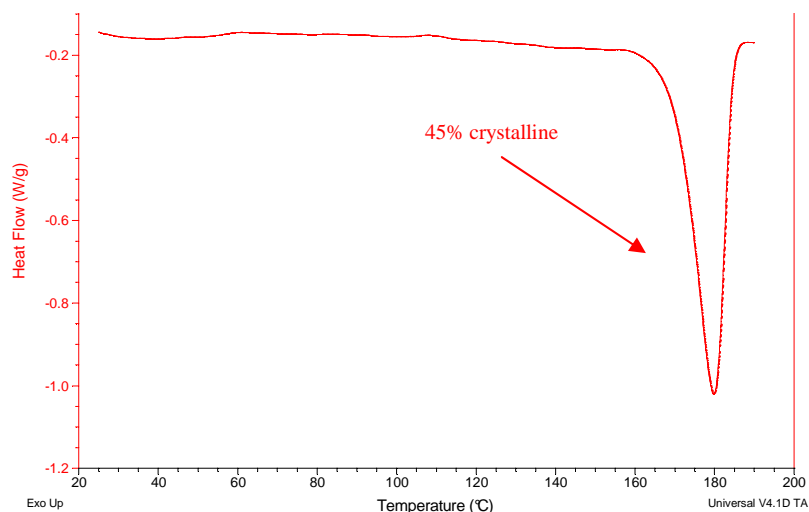
A flat transparent film was produced by heat-pressing a PLLA-core/PDLLA-shell fibre mat, having an average fibre diameter of  $1518 \pm 271 \text{ nm}$  (Figure 5.16).



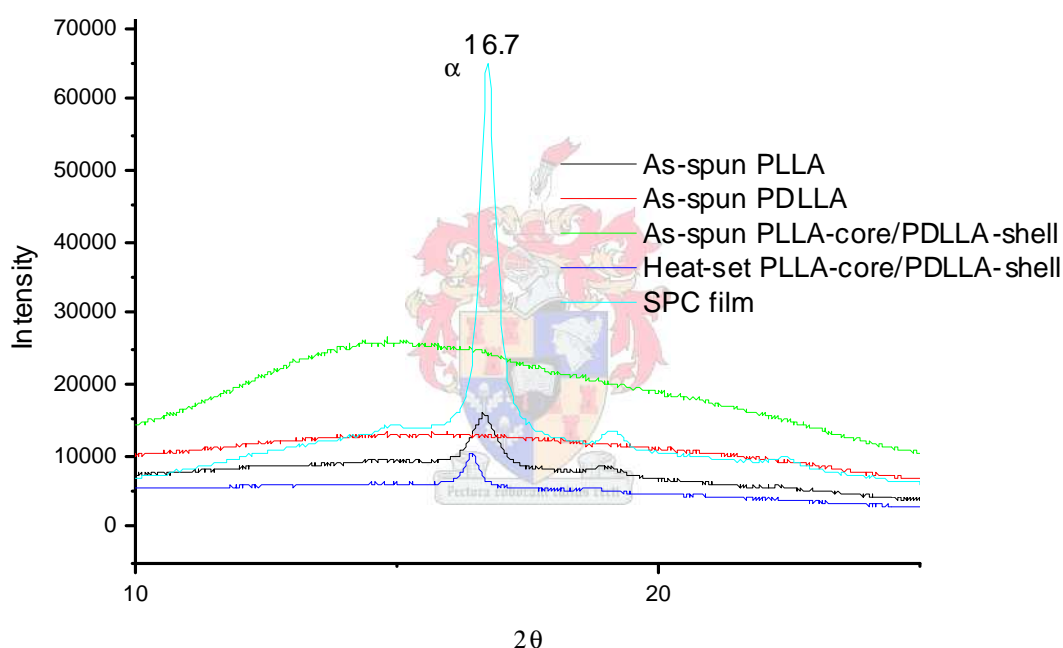
**Figure 5.16** Coaxial electrospun PDLLA-PLLA mat before heat pressing (left) and the SPC film in front of a piece of paper with the word 'FILM' written on it to show the transparency of the film

The fine structure of the film was studied with DSC and XRD. The DSC thermogram for the film showed a very sharp melt endotherm (peak maximum  $180^\circ\text{C}$ ) and no cold-crystallisation peak (Figure 5.17). The PLLA molecules in the film were therefore packed into very ordered crystal structures.

An x-ray diffractogram for the SPC film is compared with diffractograms of yarns prepared from as-spun PLLA, PDLLA and PLLA-core/PDLLA-shell and heat-set PLLA-core/PDLLA-shell (Figure 5.18). A sharp intense XRD crystal peak was present at  $16.7^\circ$  and a less pronounced peak at  $18.9^\circ$  was indicative of the presence of extensive  $\alpha$  crystallographic packing. What is interesting to note is that the peak at  $16.7^\circ$  is about six orders of magnitude greater than the heat-set yarn. This illustrates the importance of pressure applied in conjunction with heat as a means for increasing crystallinity. This resulted therefore in more perfect  $\alpha$  crystalline packing.



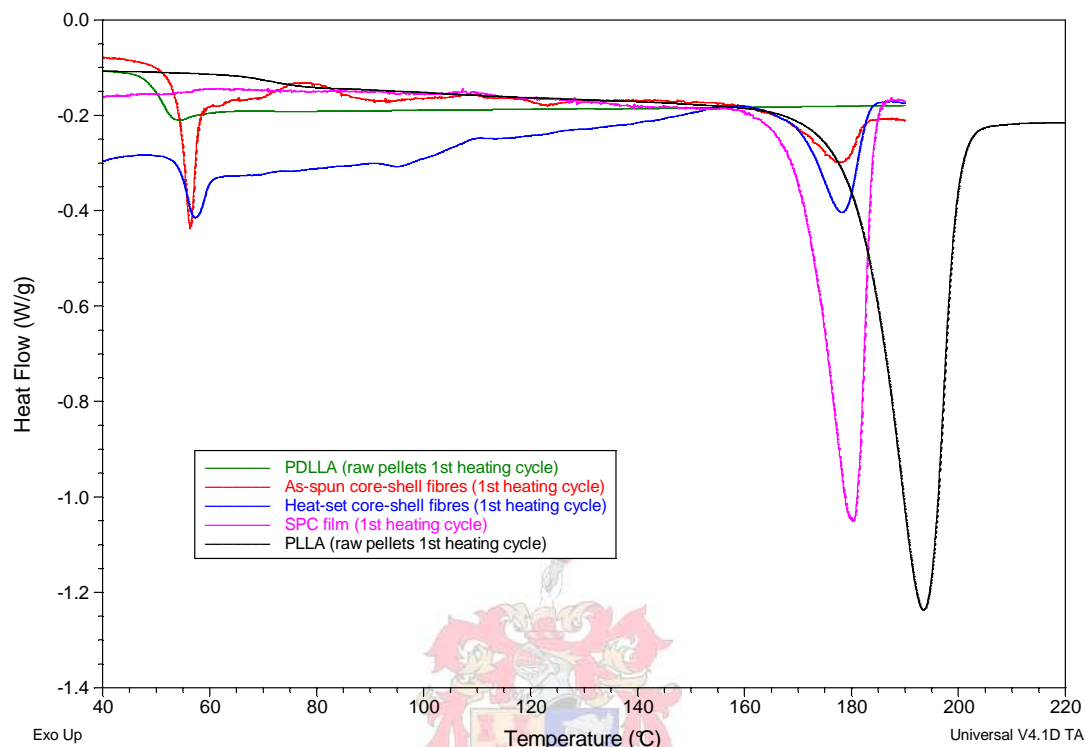
**Figure 5.17** DSC thermogram showing 1<sup>st</sup> heating cycle of the heat-pressed film



**Figure 5.18** XRD diffractogram comparing electrospun PDLLA, PLLA, PLLA-PDLLA core-shell and heat-set PLLA-PDLLA core-shell fibre yarns with that of the SPC film

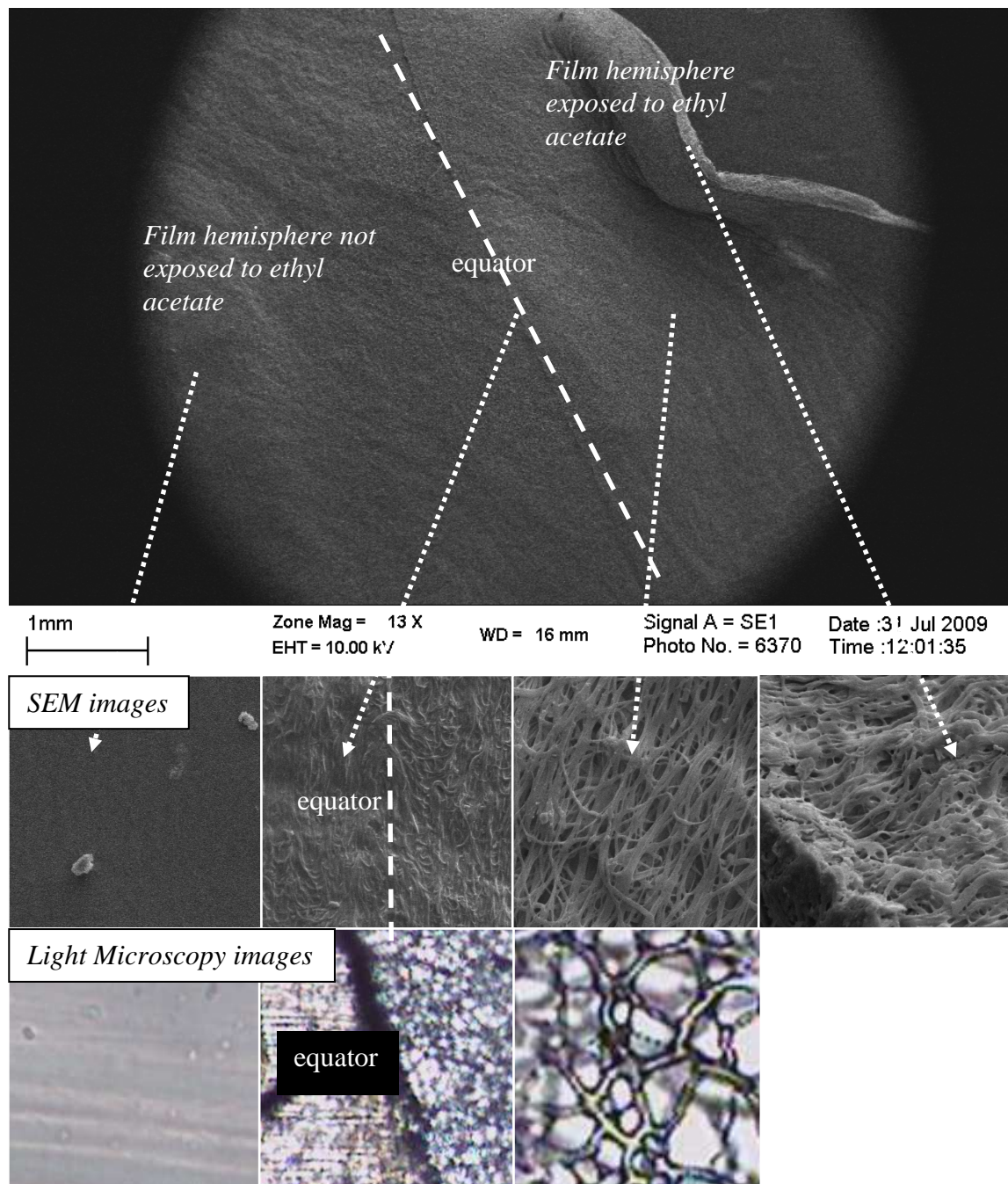
DSC thermograms of PDLLA and PLLA raw polymer, a yarn prepared from PLLA-core/PDLLA-shell fibres, a heat-set yarn of the same, and the SPC film are compared in Figure 5.19. The samples were arranged in terms of percentage crystallinity in order from highest to lowest: PLLA pellets > SPC film > Heat-set core-shell fibres > as-spun core-shell fibres > PDLLA pellets. This comparison shows the extensive crystallisation of the PLLA reinforcing fibrils in the SPC film. This once again

confirms the importance of pressure in conjunction with heat for the enhancing crystallinity (although the same crystallinity may be possible by annealing without pressure over a longer period of time).



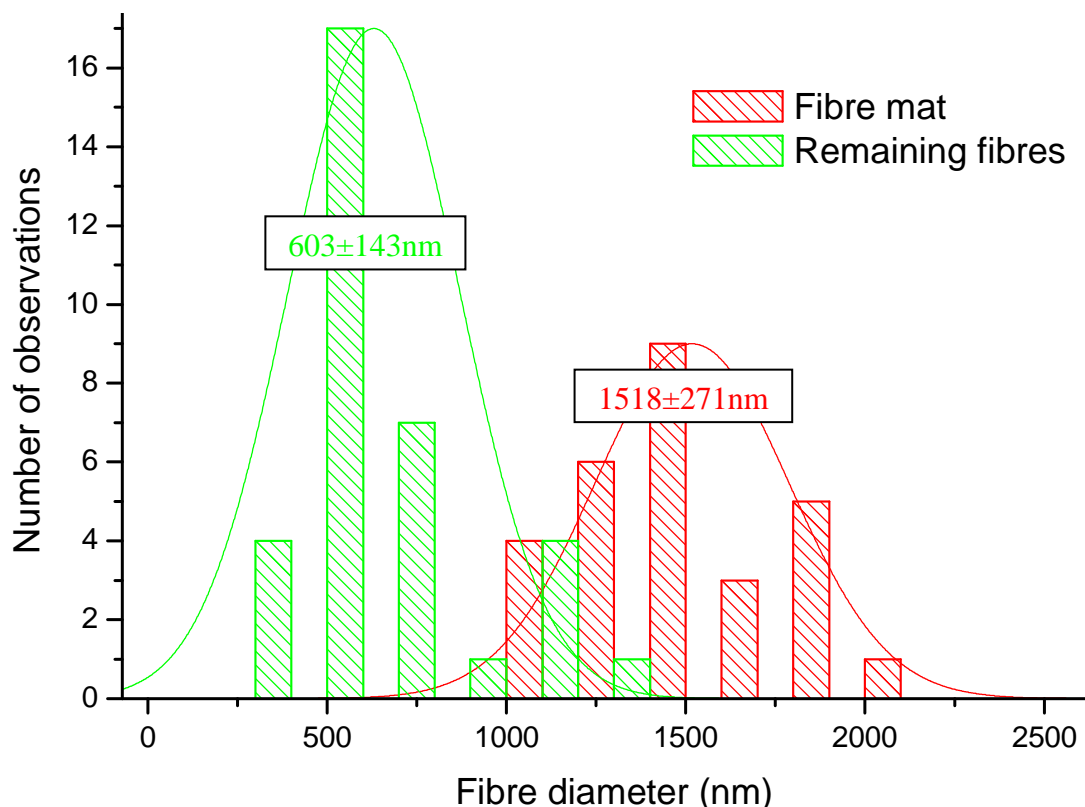
**Figure 5.19** DSC thermograms of PDLLA and PLLA raw polymer, a yarn prepared from PLLA-core/PDLLA-shell fibres, a heat-set yarn of the same, and the SPC film

On selectively dissolving away the PDLLA matrix material from the one section of the film, fibres remained (Figure 5.20). The average diameter of these fibres was  $(603 \pm 143 \text{ nm})$ . The fibre diameter distributions of the fibre mat before heat-pressing and of those fibres remaining after the PDLLA was selectively dissolved from the SPC film is shown in Figure 5.21.



**Figure 5.20** SEM and light microscopy images of a film having one hemisphere soaked in ethyl acetate



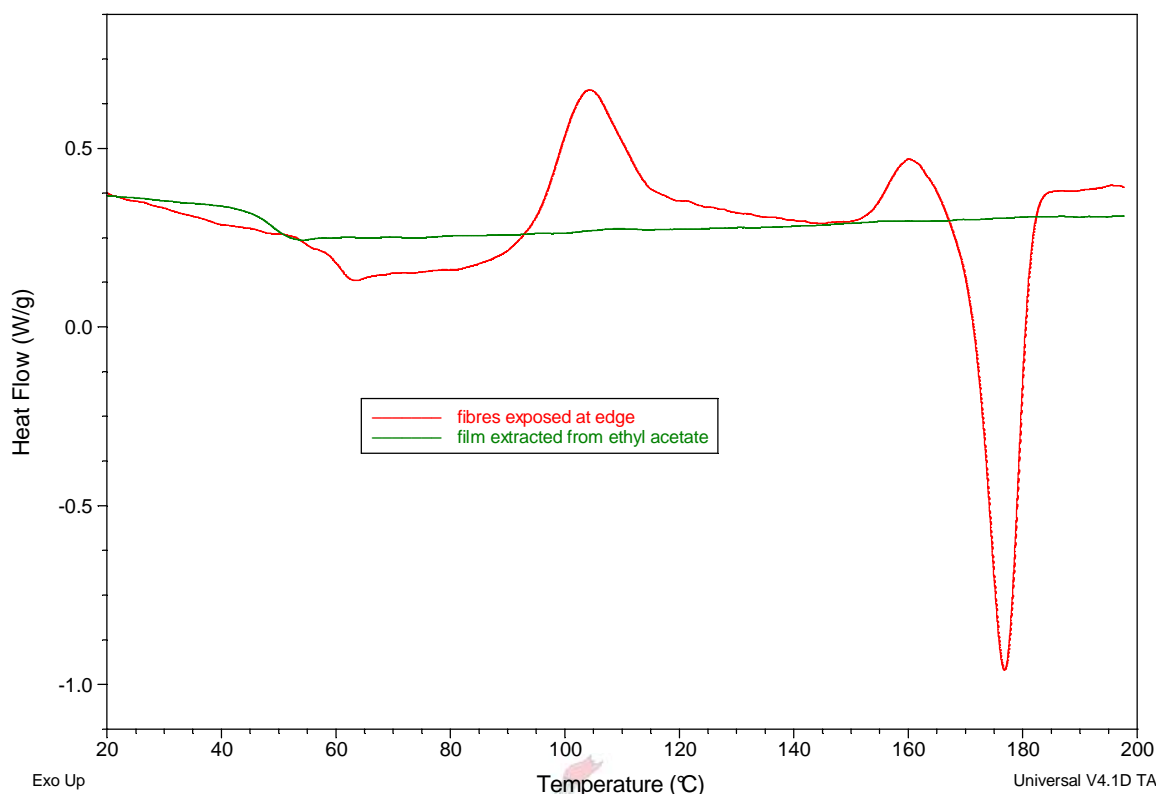


**Figure 5.21** *Fibre diameter distributions of fibre mat before heat pressing and the exposed remaining fibres after selective dissolution of PDLLA from the film with ethyl acetate (average fibre diameters are shown in boxes)*

After washing the film with ethyl acetate, the solvent was evaporated and a film left behind. DSC analysis confirmed that the remaining fibres and the extracted film were in fact semi-crystalline PLLA core material and the amorphous PDLLA matrix material respectively (Figure 5.22). This was evidenced by a sharp melt endotherm present for the remaining fibres and the absence of any endotherm for the extracted film. The remaining fibres showed optical activity (specific rotation  $-191^\circ$ ) and film extract did not (zero).

A transparent fibre reinforced film was therefore created that had a reinforcing component that had extensive crystallinity and a matrix material that pre-impregnated the reinforcing material. The transparency of the film may be attributed to the similar light diffraction coefficients of the polymers and also the fine diameters of the cores in the transparent amorphous matrix.





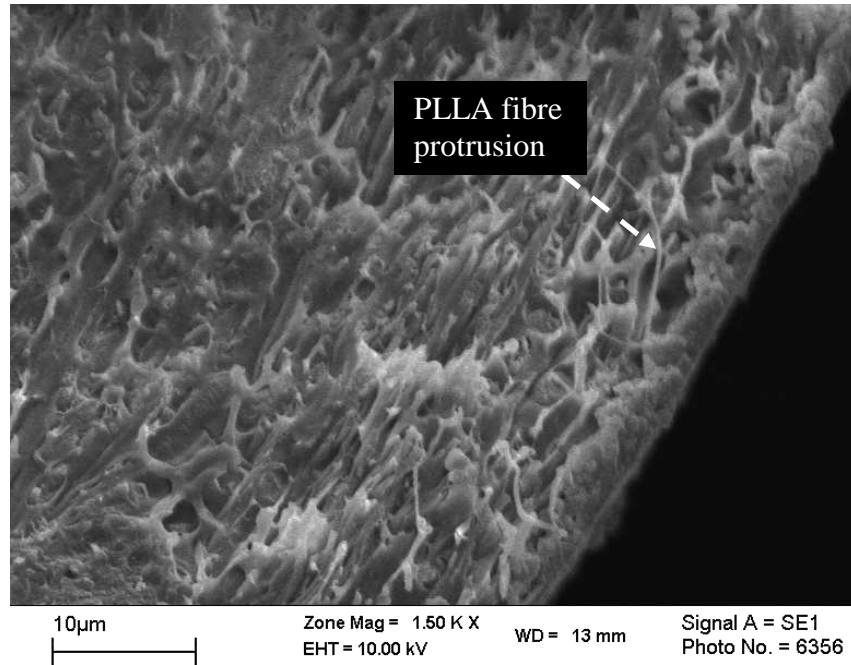
**Figure 5.22** DSC thermogram of the fibres exposed at the film edge after selective dissolution by ethyl acetate, compared with the polymer that was extracted with ethyl acetate

Cryo fracturing of the SPC films exposed fibrous structures at the point of fracture which confirms that the cores remained intact as fibrous structures (Figures 5.23 and 5.24).<sup>VI</sup> A reference PDLLA fibre mat was prepared by single capillary electrospinning. A film was prepared by heat-pressing the PDLLA plied fibre mat at 60°C for 1h. The PDLLA film was then cryo-fractured.<sup>VII</sup> There was no evidence at the point of fracture of any reinforcing fibres. This film was processed under milder conditions as previous attempts to process a PDLLA film under the same conditions as the PLLA-PDLLA fibre mat was not successful as the PDLLA film disintegrated and flowed out of the mould. This confirms that the fibres protruding from the SPC film were only PLLA fibrils.

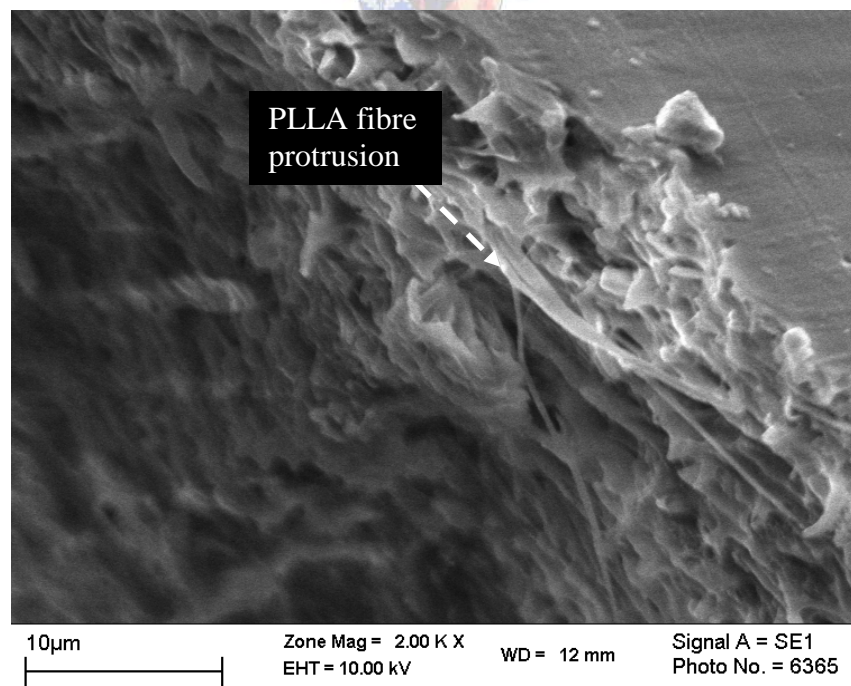
<sup>VI</sup> Appendix C: Figure C.31a and C.31b

<sup>VII</sup> Appendix C: Figure C.32

The cryo fracture samples showed some loose PLLA fibrils protruding from the point of fracture but more commonly the fibres were shown to be in intimate contact with the matrix which is favourable in terms of the materials resistance to delamination.



**Figure 5.23** *Cryo fractured film*

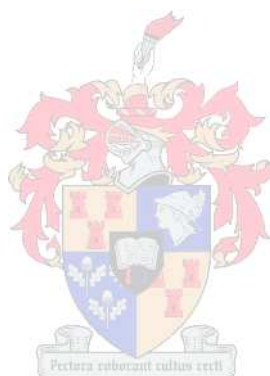


**Figure 5.24** *Cryo fractured film*

## References

1. Zong X, Ran S, Kim K-S, Fang D, Hsiao BS, Chu B. Structure and morphology changes during in vitro degradation of electrospun poly(glycolide-co-lactide) nanofiber membrane. *Biomacromolecules*. 2003;4:416-23.
2. Li R, Yao D. Preparation of single poly(lactic acid) composites. *Journal of Applied Polymer Science*. 2007 10/08/2007;107:2909-16.
3. Zong X, Kim K, Fang D, Ran S, Hsiao BS, Chu B. Structure and process relationship of electrospun bioabsorbable nanofiber membranes. *Polymer*. 2002;43:4403-12.
4. Zhou H, Green TB, Joo YL. The thermal effects on electrospinning of polylactic acid melts. *Polymer*. 2006 2006;47:7497-505.
5. Derch R, Liu T, Schaper AK, Greiner A, Wendorff JH. Electrospun nanofibers: internal structure and intrinsic orientation. *Journal of Polymer Science*. 2003;41:545-53.
6. Tan PS, Lim CT. Effects of annealing on the structural and mechanical properties of electrospun polymeric nanofibres. *Nanotechnology*. 2006;17:2649-54.
7. Wang C, Chien H-S, Yan K-W, et al. Correlation between processing parameters and microstructure of electrospun poly(D,L-lactic acid) nanofibers. *Polymer*. 2009;10.1016/j.polymer.009.10.025.
8. Inai R, Kotaki M, Ramakrishna S. Structure and properties of electrospun PLLA single nanofibres. *Nanotechnology*. 2005;16:208-13.
9. Garlotta D. A Literature review of poly(lactic acid). *Journal of Polymers and the Environment*. 2002;9(2):63-84.
10. Hoogsteen W, Postema AR, Pennings AJ, ten Brinke G. Crystal structure, conformation, and morphology of solution-spun poly(L-lactide) fibers. *Macromolecules*. 1990;23:634-42.
11. Yasuniwa M, Tsubakihara S, Iura K, Ono Y, Dan Y, Takahashi K. Crystallization behaviour of poly(L-lactic acid). *Polymer*. 2006;47:7554-63.
12. O'Connor A, Riga A, Turner II JF. Determination of crystalline content gradients in cold-drawn poly-L-lactic acid films by DSC. *Journal of Thermal Analysis and Calorimetry*. 2004;76:455-70.
13. Zhou H, Kim K-W, Giannelis EP, Joo YL. Nanofibers from polylactic acid nanocomposites: effect of nanoclays on molecular structures. *ACS Symposium Series*. 2006;918:217-30.
14. Yasuniwa M, Sakamo K, Ono Y, Kawahara W. Melting behaviour of poly(L-lactic acid): X-ray and DSC analyses of the melting process. *Polymer*. 2008;49:1943-51.
15. Pan P, Zhu B, Kai W, Dong T, Inoue Y. Effect of crystallization temperature on crystal modifications and crystallization kinetics of poly(L-lactide). *Journal of Applied Polymer Science*. 2007;DOI 10.1002/app.27102.
16. Zhang J, Tashiro K, Domb AJ, Tsuji H. Confirmation of disorder alpha form of poly(L-lactic acid) by x-ray fiber pattern and polarized IR/raman spectra measured for uniaxially-oriented samples. *Macromolecules Symposium*. 2006;242:274-8.
17. Pan P, Liang Z, Zhu B, Dong T, Inoue Y. Blending effects on polymorphic crystallization of poly(L-lactide). *Macromolecules*. 2009;42:3374-80.

18. Cho T-Y, Strobl G. Temperature dependent variations in the lamellar structure of poly(L-lactide). *Polymer*. 2006;47:1036-43.
19. Gupta BS, Revagade N, Hilborn J. Poly(lactic acid) fiber: An overview. *Progress in Polymer Science*. 2007;32:433-82.
20. Hu W, Haung Z-M. Biocompatibility of braided poly(L-lactic acid) nanofiber wires applied as tissue sutures. *Polymer International*. 2009;DOI:10.1002/pi.2695.



# Chapter 6

## *Conclusions and recommendations for further study*

*This chapter details how those specific objectives set in the beginning of this study were met and the recommendations for further study.*

### 6.1. Conclusions specific to set objectives

- A. *Development of a coaxial electrospinning process that could produce core-shell fibres from miscible solutions of amorphous PDLLA and semi-crystalline PLLA*

A coaxial electrospinning set-up was constructed with commercially available materials. The core and shell solutions were delivered to the coaxial spinneret in a controlled and reproducible manner. The existence of a compound Taylor cone and the streaming of a dyed core-solution into the electrospinning shell solution jet were visually confirmed using a magnifying glass. A single core-shell electrospinning jet was observed and the applied voltage was controlled as to prevent multiple jetting caused by excessive charge build-up in the Taylor cone. At no point did the core and shell streams split from each other to form two jets, and therefore a composite fibre consisting of both core and shell polymer was prepared.

There is an ongoing debate among electrospinning researchers that believe solution immiscibility is paramount to the formation of core-shell fibres and those who disagree. Miscible polymer solutions can be electrospun into core-shell fibres since the rate of diffusion of polymer molecules is significantly slower than the rate of electrospinning<sup>1</sup>, although some small scale blending is seen by an ill defined interface between the two components. This study, in agreement with Sun *et al*<sup>1</sup>, shows that miscible solutions may also be used to coaxial electrospinn core-shell fibres.

**B.** *Development of a method to analyse the core-shell fibre structure and study the effects of solution and other electrospinning process parameters on fibre morphology*

The coaxial electrospun PLLA-PDLLA core-shell fibres could not be analysed with TEM. The fibres were too sensitive to radiation and did not consistently provide contrast in order to discern between the two components. Other techniques such as light microscopy or SEM of yarn cross sections were also not successful.

Fluorescence microscopy of core-shell fibres with a fluorescently labelled core suggested the formation of both core-shell and twin fibre structures, where the PLLA material was continuous along the length of the fibre.

An indirect approach, consisting of the separation of the core and shell components by dissolution of the shell component in ethyl acetate was successful and confirmed by DSC and polarimetry. Continuous fibres remained after washing with ethyl acetate. These remaining fibres, when dissolved in chloroform, displayed optical activity indicative of PLLA polymer. The polymer remaining in ethyl acetate solution formed a clear film when dried under vacuum. This film dissolved in chloroform showed zero optical activity indicative of PDLLA polymer. The fibres, remaining after washing in ethyl acetate, demonstrate a significant increase in the melt endotherm in DSC thermograms associated with melting of semi-crystalline PLLA polymer. The polymer film, from the ethyl acetate extract, displays no melt endotherm in DSC thermograms associated with lack of crystalline order of amorphous PDLLA polymer.

The core solution concentration and flow rate can be used to control the ratio of core:shell material. These variables can be used to adjust the ratio of either material in the core-shell structure and thereby tailor the fibre properties to meet desired performance requirements. The core solution flow rate was the most significant parameter in influencing core fibre diameter compared with core solution concentration. Shell solution concentration and flow rate had a significant influence on the core fibre diameter and total fibre morphology in the ranges used.



C. *Evaluation of internal molecular arrangement within the fibres and the potential to enhance the crystallinity of the core and heat-bond neighbouring fibres within the thermal operating window*

XRD and DSC studies on as-spun coaxial electrospun PLLA-PDLLA core-shell fibre yarns show that the polymer molecules were highly oriented along the fibre axis. Heat setting the yarns above the glass transition temperature of PDLLA and using the cold-crystallisation temperature of PLLA increased the crystallinity within the fibre cores and fused the fibre shells where they overlapped. Mechanical testing of the heat-set yarns showed that the increase in crystallinity imparted greater yield strength and an increase in Young's modulus to the fibres. This was at the expense of toughness.

A single polymer composite film was prepared by heat-pressing a plied core-shell fibre mats between the glass transition temperature of the shell and the melting temperature of the core material. The shell components were induced to flow under pressure and created the matrix of the composite material. XRD studies showed the transparent film to be highly crystalline. Washing the film in ethyl acetate exposed fibres. These fibres were determined to be PLLA by DSC and optical rotation measurements, and also the fact the PLLA is insoluble in ethyl acetate and does not melt under the processing conditions used. Therefore the novelty of the SPC core-shell fibres and its potential in composite yarns and structures for biodegradable products has been validated.

The core-shell fibre system in this study is favourable for the preparation of fibre reinforced composite materials. Defects such as poor interfaces and differences in refractive index between reinforcing fibres and resin matrices are avoided with this system as the cores are in intimate contact with the matrix as a result of the fine diameters of the cores and their chemical compatibility.<sup>2</sup> This means that composites prepared from these fibres will be less prone to delamination, will be transparent (as essentially a one phase material) and due to their chemical similarity, these composites can be more easily re-applied, re-cycled or composted than heterogeneous composites.

Furthermore creating a core-shell fibre structure where the shell component can form the matrix and the core the reinforcing continuous fibre component, is a far simpler route to disperse nano-fibres homogeneously in a transparent matrix resin (as opposed to solvent casting impregnation methods).<sup>2</sup>

## 6.2 Recommendations for further study

Future work could involve a more comprehensive look into processing composites from these materials. The yarns made in this study did not have sufficient mechanical properties for use as suture materials and therefore these properties could be improved on by different processing conditions e.g. linear density, twists/cm, processing times and temperatures, drawing steps etc. Perhaps heating the fibres to the cold-crystallization temperature would ensure maximum crystallinity. Additionally other mechanical tests should be done that are more application specific e.g. knot strength in suture applications.

Medical products have to meet strict toxicity requirements. The solvents used in the study are harmful to human beings. Although during the electrospinning process most of the solvent is evaporated, trace amounts of solvents could be a potential hazard for implantable materials. It is recommended that future work be aimed at creating a solvent system that is less toxic than the one currently used. Solubility parameters can be tailored by adding various solvents in specific combinations, adding ionic salts and also changing the temperature of the solution (adding ion salts to a less hazardous solvent such as ethyl acetate or ethyl lactate solvent can theoretically be used to achieve the correct solubility parameters to dissolve the polymers).

Further work may also include using other biodegradable polymers and their copolymers in various combinations to form other SPC's to provide specific properties. It would be of considerable interest to include specific active components into the shell and/or core material for controlled release applications. The active species may be hydrophilic or hydrophobic to control release rates i.e. hydrophobic species will only be released when the polymer degrades whereas hydrophilic species usually show faster release rates.<sup>3</sup> As part of any tissue engineering application

biodegradation characteristics and biocompatibility of the material should be assessed by *in vivo* and *in vitro* studies.<sup>4</sup>

Molecular orientation and crystallographic packing are important for mechanical as well as degradation properties of biodegradable fibres. These kinds of fine structure require greater investigation and this could be achieved using polarized FTIR (Fourier transform infrared spectroscopy)<sup>5</sup>, dynamic sonic modulus<sup>6</sup> and solid-state NMR (nuclear magnetic resonance)<sup>7</sup> analysis. To further explain the original nature of crystal structures present in as-spun fibres the molecular structure changes during a heating cycle can be studied using temperature-dependent XRD analysis.

#### References

1. Sun Z, Zussman E, Yarin AL, Wendorff JH, Greiner A. Compound core-shell polymer nanofibers by co-electrospinning. *Advanced Materials*. 2003;15(2003):1929-32.
2. Chen L-S, Haung Z-M, Dong G-H, Liu L, Hu Y-Y, Li Y. Development of a transparent PMMA composite reinforced with nanofibers. *Polymer Composites*, 2009.
3. Haung Z-M, He C-L, Yang A, et al. Encapsulating drugs in biodegradable ultrafine fibers through co-axial electrospinning. *Wiley Periodicals*. 2005;DOI: 10.1002/jbm.a.30564.
4. Li W-J, Cooper Jr JA, Mauck RL, Taun RS. Fabrication and characterization of six electrospun poly( $\alpha$ -hydroxy ester)-based fibrous scaffolds for tissue engineering applications. *Acta Biomaterialia*. 2006;2:377-85.
5. Zhang J, Duan Y, Sato H, et al. Crystal modifications and thermal behaviour of poly(L-lactic acid) revealed by infrared spectroscopy. *Macromolecules*. 2005;38:8012-21.
6. Ghosh S, Vasanthan N. Structure development of poly(L-lactic acid) fibers processed at various spinning conditions. *Journal of Applied Polymer Science*. 2005;101:1210-6.
7. Ito T, Maruhashi Y, Demura M, Asakura T. Carbon-13 solid state NMR study on uniaxially oriented poly(L-lactic acid) films. *Polymer*. 2000;41:859-66.

# Appendix A

## Single Capillary Electrospinning

Single capillary electrospinning is a logical preamble to coaxial electrospinning. Successful coaxial electrospinning requires that the shell solution be electrospinnable and that the core solution should be of sufficient viscosity that it may be dragged into the electrospinning jet. Solvent ratio and solution concentration were varied systematically to determine the optimal solution parameter range that would yield smooth fibres and a stable electrospinning process. The information gathered was then used to prepare solutions for coaxial electrospinning. Determination of the Berry number, a calculation of solution concentration and intrinsic viscosity, as an a priori means to predict 'electrospinnability' was tested with the two polymer systems.

### A.1 Experimental

#### A.1.1 Solution preparation and electrospinning

Solution preparation and single capillary electrospinning was carried out as described in Sections 3.1.2 and 3.2 in (Chapter 3). Analysis of the fibre diameters and morphology was performed by SEM as described in Section 3.2.3 (Chapter 3).

#### A.1.2 Determination of Solution Viscosity

Viscosity measurements were performed on polymer solutions using a Brookfield Digital Viscometer (Model RVTD) with a cone spindle (nr21), small solution chamber (held at 25°C) and shear rates of 10rpm and 50rpm. PLLA and PDLLA solutions were prepared to have 4, 6, 8, 10, 12wt% concentrations in 70/30 DCM/DMF. 10mL Solutions were allowed to stir for four days at 100rpm (25°C) in poly tops. Approximately 5mL solution were added to the chamber and allowed to condition at the solution chamber conditions (25°C). Measurements were recorded after 1 and 3 min and the average readings calculated. The inherent viscosity can be calculated from the instrument reading by multiplying the instrument reading with a factor that takes the rpm and spindle size into consideration.

## A.2 Results and Discussions

### A.2.1 Solution parameter effects on fibre diameter, fibre morphology, and process stability

The influence of various key parameters on the electrospinning process, fibre diameter and fibre morphology is discussed in detail in various papers as presented in Chapter 2 – Literature Review. A starting point in any electrospinning experiment is to configure the solution properties first at constant ambient and processing conditions that produce a consistent and stable electrospinning jet, and uniform fibres of a required dimension. Optimisation of the electrospinning process by careful control of the ambient and process parameters is then later sought for reproducibility and fine tuning.

A basic electrospinning set-up was used as described in Chapter 3 (Section 3.2) using a single capillary. The effects of solvent ratio and polymer solution concentration on fibre morphology were investigated.

Based on preliminary work done in our group and what exists in literature<sup>1</sup>, on electrospinning polylactic acid solutions, a solvent combination of a dichloromethane (DCM) and dimethyl formamide (DMF) were chosen as the solvent pair. In this specific case DCM is the main solvent for both polymers; DMF is a solvent for PDLLA but it is not a solvent for PLLA. DCM is highly volatile and has low polarity relative to the low volatile-highly polar DMF. Electrospinning from DCM alone results in precipitation and gelling in the Taylor cone and needle blocking. This does not contribute to stable electrospinning and uniform fibres. DMF reduces this phenomenon and increases the charge carrying capacity of the jet. An optimum ratio of the two solvents will give an electrospinning solution with the correct combination of volatility and fibre draw, and ultimately result in dry smooth fibres.

Coaxial electrospinning requires that at least the shell solution be electrospinnable. Single capillary electrospinning PDLLA solutions were investigated to determine in which parameter range the shell solution was electrospinnable and where smooth uniform fibres could be obtained. Electrospinnability of the PLLA core solutions were

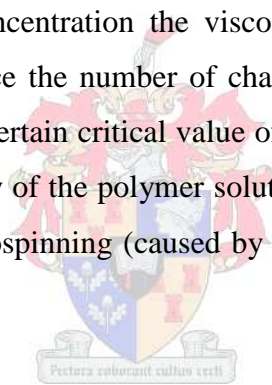
also investigated to note any changes that may occur to the resultant PLLA fibrous component when spinning with a single versus a coaxial electrospinning system.

The influence of varied concentration and solvent ratio on resultant fibre diameter and morphology was analysed by SEM. The effects of concentration and solvent ratio on average fibre diameter, fibre morphology and needle blockage are summarised in Tables A.1 and A.2. Fixed parameters included a flow rate of 1.5ml/hr and 15kV applied voltage over a 15cm spinning distance. Temperature and humidity was 21.7-22.6°C/51-61%rH. Fibres were collected statically on a grounded flat aluminium covered collector.

### A.2.1.1 Electrospinning PLLA and PDLLA solutions

#### *i) Effect of concentration*

On increasing the solution concentration the viscosity increases as more polymer chains are in solution and hence the number of chain entanglements also increases. This effect is observed after a certain critical value of concentration (and viscosity) is exceeded and the viscoelasticity of the polymer solution increases and suppresses the Raleigh instability when electrospinning (caused by the surface tension forces of the solvent).



The fibre morphology changes from electrospaying droplets (<4wt%), to beads-on-string (4wt%) and as PLLA and PDLLA solution concentrations reach a critical concentration (6wt%) smooth fibres are obtained. The transformation from beads-on-string morphology to smooth fibres for DCM/DMF solvent ratios 80/20, 70/30, and 60/40 can be seen in the Figures A.1 and A.2 and further detail is given in Section 1.3 (supporting information at the end of this Annexure) in Figures A.11, A.13, A.14, A.16, A.18 and A.19.

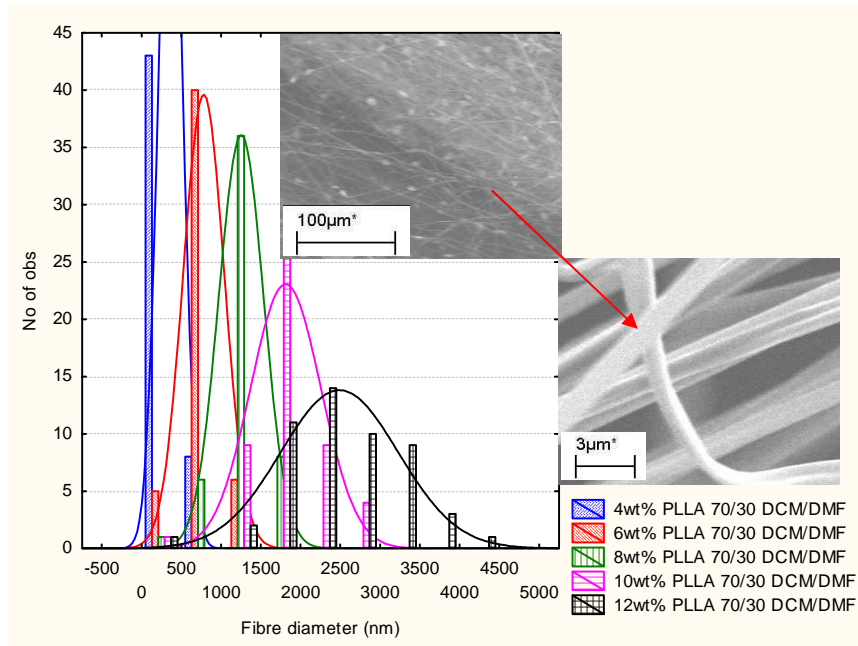


**Table A.1** Effect of concentration and solvent ratio on *average fibre diameters (nm)* of electrospun PLLA and PDLLA solutions

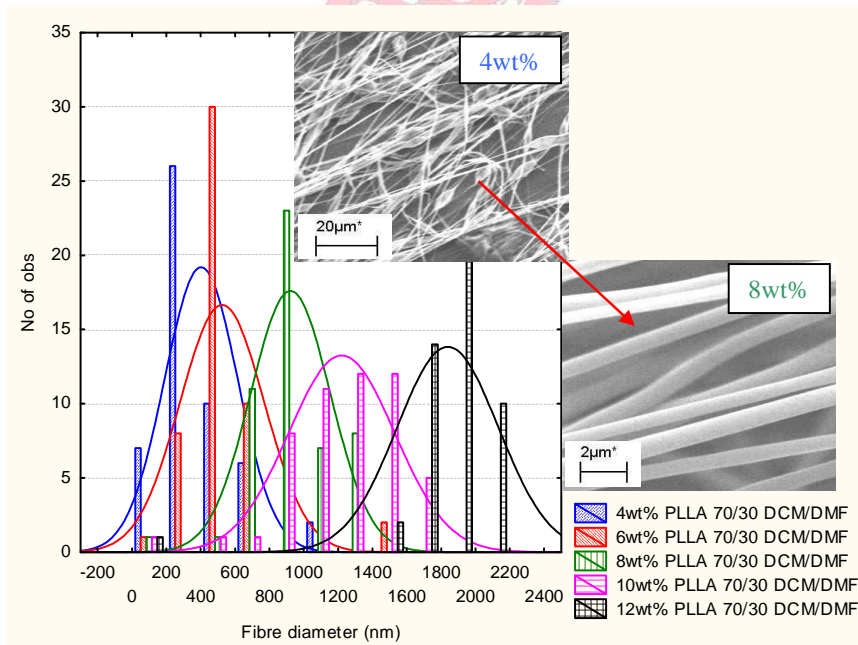
Polymer conc. (wt%)	PLLA			PDLLA		
	Solvent Ratio					
	80/20	70/30	60/40	80/20	70/30	60/40
4%	481	363	365	407	405	399
6%	1207	788	647	680	529	841
8%	2060	1266	893	1199	933	840
10%	2291	1834	1694	1643	1236	1573
12%	3353	2521	Gelled	1687	1863	1687

**Table A.2** Effect of concentration and solvent ratio on electrospinning conditions and resultant fibre morphology

Solvent Ratio (v/v) DCM/DMF	Polymer conc. (wt% based on solvent mass)									
	4%		6%		8%		10%		12%	
	Appearance	Blocking	Appearance	Blocking	Appearance	Blocking	Appearance	Blocking	Appearance	Blocking
PLLAL80/20	Smooth	yes	Smooth	Yes	Smooth	Yes	Smooth	yes	Smooth	yes
PLLA70/30	Beads	yes	Smooth	No	Smooth	No	Smooth	No	Smooth	yes
PLLA60/40	Beads	No	Smooth	No	Smooth	No	Smooth	yes	gelled not spinnable	
PDLLA80/20	Beads	Yes/no	Beads	yes/no	Smooth	yes/no	Smooth	yes/no	Smooth	yes
PDLLA70/30	Beads	Yes/no	Smooth	No	Smooth	No	Smooth	No	Smooth	no
PDLLA60/40	Beads	No	Beads	No	Smooth	No	Smooth	No	Smooth	no



**Figure A.1** Fibre diameter distributions: Electrospun PLLA solutions of increasing concentration in 70/30 DCM/DMF



**Figure A.2** Fibre diameter distributions: increasing polymer wt% concentration of PDLLA solutions spun from 70/30 DCM/DMF

The electrospinning process is governed by complex solution, process and ambient variables. The complex interplay of these variables results in fibre diameter distributions. A narrow fibre distribution indicates homogenous and complementary parameter (solution, process and ambient) combinations.

It was observed that narrower fibre diameters and fibre diameter distributions were obtained from lower solution concentrations  $\leq 8\text{wt}\%$  solutions. However beads-on-string morphology was observed at  $4\text{wt}\%$  solutions for all solvent ratios. Fibre distributions at varying solution concentrations for the PLLA and PDLLA solutions with 70/30 DCM/DMF solvent ratio are shown in Figures A.1 and A.2. Distributions for the other solvent ratios investigated can be observed in Figures A.12, A.15, A.17 and A.20 (Section 1.3).

ii) *Effect of solvent ratio*

The DCM/DMF solvent ratio determines the balance of: *low polarity + high volatility vs. high polarity + low volatility*. The solvent properties of DCM and DMF are compared in Table A.3.

**Table A.3** *DCM and DMF solvent properties*

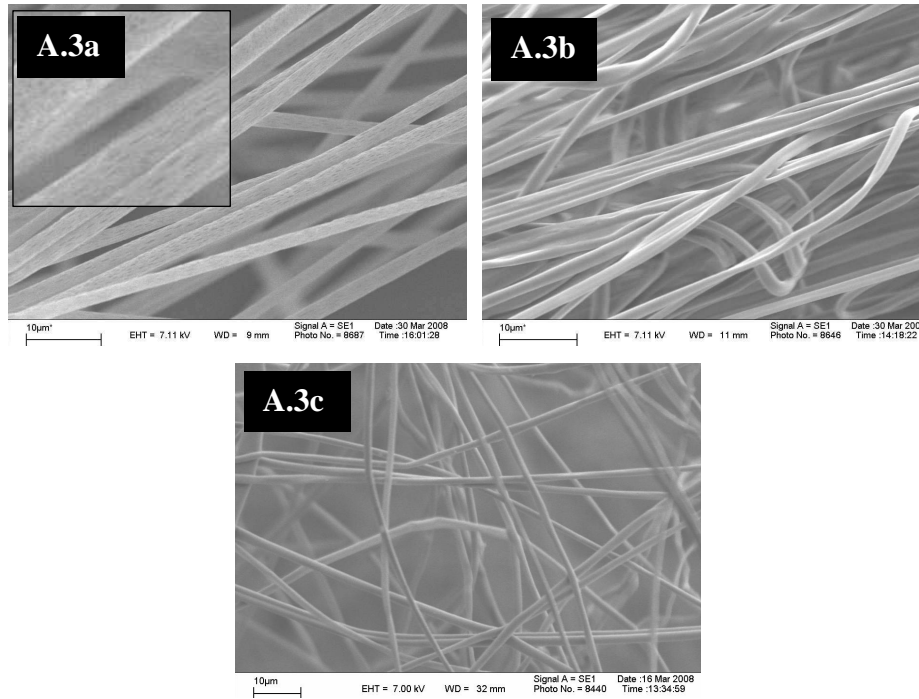
Solvent	Formulae	Molecular weight (g/mol)	Boiling point (C)	Density (g/mL)	Solubility in water (g/100g)	Dielectric constant
DCM	CH <sub>2</sub> Cl <sub>2</sub>	84.93	39.8	1.326	1.32	9.08
DMF	C <sub>3</sub> H <sub>7</sub> NO	73.09	153	0.944	Miscible	58

DCM is the main solvent and approximates a  $\theta$  solvent at room temperature for PLLA and PDLLA. A solvent combination of less than 50% (v) DCM, with DMF as the other solvent, limits the concentration range for PLLA. Below 50% DCM the polymer gels and precipitates out of solution. This does not occur with PDLLA as DMF is a solvent for this polymer. Solvent ratios of 60/40, 70/30 and 80/20 DCM/DMF were investigated over a broad concentration range for PLLA solutions. Fibres spun from an 80/20 solvent ratio had a greater portion of volatile component and lesser amount of polar species.

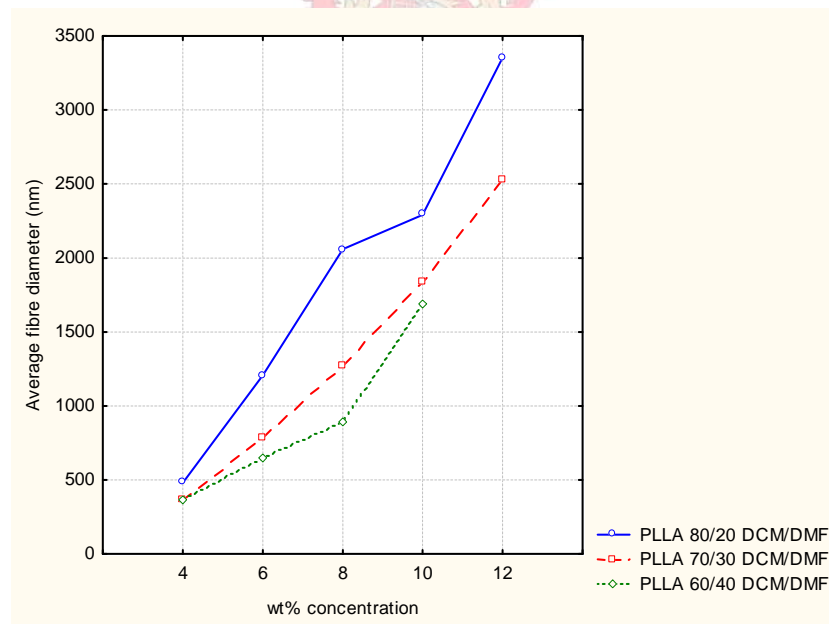
Solutions with 80/20 solvent ratio lost more solvent more rapidly during electrospinning and solidified faster.

A greater rate of solidification and reduced charge carrying capacity (as a result of more DCM) affected the time and degree of drawing by the electrostatic force respectively. This resulted in larger fibres diameters with porous surface structures for fibres spun from 80/20 DCM/DMF solvent ratio (Figure A.3a and A.5a). Pores are seen for all samples with 80/20 solvent ratio; but it is more predominant in the PLLA solutions. This was attributed to: firstly the high volatility of DCM and secondly to the immiscibility of moisture in the ambient air (and also DMF) with PLLA. As the DCM evaporated from the fibre surface during electrospinning the ambient moisture replaced it and created regions of concentrated DMF and H<sub>2</sub>O. DMF and H<sub>2</sub>O are non-solvents for PLLA and cause phase separation resulting in porosity at the fibre surfaces.

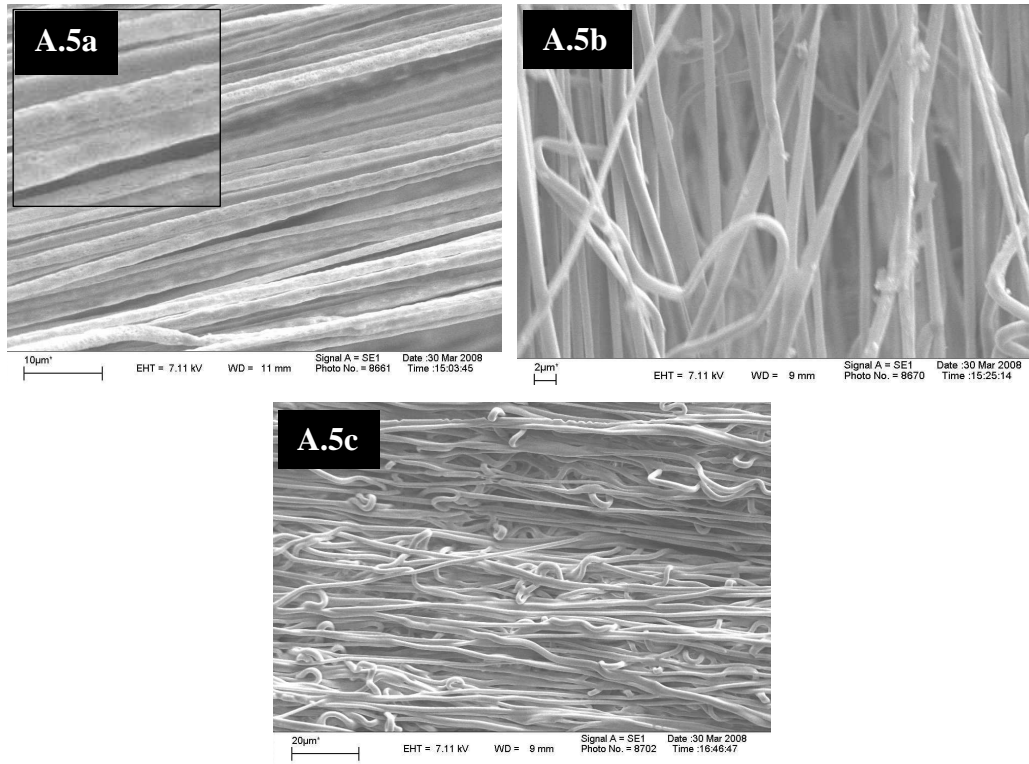
Solutions, more specifically PLLA solutions, with a 60/40 DCM/DMF solvent ratio had limited solubility at higher concentrations (>10wt%). This placed limitations on potential processing ranges to create fibres with various diameters and morphologies. The influence of solvent ratio, with increasing solution concentration, on average fibre diameters is shown in Figures A.3, A.4 and A.5, A.6 for PLLA and PDLLA solutions respectively. The fibre diameter increases almost linearly for solution made from the 70/30 DCM/DMF solvent ratio. Other solvent ratios show staggered increments of average fibre diameter with increasing concentration. The distribution of average fibre diameters for 8wt% PLLA and 10wt% PDLLA solutions at varying solvent ratios are shown in Figures A.7 and A.8 respectively. It was clearly seen that a 70/30 solvent ratio for both solutions yielded fibres with the narrowest fibre diameter distributions.



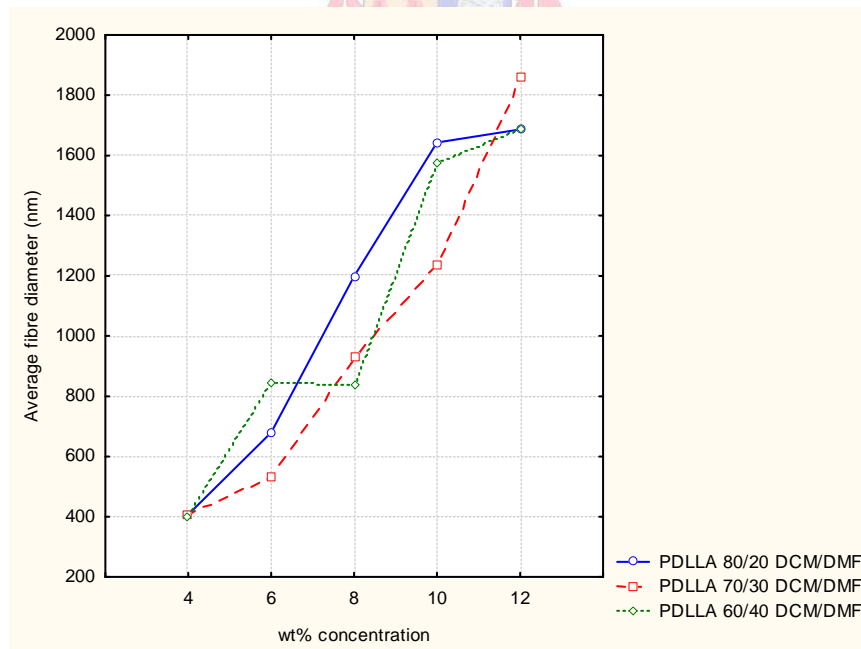
**Figure A.3** SEM images illustrating a change in fibre morphology on varying solvent ratio of an 8wt% PLLA solution with a) 80/20, b) 70/30, c) 60/40 DCM/DMF solvent ratio



**Figure A.4** Average fibre diameter (nm) vs. polymer wt% concentration of PLLA solutions spun from 80/20, 70/30, 60/40 DCM/DMF solvent ratios

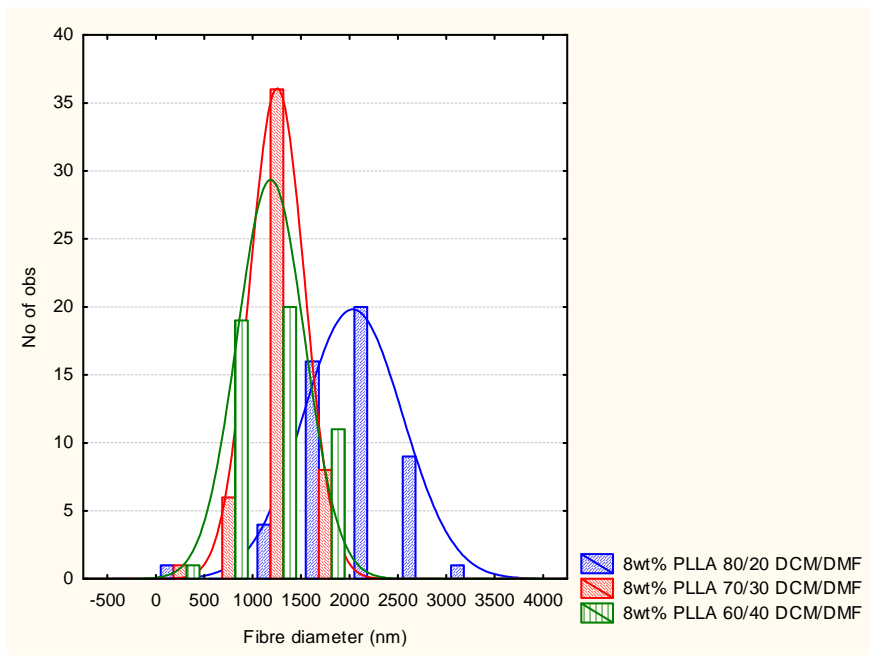


**Figure A.5** SEM images illustrating a change in fibre morphology on changing the solvent ratio of an 8wt% PDLA solution with a) 80/20, b) 70/30, c) 60/40 DCM/DMF solvent ratio

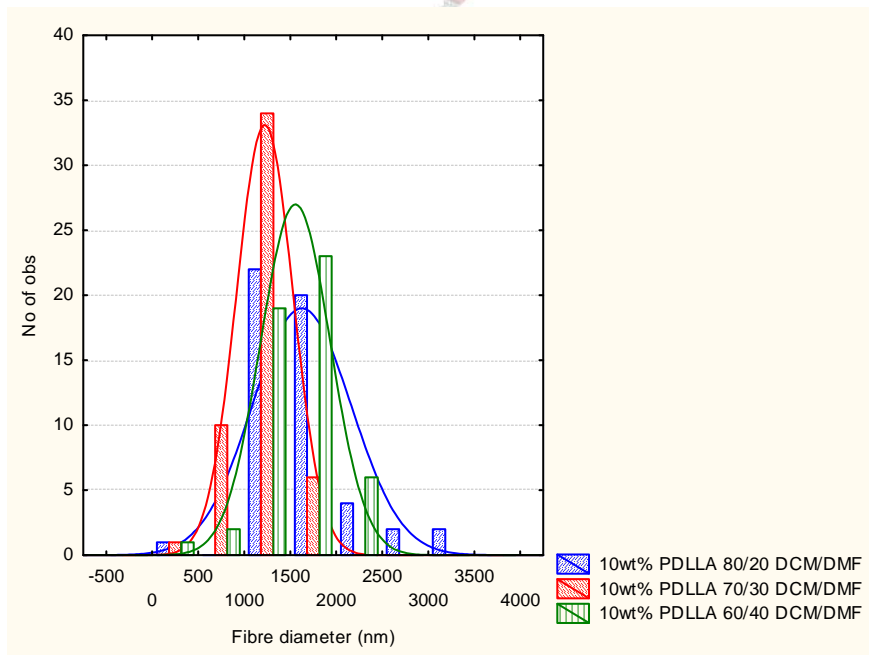


**Figure A.6** Average fibre diameter (nm) vs. polymer wt% concentration of PDLA solutions spun from 80/20, 70/30, 60/40 DCM/DMF solvent ratios





**Figure A.7** *Fibre diameter distributions: comparison of 8wt% concentration of PLLA solutions spun from DCM/DMF*



**Figure A.8** *Fibre diameter distributions: comparison of 10wt% concentration of PDLLA solutions spun from DCM/DMF*

### A.2.2 Determination of solution viscosity (Berry number ( $Be$ ))

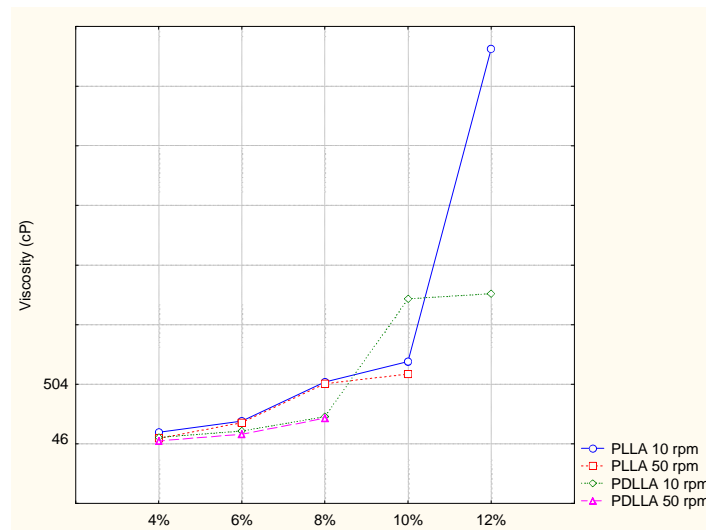
Single capillary electrospinning parameter studies have shown that a 70/30 DCM/DMF solvent ratio is the most optimum for forming smooth uniform fibres.

The relevance of polymer chain entanglements, and therefore viscosity, and the effect it has on the resulting morphology of fibres has been described by Kenawy et al.<sup>2</sup> Polymer chain entanglements stabilize the jet as the solvent evaporates during the fiber formation process during electrospinning. Below a critical concentration of polymer, chain entanglements are insufficient to stabilize the jet, leading to the breakup of the liquid jet into droplets via a Rayleigh instability. The spraying of droplets is called electro spraying rather than electrospinning. On the other end of the spectrum there also exists a maximum concentration where uniform fibers are no longer produced as a result of high solution viscosity.<sup>2,3</sup> A method for a priori prediction of fiber/bead formation as a function of concentration and molecular weight was demonstrated by Shenoy et al.<sup>3</sup>

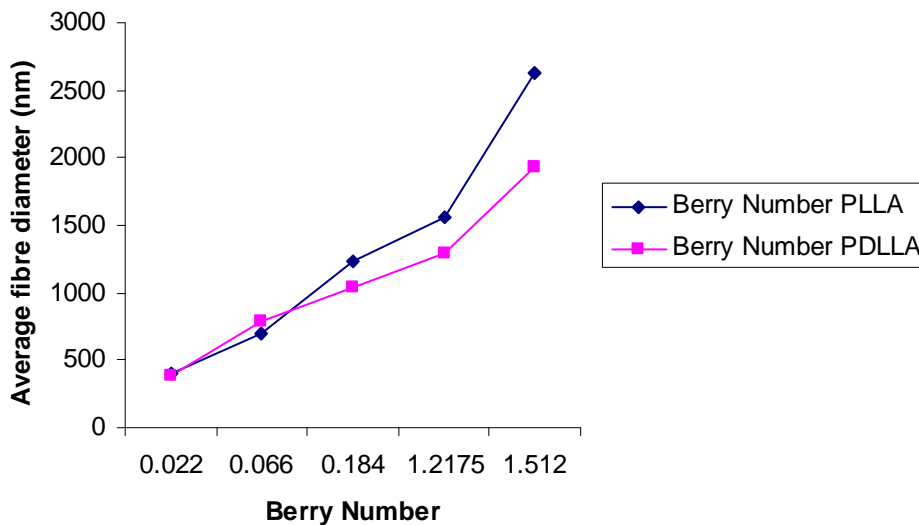
The Berry number ( $Be$ ) is a dimensionless parameter employed by the group of Frank K. Ko to study a poly(L-lactic acid) in chloroform solution.<sup>4</sup> It provides an indication of the degree of entanglement of polymer chains in solution or molecular conformation by correlating fiber diameter/morphology to  $Be$ .  $Be$ , the product of intrinsic viscosity ( $[\eta]$  = the ratio of specific viscosity to concentration at infinite dilution) and polymer concentration, has shown to affect fiber diameter/morphology and spinnability of polymer solutions. According to them there are four regions of Berry number corresponding to the distribution of polymer chain conformation and fiber morphology. It is described that for  $Be < 1$ , the polymer is in a very dilute solution, and the polymer molecules are so far apart in the solution that individual molecules hardly ever touch each other. When the polymer concentration is increased,  $Be > 1$ , at a certain point molecules interact and entangle. Ko *et al*<sup>4</sup> used this to study a poly(L-lactic acid)/chloroform system which produced Berry numbers where fiber formation occurs for  $Be > 1$ .

The viscosity of PLA solutions of increasing concentration with 70/30 DCM/DMF solvent ratio was determined and is shown in Figure A.9. The Berry numbers for each

concentration interval was calculated and is shown in Figure A.10 to indicate the range where entanglements become most significant. Electrospinning these solutions have shown that entanglements become significant and smooth fibres are formed above 8wt% for PDLLA and 6wt% for PLLA. Viscosity data showed that a sharp increase in solution viscosity occurred for concentrations  $>8\text{wt}\%$  for PDLLA and  $>10\text{wt}\%$  for PLLA. 10 & 12wt% PDLLA have been shown to be electrospinnable and because the viscosities of these solutions are sufficiently higher than 8wt% PLLA solutions the shell should encapsulate the core material to form core-shell fibres. PDLLA solutions  $>8\text{wt}\%$  should be used for the shell solution and PLLA solutions  $\leq 8\text{wt}\%$  should be used for the core solution.



**Figure A.9** Viscosity readings for PLLA and PDLLA 70/30 DCM/DMF solutions with concentration intervals 4,6,8,10,12wt%



**Figure A.10** Effect of increasing solution concentration and viscosity of average fibre diameter

It is reported that usually solutions are electrospinnable if they have Berry numbers ( $Be$ )  $>1$ . The concentration and molecular weight affect the number of entanglements in a polymer solution and because the polymers used in this work have large molecular masses the solutions are electrospinnable for  $Be <1$ . Therefore in this case the  $Be$  would have been useful for a *priori* prediction of solution concentrations that would produce smooth un-beaded electrospun fibres. However, some solutions with  $Be <1$  were also electrospinnable. Therefore there is a risk of eliminating solutions of lower concentrations that do indeed produce smooth fibres and could yield smaller uniform fibres.

### A.3 Conclusions

The influence of polymer solution concentration and solvent ratio on fibre morphology is significant as seen in the ranges studied. An increase in concentration in 2wt% intervals showed a significant increase in fibre diameter (Average 451nm) for all PLLA and PDLLA solutions as would be expected from electrospinning literature. Beads-on-string morphology is seen below 6 wt% for all polymer solutions except the 4wt% PLLA 80/20 DCM/DMF solution. PDLLA solutions show beads additionally at 6wt% solutions with 80/20 and 60/40 DCM/DMF solvent ratios.

The fibres formed about the critical viscosity or  $Be$  value, which is near 8wt% for solutions of both polymers, show mostly smooth fibres with uniform diameters. Pores are seen for samples when using 80% dichloromethane content; but it is more predominant in the PLLA solutions. This was attributed to: firstly the high volatility of DCM and secondly to the immiscibility of moisture in the ambient air (and also DMF) with PLLA. As the DCM evaporated from the fibre surface during electrospinning the ambient moisture replaced it and created regions of concentrated DMF and H<sub>2</sub>O. DMF and H<sub>2</sub>O are non-solvents for PLLA and cause phase separation resulting in porosity at the fibre surfaces.

Solutions having a  $>40\%$  DMF content resulted in fused fibres on the collector. This indicates that not all of the DMF was removed during the electrospinning process resulting in fibre fusion on the collector. Fibres spun from higher DMF content solutions produced broader fibre diameter distributions as a result of changing

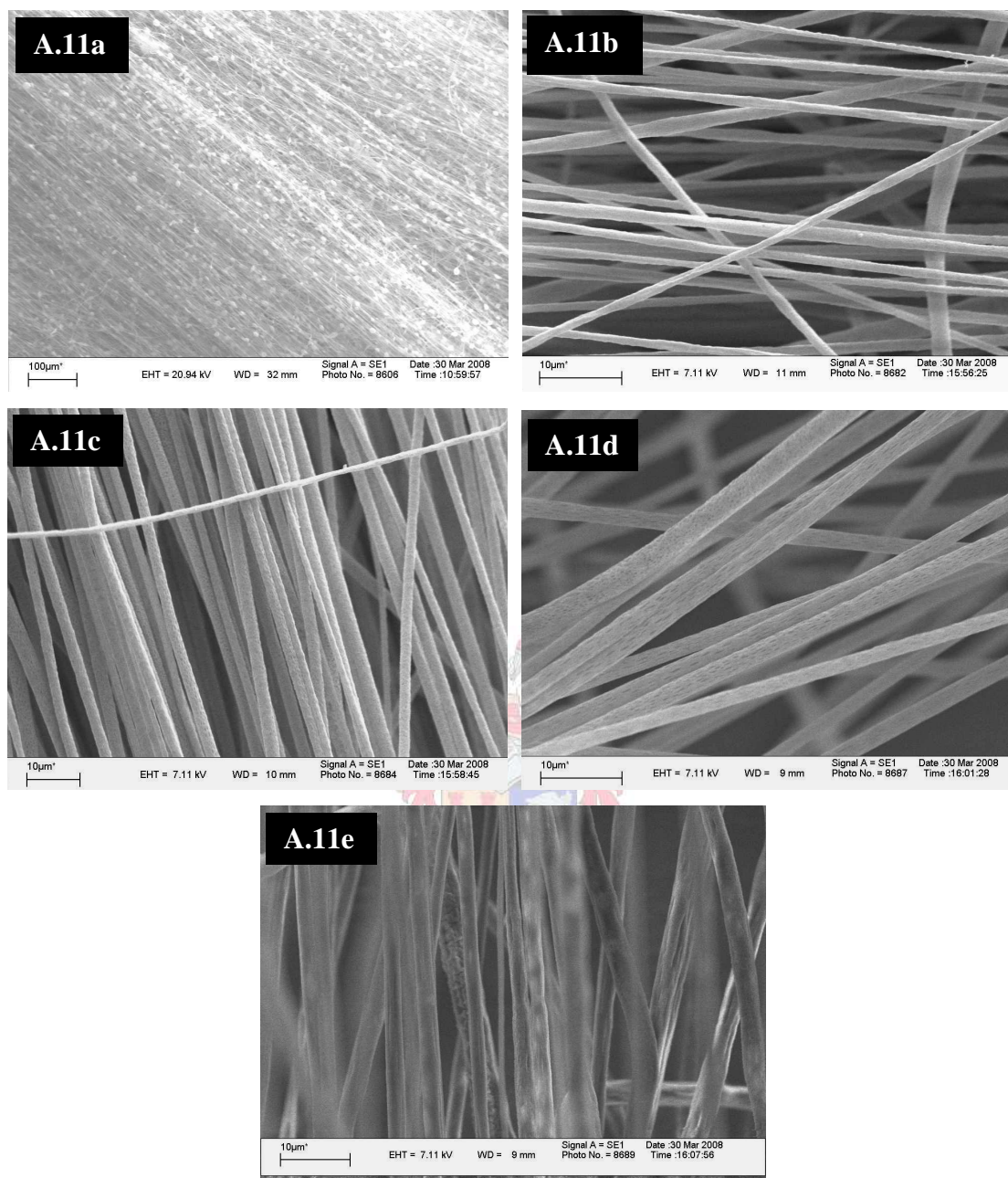
solubility and concentration parameters during the course of the electrospinning process.

The other apparent morphological feature is that of a collapsed ribbon. This structure is a result of rapid evaporation of a volatile solvent from the surface of the fibre. A skin forms on the fibre surface and sealing off solvent in the inner parts of the fibre. At a later stage in electrospinning or even later on the collector the solvent encapsulated inside the skin will evaporate. The solvent can escape through tiny pores on the lower nanoscale range not seen in SEM images. One possible mechanism that could lead to this morphology is where the latent evaporation from core induces a gradient whereby the solvent leaves and the inside polymer solution forms a lining on the inside of the solid skin. The inner solution eventually retracts enough to form a slug/hollow portion which will continue lining the entire length of the fibre until all the solvent has evaporated. A hollow fibre structure remains. This is similar to what was observed by Dror et al.<sup>5</sup> If the fibre walls are not thick or tough enough they collapse in the presence of the vacuum, during coating and SEM imaging, resulting in the collapsed ribbon structure.

Based on the solution parameters studied a 70/30 DCM/DMF solvent ratio will provide a stable electrospinning process, uniform fibres and narrow fibre diameter distributions. The average fibre diameters for this solvent ratio combination also increase approximately linearly for each concentration interval. This was determined to be valuable for later investigations where a linear increase in core concentration would be sought to produce a linear increase in core-shell fibre diameter.

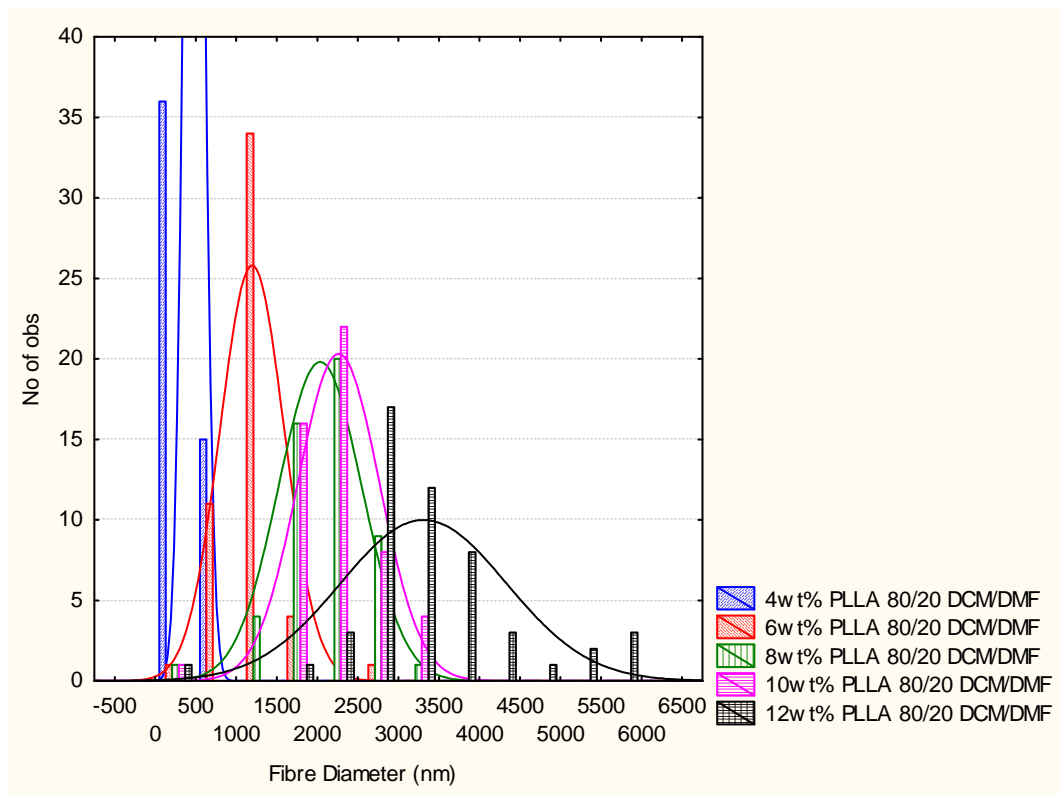
To translate this information into a stable coaxial electrospinning set-up the solution concentrations for the shell should be preferably >8wt% and the core concentrations can vary.

## A.4 Supporting Information

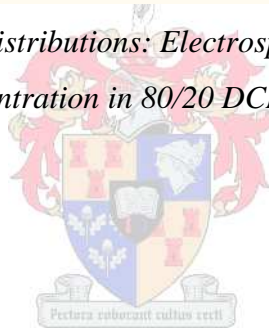


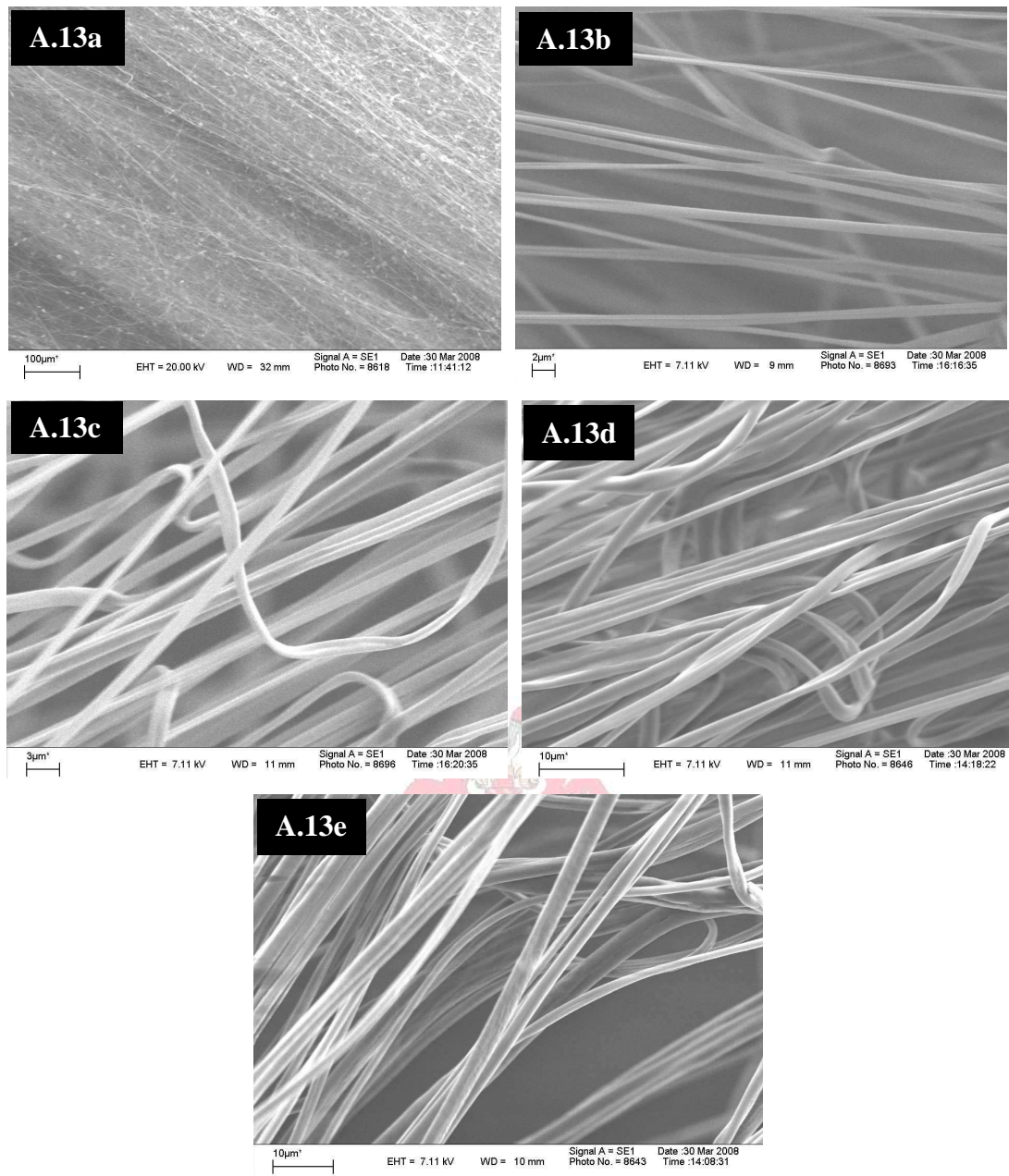
**Figure A.11** SEM images illustrating a change in fibre morphology and distribution with on increasing PLLA polymer solution concentration a) 4wt%, b) 6wt%, c) 8wt%, d) 10wt%, e) 12wt% polymer solution with 80/20 DCM/DMF solvent ratio



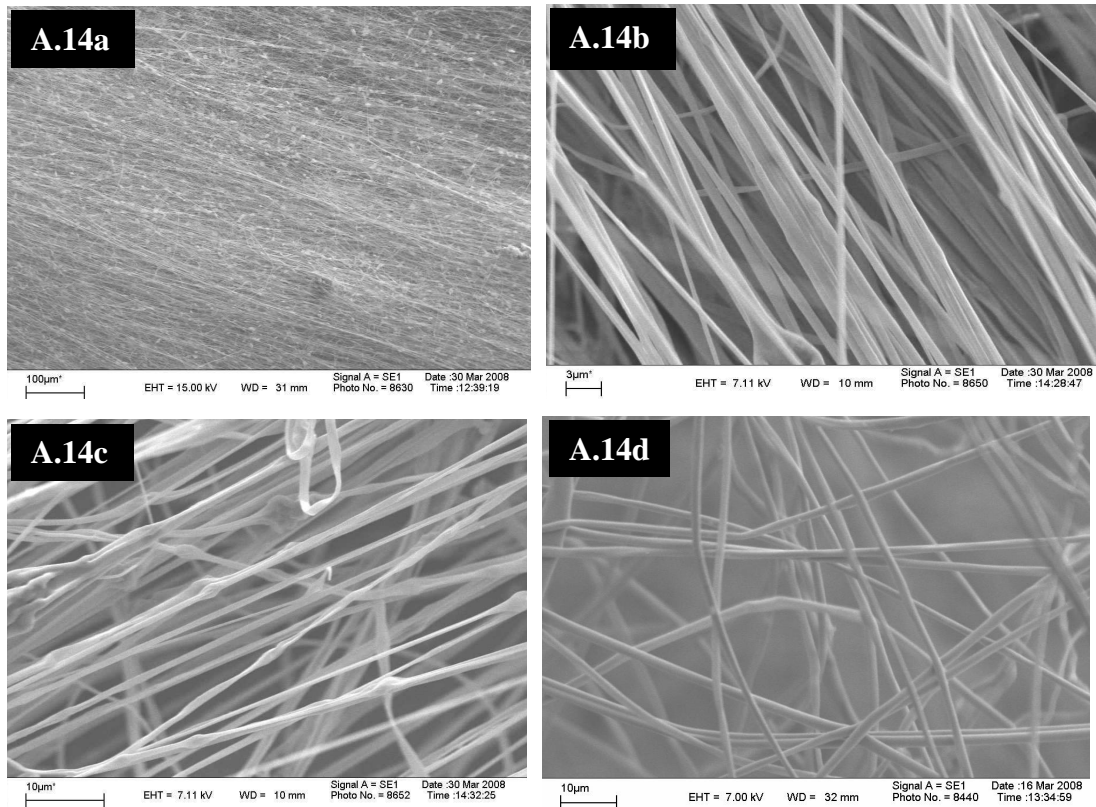


**Figure A.12** Fibre diameter distributions: Electrospun PLLA solutions of increasing concentration in 80/20 DCM/DMF

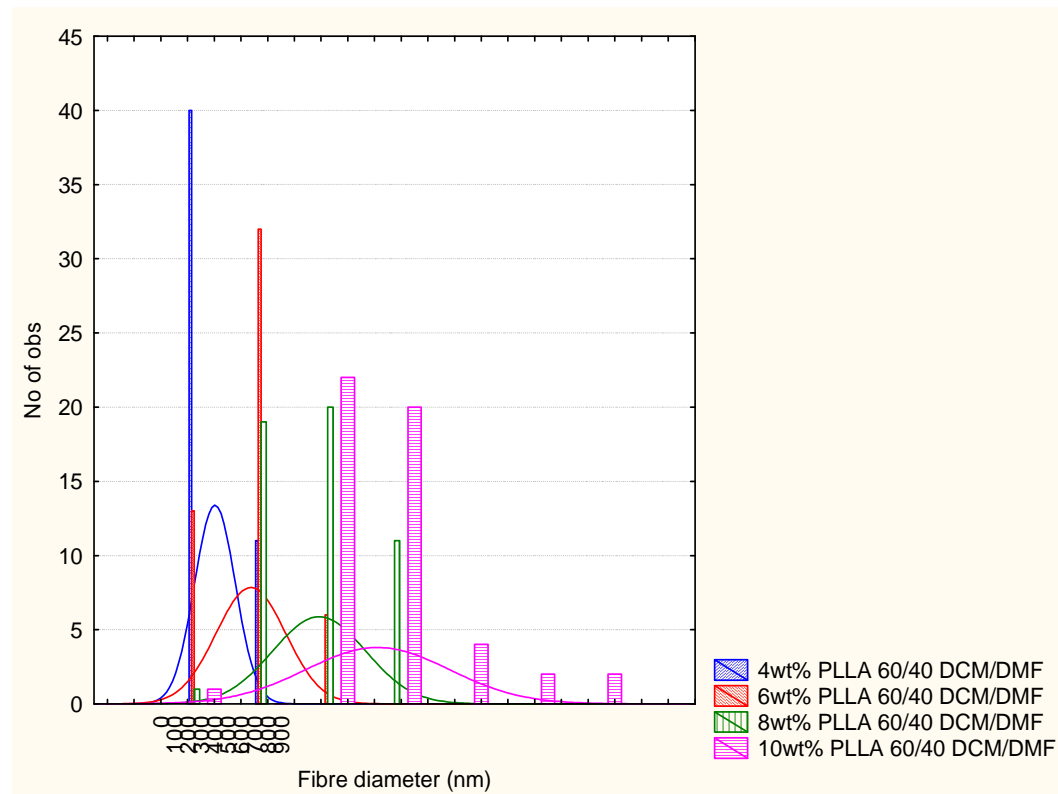




**Figure A.13** SEM images illustrating a change in fibre morphology with on increasing PLLA polymer solution concentration a) 4wt%, b) 6wt%, c) 8wt%, d) 10wt%, e) 12wt% polymer solution with 70/30 DCM/DMF solvent ratio



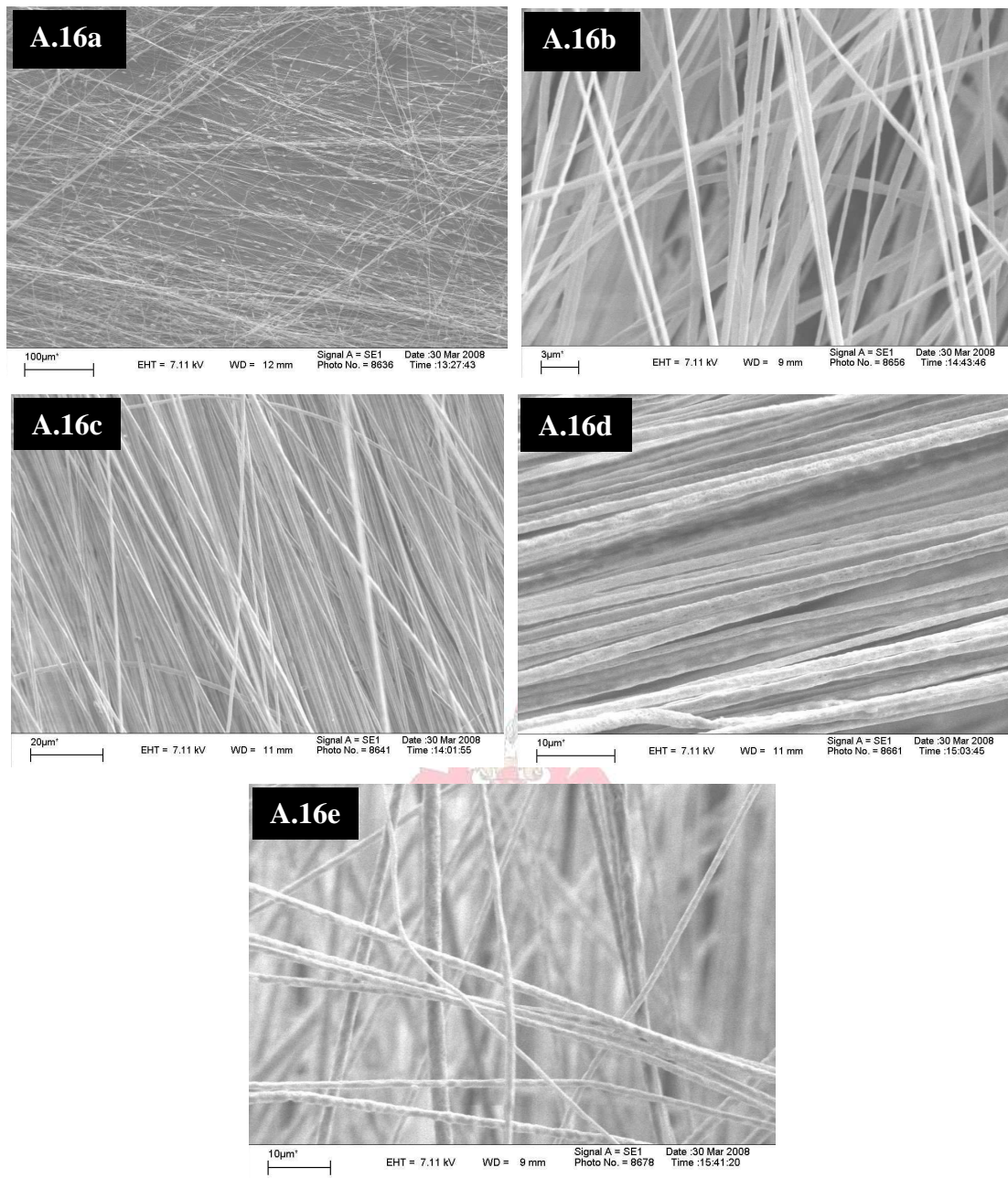
**Figure A.14** SEM images illustrating a change in fibre morphology with on increasing PLLA polymer solution concentration a) 4wt%, b) 6wt%, c) 8wt%, d) 10wt% polymer solution with 60/40 DCM/DMF solvent ratio



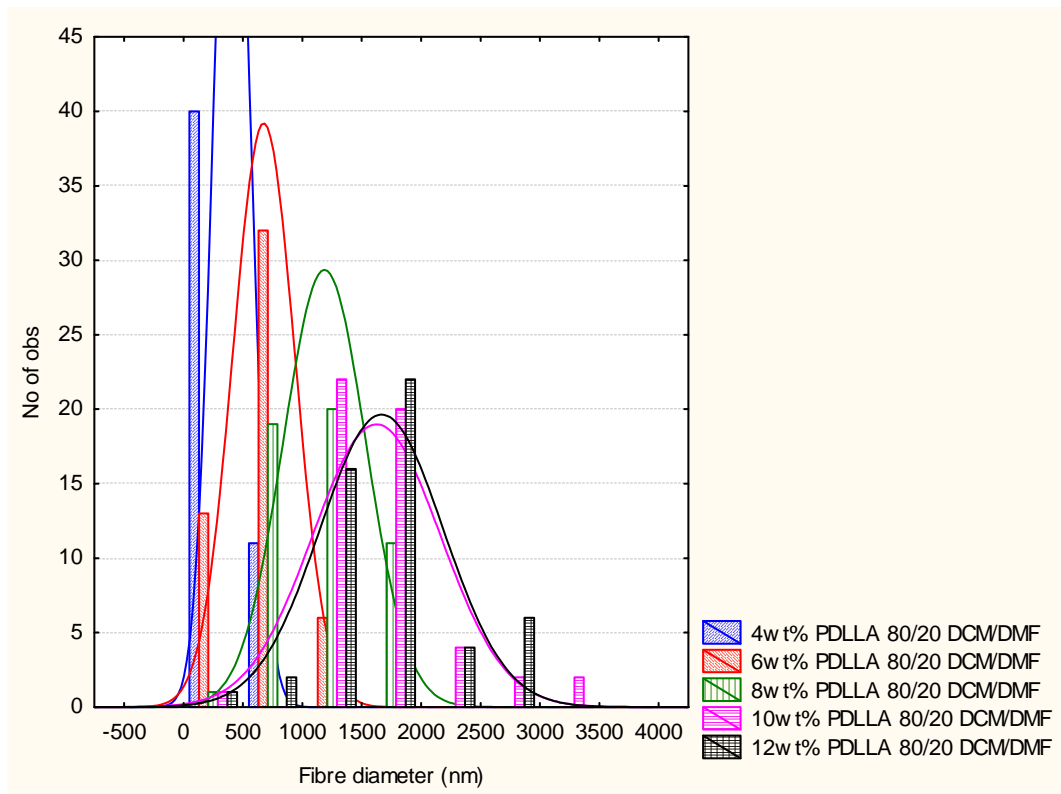
**Figure A.15** Fibre diameter distributions: increasing polymer wt% concentration of PLLA solutions spun from 60/40 DCM/DMF







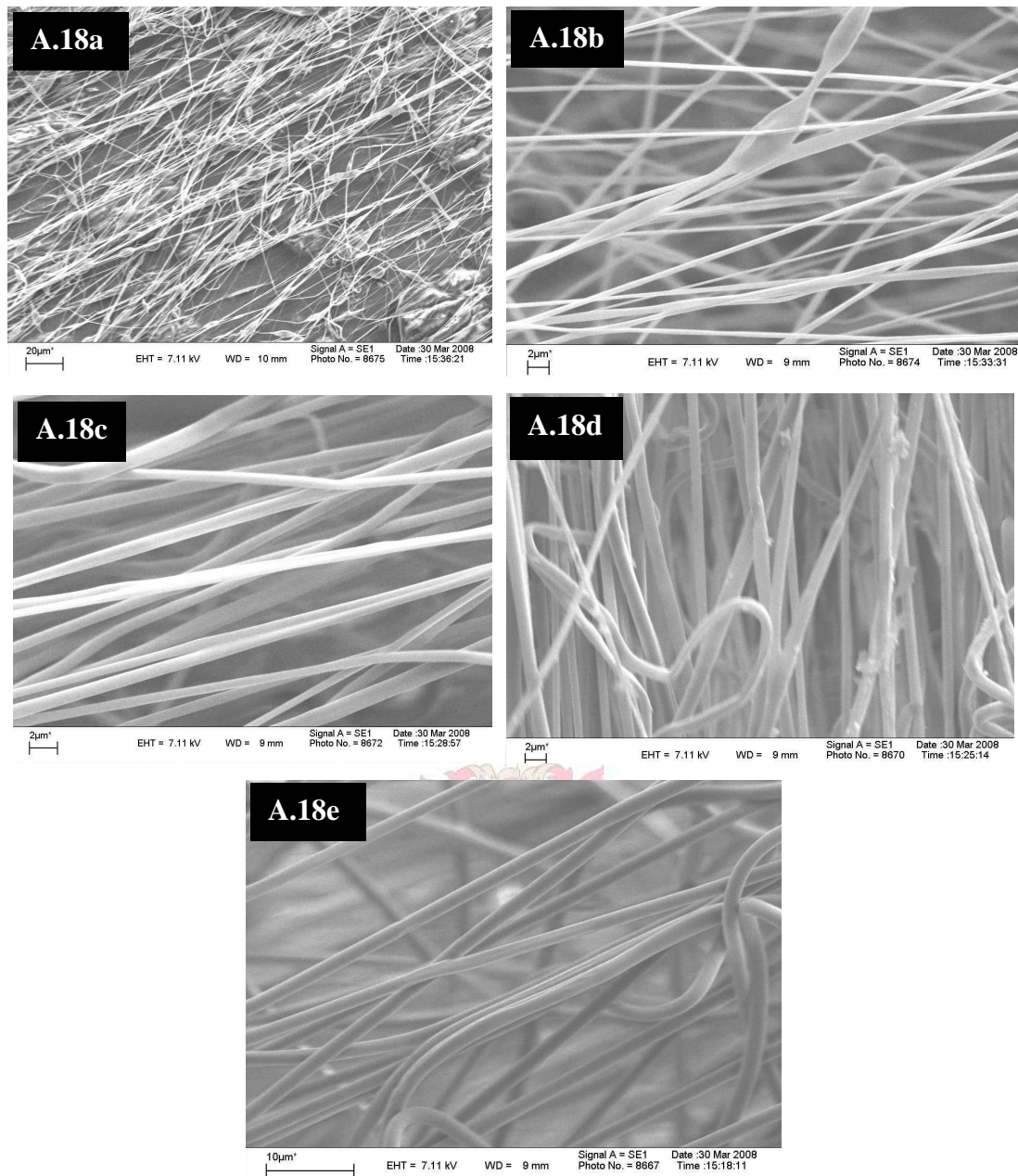
**Figure A.16** SEM images illustrating a change in fibre morphology with on increasing PDLLA polymer solution concentration a) 4wt%, b) 6wt%, c) 8wt%, d) 10wt%, e) 12wt% polymer solution with 80/20 DCM/DMF solvent ratio



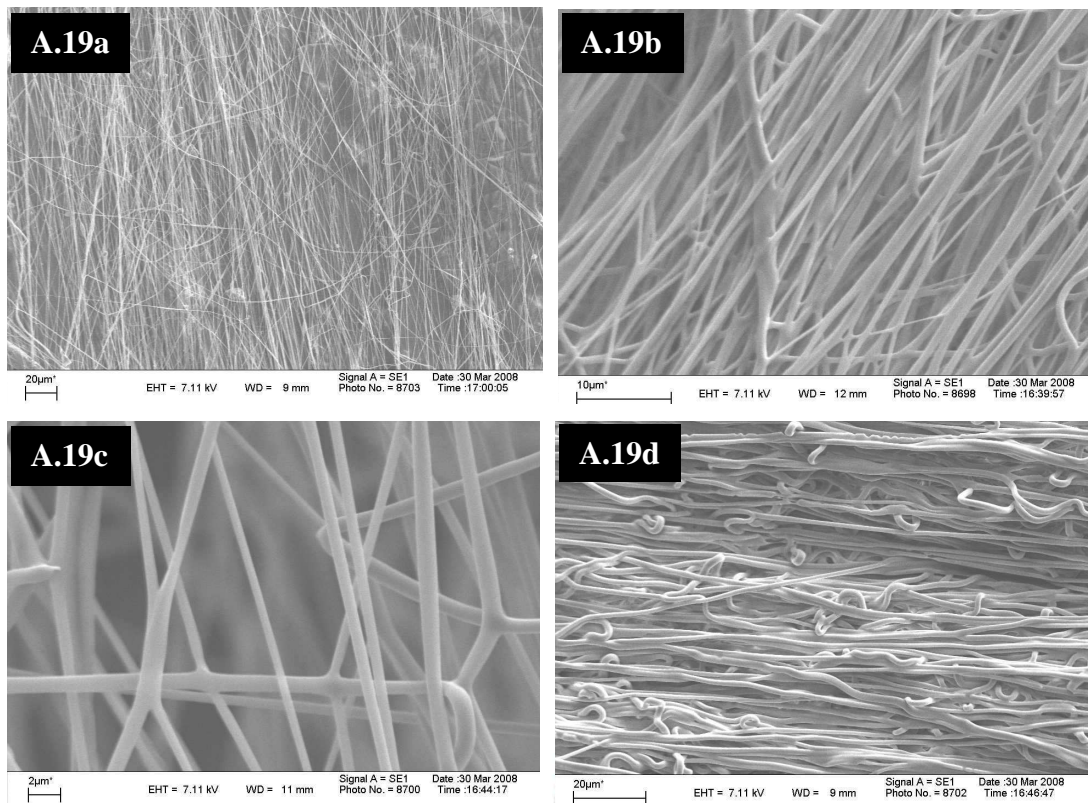
**Figure A.17** Fibre diameter distributions: increasing polymer wt% concentration of PDLLA solutions spun from 80/20 DCM/DMF



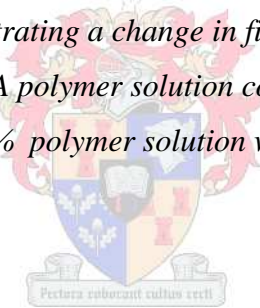


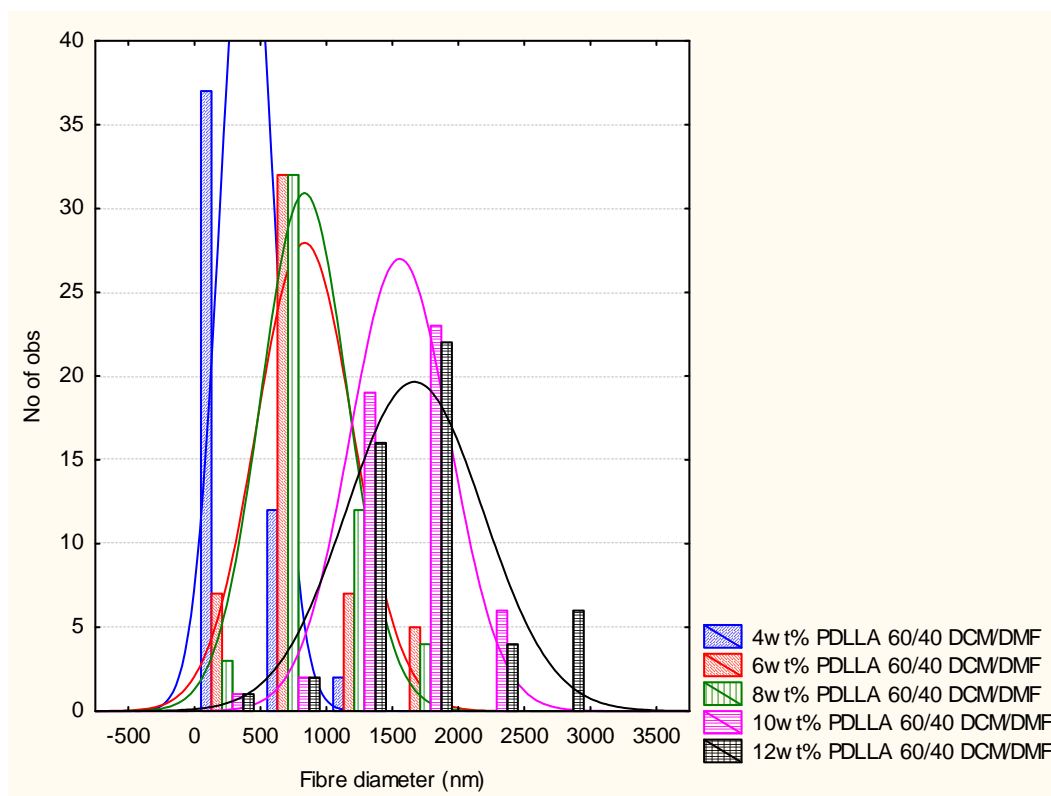


**Figure A.18** SEM images illustrating a change in fibre morphology on increasing PDLLA polymer solution concentration a) 4wt%, b) 6wt%, c) 8wt%, d) 10wt%, e) 12wt% polymer solution with 70/30 DCM/DMF solvent ratio



**Figure A.19** SEM images illustrating a change in fibre morphology with on increasing PDLA polymer solution concentration a) 4wt%, b) 6wt%, c) 8wt%, d) 10wt% polymer solution with 60/40 DCM/DMF solvent ratio





**Figure A.20** Fibre diameter distributions: increasing polymer wt% concentration of PDLA solutions spun from 60/40 DCM/DMF

#### References

1. Zong X, Kim K, Fang D, Ran S, Hsiao BS, Chu B. Structure and process relationship of electrospun bioabsorbable nanofiber membranes. *Polymer*. 2002;43:4403-12.
2. Kenawy E-R, Layman JM, Watkins JR, et al. Electrospinning of poly(ethylene-co-vinyl alcohol) fibers. *Biomaterials*. 2003;24:907-13.
3. Shenoy SL, Bates WD, Frisch HL, Wnek GE. Role of chain entanglements on the fiber formation during electrospinning of polymer solutions: good solvent, non-specific polymer-polymer interaction limit. *Polymer*. 2005;46:3372-84.
4. Ko FK. Nanofiber Technology: Bridging the gap between nano and macro world. NATO ASI on Nanoengineered Nanofibrous Materials, 2004.
5. Dror Y, Salalha W, Avrahami R, et al. One-step production of polymeric microtubes by co-electrospinning. *Small*. Volume 3, 2007.

## Appendix B

### ***Direct methods for core-shell fibre structure validation***

*Appendix B deals with a significant amount of work that was conducted to exhaust direct strategies to validate a core-shell fibre structure. Various sample preparation strategies and analyses using light microscopy, scanning electron microscopy and transmission electron microscopy were used. These methods were not ideal for analysis of coaxial electrospun core-shell fibres. The fibres showed optical effects and were on the lower limits of resolution for analysis with light microscopy. Electrospun PLA polymers were highly strained and were radiation sensitive which made SEM and TEM analyses problematic. Contrast between the core and shell, in all forms of transmission microscopy used, was not sufficient as the polymers have the same chemistry and addition of compounds for contrast during electrospinning altered the spinning conditions. These methods suggested that a core-shell fibre structure may have been obtained but these results were inconclusive.*

### ***B.1 Experimental***

#### **B.1.1 Outline**

Coaxial electrospun fibres collected *in situ* (intercepted during electrospinning) on glass slides were analysed with light microscopy (fibres observed in lateral view) to investigate a possibility of contrast between a core component that is more crystalline than the shell component that is amorphous. Coaxial electrospun fibres with exposed cross-sections were analysed via SEM. It was hoped that a phase-difference or phase boundary between the core and shell components would be observed. Coaxial electrospun fibres were observed in lateral and cross-sectional view with TEM under standard and cryo conditions as well as in dark-field mode. Lateral samples were collected *in situ* on carbon coated grids. Cross-sections were observed by embedding the core-shell fibre yarns in a matrix material (resin, sucrose, polyvinyl alcohol) and cutting thin slides (of 100nm thickness) perpendicular to the yarn axis with ultramicrotomy. It was hoped that under certain conditions i.e. high accelerating voltage, cryo conditions, dark-field mode and use of contrasting agents in the core, that the fibres would be stable under the electron beam and there would be sufficient

contrast between the core and shell that would allow the observation of the core-shell fibre structure.

### B.1.2 Raw Materials

The raw materials were used as received from the supplier. The materials were:

<i>Raw Material</i>	<i>Supplier</i>
<i>Preparation of electrospinning solutions</i>	
Poly(L-lactic acid) (PL24, Mw $\cong$ 291k)	Purac Biomaterials, Netherlands
Poly(D,L-lactic acid) (PDL20, Mw $\cong$ 265k)	Purac Biomaterials, Netherlands
Analytical grade N,N Dimethylformamide (DMF) (98%)	Sigma Aldrich, South Africa
Industrial grade Dichloromethane (DCM)	Sasol Solvents, South Africa
<i>Contrasting agents added to core polymer solution</i>	
DIANIX SBR blue dye	Dye Star, South Africa
PVP-capped ZnS Particles (ave 30nm) <sup>1</sup>	Department of Chemistry and Polymer Science, Stellenbosch University
AgNO <sub>3</sub>	Sigma Aldrich, South Africa
<i>Resins for sample preparation to analyse fibre cross-sections</i>	
Spurrs Resin	Agar Scientific Ltd, UK
LR White Resin	Agar Scientific Ltd, UK

### B.1.3 Light microscopy

Light microscopy was conducted on fibres that were intercepted with glass slides during the electrospinning process. Analysis was conducted as described in Chapter 3 (Section 3.4.1).

### B.1.4 Cryo-SEM

Samples were mounted to stand up-right in a sample holder which were inserted into a special chamber held under cryo conditions (liquid nitrogen -196°C) (Figure B.1). A force was applied to the sample with a lever in an attempt to shatter the fibres to

<sup>1</sup> Appendix D: Section D.2



expose the cross-section of the fibres. Standard SEM analysis that was performed was conducted as described in Chapter 3 (Section 3.2.2). SEM analysis was also conducted on cross-sections prepared by embedding coaxial electrospun fibre yarns in resin followed by ultramicrotomy perpendicular to the yarn axis to expose the fibre ends.



**Figure B.1** *Attempting to break ductile yarn sample under Cryo-SEM conditions*

### **B.1.5 Transmission electron microscopy (TEM)**

TEM analysis was used to analyse the fibre structure in lateral and cross-sectional views to validate a core-shell fibre structure. Analysing the fibres under cryo-conditions and also in dark-field mode were strategies used to reduce charge build-up on and within fibre samples. Various agents were mixed with the core solution to assist in the validation of the core-shell fibre by increasing the contrast between the core and shell components.

#### **B.1.5.1 Standard**

Fibres were intercepted during electrospinning on carbon coated grids. The fibres were analysed using 100kV and 120kV accelerating voltage with the Leo Omega 912 (Zeiss Vienna, Austria) JEOL 1200EXII CRYO TEM (JEOL – Japan) under standard and cryo conditions. TEM analysis was also conducted in the Dark-field mode. Dark-field TEM transmits indirect electrons through the sample and was used in an attempt to obtain greater contrast between possible core and shell components and reduce the number of electrons interacting with the sample.

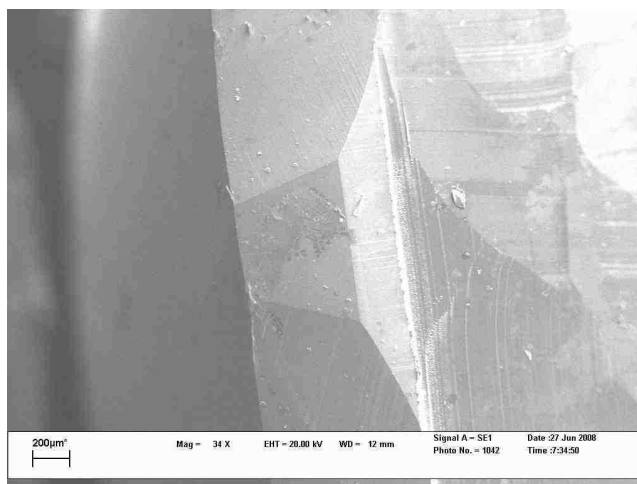


### B.1.5.2 Cryo-TEM

To reduce the effect of heat build-up as a result of electron collisions with the sample the fibre deposited on grids were viewed under cryo conditions using 120kV accelerating voltage with the JEOL 1200EXII CRYO TEM (JEOL – Japan).

### B.1.5.3 Cross-sections

In one sample preparation step (1) Yarns were set in Spurr's resin (in a tablet forming template) and allowed to set for 48hrs at 30°C in a convection oven. In a different sample preparation step (2) yarns were coated in polyvinyl alcohol by dipping in an aqueous solution of 10wt% polyvinyl alcohol ( $M_w$ 99k). These polyvinyl alcohol coated yarns were placed in Spurr's resin and set as mentioned previously. In a third sample preparation step (3) yarns were dipped in sucrose solutions prior to analysis. The resin slides of yarn/fibre cross-sections were prepared under standard and cryo conditions with the Reichert Ultracut S and with Reichert FCS Cryo Ultramicrotome unit (Leica Vienna, Austria) respectively. The Reichert FCS cryo-sectioning accessory, consisting of a liquid nitrogen dewar, cryochamber, control unit, and liquid nitrogen pump, was used to cut samples under cryo conditions. An automatic pumping system maintains a stable low temperature environment around the frozen specimen and the knife. The 100nm slides were cut from a trapezium shaped area carved into the resin tablet (Figure B.2) were viewed with TEM under standard and cryo conditions.

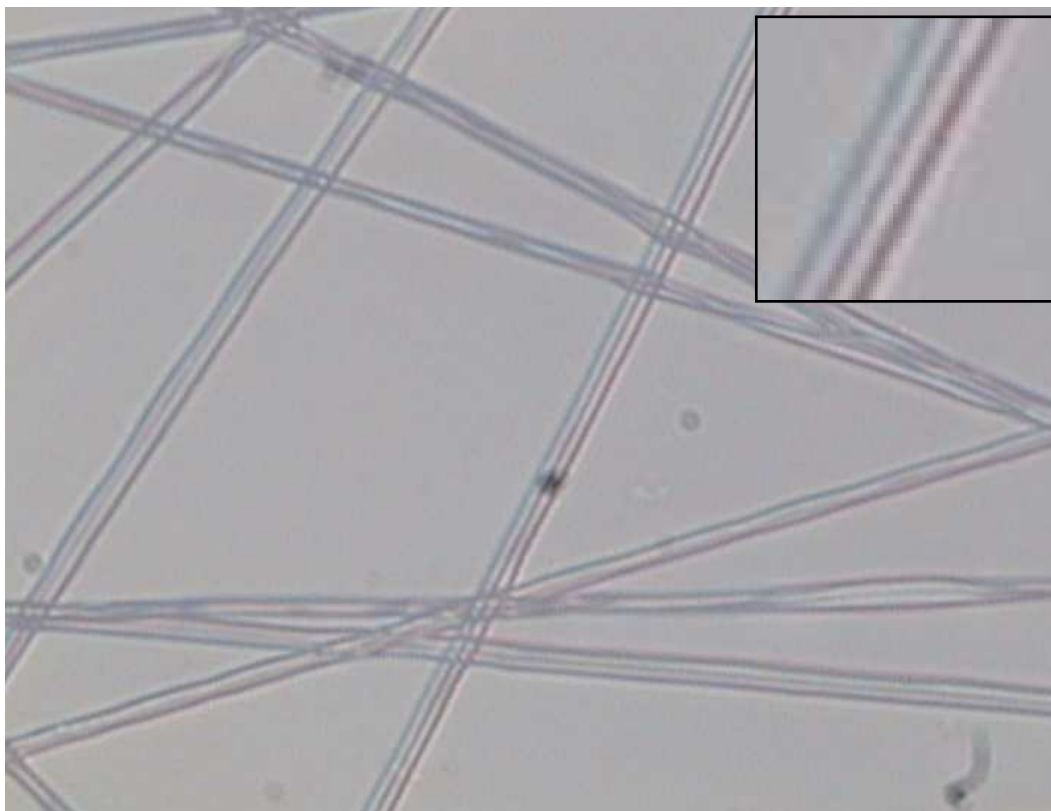


**Figure B.2** Trapezium cut resin tablet with coaxial electrospun fibre yarn

## B.2 Results and Discussions

### B.2.1 Light microscopy

Coaxial electrospun fibres collected on glass slides were analysed with 400X magnification with a light microscope. The fibres are on average  $<2\mu\text{m}$  and display optical effects from light diffraction through and around the fibre (Figure B.3). The effects created by light reflection and diffraction generate uncertainty about the true fibre structure. Under first observations the fibres appeared to have core-shell structures but this could be an optical effect or a function of fibre geometry (ribbons or collapsed structures) or the effect of twin and/or overlapping fibres.



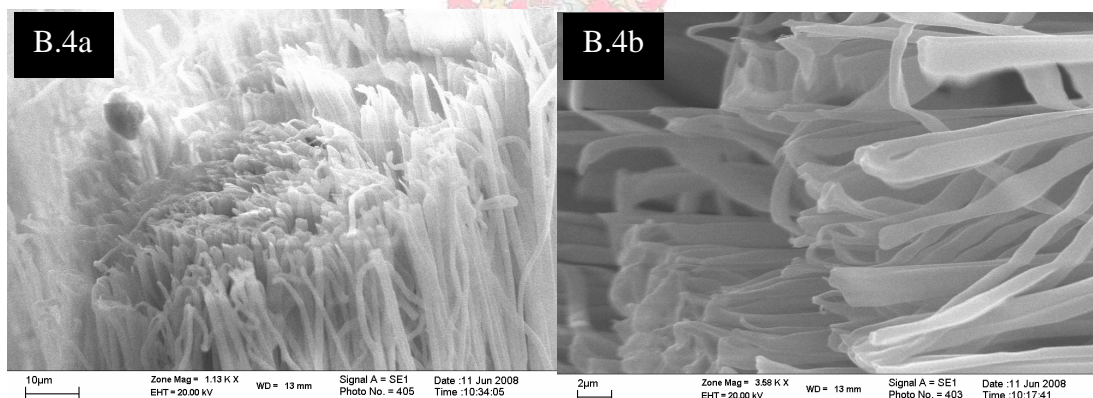
**Figure B.3** *Light microscope image of coaxial electrospun fibres under 400X magnification*

### B.2.2 SEM

Core-shell solutions (8wt% PLLA and 10wt% PDLLA) were coaxially electrospun to prepare yarns. Yarn samples that were **A**) cut under cryo conditions/‘cryo fractured’ (liquid nitrogen  $\cong -196^\circ\text{C}$ ) or **B**) set in resin and cut with a microtome were analysed

by SEM. These samples in general were sensitive under the electron beam. The electron beam effects were more apparent in raised areas and where gold coating was not complete and where some fibres changed morphology as well as position because of heat generation causing charge build-up.

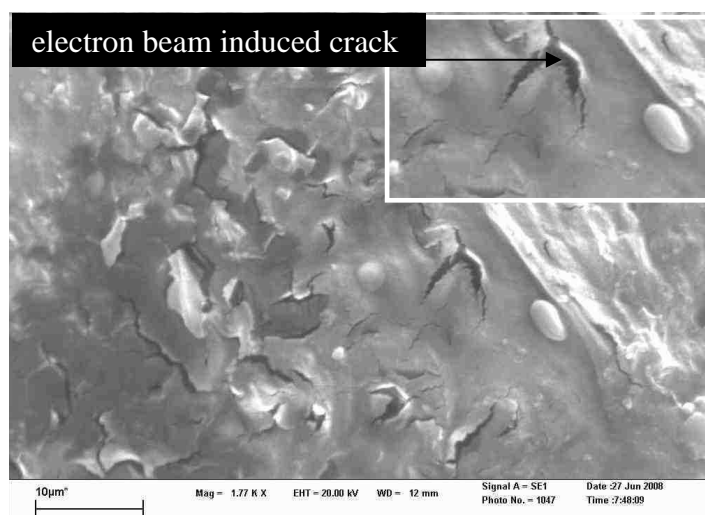
**A)** As-spun yarns that were cut did not yield clear or clean-cut cross-sections (Figure B.4a and b). The fibres showed incredible ductility under cryo conditions and would not shatter and therefore cross-sections could not be obtained with this method as the fibres could only be bent and stretched. This ductility below the glass transition temperature ( $T_g$ ) of both materials was attributed to the fine diameters and reduced number and size of flaws present within material of this scale ( $<2\mu\text{m}$ ). These fibres therefore show potential for applications requiring materials that deliver mechanical performance at cryo temperatures. This ductility under cryo conditions was seen for coaxial electrospinning as well as single capillary electrospinning of PLLA and PDLA.



**Figure B.4** SEM images of exposed fibre ends under a) low and b) high magnification

**B)** Yarns set in resin were microtomed to expose the fibre cross-sections (Figure B.5). The resin appeared to penetrate the fibres at their surfaces which created one continuous resin-fibre polymeric phase. The fibres as a result were not easily analysed. In some cases clear fibre ends were seen from the delamination of the fibres from the resin (Figure B.16 Section 1.3 - supporting information) from thermal shrinkage under the electron beam or by other means. The cross-sections were not always clear and it was difficult to observe as the morphology of the fibre was

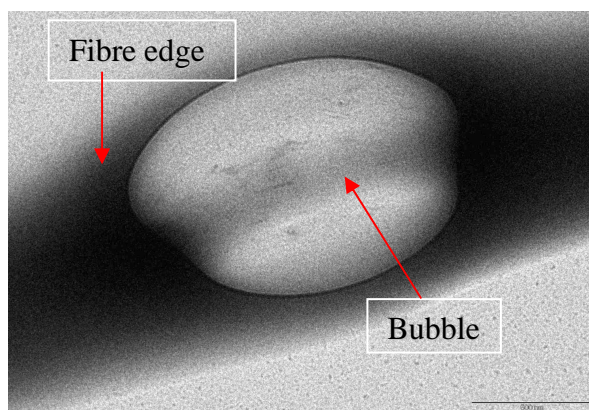
changed instantly when exposed to the electron beam. There were some indications of possible core-shell cross-sections, however these were not observed in any great number to be significant. The resin also seemed to crack on exposure to the electron beam. The consistencies of the observations of a core-shell structure were neither reproducible nor consistent enough to make any absolute validation of such a structure.



**Figure B.5** *Resin tablet edge exposed by ultramicrotomy showing fibres sticking out of the resin*

### B.2.3 TEM

Transmission electron microscopy of the coaxial electrospun fibres (collected directly on carbon coated TEM grids) was challenging. Various PLA core-shell solutions (4-8wt% PLLA and 10-12wt% PDLLA) were coaxially electrospun. The fibres were not stable at accelerating voltages <120kV, and only semi-stable at 120kV, where they had a tendency to change position and morphology. These instabilities are a result of the intrinsic radiation sensitivity (observed experimentally) of PLA polymer and the stressed (high strain by rapid elongation frozen-in by rapid solidification in the electrospinning process) internal structure of electrospun fibres that is released when the fibre is heated by interactions with the electrons from the electron beam. Additionally the fibres bubbled (Figure B.6) and crimped (shriveled to a curled morphology) as a result of this heat build up from electron collisions with the polymers. The bubbles generally ‘popped’ and destroyed the fibre removing it from view.

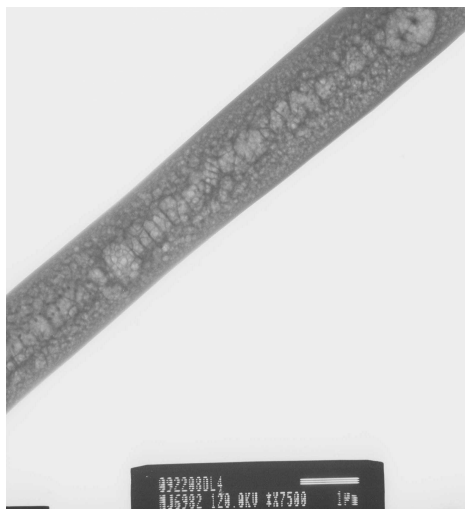


**Figure B.6** *Bubble formation from interaction between electrons and coaxial electrospun PLA fibre*

An accelerating voltage of 120kV resulted in fewer collisions between the electrons from the incident beam with the electrons in the PLA polymer in the fibre samples. This was the result of the greater speed with which the electrons passed through the sample. At lower accelerating voltages the incident electrons spent a longer time in the fibres which translated into more collisions and hence greater heat build-up within the fibres. An accelerating voltage of 120kV was however still not ideal as the fibres eventually became unstable after several seconds of exposure at high accelerating voltages. Higher accelerating voltages are possible on other instruments but the drawback is the loss of contrast which would not have aided the investigation of the core-shell structure with these polymers which have the same chemistry.

In an attempt to offset this heat build-up within samples, sample analysis was conducted under cryo conditions (liquid nitrogen  $\cong -196^{\circ}\text{C}$ ) at 120kV accelerating voltage. This was not very successful as the fibre inner structure was altered still by heat build-up. However, an interesting phenomenon observed was that a multitude of nano-pores nucleated from the centre out towards the periphery of the fibres (Figure B.7). This phenomenon demonstrated a potential inexpensive avenue to create highly porous fibres where very high surface areas are desirable.

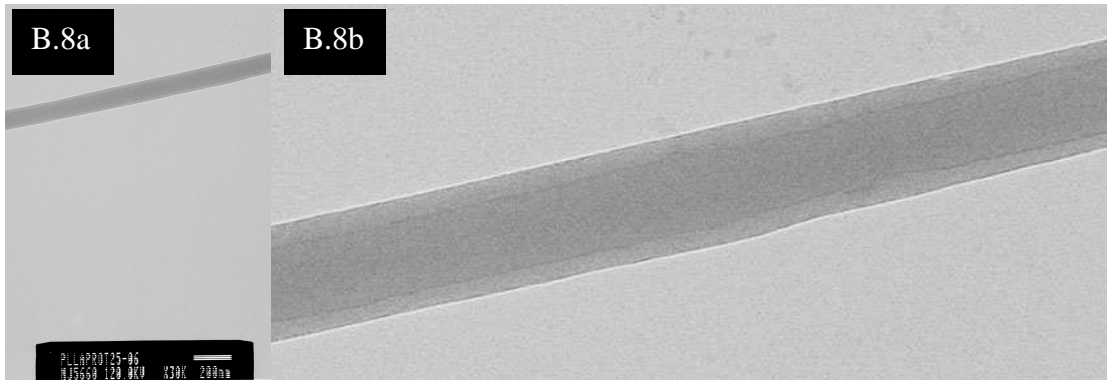




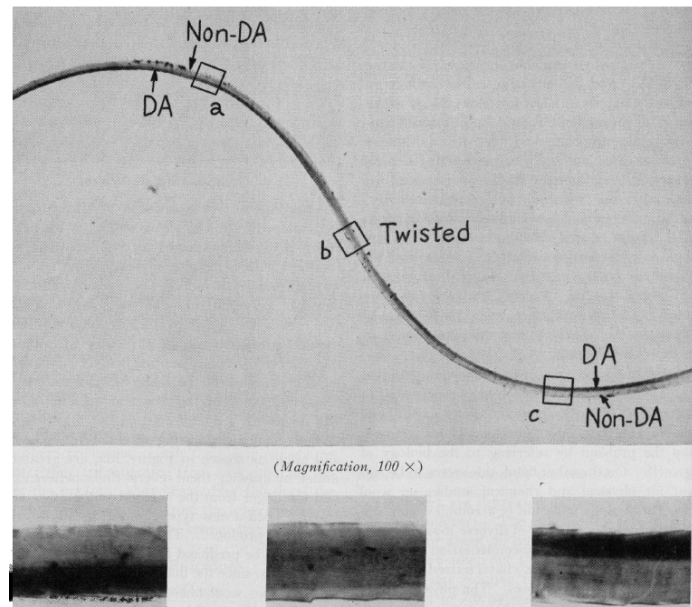
**Figure B.7** *Nucleation of pores within the coaxial electrospun PLA fibres observed under cryo conditions*

In some instances, where fibres remained stable under the electron beam, the fibres appeared to have core-shell structures (Figures B.8a and b). As the images are only of lateral views of the fibres the possibility of these fibres being twisted side-by-side (as seen when preferential stained wool fibres twist (Figure B.9), overlapping or collapsed ribbon fibres are quite likely. To distinguish the other structural possibilities from core-shell fibre structures with absolute certainty is not possible. It was assumed a priori that there would be some contrast between the core and shell material as the core should be denser (disordered crystals shown and explained by x-ray diffraction and differential scanning calorimetry analysis in later sections) and allow fewer electrons to pass through the fibres as compared with the shell which has larger free volume between polymer molecules and no crystal structures. Once more there was no reproducible evidence from this approach that could without uncertainty validate a core-shell fibre structure.



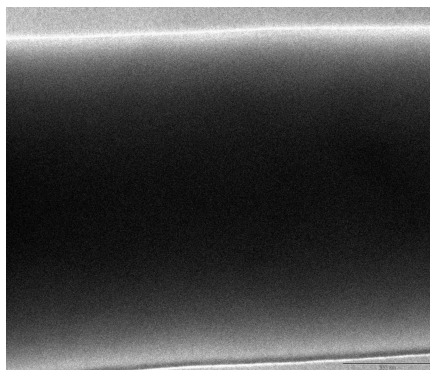


**Figure B.8** a) TEM image and b) expanded view of a coaxial electrospun PLA fibre stable under the electron beam showing contrast of a continuous core (much too large a core and therefore contrast could be due to edge effects)



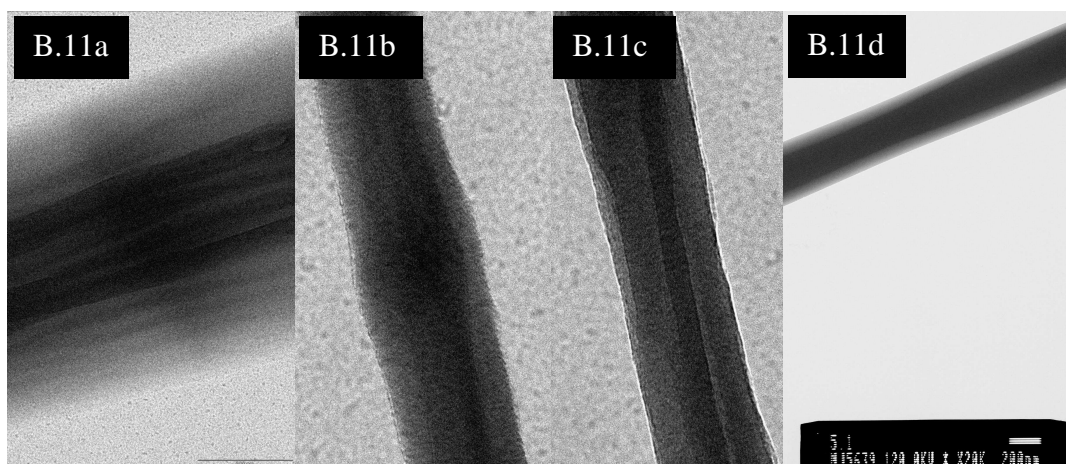
**Figure B.9** Wool fibre with preferential staining of ortho- and para-cortex (DA – dye accepted sites)<sup>1</sup>

In many instances the electron beam could not transmit through the fibre samples as they were too thick (a rule of thumb in TEM analysis is that samples should be <200nm in thickness to allow sufficient transmission of electrons). In such case solid black fibres were observed (Figure B.10)

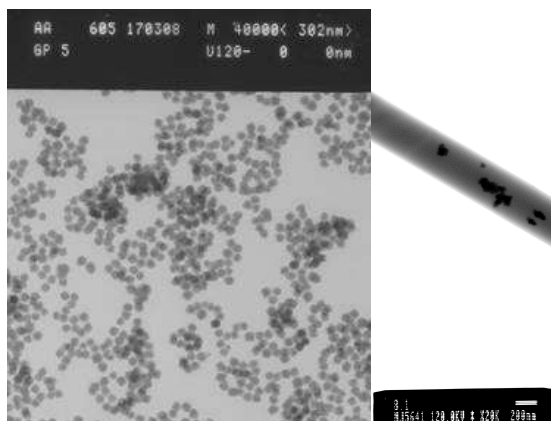


**Figure B.10** Coaxial electrospun fibre that shows a lighter peripheral region and a darker interior which is too thick to allow transmission of electrons

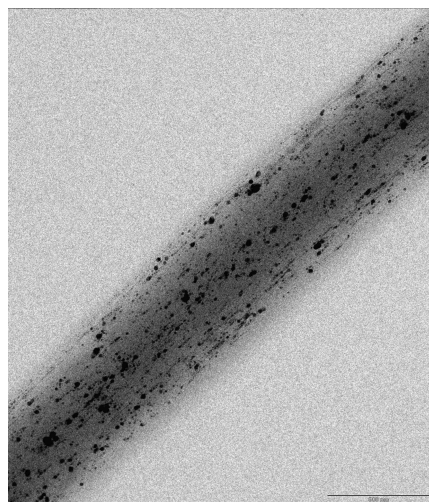
A **dye** (Figures B.11a), b), c), d) and Figure B.17 Section 1.3 – supporting information), **ZnS-PVP particles** (Figures B.12a), b) and Figure B.18 Section 1.3 – supporting information) and **AgNO<sub>3</sub>** (Figure B.13) particles were added on separate occasions to the core solution at 0.1wt% (dry fibre weight) and allowed to homogenise (for 2-4hrs) prior to spinning to ultimately achieve contrast under TEM analysis of coaxially electrospun fibres. These additions yielded results of varying success, showing likely core-shell structures in some cases, but once again the absolute certainty of a core-shell structure was still elusive. What should be noted is that electrospinning with core solutions containing **AgNO<sub>3</sub>** was problematic as the solution was very conductive and stable electrospinning was rarely achieved (forming of multiple jets occurred).



**Figure B.11** a), b), c), and d) Coaxial electrospun fibres with 0.1wt% (of dry fibre mass) dye in the core



**Figure B.12** a) ZnS-PVP particles and b) Coaxial electrospun PLA fibres with 0.1wt% (of dry fibre mass) ZnS-PVP in the core

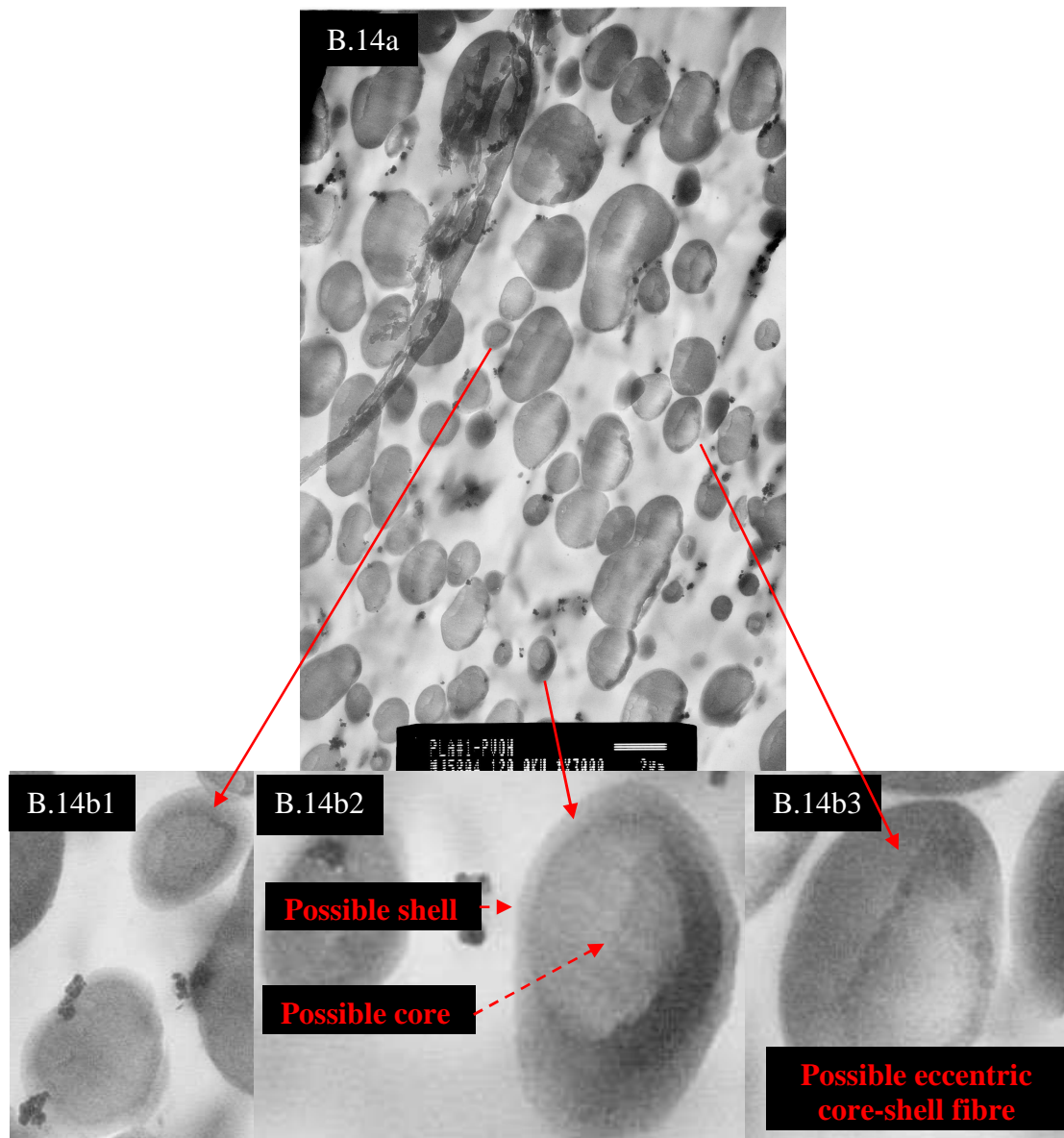


**Figure B.13** Coaxial electrospun PLA fibres with 0.1wt%  $\text{AgNO}_3$  particles (of dry fibre mass) in the core

In attempt to support the evidence of possible core-shell structures seen in lateral view TEM images, cross-sections of the core-shell fibre yarns were prepared. These were prepared by ultramicrotomy of as-spun yarns embedded in resin (with and without contrasting agents in the core). Slides 100nm thick were cut and analysed under TEM.

Stability (under the electron beam) of the fibres embedded in the thin resin slides was slightly better than with the fibres collected on the TEM grids. The reason for this is due to fewer collisions of incident electrons with the samples because the electrons only had to travel through 100nm samples (oppose to  $\cong 1\mu\text{m}$  fibre samples in lateral viewing).

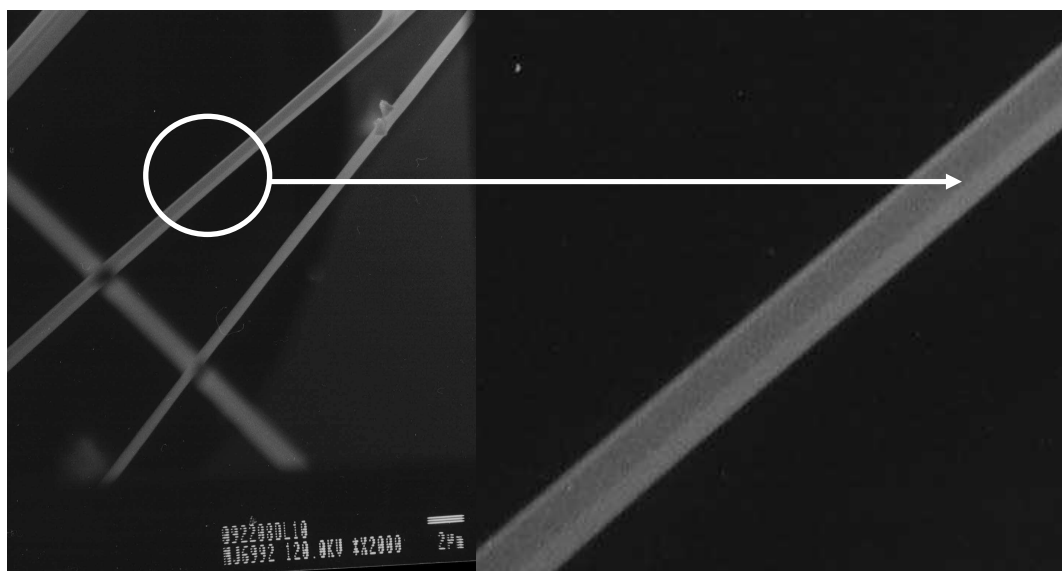
The microtome slides showed evidence of concentric and eccentric core-shell fibre cross-sections (Figure B.14a) and b) 1-3). Similar structures were however also picked up on analysis of a reference PLLA yarn which indicated that the fibres were not parallel but some were mounted at an angle and it was still difficult to observe unambiguously the core-shell structure (Figure B.19 Section 1.3 – supporting information).



**Figure 5.14** a) and b) 1-3) coaxial electrospun fibre cross-section prepared by ultramicrotomy of yarns embedded in resin.

Additionally lateral fibres on TEM grids were viewed under *dark-field* TEM mode (Figure B.15a) and b)). Dark-field TEM transmits indirect electrons through the

sample and was used in attempt to obtain greater contrast between possible core and shell components and reduce the number of electrons interacting with the sample. Although some images indicated an eccentric core-shell structure (Figure B.15b) and contrast was seen, neither significant improvement (compared with incident electrons) nor absolute proof of a core-shell structure could be visualised with this method.



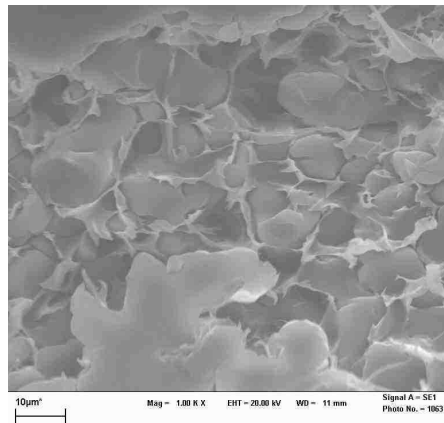
**Figure B.15** a) Dark field TEM image of coaxial electrospun PLA fibres and b) expanded view of the fibre showing a possible eccentric core-shell fibre

### B.3 Conclusions

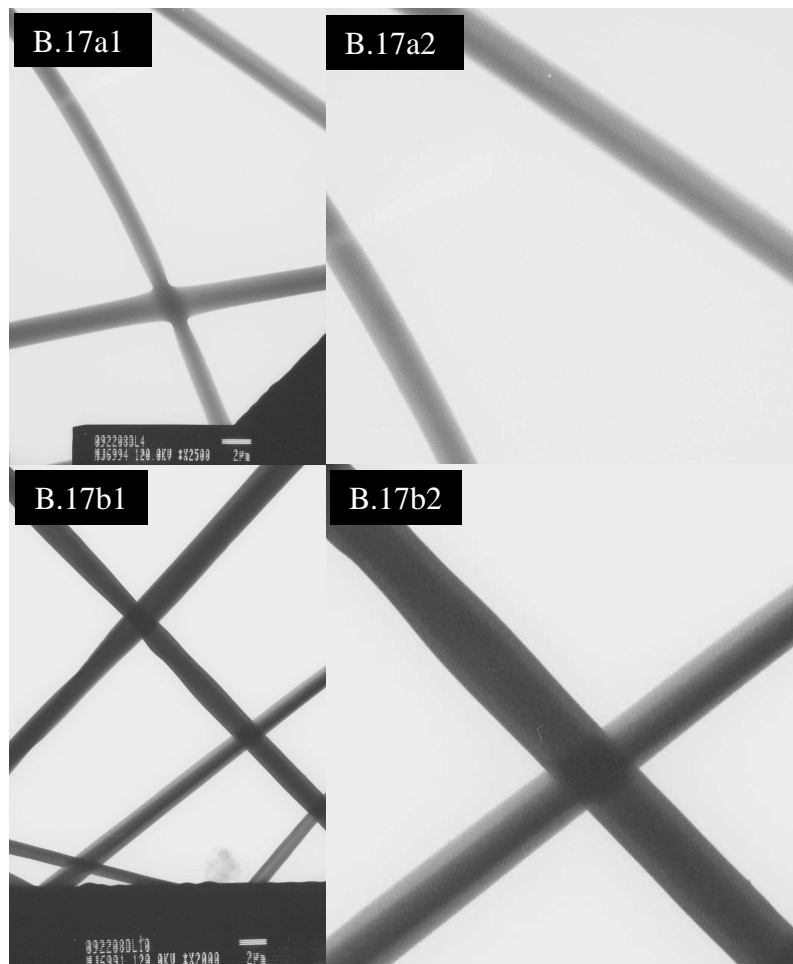
Microscopy strategies used to validate the core-shell fibre structure proved to be inconclusive. There were cases where fibres, stable under the electron beam (TEM), showed sufficient contrast and a core-shell fibre structure. However, it could not be said with absolute certainty that this was a concentric core-shell fibre, a twist twin fibre or some aberration. Core-shell fibres structures were also not seen often enough in fibres of the same collected sample and between different samples. Based on this uncertainty it would be presumptuous to assume that core-shell spinning was successful. An alternative method or methods to investigate the core-shell fibre structure was therefore required.



## B.4 Supporting Information

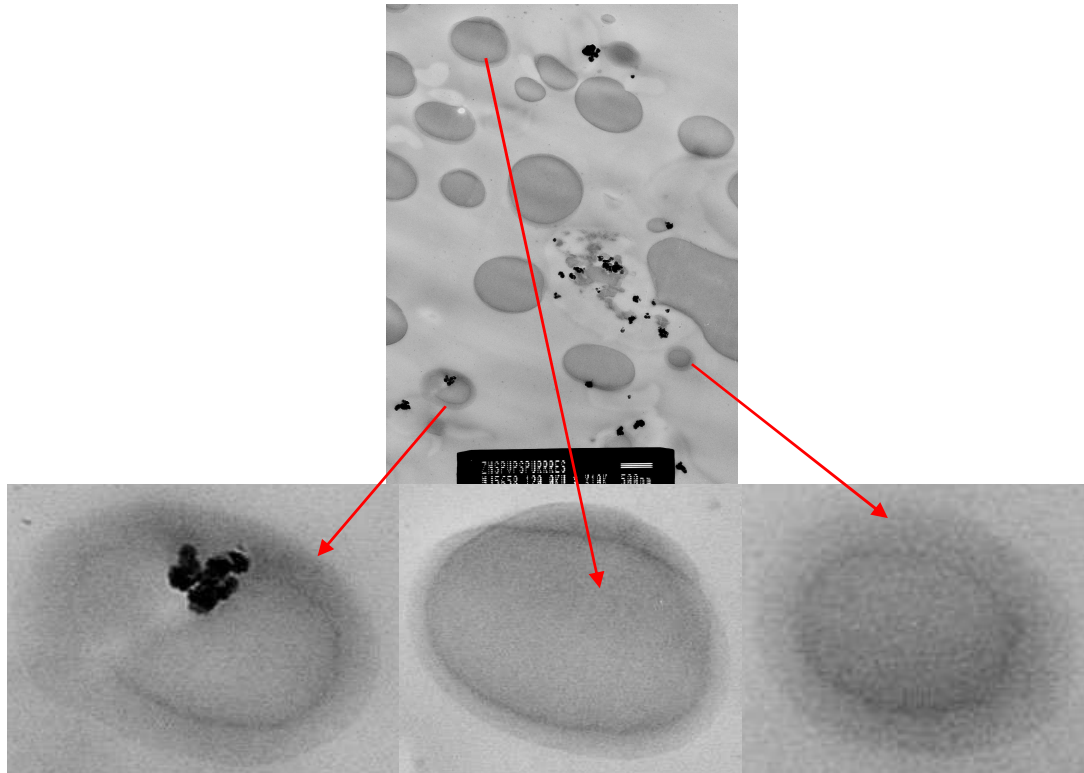


**Figure B.16** *Fibres exposed from microtomed resin tablet*

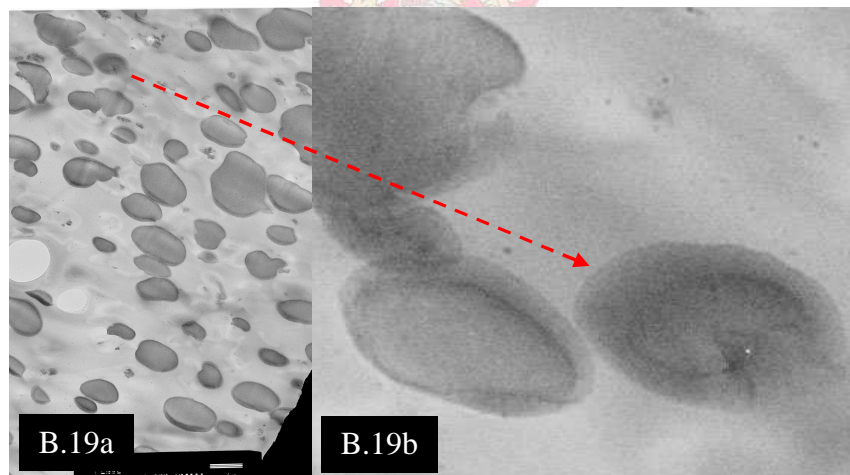


**Figure B.17** *a1&2) TEM images and b1&2) expanded view of coaxial electrospun fibres on grids*





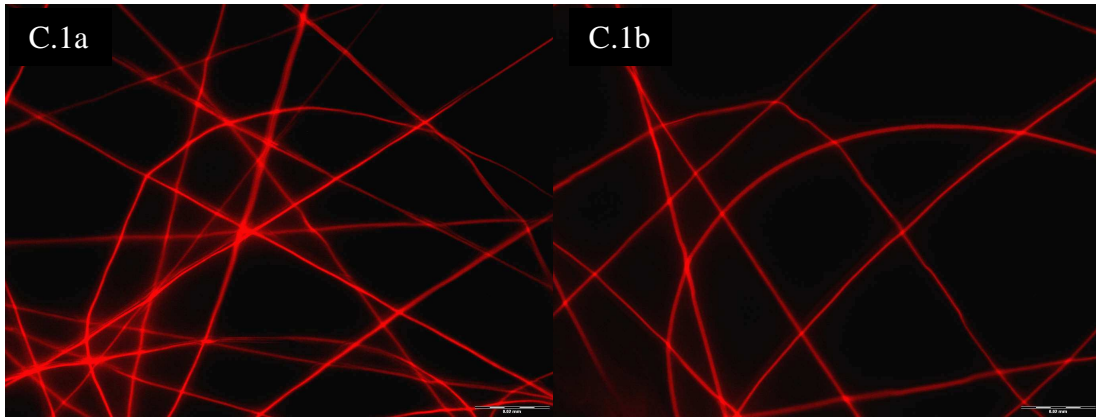
**Figure B.18** TEM images of ZnS-PVP loaded core-shell fibres cross-sections



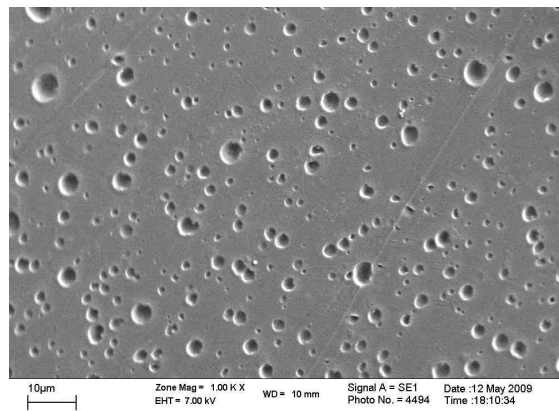
**Figure B.19** a) TEM image and b) expanded view of electrospun PLLA yarn cross-sections

#### References

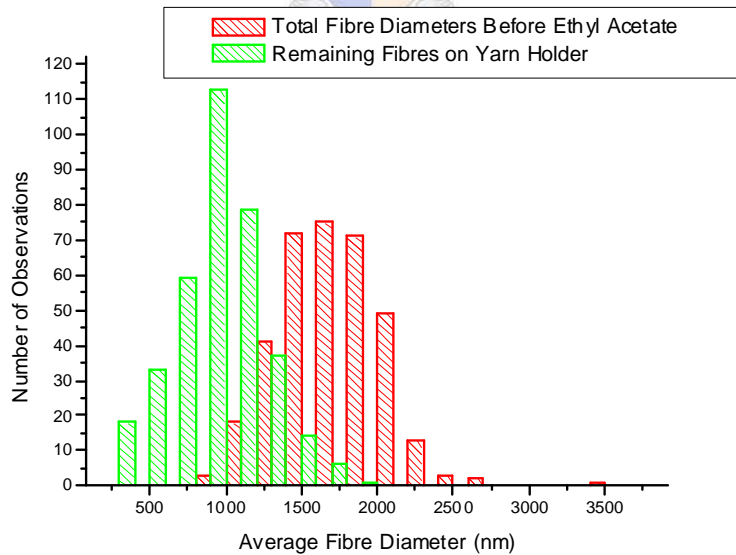
1. Horio M, Kondo W. Crimping of Wool Fibers. *Textile Research Journal*. 1953;23:373-86.



**Figure C.1** a) and b) Coaxial electrospun PLLA(Rhodamine B)-PLLA fibres with 0.1 and 0.3ml/h core flow rate respectively



**Figure C.2** PDLLA polymer film after evaporation of ethyl acetate



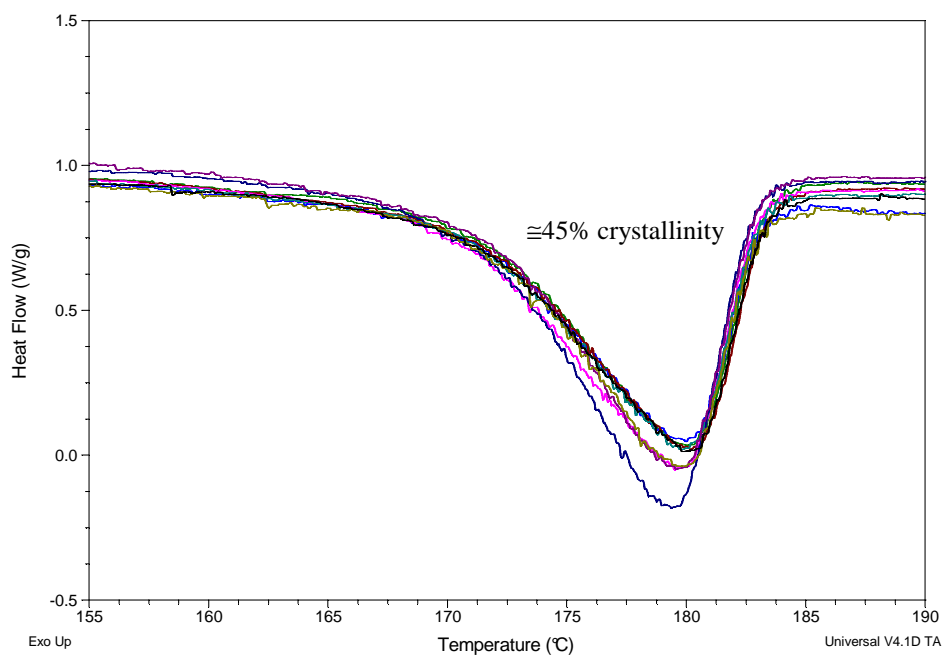
**Figure C.3** Average fibre diameter distributions of coaxial electrospun fibres before and after washing in ethyl acetate

**Table C.1** Specific optical rotation measurements for cores and films dissolved in chloroform

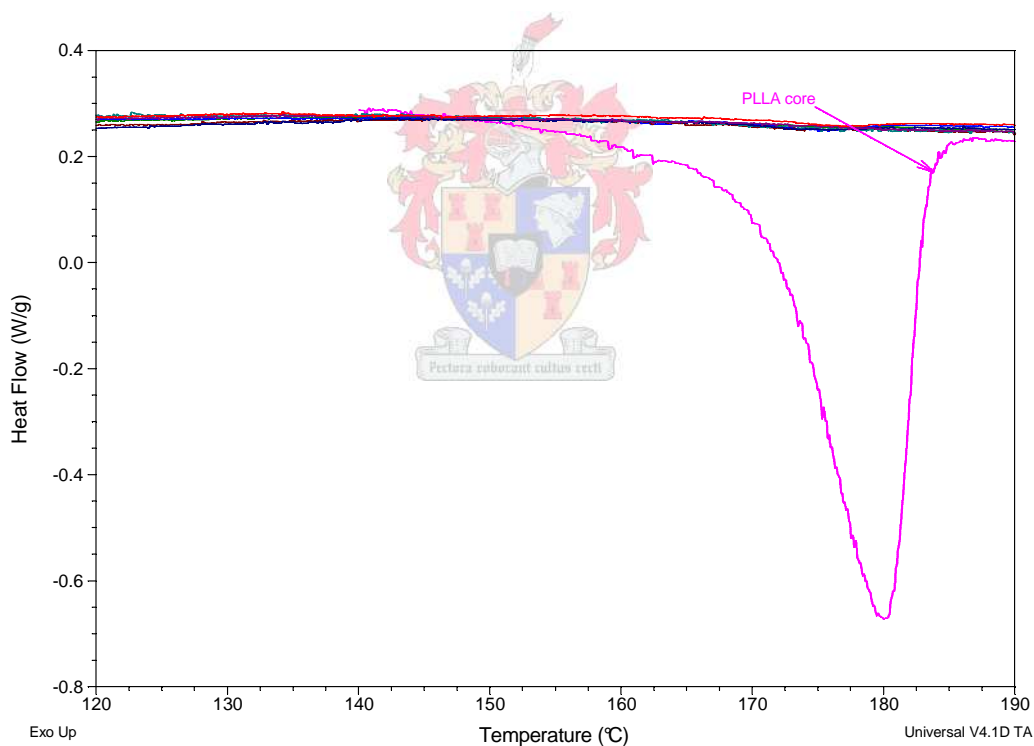
Specific optical rotation for core ( $[\alpha]_{\lambda}^{\theta}$ )	Specific optical rotation for shell ( $[\alpha]_{\lambda}^{\theta}$ )
-190.17	0
-200.39	0
-193.74	0
-250.63	0
-195.12	0
-207.81	0
-298.33	0
-161.19	0
-187.27	0
-222.04	0
-207.33	0
-186.73	0

**Table C.2** Specific optical rotation measurements for cores and films dissolved in chloroform

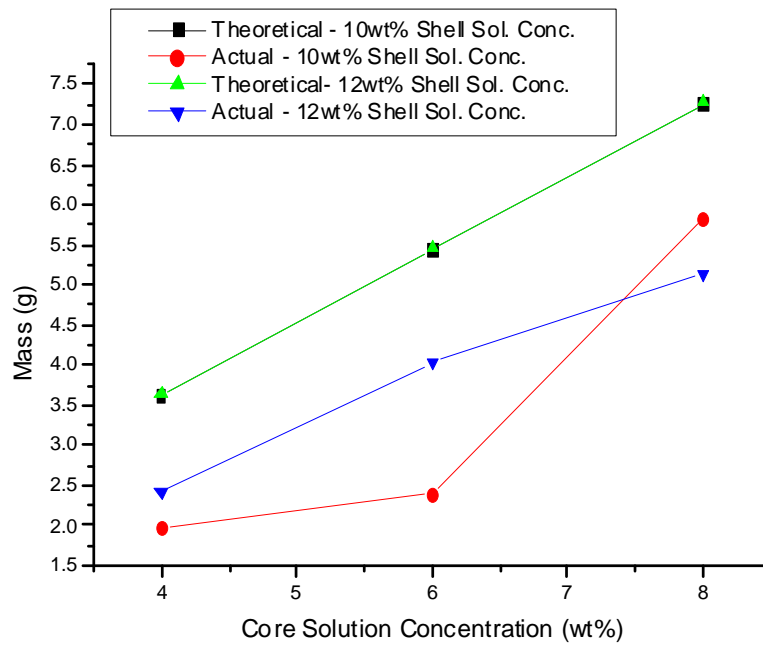
Core solution conc. (wt%)	Shell solution conc. (wt%)	Core solution flow rate (ml/h)	Shell solution flow rate (ml/h)	Remaining fibres on yarn holder concentration in 5ml Chloroform solution (wt%)	Polymer film extracted from ethyl acetate concentration in 5ml Chloroform solution (wt%)	Specific optical rotation of remaining fibres on yarn holder ( $[\alpha]_{\lambda}^{\theta}$ )	Specific optical rotation of polymer film extracted from ethyl acetate ( $[\alpha]_{\lambda}^{\theta}$ )
4%	10%	0.3	1.2	0.05%	0.12%	-218.24	0
6%	10%	0.3	1.2	0.08%	0.07%	-195.29	0
8%	10%	0.3	1.2	0.14%	0.10%	-171.17	0
4%	12%	0.3	1.2	0.05%	0.04%	-157.29	0
6%	12%	0.3	1.2	0.12%	0.15%	-220.61	0
8%	12%	0.3	1.2	0.16%	0.18%	-188.38	0
8%	10%	0.1	1.2	0.03%	0.06%	-334.94	0
8%	10%	0.2	1.2	0.10%	0.09%	-144.2	0
8%	10%	0.3	1.2	0.14%	0.10%	-171.17	0
8%	10%	0.1	1.4	0.03%	0.15%	-240.65	0
8%	10%	0.2	1.4	0.09%	0.10%	-180.3	0
8%	10%	0.3	1.4	0.15%	0.05%	-343.15	0
5mg REF	N/A	N/A	N/A	0.07%	0.00%	-223.8	0
10mg REF	N/A	N/A	N/A	0.13%	0.00%	-193.96	0
15mg REF	N/A	N/A	N/A	0.20%	0.00%	-253.64	0
Blank Chloroform						0	0



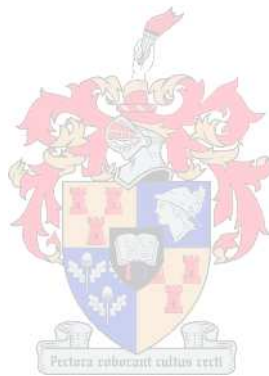
**Figure C.4** DSC thermogram showing the melt endotherms of the cores



**Figure C.5** DSC thermogram of the separated shell components compared with one PLLA core sample



**Figure C.6** *Effects of solution concentration on actual vs. theoretical core mass yield*

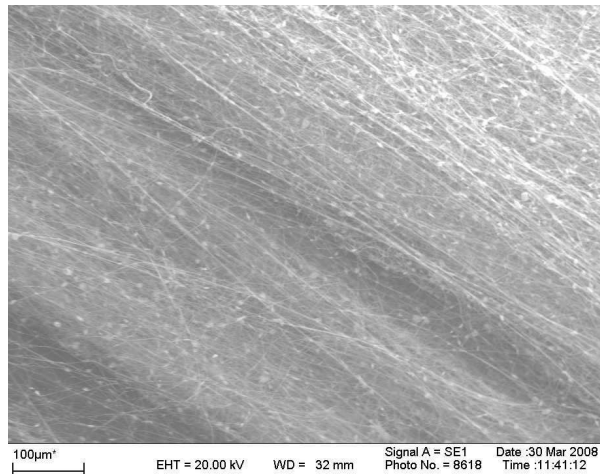


**Table C.3** *Parameter effects on as-spun yarn mass before and after washing in ethyl acetate*

Core wt% conc.	Shell wt% conc.	Core-flow rate (ml/h)	Shell flow rate (ml/h)	Total yarn mass (mg)	Core mass (mg)	Shell Mass (mg)	core:total yarn mass	Theoretical total yarn mass (mg)	Theoretical core mass (mg)	Theoretical shell mass (mg)	Theoretical core:total yarn mass
4%	10%	0.3	1.2	23.91	1.98	16.49	8.27%	39.98	3.63	36.34	9.09%
6%	10%	0.3	1.2	19.21	2.40	13.03	12.49%	41.79	5.45	36.34	13.04%
8%	10%	0.3	1.2	21.78	5.83	17.24	26.79%	43.61	7.27	36.34	16.67%
4%	12%	0.3	1.2	27.97	2.42	19.67	8.66%	47.24	3.63	43.61	7.69%
6%	12%	0.3	1.2	32.03	4.03	22.87	12.58%	49.06	5.45	43.61	11.11%
8%	12%	0.3	1.2	27.74	5.13	15.90	18.50%	50.88	7.27	43.61	14.29%
8%	10%	0.1	1.2	26.61	1.70	18.83	6.39%	38.76	2.42	36.34	6.25%
8%	10%	0.2	1.2	26.06	4.20	16.77	16.12%	41.19	4.85	36.34	11.76%
8%	10%	0.3	1.2	21.78	5.83	17.24	26.79%	43.61	7.27	36.34	16.67%
8%	10%	0.1	1.4	32.87	1.51	21.57	4.60%	44.82	2.42	42.40	5.41%
8%	10%	0.2	1.4	33.36	3.16	20.07	9.49%	47.24	4.85	42.40	10.26%
8%	10%	0.3	1.4	32.83	4.63	13.83	14.11%	49.67	7.27	42.40	14.63%







**Figure C.7** *Beads-on-string morphology of fibres electrospun from 4wt% PLLA (70/30 v/v DCM/DMF) solutions*

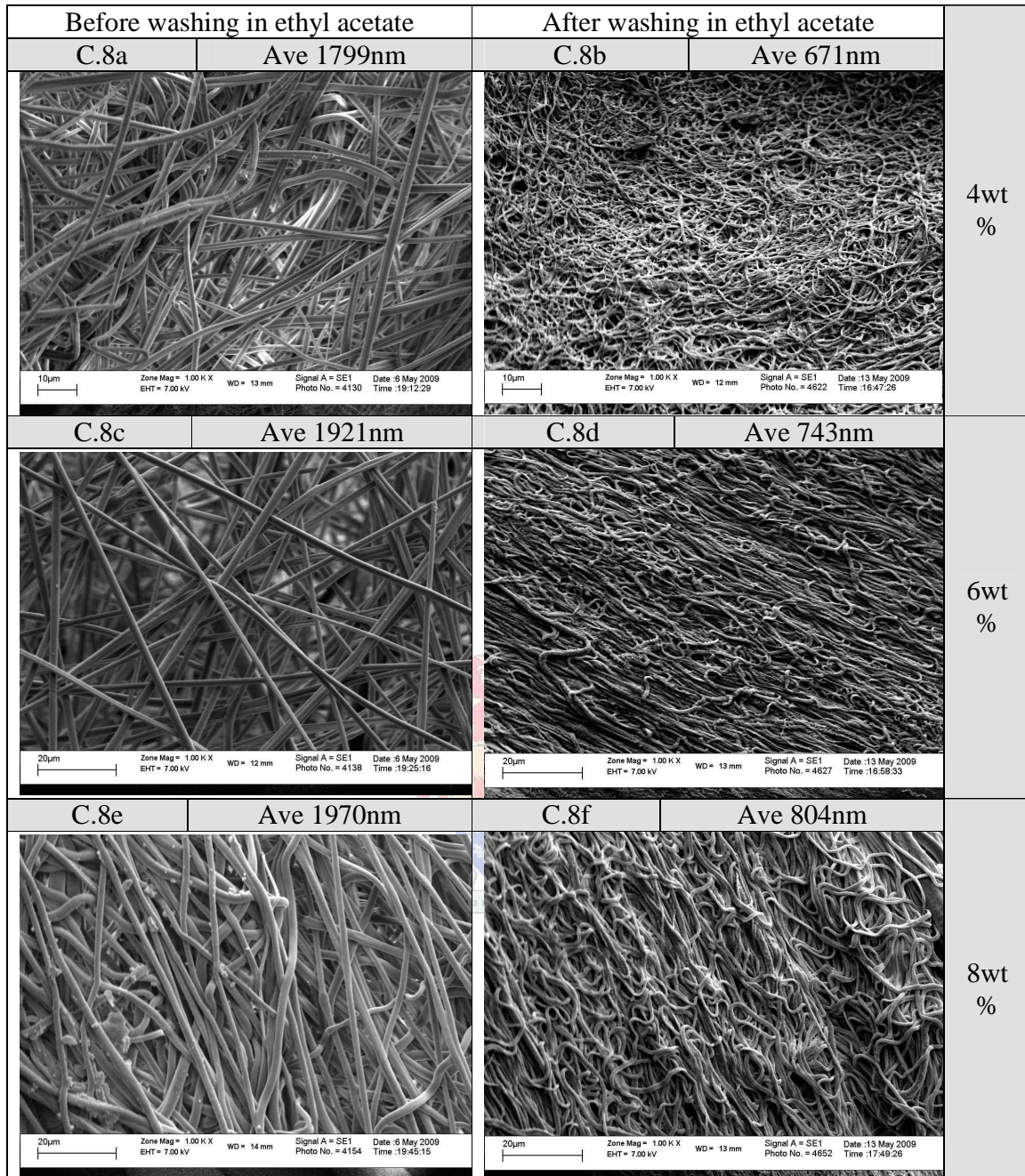
**Table C.4** *Parameters investigated: A) effects of solution concentration and B) effects of solution flow rate on resultant fibre diameters*

A. <sup>1</sup> Core concentration (wt%)	Shell concentration. 10wt%		Shell concentration. 12wt%	
	Ave. core diameter (STDEV)	Ave. total diameter (STDEV)	Ave. core diameter (STDEV)	Ave. total diameter (STDEV)
4%	630 (±174)	1725 (±287)	671 (±218)	1799 (±234)
6%	689 (±193)	1720 (±518)	743 (±162)	1921 (±238)
8%	675 (±155)	1534 (±390)	804 (±210)	1969 (±273)

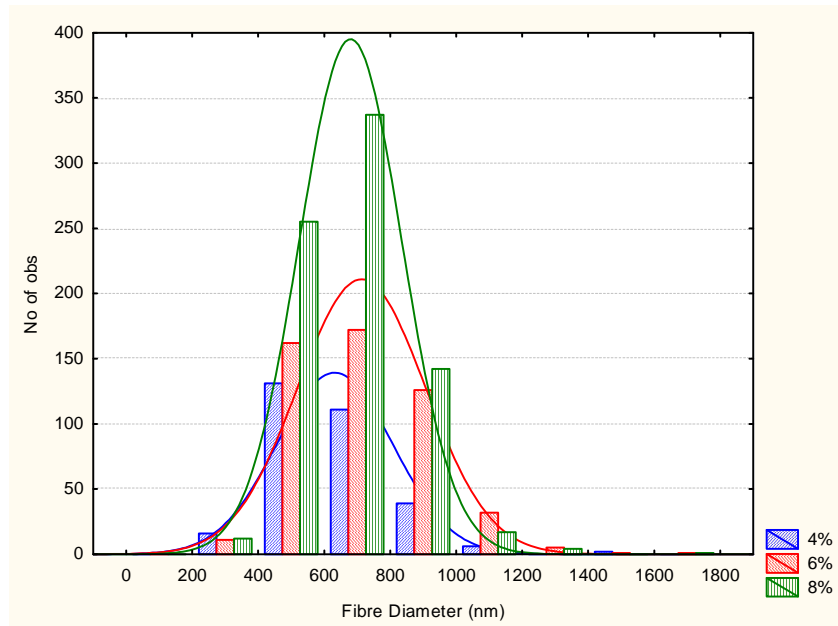
B. <sup>2</sup> Core flow rate (ml/h)	Shell flow rate 1.2ml/h		Shell flow rate 1.4ml/h	
	Ave. core diameter (STDEV)	Ave. total diameter (STDEV)	Ave. core diameter (STDEV)	Ave. total diameter (STDEV)
0.1	472 (±125)	1436 (±279)	416 (±107)	1617 (±225)
0.2	577 (±169)	1500 (±188)	540 (±167)	1490 (±345)
0.3	675 (±155)	1534 (±292)	638 (±215)	1461 (±244)

<sup>1</sup> First (A) the effect of varying the core solution concentration at 10wt% and 12wt% shell solution concentrations on the resultant fibre diameters was investigated. The core and shell solution flow rates were held constant at 0.3 ml/h and 1.2 ml/h respectively.

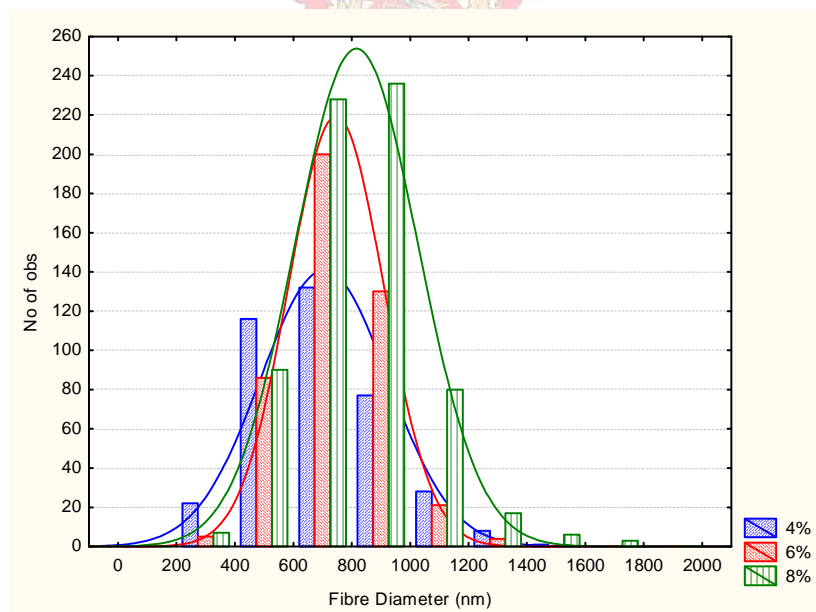
<sup>2</sup> The effect of core flow rate at 1.2 ml/h and 1.4 ml/h shell solution flow rates on resultant fibre diameters was also investigated (B).



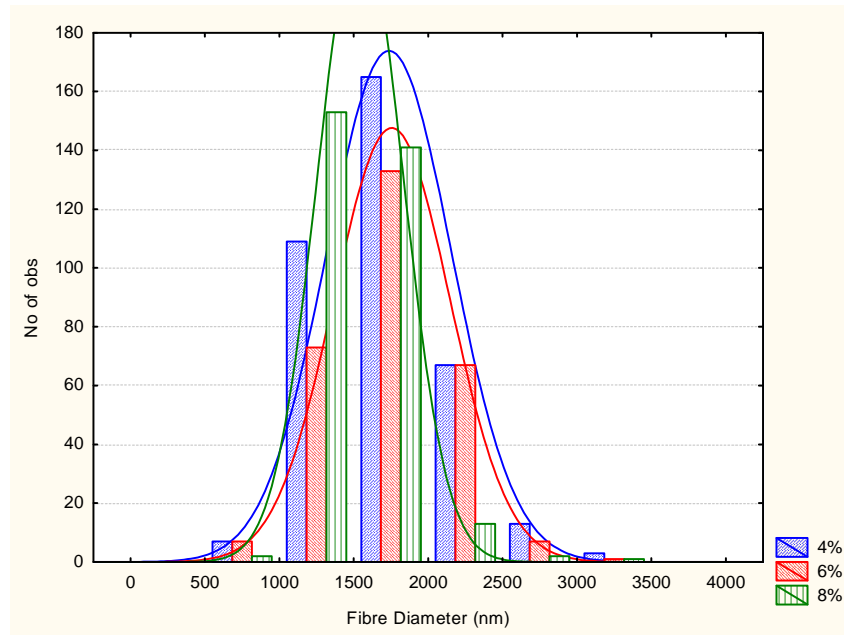
**Figure C.8** Core-shell fibre diameters as a function of core polymer concentrations a-b) 4wt%, c-d) 6wt%, e-f) 8wt% before and after washing in ethyl acetate. The core and shell solution flow rates during electrospinning were 0.3 and 1.2 ml/h respectively. The shell solution concentration was 12wt%



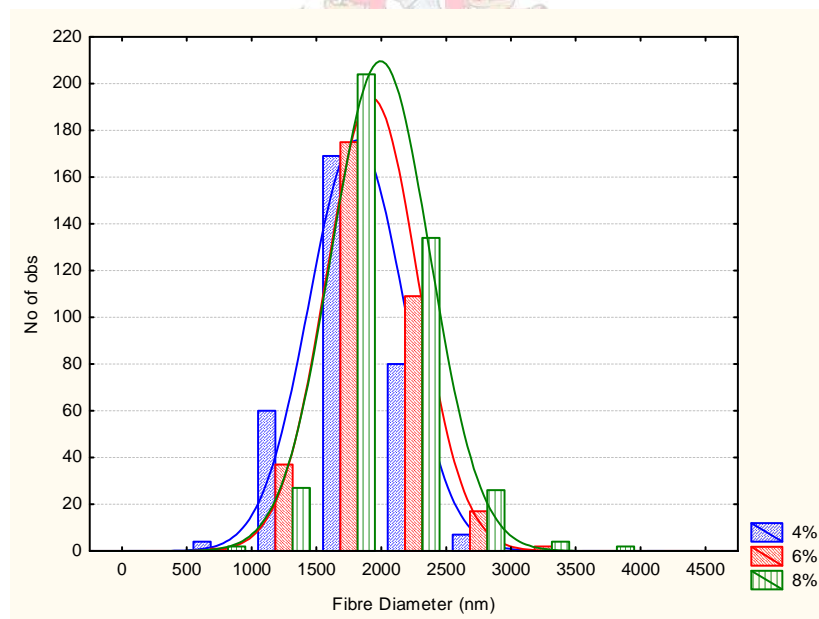
**Figure C.9** *Fibre remaining after washing in ethyl acetate - fibre diameter distributions: Effect of increasing core solution concentration at 10wt% shell solution concentration*



**Figure C.10** *Fibre remaining after washing in ethyl acetate - fibre diameter distributions: Effect of increasing core solution concentration at 12wt% shell solution concentration*



**Figure C.11** *As-spun fibre diameter distributions: Effect of increasing core solution concentration at 10wt% shell solution concentration*

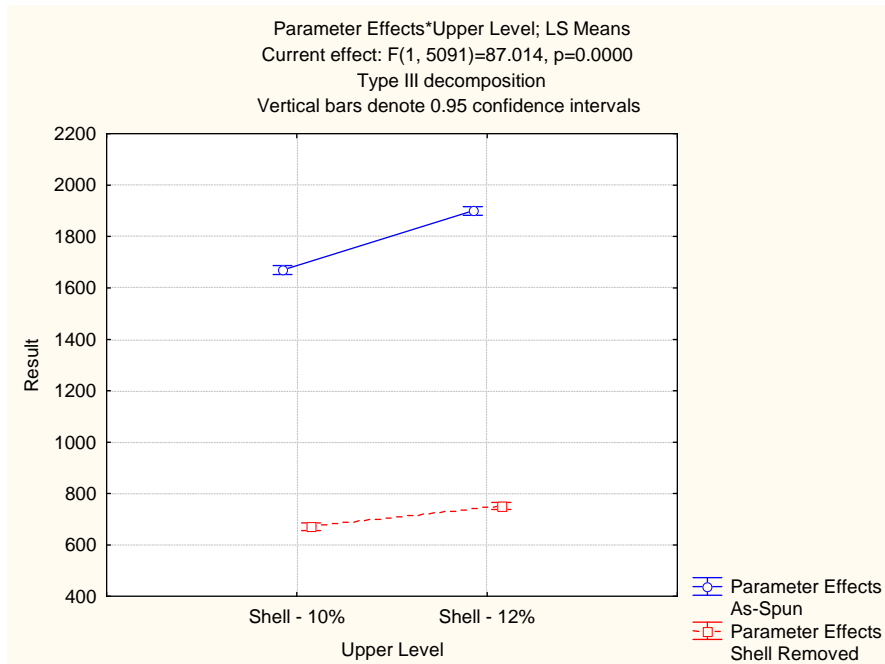


**Figure C.12** *As-spun fibre diameter distributions: Effect of increasing core solution concentration at 12wt% shell solution concentration*

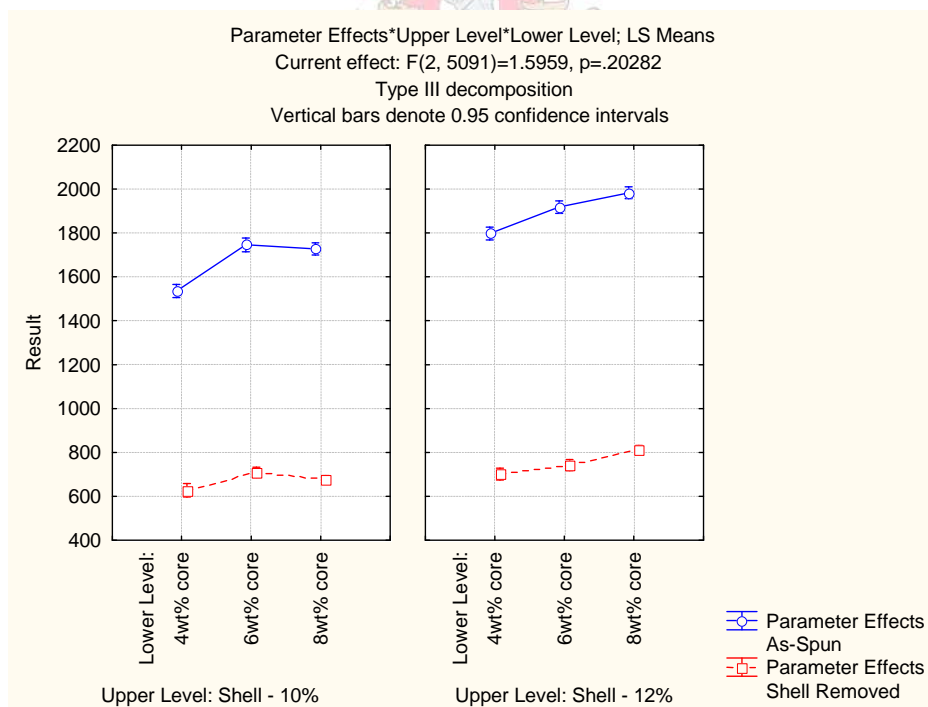
**Table C.5** Bonferroni Tests for significance from ANOVA of solution concentration effects on core and core-shell fibre diameters

Bonferroni test; variable Result (FibreDiameters_Concentration in Analyses - 09Nov2009.stw)															
Probabilities for Post Hoc Tests															
Error: Between MS = 74533., df = 5091.0															
No.	Parameter Effects	Upper Level	Lower Level	{1}	{2}	{3}	{4}	{5}	{6}	{7}	{8}	{9}	{10}	{11}	{12}
				1535.4	1745.6	1727.3	1797.5	1917.5	1982.9	628.31	709.29	675.98	701.70	742.29	811.71
1	As-Spun	10wt% shell	4wt% core		0.00	0.00	0.00	0.00	0.00	0.00	0.00	0.00	0.00	0.00	0.00
2	As-Spun	10wt% shell	6wt% core	0.00		1.00	1.00	0.00	0.00	0.00	0.00	0.00	0.00	0.00	0.00
3	As-Spun	10wt% shell	8wt% core	0.00	1.00		0.05	0.00	0.00	0.00	0.00	0.00	0.00	0.00	0.00
4	As-Spun	12wt% shell	4wt% core	0.00	1.00	0.05		0.00	0.00	0.00	0.00	0.00	0.00	0.00	0.00
5	As-Spun	12wt% shell	6wt% core	0.00	0.00	0.00	0.00		0.08	0.00	0.00	0.00	0.00	0.00	0.00
6	As-Spun	12wt% shell	8wt% core	0.00	0.00	0.00	0.00	0.08		0.00	0.00	0.00	0.00	0.00	0.00
7	Shell Remove	10wt% shell	4wt% core	0.00	0.00	0.00	0.00	0.00	0.00		0.00	0.65	0.03	0.00	0.00
8	Shell Remove	10wt% shell	6wt% core	0.00	0.00	0.00	0.00	0.00	0.00	0.00		1.00	1.00	1.00	0.00
9	Shell Remove	10wt% shell	8wt% core	0.00	0.00	0.00	0.00	0.00	0.00	0.65	1.00		1.00	0.00	0.00
10	Shell Remove	12wt% shell	4wt% core	0.00	0.00	0.00	0.00	0.00	0.00	0.03	1.00	1.00		1.00	0.00
11	Shell Remove	12wt% shell	6wt% core	0.00	0.00	0.00	0.00	0.00	0.00	0.00	1.00	0.00	1.00		0.00
12	Shell Remove	12wt% shell	8wt% core	0.00	0.00	0.00	0.00	0.00	0.00	0.00	0.00	0.00	0.00	0.00	



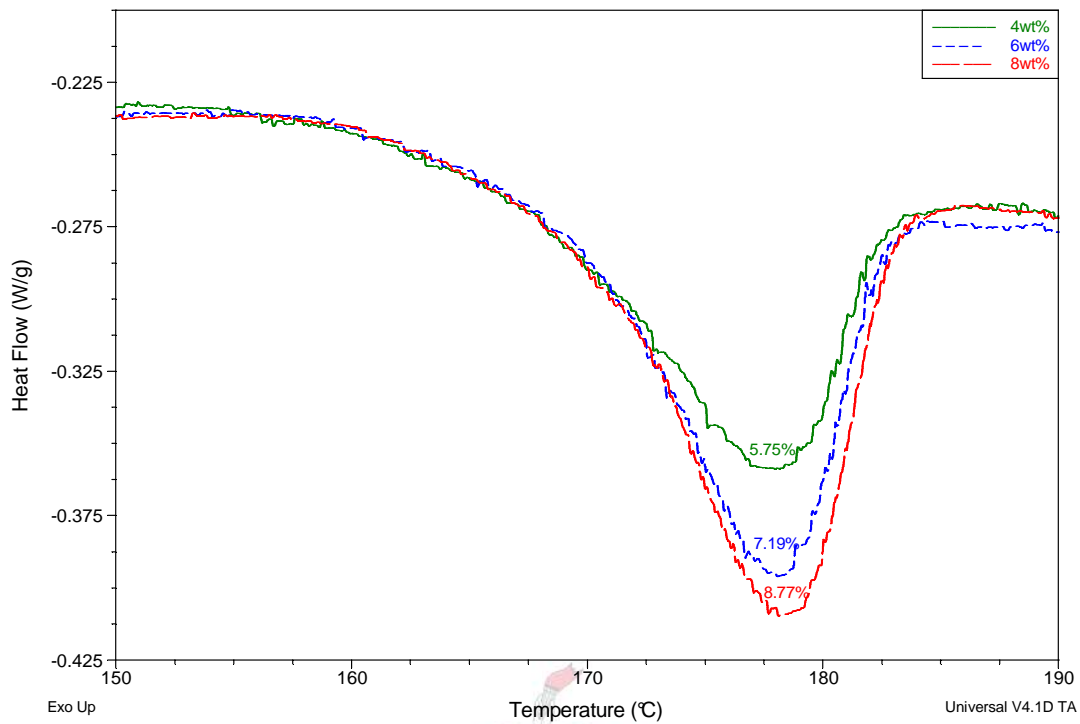


**Figure C.13** Shell solution concentration effects on core (shell removed) and core-shell (As-spun) fibre diameter - Parameter Effects\*Upper Level; Least-square (LS) Means

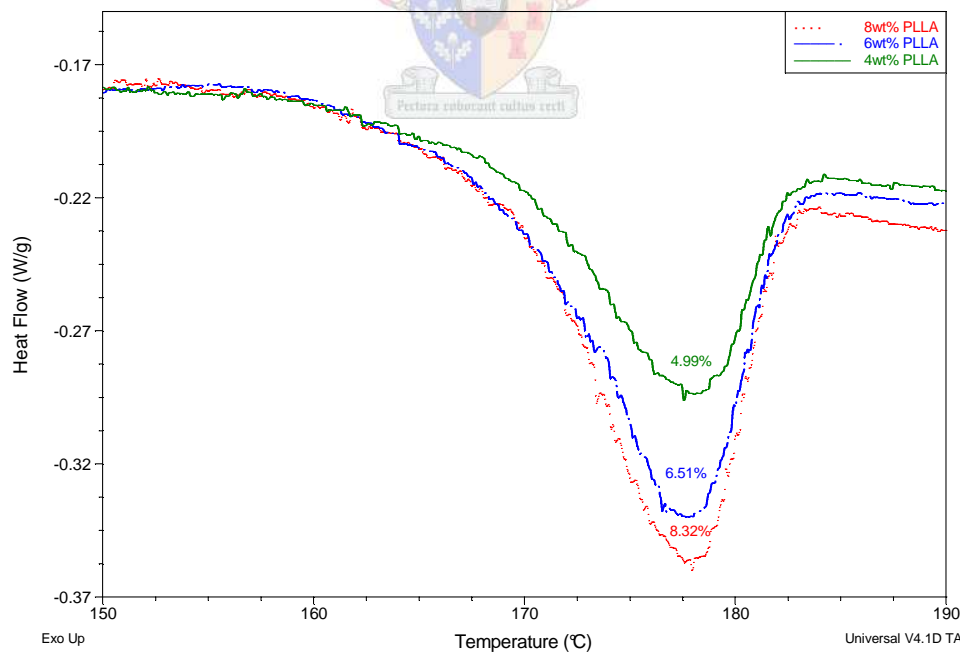


**Figure C.14** Solution concentration effects on core (shell removed) and core-shell (As-spun) fibre diameter - Parameter Effects\*Upper Level\*Lower Level; LS Means





**Figure C.15** Solution concentration effects on the melt endotherm of coaxial electrospun fibre yarns at a 10wt% shell solution concentration



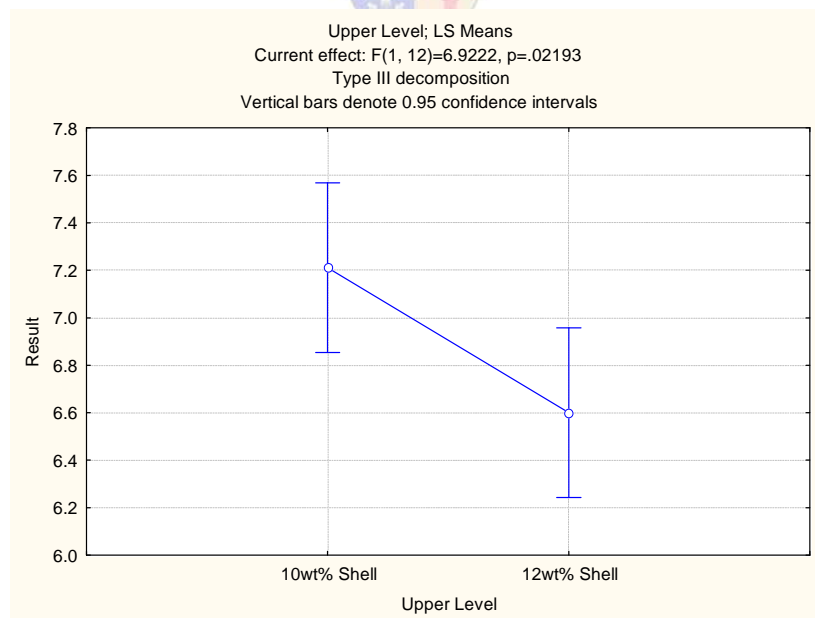
**Figure C.16** Solution concentration effects on the melt endotherm of coaxial electrospun fibre yarns at a 12wt% shell solution concentration

**Table C.6** Bonferroni Tests for significance from ANOVA of increasing core solution concentration effects on core-shell fibre crystallinity: 10wt% shell solution concentration

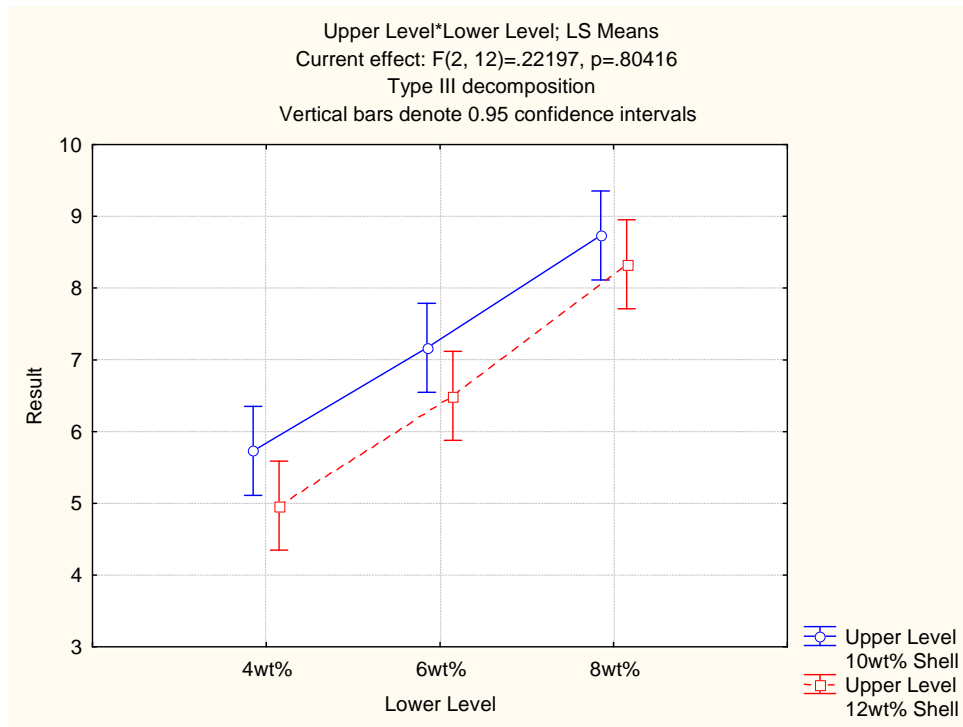
Upper Level=10wt% Shell Bonferroni test; variable Result (Spreadsheet in Analyses - 09Nov2009.stw) Probabilities for Post Hoc Tests Error: Between MS = .12000, df = 6.0000				
No.	Lower Level	{1}	{2}	{3}
		5.7333	7.1667	8.7333
1	4wt%		0.01	0.00
2	6wt%	0.01		0.00
3	8wt%	0.00	0.00	

**Table C.7** Bonferroni Tests for significance from ANOVA of increasing core solution concentration effects on core-shell fibre crystallinity: 12wt% shell solution concentration

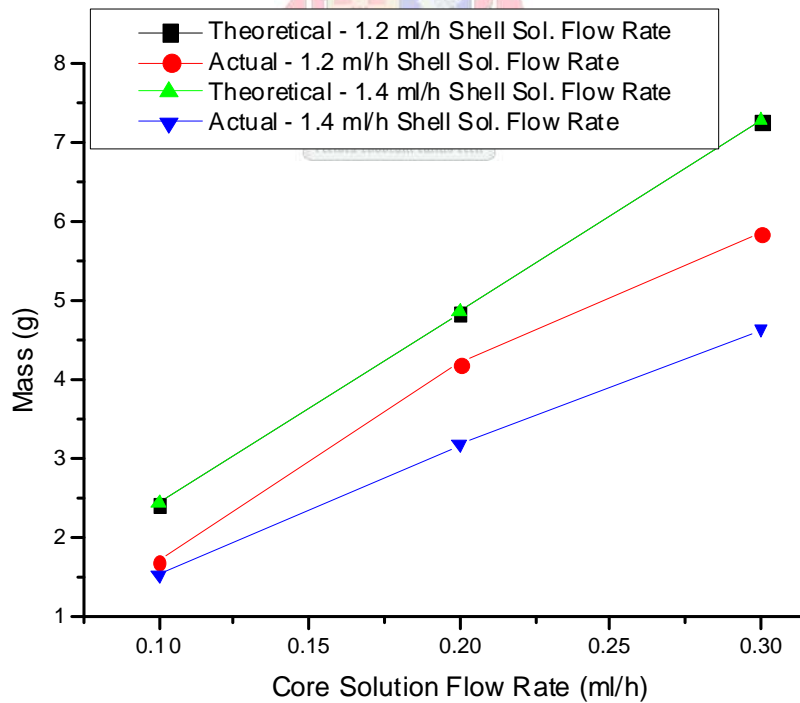
Upper Level=12wt% Shell Bonferroni test; variable Result (Spreadsheet in Analyses - 09Nov2009.stw) Probabilities for Post Hoc Tests Error: Between MS = .36556, df = 6.0000				
No.	Lower Level	{1}	{2}	{3}
		4.9667	6.5000	8.3333
1	4wt%		0.06	0.00
2	6wt%	0.06		0.03
3	8wt%	0.00	0.03	



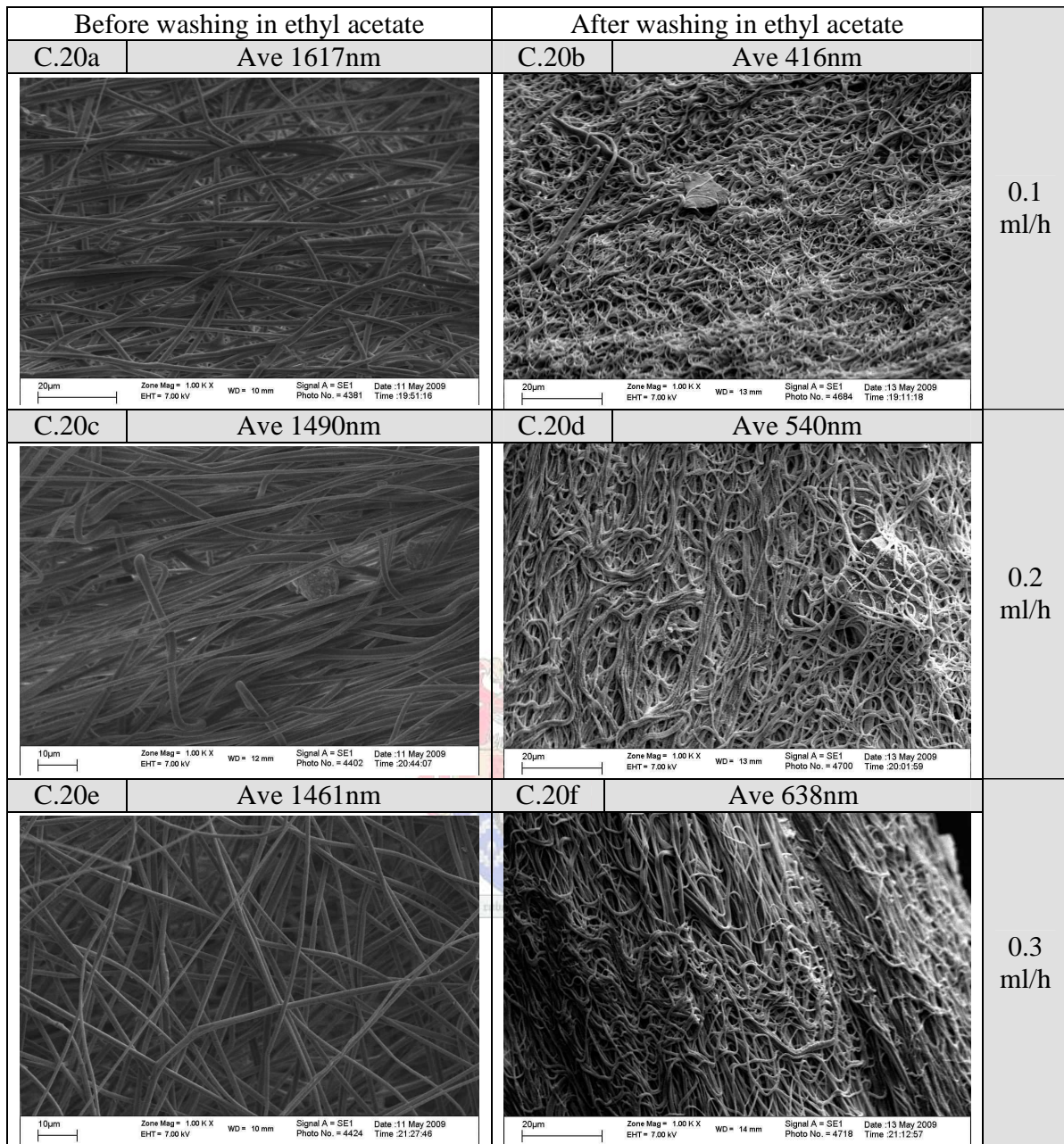
**Figure C.17** Solution concentration effects on core-shell fibre crystallinity – UpperLevel; Least-square (LS) Means



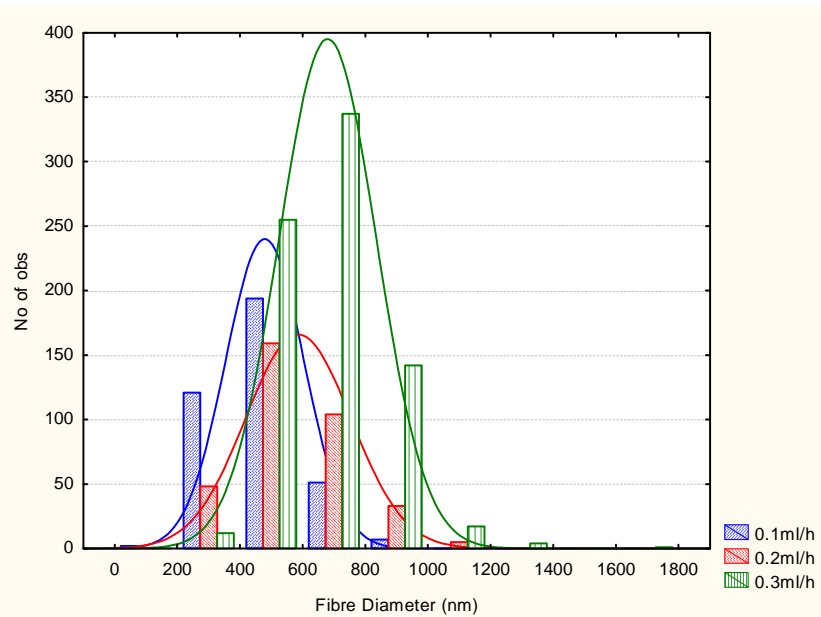
**Figure C.18** Solution concentration effects on core-shell fibre crystallinity – Upper Level\*Lower Level; LS means



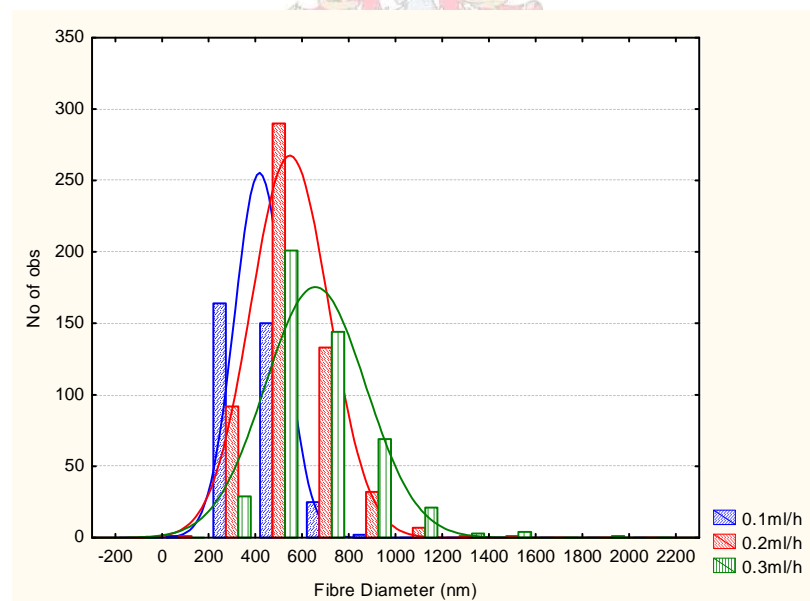
**Figure C.19** Effects of solution concentration flow rate on actual vs. theoretical core mass yield



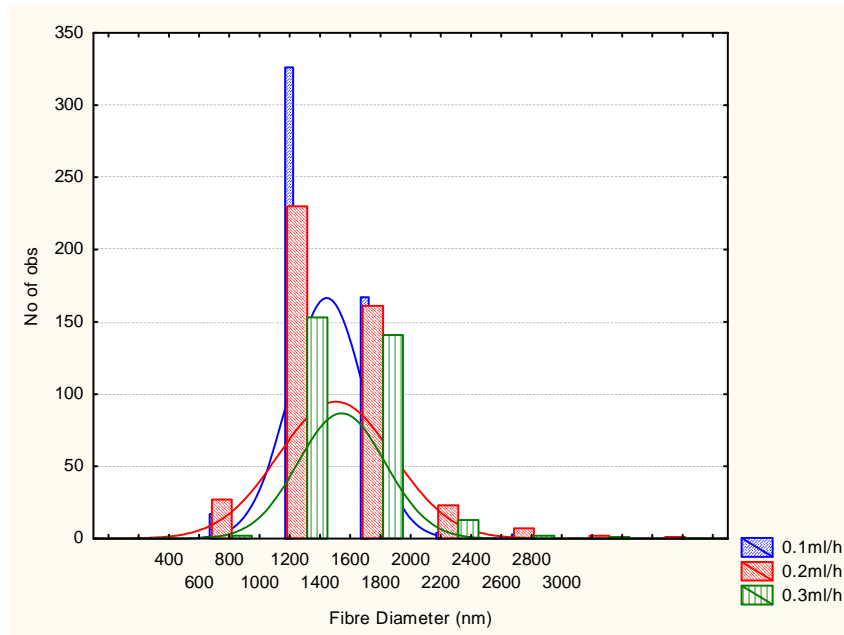
**Figure C.20** SEM images showing core-shell fibres spun with PLLA core solution flow rates a-b) 0.1ml/hr, c-d) 0.2ml/hr, e-f) 0.3ml/h and a shell solution flow rate of 1.4 ml/h before and after washing in ethyl acetate. The core and shell solution concentrations used were 8wt% PLLA and 10wt% PDLLA respectively



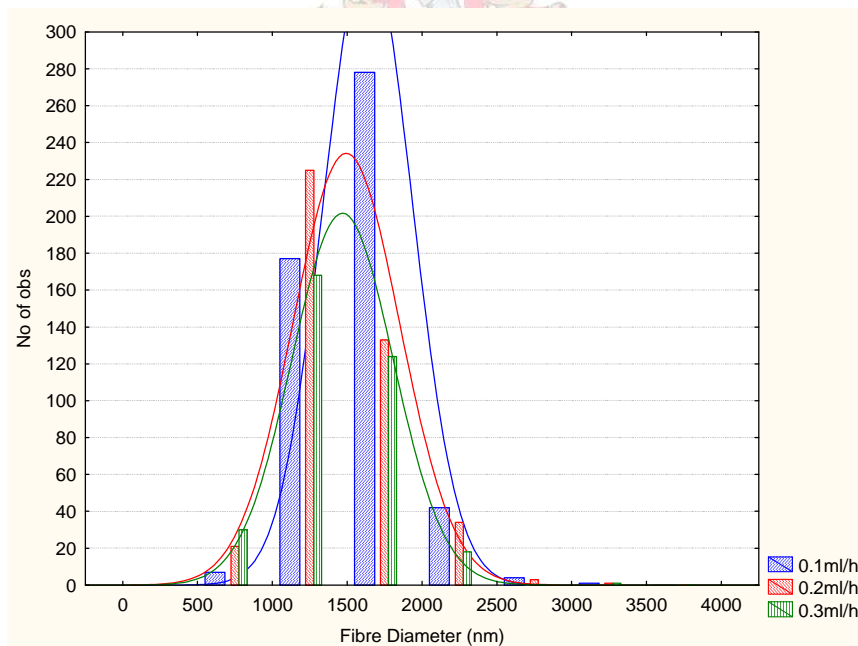
**Figure C.21** Fibre remaining after washing in ethyl acetate - fibre diameter distributions: Effect of increasing core solution flow rate at 1.2ml/h shell solution flow rate



**Figure C.22** Fibre remaining after washing in ethyl acetate - fibre diameter distributions: Effect of increasing core solution flow rate at 1.4ml/h shell solution flow rate



**Figure C.23** *As-spun fibre diameter distributions: Effect of increasing core solution flow rate at 1.2ml/h shell solution flow rate*



**Figure C.24** *As-spun fibre diameter distributions: Effect of increasing core solution flow rate at 1.4ml/h shell solution flow rate*

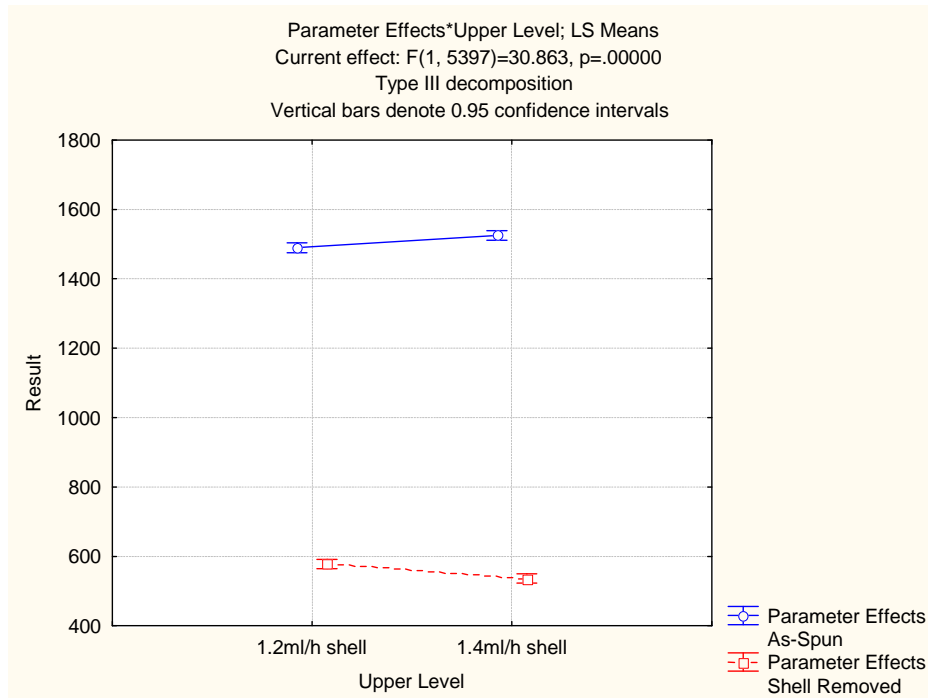


**Table C.8** *Bonferroni Tests for significance from ANOVA of solution flow rate concentration effects on core-shell (as-spun) fibre diameters*

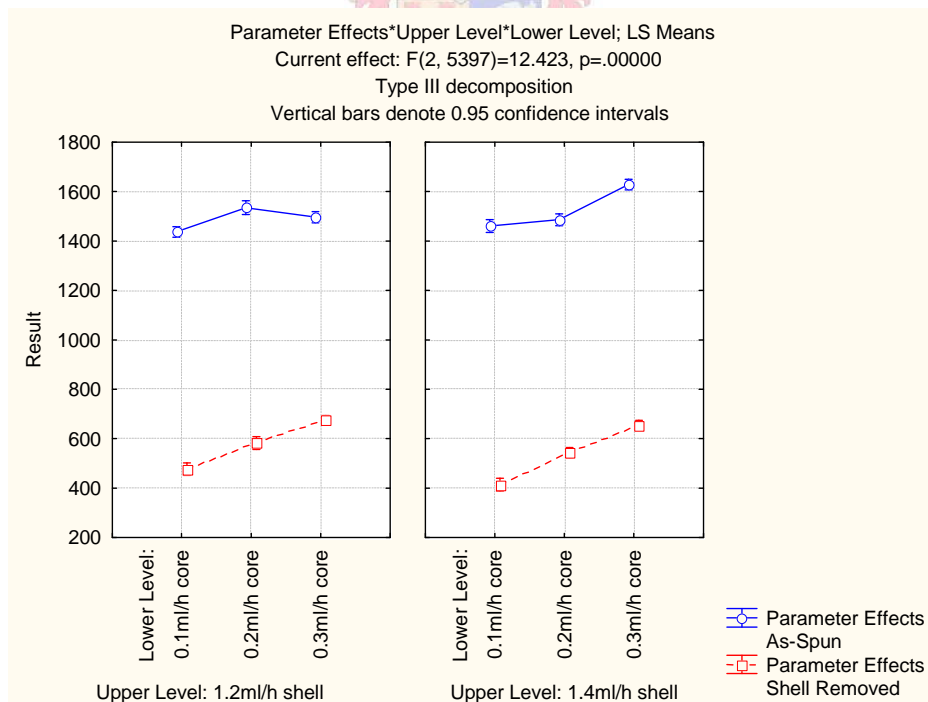
Parameter Effects=As-Spun Bonferroni test; variable Result (Spreadsheet in Analyses - 09Nov2009.stw) Probabilities for Post Hoc Tests Error: Between MS = 1013E2, df = 2540.0								
No.	Upper Level	Lower Level	{1}	{2}	{3}	{4}	{5}	{6}
			1437.0	1535.1	1496.5	1460.4	1486.5	1628.7
1	1.2ml/h shell	0.1ml/h core		0.00	0.06	1.00	0.27	0.00
2	1.2ml/h shell	0.2ml/h core	0.00		1.00	0.04	0.62	0.00
3	1.2ml/h shell	0.3ml/h core	0.06	1.00		1.00	1.00	0.00
4	1.4ml/h shell	0.1ml/h core	1.00	0.04	1.00		1.00	0.00
5	1.4ml/h shell	0.2ml/h core	0.27	0.62	1.00	1.00		0.00
6	1.4ml/h shell	0.3ml/h core	0.00	0.00	0.00	0.00	0.00	

**Table C.9** *Bonferroni Tests for significance from ANOVA of solution flow rate concentration effects on core (shell removed) fibre diameters*

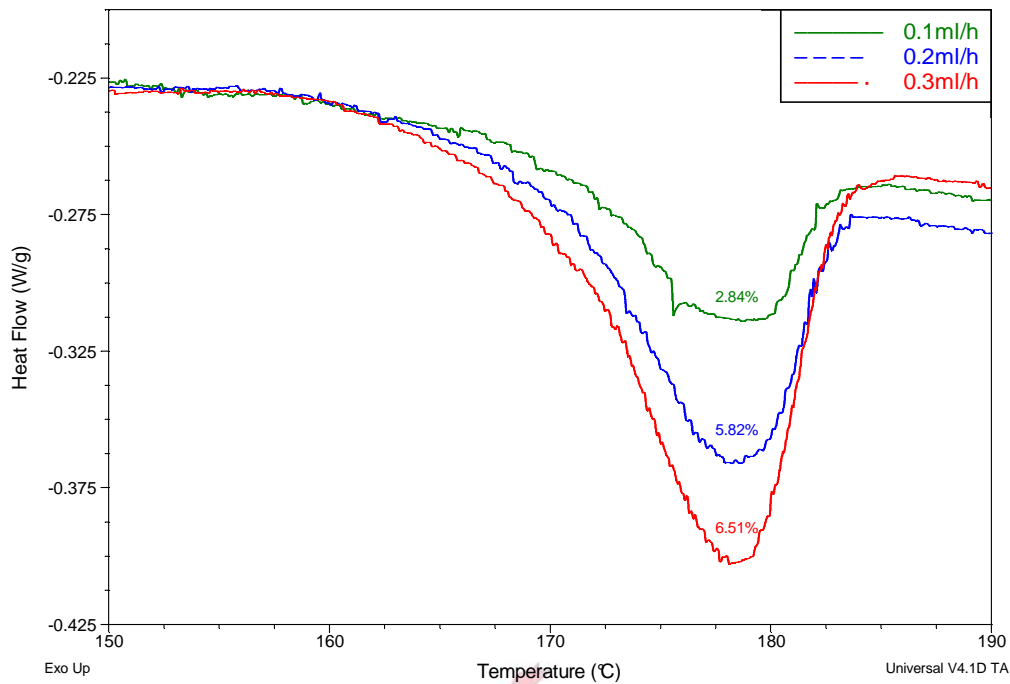
Parameter Effects=Shell Removed Bonferroni test; variable Result (Spreadsheet in Analyses - 09Nov2009.stw) Probabilities for Post Hoc Tests Error: Between MS = 26241., df = 2857.0								
No.	Upper Level	Lower Level	{1}	{2}	{3}	{4}	{5}	{6}
			476.20	582.33	675.98	413.97	543.17	652.37
1	1.2ml/h shell	0.1ml/h core		0.00	0.00	0.00	0.00	0.00
2	1.2ml/h shell	0.2ml/h core	0.00		0.00	0.00	0.01	0.00
3	1.2ml/h shell	0.3ml/h core	0.00	0.00		0.00	0.00	0.19
4	1.4ml/h shell	0.1ml/h core	0.00	0.00	0.00		0.00	0.00
5	1.4ml/h shell	0.2ml/h core	0.00	0.01	0.00	0.00		0.00
6	1.4ml/h shell	0.3ml/h core	0.00	0.00	0.19	0.00	0.00	



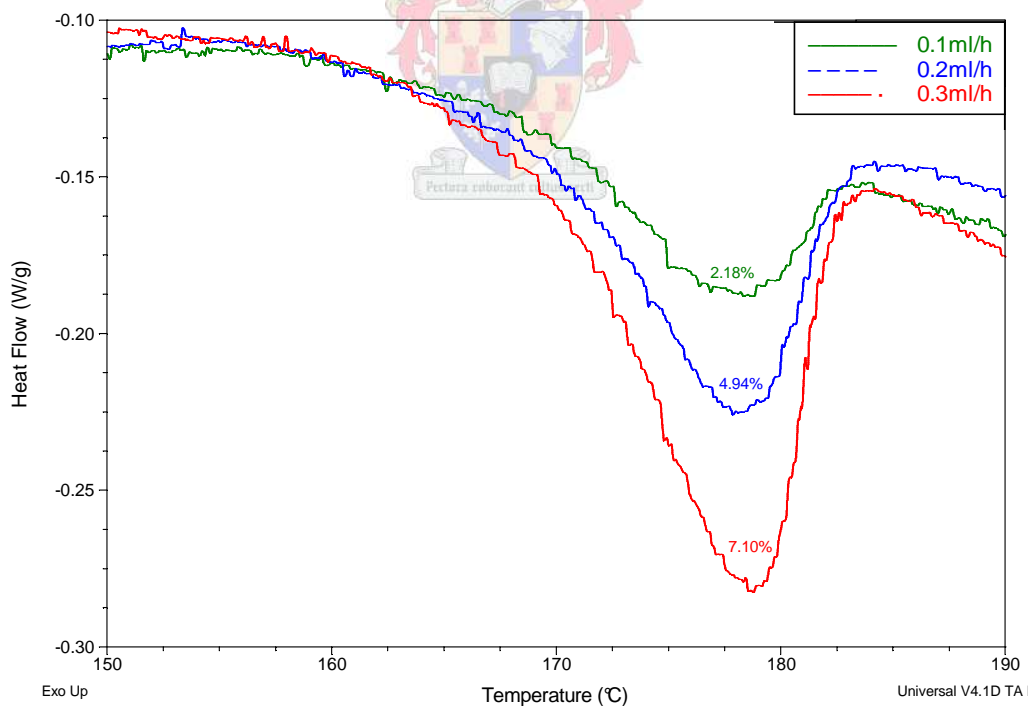
**Figure C.25** Shell solution flow rate effects on core (shell removed) and core-shell (As-spun) fibre diameter - Parameter Effects\*Upper Level; Least-square (LS) Means



**Figure C.26** Solution flow rate effects on core (shell removed) and core-shell (As-spun) fibre diameter - Parameter Effects\*Upper Level\*Lower Level; LS Means



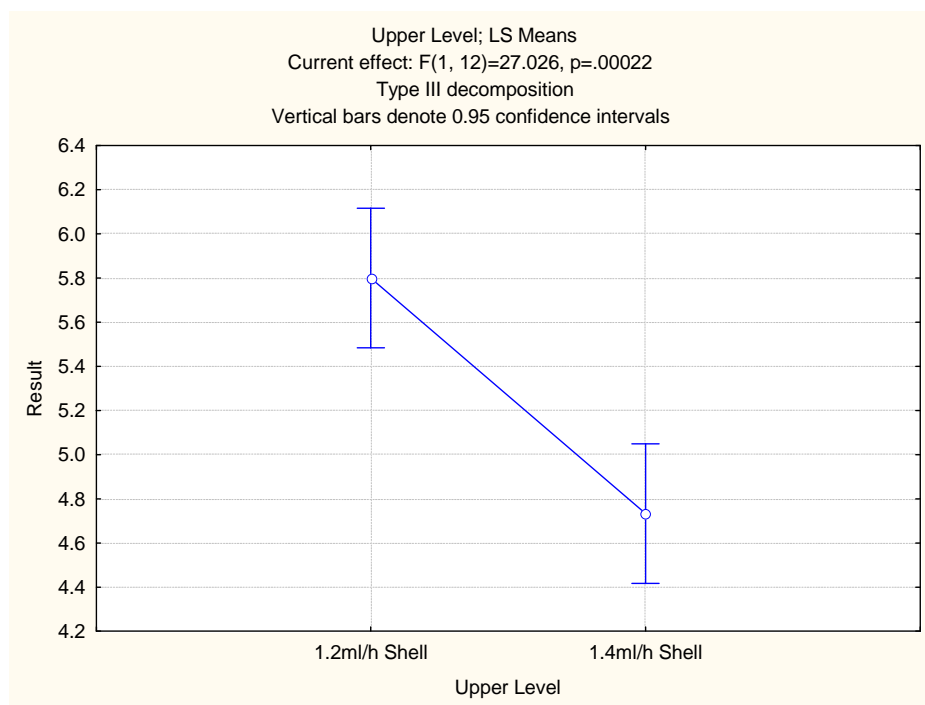
**Figure C.27** Solution flow rate concentration effects on the melt endotherm of coaxial electrospun fibre yarns at a 1.2 ml/h shell solution flow rate



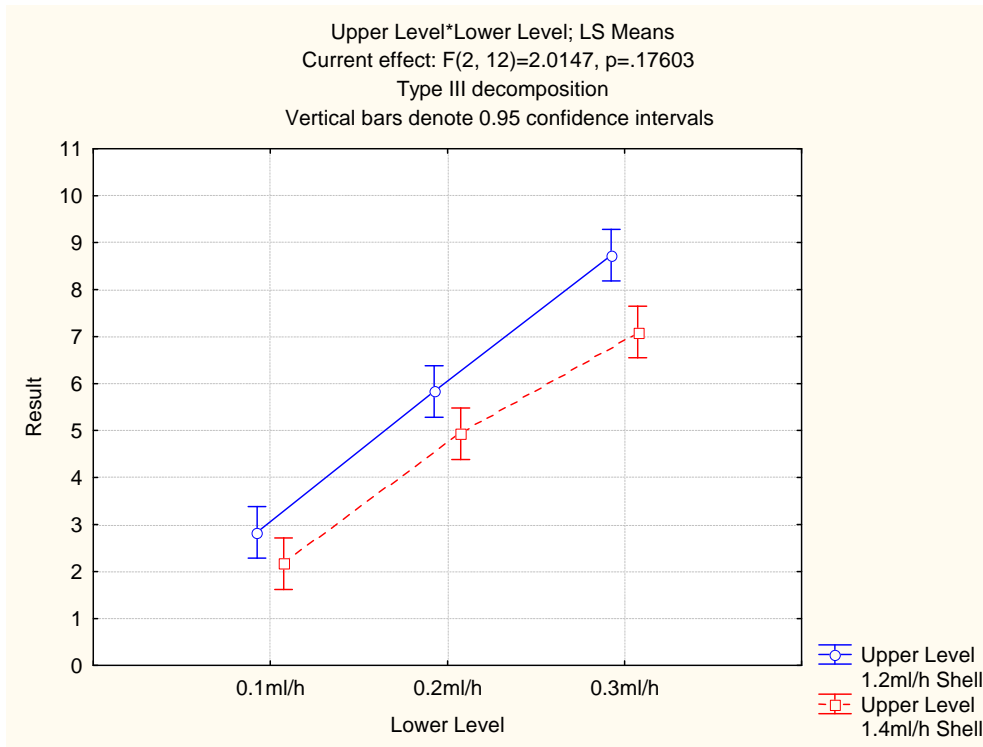
**Figure C.28** Solution flow rate effects on the melt endotherm of coaxial electrospun fibre yarns at a 1.4 ml/h shell solution flow rate

**Table C.10** Bonferroni Tests for significance from ANOVA of increasing core solution flow rate effects on core-shell fibre crystallinity: 1.2ml/h and 1.4ml/h shell solution flow rate

Bonferroni test; variable Result (Crystallinity_FlowRate in Analyses - 09Nov2009.stw)								
Probabilities for Post Hoc Tests								
Error: Between MS = .18944, df = 12.000								
No.	Upper Level	Lower Level	{1}	{2}	{3}	{4}	{5}	{6}
			2.8333	5.8333	8.7333	2.1667	4.9333	7.1000
1	1.2ml/h Shell	0.1ml/h		0.00	0.00	1.00	0.00	0.00
2	1.2ml/h Shell	0.2ml/h	0.00		0.00	0.00	0.39	0.06
3	1.2ml/h Shell	0.3ml/h	0.00	0.00		0.00	0.00	0.01
4	1.4ml/h Shell	0.1ml/h	1.00	0.00	0.00		0.00	0.00
5	1.4ml/h Shell	0.2ml/h	0.00	0.39	0.00	0.00		0.00
6	1.4ml/h Shell	0.3ml/h	0.00	0.06	0.01	0.00	0.00	



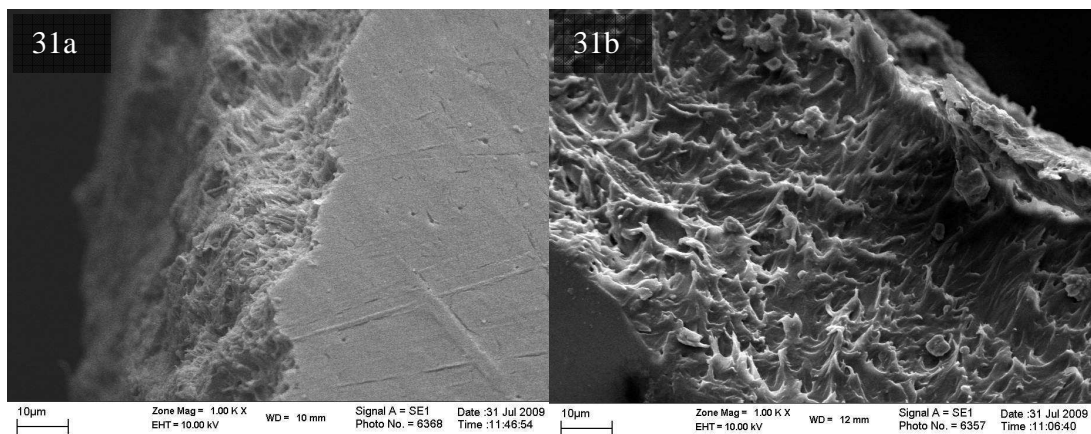
**Figure C.29** Solution flow rate effects on core-shell fibre crystallinity – UpperLevel; Least-square (LS) Means



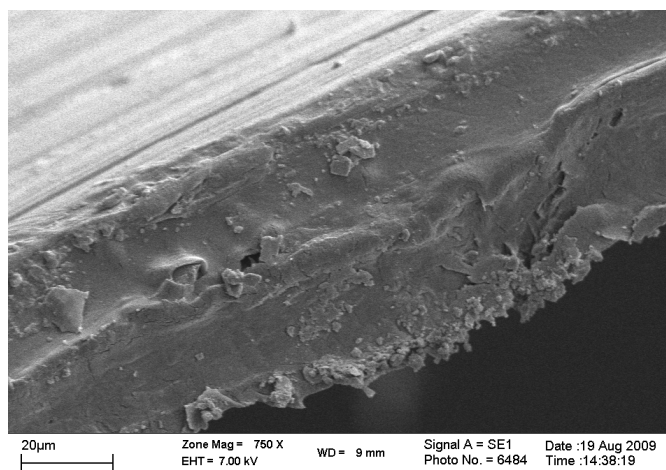
**Figure C.30** Solution solution effects on core-shell fibre crystallinty – Upper Level\*Lower Level; LS means

**Table C.11** Young’s modulus (E) for as-spun and heat-set yarns

	As-spun	Heat-set
	E (MPa)	E (MPa)
	50.2	167.8
	53.6	632.4
	90.6	254.6
	59.6	177.7
	63.9	191.2
	57.0	161.4
	60.8	133.4
	85.6	145.1
	70.2	145.9
	83.6	145.5
AVE	67.5	215.5
STDEV	14.3	150.6



**Figure C.31** a) and b) Cryo fractured film prepared from coaxial electrospun PLLA-PDLLA fibres



**Figure C.32** Cryo fractured film prepared from single capillary electrospun PDLLA fibres



## Appendix D

### D.1 Fluorescent labelling of PLLA

To study the core-shell fibre structure the core was fluorescently labelled with Rhodamine B. PLLA(Rhodamine B)-PDLLA core-shell solutions were coaxially electrospun and analysed at an excitation wavelength of 479nm (specified for Rhodamine B). Rhodamine B was covalently bonded to the hydroxyl end-group on the C-terminus of the PLLA chain (the other end is capped with an ester) using N, N'-dicyclohexylcarbodiimide (DCC). DCC was used to prepare a better leaving group by enhancing the electrophilicity of the carboxylate group of Rhodamine B. The negatively charged oxygen acts as a nucleophile, attacking the central carbon in DCC. DCC is temporarily attached to the former carboxylate group (now an ester group) allowing for the nucleophilic attack by the alcohol group of PLA and a dehydration coupling reaction of the PLA and Rhodamine B.

#### Reagents

Poly(L-lactic acid) (PL24, Mw $\cong$ 291k)	Purac Biomaterials, Netherlands
Rhodamine B (479.01 g/mol)	Sigma Aldrich, South Africa
N,N' Carbodiimidazole (206.33g/mol)	Sigma Aldrich, South Africa
Distilled Water	Department of Chemistry and Polymer Science, Stellenbosch University
Industrial grade Dichloromethane (DCM)	Sasol Solvents, South Africa
Analytical grade Diethyl ether	Saarchem/Merck, South Africa

**Method**

DCC (0.005g) was dissolved in 10mL DCM and stirred for 15min. At this point the Rhodamine-B (0.001g) was added and the mixture was stirred for 30min. PLA (0.505g) was dissolved in 10mL of DCM. The two solutions were mixed and stirred for a week at room temperature (RT -  $\pm 22^{\circ}\text{C}$ ). The polymer was precipitated into diethyl ether. The precipitate was washed several times with distilled water to extract any unreacted Rhodamine B. The polymer was dried overnight under reduced pressure (50mBar). The dried polymer was dissolved in chloroform and washed with methanol/distilled water. The organic layer was dried overnight under reduced pressure (50mBar).

**D.2 Synthesis of Zinc Sulphide (ZnS) particles capped with polyvinylpyrrolidone (PVP)**

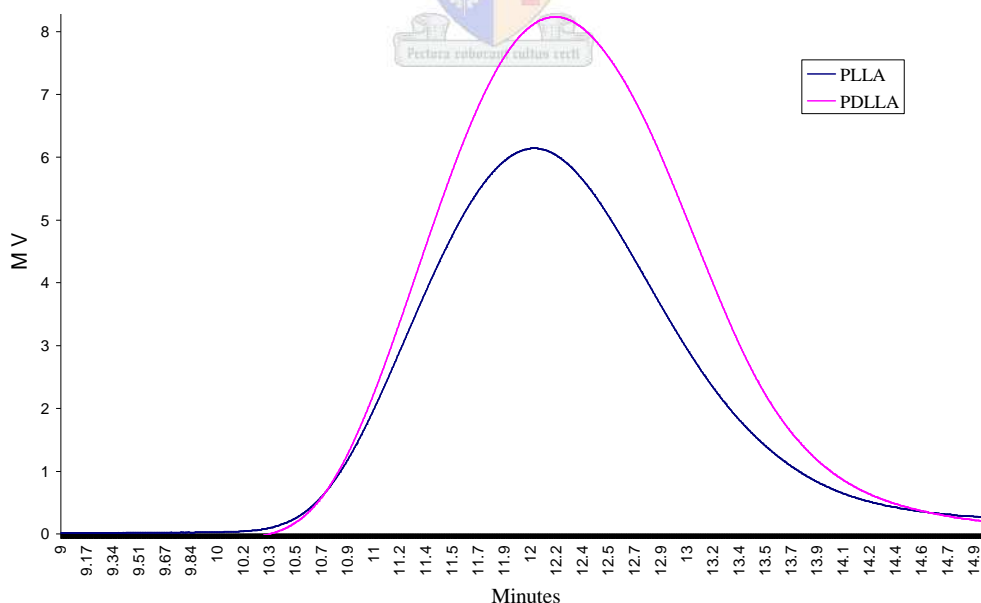
ZnS-PVP particles were synthesized for other purposes by colleagues in our Department. These particles were kindly donated to us to experiment with different contrasting strategies for analysing the core-shell fibre structures. The synthetic route used to prepare these particles can be found in literature.<sup>1</sup>

**D.3 Determination of molecular mass of PLLA and PDLLA with size exclusion chromatography (SEC)/gas permeation chromatography (GPC)****Materials**

<i>Raw Material</i>	<i>Supplier</i>
<i>Gel permeation chromatography GPC (mobile phase)</i>	
HPLC grade Tetrahydrofuran (THF) solvent (0.125% BHT stabilised)	Chromasolve

This chromatographic technique separates polymer molecules according to size, or more correctly hydrodynamic volume. When the chromatographic medium is a gel, the technique is also referred to as gel permeation chromatography (GPC).

The SEC instrument used in this project is comprised of the following units: Waters 1515 isocratic HPLC pump; Waters 717 plus Autosampler; Waters 2487 Dual  $\lambda$  Absorbance detector; Waters 2414 Refractive index (RI) detector at 30°C and data processing was performed using Breeze Version 3.30 SPA (Waters) software. Separation was achieved using two PLgel (Polymer Laboratories) 5 $\mu$ m Mixed-C (300 $\times$ 7.5mm) columns connected in series along with a PLgel 5 $\mu$ m guard column (50 $\times$ 7.5mm). The columns were kept at a constant temperature of 30°C. THF Chromasolve HPLC grade solvent (0.125% BHT stabilised) was used as mobile phase at a flow rate of 1ml/min. PLLA and PDLLA samples were dissolved in the stabilised THF at a concentration of 5mg/ml and 100 $\mu$ l injection volumes were used. The system was calibrated using Polymer Laboratories Easivial PS Standards (10 Standards ranging from 580g.mol<sup>-1</sup> to 3 000 000g.mol<sup>-1</sup>). The SEC curves and polymer molecular weight distributions of the PLA used in this work are shown in Figure E.2 and Table E.1 respectively.



**Figure D.1** GPC curve for PLLA and PDLLA polymer in THF

**Table D.1** *Molecular weight distributions*

Polymer	$M_n$ (number ave. molecular weight)	$M_w$ (weight ave. molecular weight)	PDI ( $M_w/M_n$ ) (poly dispersity index)
PLLA	146250	291328	1.99
PDLLA	132722	265153	2.00

## References

1. Wang C, Tao X-T, Yang J-X, Ren Y, Liu Z, Jiang M-H. Preparation and characterization of the ZnS nanospheres with narrow size distribution. *Optical Materials*. 2006;28:1080-3.

